A Study of Nanomaterials and Endocytic Marked Compartments in Cells using Image Correlation Spectroscopy Analysis

by

Lindsay Shearer

A thesis submitted in partial fulfillment of the requirements for the degree of

Doctor of Philosophy

Department of Chemistry

University of Alberta

Abstract

Nanomaterials have gained interest due to their unique physical and chemical phenomena that is only observed for materials in this size regime. In the biohealth sector, gold nanoparticles are good platforms for use in curative treatments and detection of cancer and disease. However, their effectiveness depends on how well they are internalized and destined to travel in cells. One pathway gold nanoparticles use to travel in cells is clathrin mediated endocytosis. In this pathway, gold nanoparticles are encapsulated in membrane vesicles that undergo fusions and maturations with four intracellular vesicles (endosomes) before being directed to the lysosome for degradation. There are four proteins which "mark" the pathway; Rab5 (Early Endosome), Rab11 (Recycling Endosome), Rab7 (Late Endosome), and LAMP-1 (Lysosome).

In this work, we first studied the distribution and co-localization of the four proteins which "mark" the pathway to determine the extent to which these markers are unique for specific endosomes or co-exist with other markers on endosomes. This study was done for C2C12 and A549 cells to determine if the distribution and co-localization of markers was cell type specific. We determined that markers are not unique for specific endosomes and markers can co-exist in the same endosome, the distribution and co-localization of markers in cells is cell type specific and the distribution of ternary complexes varies with cell type.

We then studied the time dependent internalization and uptake of phospholipid coated gold nanoparticles and the extent of co-localization of phospholipid coated gold nanoparticles with markers in C2C12 and A549 cells. C2C12 and A549 cells are able to continuously internalize phospholipid coated gold nanoparticles with time, but to different extents. It was also observed that the ability for cells to withhold phospholipid coated gold nanoparticles in a

nanoparticle free extracellular environment depends on cell type. We also found that binary and ternary complex formation in A549 and C2C12 cells varied. A fraction of binary complexes consisting of one marker and phospholipid coated gold nanoparticles may also include ternary complexes in both cell types. This work was consistent with results obtained in Chapter 3.

As we were able to effectively study the endocytic pathway and uptake of phospholipid coated gold nanoparticles in two different cell types, we chose to study α −synuclein (α −syn) in SH-SY5Y cells. α −syn is a protein associated with Parkinson's disease; until recently, oligomeric forms of the protein are understood to be toxic and are the current focus of study for scientists for detection and curative methods. Thus, we applied the same logic and methods in Chapters 3 and 4 to study oligomeric forms of α −synuclein. We studied the time dependent uptake of oligomers, distribution and extent of co-localization of markers, extent of co-localization of oligomers, and the extent of co-localization of oligomers with markers in SH-SY5Y cells. The oligomers chosen for this study were monomers, as well as engineered dimers and tetramers. We found each oligomer was able to passively enter cells and each oligomer was observed to also undergo clathrin mediated endocytosis. Each oligomer had shown to be internalized and taken up in cells in a time dependent manner; however, the degree of aggregation of monomers decreases the most with time.

Real-time observation of monomers, dimers, and tetramers of α −synuclein in SH-SY5Y cells was also studied. This was the first time real-time observation was to be undertaken for this study; we determined an experiment consisting of 50 images is sufficient to estimate the diffusion time, diffusion coefficient, and temporal auto correlation amplitude. We also observed that the diffusion time of oligomers in cells was proportional to the size of the oligomer.

In this work, membrane trafficking and possible roles of endocytic proteins was studied along with the endocytic uptake of two nanomaterial systems of interest for potential therapeutic and diagnostic applications. This is the first ICS analysis of endocytic marker and gold nanoparticle association and distribution and the first successful *quantitative* three color co-localization performed in-vitro in C2C12 and A549 cells, using Image Correlation Spectroscopy analysis. The work presented in this thesis significantly contributes to the field of nanotechnology and cell biology.

The work in this thesis was accomplished using Image Correlation Spectroscopy analysis of images obtained using a laser scanning confocal microscope.

Preface

Triple Image Cross Correlation Spectroscopy Analysis was developed by Dr. Nils O. Petersen and Dr. Max Anikovsky. This work has not yet been published.

Phospholipid coated gold nanoparticle synthesis and characterization was developed by Meijing Wang.[1,2]

Oligomeric constructs of α −synuclein synthesis and characterization was developed by Xi Li and co-workers. This work is currently under review.

The data and analysis presented in this thesis belongs to Lindsay J. Shearer and is not yet published; manuscripts for publication in progress.

For Mom, Dad, & Alison.

Acknowledgements

First and foremost, I would like to thank my supervisor, Dr. Nils O. Petersen for his guidance and support during my PhD studies for which this thesis would not be possible. I am very grateful for your willingness to be available to teach and challenge me in research; with every discussion in the past five years, I have always learned something new. Thank you for providing me with the opportunity to study; it has been a pleasure working with you.

I would like to acknowledge the following organizations for which this research opportunity would not be possible; Alberta Innovates Health Solutions, NSERC, National Institute for Nanotechnology, and the University Of Alberta Department Of Chemistry.

I would like to thank my colleagues from the Petersen Lab; Xi Li, Chunhua Dong, Meijing Wang, Nick Smisdom, and Max Anikovsky. I would also like to thank Dr. Xuejun Sun and Gerry Barron for providing me with a wealth of information in laser scanning confocal microscopy, and allowing use of the microscope at the Cross Cancer Institute for this thesis. At the National Institute of Nanotechnology, I would like to thank Angela Brigley, Cathy de Guzman, and Bethany Griffith. I would like to thank Dr. Michael Woodside and the Woodside lab for their help and guidance.

I am forever grateful for the friends I have made in Edmonton during my PhD studies; Charles Vaudry, Tran Tran, Jyoti Minhas, Tina Djurjevic, Claude Larrivee Aboussafy, Amy Edgington, Aleona Shynkaruk, Amanda Nagyl, Paul Lummis, and many more.

Last but not least, I would like to thank my family; Gil Shearer, Roz Shearer, and Alison Shearer for their continuous support and encouragement; always.

Table of Contents

List of Tables

List of Figures

List of Abbreviations

A	Fitted Auto Correlation Amplitude
A549	Human Lung Adenocarcinoma Cells
α −Synuclein	Alpha Synuclein
α −Syn	Alpha Synuclein
AU	Airy Unit
BSA	Bovine Serum Albumin
C2C12	Mouse Muscle Myoblastoma Cells
$C_6H_8O_6$	Ascorbic Acid
CD	Cluster Density
CO_2	Carbon Dioxide
Cy5	Cy5-Tetrazine
Cy3	Cy3-Tetrazine
$\Delta\tau$	Delay Time Between Images
DA	Degree of Aggregation
DMEM	Dulbecco's Modified Eagle Medium
DLS	Dynamic Light Scattering
Ds	Dimers
Ds-488	Dimers with a 488 nm fluorescent probe
Ds-561	Dimers with a Cy3 fluorescent probe
Ds-633	Dimers with a Cy5 fluorescent probe

DIC	Differential Interference Contrast
EE	Early Endosome
$F(b\|gr)$	Fraction of Clusters with Blue Containing Green and Red
$F(bg\|r)$	Fraction of Clusters with Blue and Green Containing Red
$F(br\|g)$	Fraction of Clusters with Blue and Red Containing Green
$F(g\|r)$	Fraction of Clusters with Green Containing Red
$F(g\|rb)$	Fraction of Clusters with Green Containing Red and Blue
$F(gb\|r)$	Fraction of Clusters with Green and Blue Containing Red
$F(gr\|b)$	Fraction of Clusters with Green and Red Containing Blue
$F(r\|g)$	Fraction of Clusters with Red Containing Green
$F(r\|gb)$	Fraction of Clusters with Red Containing Green and Blue
$F(rb\|g)$	Fraction of Clusters with Red and Blue Containing Green
$F(rg\|b)$	Fraction of Clusters with Red and Green Containing Blue
F-12K	Ham's F12 K Medium
FBS	Fetal Bovine Serum
FITC	Fluoroscein Isothiocyanate
GNPs	Phospholipid Coated Gold Nanoparticles
g(0,0)	Auto Correlation Amplitude
$g(0,0,0)$	Temporal Auto Correlation Amplitude
$g(\alpha,\beta,\tau)$	Temporal Auto Correlation Function
$g_{gr}(\alpha,\beta)$	Normalized Cross Correlation Function

$g_{grb}(\alpha,\beta,\theta,\rho)$	Normalized Triple Cross Correlation Function
$\langle g(0,0) \rangle$	Average Auto Correlation Amplitude
$\langle g(0,0,0) \rangle$	Average Temporal Auto Correlation Amplitude
$\langle g_b(0,0) \rangle$	Average Auto Correlation Amplitude for blue channel
$\langle g_g(0,0) \rangle$	Average Auto Correlation Amplitude for green channel
$\langle g_{gb}(0,0) \rangle$	Average Cross Correlation Amplitude for green/blue channel
$\langle g_{gr}(0,0) \rangle$	Average Cross Correlation Amplitude for green/red channel
$\langle g_r(0,0) \rangle$	Average Auto Correlation Amplitude for red channel
$\langle g_{rb}(0,0) \rangle$	Average Cross Correlation Amplitude for red/blue channel
$I_{avg.}$	Average Intensity
$\langle I_{avg.} \rangle$	Average of the Average Intensity
ICS	Image Correlation Spectroscopy
ICCS	Image Cross Correlation Spectroscopy
$KAuCl_4$	Potassium Gold (III) Chloride
λ	Wavelength of excitation
LAMP-1	Lysosomal Associated Membrane Protein 1
LAMP-1-488	Lysosomal Associated Membrane Protein 1 with a 488 nm fluorescent probe
LAMP-1-561	Lysosomal Associated Membrane Protein 1 with a 555 nm fluorescent probe
LAMP-1-633	Lysosomal Associated Membrane Protein 1 with a 647 nm fluorescent probe
LE	Late Endosome
Lys	Lysosome

mm	Millimeter
mL	Milliliter
mM	Millimolar
Ms	Monomers
Ms-488	Monomers with a 488 nm fluorescent probe
Ms-561	Monomers with a Cy3 fluorescent probe
Ms-633	Monomers with a Cy5 fluorescent probe
N.A	Numerical Aperture
n_{images}	Number of Images
$n_{species}$	Number of Clusters Containing Species
$\langle n_{species} \rangle$	Average Number of Clusters Containing Species
NBD-SOPG	Nitro-benzoxadiazol conjugated SOPG lipid
NINT	National Institute of Nanotechnology
RE	Recycling Endosome
$NaBH_4$	Sodium Borohydride
$Na_3C_6H_5O_7$	Trisodium Citrate
$\langle N_b \rangle$	Average number of clusters with only blue
$\langle N_g \rangle$	Average number of clusters with only green
$\langle N_{gb} \rangle$	Average number of clusters with only green and blue
$\langle N_{gr} \rangle$	Average number of clusters with only green and red
$\langle N_{grb} \rangle$	Average number of clusters with only green, red, and blue

$\langle N_r \rangle$	Average number of clusters with only red
$\langle N_{rb} \rangle$	Average number of clusters with only red and blue
nm	Nanometer
PBS	Phosphate Buffered Saline
PFA	Paraformaldehyde
Rab5	Rabaptin 5
Rab5-561	Rab5 with a fluorescent Cy3 probe
Rab7	Rabaptin 7
Rab7-488	Rab7 with a fluorescent 488 nm probe
Rab7-633	Rab7 with a fluorescent 647 nm probe
Rab11	Rabaptin 11
Rab11-633	Rab11 with a fluorescent 647 nm probe
SH-SY5Y	Human Bone Marrow Neuroblastoma Cells
SOPG	1-stearoyl-2-oleoyl-sn-glycero-3-phospho-(1'-rac-glycerol) (sodium salt)
SEM	Scanning Electron Microscope
τ	Time in seconds
TEM	Transmission Electron Microscope
TICS	Temporal Image Correlation Spectroscopy
TRICCS	Triple Image Cross Correlation Spectroscopy
Ts	Tetramers
Ts-488	Tetramers with a 488 nm fluorescent probe

Ts-561	Tetramers with a Cy3 fluorescent probe
Ts-633	Tetramers with a Cy5 fluorescent probe
μL	Microliter
μm	Micrometer or microns
μM	Micromolar
μs	Microsecond
ω (μm)	General term for fitted laser beam width obtained in ICS
ω_o (μm)	"True" fitted laser beam width obtained in ICS
ω_{DL} (μm)	Theoretical Diffraction Limited Laser Beam Width
ω_{Exp} (μm)	Experimental fitted laser beam width obtained in ICS
⟨ω (μm)⟩	Average Fitted Laser Beam Width obtained in ICS
WT	Wild Type

Chapter 1

Motivation and Purpose for a Study of Nanomaterials in Cells and Endocytic Marked Compartments using Image Correlation Spectroscopy Analysis

1 Motivation and Purpose for a Study of Nanomaterials and Endocytic Markers using Image Correlation Spectroscopy Analysis

1.1 Importance of Nanotechnology

Nanotechnology is defined as the science and study of matter at dimensions ranging between 1-100 nanometers. The field of nanotechnology began to emerge approximately fifty years ago. Specifically, in 1957, Dr. Richard Feynman, an American physicist, gave a lecture titled *There's Plenty of Room at the Bottom* at the California Institute for Technology for which the overall concept of nanotechnology began to emerge. Proceeding into the early 1970s, the term "Nano-technology" was first defined by Dr. Norio Taniguchi,"'Nano-technology' is the production technology to get the extra high accuracy and ultra fine dimensions, i.e the preciseness and fineness of the order of 1 nm (nanometer), 10^{-9} m in length". Ultimately, by the early 1980s, Dr. Eric Drexler published several works related in the field and was the first to receive a doctoral degree on the topic of molecular nanotechnology.[3]

Nanotechnology has become important due to the physical and chemical phenomena that are only observed for materials in this size regime. Unlike at the macromolecular and bulk scale, *nanomaterials* possess properties that are actually dependent on the relative size of the material. Specifically, quantum effects begin to govern the behavior and properties of particles at this scale. Material characteristics such as the melting point, fluorescence, electrical conductivity, magnetic permeability and chemical reactivity change as a function of the particle size within this 1-100 nanometer regime.[4] Thus, a significant amount of work has been studied in the last thirty years by chemists, biologists, physicists, and engineers to further understand this phenomenon and develop numerous devices of ranging sizes and morphologies for specific applications in fields of electronics, energy, agriculture and forestry, and biohealth.

In the biohealth sector, nanomaterials have shown promise to serve as platforms for curative treatments and detection of cancer and disease.

1.2 Types of Nanomaterials

In this thesis, two types of nanomaterial systems of interest were studied; phospholipid coated gold and α −synuclein oligomer constructs.

1.2.1 Gold

As a means to add to current methods and alleviate associated drawbacks and unwanted side effects, scientists have made great efforts to develop a number of nanomaterials to serve as platforms for drug delivery and radiation and heat therapy. One material in particular that has been widely used is nanoscale gold.

For the last thirty years, it is has been known that gold has the ability to bind with thiol groups.[5] This is incredibly advantageous for the field of biohealth because scientists can modify a molecule of interest with a thiol group to be able to bind with a gold surface.[6,7] As an example in drug delivery applications, many have functionalized gold nanoparticles with thiol-capped polyethylene glycol (PEG) monolayers by means of protecting gold nanoparticles from being directed out of circulation in the bloodstream and taken up by the reticuloendothelial system (RES) for degradation and excretion.[8,9,10]

Gold nanoparticles can be functionalized with thiolated poly(ethylene glycol) but *also* with molecules currently known to treat cancer such as doxorubicin and oxaliplatin, as a means to increase the likelihood of drug delivery to cells without being recognized and degraded by the RES. [11,12, 13]

An important consideration of nanomaterials in general is that due to their size they are able to passively target to solid tumors. This is due to the leaky vasculature of solid tumors where nanoparticles can passively penetrate through these openings and reach the tumor cells. This process is referred to as the enhanced permeability and retention effect.[14]

Another interesting use of gold is the potential to prepare gold nanoparticle-antibody hybrids; depending on the application, antibodies can be functionalized to gold to actively target a *specific cell type* that expresses the respective antigen for photothermal therapy applications.[15] Due to the strong electron dense nature of gold, gold can release heat to its surroundings upon interaction with electromagnetic radiation for heat therapy. This occurs by phonon-phonon

relaxation. Or, antibodies can be functionalized to gold nanoparticles with the goal of activating a specific immune response.[16,17]

Like gold, deoxyribonucleic acid (DNA) molecules are nanomaterials; specifically, DNA is approximately 2 nanometers in diameter. DNA molecules encode specific genetic information responsible for the growth, development, and reproduction of living organisms and viruses. Thus, many people have done work towards developing gold-DNA- hybrids for enhanced drug delivery and thermally dependent therapeutic applications.[18,19,20,21]

Lastly, an important feature for these nanoparticles to serve as effective platforms in photothermal, drug delivery, and photodynamic therapy applications is that these nanoparticles are not toxic. Lactate dehydrogenase (LDH) and metabolic cell activity assays (MTT) have been done to show gold nanoparticles are not toxic.[22]

Gold nanoparticles with a phospholipid coating post the potential to be biocompatible with cells and have been previously characterized. The phospholipid coated gold nanoparticles have shown to internalize but there is no clear evidence for what compartments they localize to inside cells.[2]

1.2.2 α-Synuclein

Parkinson's disease is a neurodegenerative disease commonly found in somewhat older individuals, specifically between ages 50-93 years affecting approximately 7 million people worldwide. The neurodegeneration occurring is the loss of dopaminergic pigmented neurons in the substantia nigra.[23] Individuals diagnosed with the disease can show a number of symptoms, specifically impaired dexterity, expressionless face, and monotonous quality of speech are among the common symptoms.[24] A defining characteristic associated with the root source of Parkinson's disease is the presence of Lewy bodies in neurons.[25] Lewy bodies are intracellular composites of misfolded aggregates of a protein known as α −synuclein.[26]

Protein misfolding can be very problematic; when a protein is misfolded, it exposes it's hydrophobic amino acid side chain to the environment thus being more prone to aggregation.[27] α −synuclein is a natively unfolded 140-amino acid protein that is encoded by a single gene consisting of seven exons located in chromosome 4. A30P, E46K, and A53T are among the three

known mutations or misfolded forms of α-synuclein.[28] The presence of α −synuclein in human brains has been confirmed in the past twenty years via immunoblot analysis.[29] The protein has proven to be quite toxic in vitro and in vivo. [30, 31, 32,33] The initial neuronal or cellular uptake of α −synuclein has shown to occur via a receptor mediated endocytic process.[34]

It is still a bit unclear which form of α-synuclein is truly toxic. However, recently it has been shown that prior to fibril formation, oligomer aggregation of α −synuclein is toxic.[35] In vitro studies have shown that monomer mutations A30P and A53T are consumed more quickly than the Wild Type in vitro.[36] In addition, studies have also shown pre-fibrillar mutants of α −synuclein are toxic in tissue culture cells, in mammalian neurons, and in Parkinson's Disease model organisms.[37]

In this work, we studied wild type (WT) monomers, engineered dimers, and engineered tetramers. Engineered dimers and tetramers were prepared by covalently linking 3 amino acid chains.

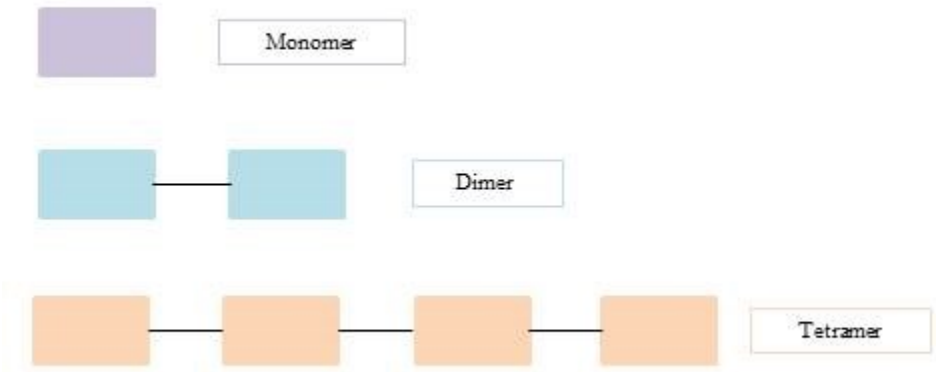

Figure 1.1 Wild Type Monomer, Engineered Dimer, and Engineered tetramer

Therefore, the extent to which various oligomeric forms of α −synuclein aggregate and internalize in cells for potential Lewy Body formation in neurons is of high interest to further explore for potential detection and therapeutic applications of Parkinson's disease.

1.3 Internalization and Uptake of Nanomaterials

Nanomaterials such as gold and α −synuclein are known to undergo a process known as Endocytosis.[38,34]

Endocytosis is broadly defined as a process in which a eukaryotic cell engulfs material from the extracellular environment. Specifically, endocytosis can be classified into four different types; phagocytosis, pinocytosis, caveolin, and clathrin mediated endocytosis.[39] Each classification of endocytosis depends primarily on the size and composition of material being engulfed.

Materials on the scale of 50 microns undergo phagocytosis. Phagocytosis is a process that is used by phagocytes to engulf large particles, pathogens, and apoptotic cells.[40] Phagocytosis means the process for devouring cells. In contrast, cell drinking is defined by pinocytosis, in which fluid-like substances and solutes undergo endocytosis. Caveolin endocytosis is specific to the internalization of material on the nanoscale and membrane invagination is dependent on the recruitment of caveolin from the cytoplasm to the membrane. The membrane domain of the internalization site is enriched with cholesterol and sphingolipids and the material endocytosed via a caveolin dependent pathway include folic acid, albumin, and cholesterol.[41] Lastly, clathrin mediated endocytosis is also specific for nanomaterials however the membrane invagination is dependent on the recruitment of clathrin from the cytoplasm to the membrane. Receptors localized to these domains include low density lipoproteins receptors, transferrin receptors, and epidermal growth factor receptors.[42]

Phagocytosis was first discovered by Elie Metchnikoff in the late 19th century.[43] However, more specific information in regard to fusion and maturation phenomena of endocytosis began to surface in the early 1960s; Werner Straus at the University of North Carolina, Chapel Hill, performed and observed an experiment in which blue stained phagosomes were able to fuse with red stained lysosomes to form purple spheres in kupfer cells.[44] As time progressed into the mid-1980s, the absolute definition of whether endocytosis was a maturation, fusion, or a maturation and fusion process still remained to be clearly defined. One hypothesized theory of endocytosis was the *Vesicle Shuttle Model* whereby endosomes are of fixed size, location, and morphology and transport of cargo would occur via smaller vesicles, transporting the cargo between the

endosomes. Another hypothesized theory of endocytosis was the *Maturation Model* whereby the endosomes and the contents move together as the organelles undergo maturation and fuse with the lysosome. To date, the later model appears to be the most commonly supported.[45,46,47] The work presented in this thesis is based on the hypothesis that endosomes undergo maturation and fusion such that these compartments are not of fixed size and location in the cytoplasm of cells.

Figure 1.2 is an illustration of the commonly proposed pathway of clathrin mediated endocytosis. The first step in clathrin mediated endocytosis is the localization of nanoparticles to the plasma membrane. Then, clathrin is recruited to the plasma membrane to assist invagination of the membrane. Clathrin, adapter proteins, and membrane bound proteins assist with pinching the invaginated membrane into the cytoplasm of the cell. After a few minutes, the clathrin coat sheds from the membrane and becomes a nanoparticle vesicle. The nanoparticle vesicle then fuses with an early endosome after approximately ten minutes has progressed. Membrane bound receptors are then "pinched" from the early endosome to form a recycling endosome to recycle receptors back to the plasma membrane. Meanwhile, the early endosome proceeds to mature into a late endosome. The endocytic pathway culminates with the fusion of the late endosome with the lysosome for possible degradation of cargo or internalized nanoparticles. On average, complete endocytosis has exhibited a length of time of approximately thirty to forty minutes. Although not shown in the figure, there are a number of key proteins that participate in the membrane coat nucleation and assembly, coated pit maturation, fission of coat, and the uncoating of the clathrin from the clathrin coated vesicle upon internalization.[48]

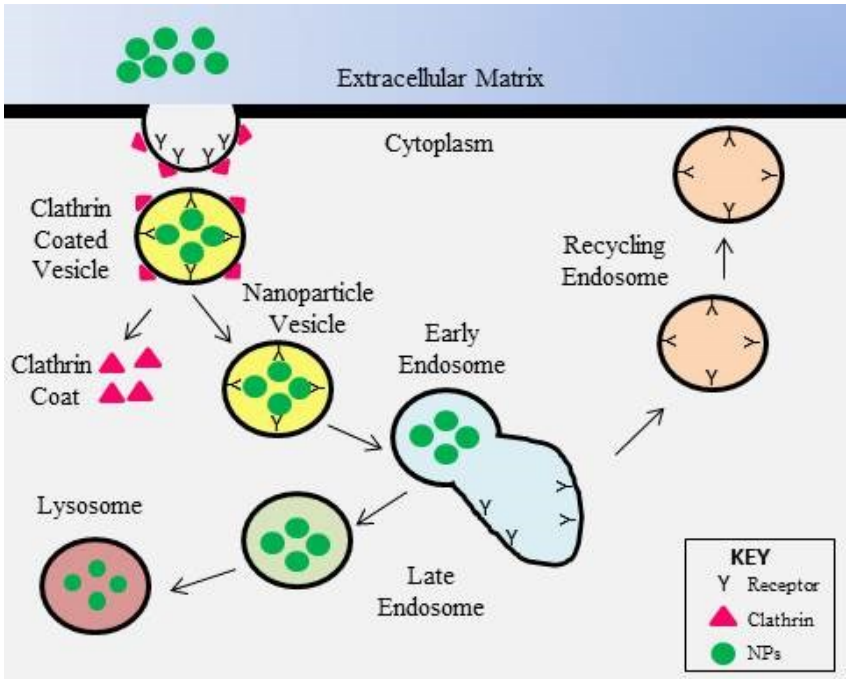

Figure 1.2 Clathrin Mediated Endocytosis

Hypothesized maturation-fusion model of Clathrin Mediated Endocytosis of nanoparticles (NPs). Adapted from International University Receptor Mediated Endocytosis.[49]

The cell contains an extremely complex network of proteins and lipids of which a fraction play a role in membrane trafficking, signaling, cellular adhesion, and nuclear transport, to name a few. Among these, the Rab-GTPase (Rab) family of proteins are associated with intracellular membrane trafficking.[50] Specific Rab proteins are known to localize to specific domains on endocytic compartments in the clathrin mediated up take pathway that help tether, fuse, and mark the presence of endosomes. These Rab proteins are referred to as *markers.* There are also a number of *effector molecules* and SNARE proteins specific for each Rab protein that form platforms on the endosomes to assist the Rab protein association with endosomes, in addition to assisting Rabs with tethering and fusing endosomes, where necessary.[51] Rabs in a guanosine triphosphate bound state (GTP) give rise to the "active" state of the Rab proteins. Few Rabs have been characterized to localize specifically to the lysosome, however the lysosomal associated membrane protein (LAMP) is among one protein or marker that associates with lysosomes, as the name implies. In this work, Rab5, Rab7, Rab11, and LAMP-1 are the markers used to study the intracellular membrane trafficking of the endocytic compartments associated with the early,

late, recycling, and lysosomal endocytic compartments, respectively, in Clathrin Mediated Endocytosis.

In relation to Figure 1.2, Rab5 is responsible for the fusion of the nanoparticle vesicle with early endosomes.[52] Rab5 appears to be the most fully understood protein in clathrin mediated endocytosis. In-Vitro cell-free assays have been established in the early 1990s to confirm the presence and specificity of clathrin mediated endocytic markers to specific compartments, such as Rab5 with early endosomes and Rab7 with late endosomes. It has been shown early and late endosomes were unique to Rab5 and Rab7, respectively. Authors also confirmed the phenomena of fusion by preparing separate fractions of early and late endosomes with HRP and avidin internalization and mixing the fractions together. The observation of early endosome fusion with incoming vesicles was observed whereas and early and late endosome fusion was not observed. This data supports the claim that Rab5 and Rab7 are unique to each compartment, such that the early endosome potentially matures into a late endosome by which Rab5 is replaced with Rab7.[53] The same authors also confirmed the in-vivo functional role of Rab5 and observed similar phenomena.[54] Studies have also been performed such that depletion of Rab5 from the cytosol restricted early endosome fusion in vitro.[55] Lastly, early endosome motility has been shown to be dependent on Rab5.[56]

The next step in the clathrin mediated endocytic pathway is the maturation of the Early Endosome into the Late Endosome. The Rab5-Rab7 transition is a maturation step whereby Rab7 replaces Rab5 to mark the maturation stage of the early to late endosome. A combination of Guanine nucleotide exchange factors (GEFs) act to displace effectors associated with Rab5 and activate Rab7 to facilitate association with the newly matured endosome, or late endosome.[57,58] Studies have shown that Rab5 is displaced by Rab7; the advantages of live-cell microscopy have been used to visualize the dissociation of Rab5 by Rab7, and shown evidence that at some point in time, Rab5 and Rab7 co-exist on the same compartment before complete displacement of Rab5 with Rab7.[59,60]

The final step of internalized cargo in Clathrin Mediated Endocytosis is the fusion of the late endosome with the lysosome. Studies have been done by similar methods of western blot analysis, and live-cell and electron microscopy; Hela cells were overexpressed with Enhanced Green Fluorescent Protein (EGFP) –tagged Rab7 wt as well as active and dominant-negative

mutant proteins. The extent of localization for each with other properties of late endocytic structures was confirmed and analyzed. Specifically, Rab7 was shown to be significant for fusion of late endocytic structures with lysosomal compartments.[61] Additionally, studies have also shown Rab7 not only localizes to late endocytic structures, but that the function of Rab7 is inhibited when cells are deficient in the lysosomal membrane proteins LAMP-1 and LAMP-2.[62] Thus, this data appears to support the claim that Rab7 and LAMP-1 are co-dependent and perhaps Rab7 marked Late Endocytic compartments fuse with lysosomes marked with LAMP-1 for delivery of cargo to the lysosome.

Last, lysosomes are membrane compartments in a cell that are the most acidic of the endosomes and are responsible for the degradation of biological macromolecules, in particularly extracellular material internalized by endocytosis can be degraded in the lysosome. Lysosome associated membrane protein-1 (LAMP-1) is a type I transmembrane protein (has a single transmembrane helix) and one of the major protein components of identifying or marking the lysosomal membrane.[63] Material has been unlikely found to be released into the extracellular medium nor transferred to other organelles after being delivered to the lysosome.[64] Thus, lysosomes are the final destination for cargo undergoing Clathrin Mediated Endocytosis.

In summary, uptake of cargo is into vesicles that fuse with early endosomes, which in turn mature into late endosomes, and ultimately fuse with lysosomes for possible degradation. Additionally, cells undergo recycling of receptors back to the cell membrane. Thus, the recycling endosome is a compartment formed from receptors and lipids that "pinch" off of the Early Endosome.[65] Similar to the Rab5 to Rab7 switch, Recycling Endosomes acquire Rab11. Studies have shown by live cell microscopy that Rab11 co-localizes to transferrin receptors, receptors within coated pits that are internalized during clathrin mediated endocytosis, and Rab11 recycles back to the membrane.[66] An interesting find to keep to consideration is both Rab5 and Rab11 have shown to localize to the same recycling endocytic compartments in A431 cells.[67] Two color imaging experiments demonstrated in this work provides qualitative evidence to support this claim and will be discussed in this Chapter 3.

A unique feature with each endosome in the clathrin mediated endocytic pathway is the acidity; the acidity of each endosome increases with progression of the endocytic pathway.

Studies have shown a potential source of pH acidity of endosomes is attributable to the Vacuolar ATPase (V-ATPase).[68]

In conclusion, the understanding of nanomaterial processing is strongly dependent on membrane trafficking, and Rab and LAMP proteins are very important at assisting with this role. Thus, it is of high interest to understand more specifics to the Rab and LAMP protein interaction and trafficking in cells for nanomaterial endocytosis and intracellular protein distribution.

1.4 Tools Available to Study Nanomaterials and Cellular Processes

In order to study nanomaterials and clathrin mediated endocytosis, we need to have tools that provide good specificity, sensitivity, and resolution. Specifically, we resort to microscopy to study these nanomaterials and cellular processes. There are three types of microscopy; electron, scanning probe, and light microscopy.

Electron microscopy is a commonly used technique to study structural information of nanomaterials and cellular compartments. Electron microscopy is advantageous to obtain structural information due to the high resolution achieved with electron microscopes, because resolution improves as the wavelength decreases.[69] In addition, electron microscopes achieve higher magnification. There are two main forms of electron microscopy used; Transmission electron microscopy (TEM) and scanning-tunneling electron microscopy (SEM)

The beam of energy of a TEM ranges 100,000-400,000 eV. Electrons are produced from an electron gun and interact with atoms in a sample specimen. The electrons that are *transmitted* through the specimen are focused by an objective lens onto an image. Many studies have used TEM to characterize gold nanoparticles.[70,71,72] TEM also provides two dimensional structures of specimens.

A scanning electron microscope also uses electrons as the illumination source; however, as opposed to an image being generated from electrons transmitted through the sample, an image is generated based on detected backscattered and secondary electrons. Properties of the specimen surface, such as its topography and composition are obtained from SEM studies (Purdue University Radiological and Environmental Management). SEM has been used to characterize

and visualize many materials, in particular gold.[73,74] In contrast to TEMs, SEMs produce three dimensional images of specimens.[75]

Electron microscopy techniques are extremely useful to obtain information in regard to the crystal structure, topography, and composition of materials with high resolution. However, electron microscopy does not provide specific quantitative information of species of interest.

Light microscopy has the disadvantage of slightly poorer resolution as excitation of light is in the UV range. However, light microscopy is more sensitive and specific for the use of antibodies, proteins, and nanomaterials in cells.[76] In addition, light microscopy can be used for real-time observation of systems in cells. Laser scanning confocal microscopy allows one to obtain images of cells fluorescently labelled for endocytic markers and fluorescent nanomaterials.

Image Correlation Spectroscopy analysis is an incredibly useful intensity fluctuation analysis technique for analysis of laser scanning confocal microscopy images of cells. The intensity of species, degree of aggregation, number of clusters, and number of clusters per square micron can be determined using Image Correlation Spectroscopy Analysis.[77]

1.5 Hypothesis

The work in this thesis focusses on three topics; the distribution and association of endocytic markers in cell lines, the association of nanomaterial systems with these markers in cell lines, and the efficiency of uptake and internalization of nanomaterial systems in a time dependent manner.

Based on the hypothesized maturation and fusion model described in Chapter 1.3, we hypothesize that markers specific for endocytic compartments may simultaneously co-exist on one compartment as fusions and maturations occur. For example, one interaction known to occur as discussed in Chapter 1.3 is the fusion of Rab7 marked late endosomes with LAMP-1 marked lysosomal endosomes; these markers may simultaneously exist on the same cluster or compartment in the observation region of the laser beam, but Rab7 and LAMP-1 markers should be *unique* for late and lysosomal endosomes, respectively. These markers are described as

unique, but found to co-localize. Thus, we want to determine which *extent* they are unique or able to co-localize.

We also hypothesize that phospholipid coated gold nanoparticles will associate with each endocytic marker of approximately 100% given the notion gold nanoparticles exhibit clathrin mediated endocytic behavior. The study of phospholipid coated gold nanoparticles with endocytic compartments in a three-way interaction will be studied in this work, and to the best of our knowledge, is the first three way color quantitative study performed to date. If successful, this study will present an understanding of the uptake and interaction of phospholipid coated gold nanoparticles with one and two markers. In addition, we hope this study will *also* serve as a model to demonstrate a technique for scientists in the field of biophysics to use to study three systems of interest simultaneously. If these phospholipid coated gold nanoparticles undergo endocytosis, the work presented will also provide insight for further use of phospholipid coated gold nanoparticles for drug delivery applications that rely on pH dependent drug release via acidic endosomes. Lastly, we hypothesize that these gold nanoparticles should be taken up in the same fashion, regardless of cell type.

Once having studied the successful pairwise and three way interaction of phospholipid coated gold nanoparticles in cells, this technique will be applied to study another nanomaterial of interest, α −synuclein. Although not a model or potential use for a drug delivery *platform*, it is of high interest to study the differences that may exist among internalized oligomeric forms of α −syn in neuronal cells to obtain more information of this Parkinson's disease associated species. We hypothesize that each oligomeric variant of α − syn will undergo endocytosis, with minor variations to be observed with oligomers upon binding.

1.6 Thesis Statement

The purpose of this work is to demonstrate the use of Image Correlation Spectroscopy analysis and laser scanning confocal microscopy to study biological systems of interest, specifically nanomaterials and markers for clathrin mediated endocytic compartments. The intracellular distribution, co-localization, and physical movements of these systems will be discussed to provide foundations and motive for potential therapeutic applications.

Chapter 2

Methods & Materials

2 Methods & Materials

Cell culture, sample labelling, and characterization completed in this study were done at the National Institute for Nanotechnology (NINT) in Edmonton, Alberta. Fluorescent imaging completed in this study was done at the Cell Imaging Facility at the Cross Cancer Institute in Edmonton, Alberta.

2.1 Cell Culture

2.1.1 C2C12 Cell Culture

Mouse muscle mybolastoma (C2C12) cells were cultured in Dulbecco's modified eagle medium (DMEM), supplemented with 10 % fetal bovine serum (FBS). Cells were grown in an incubator chamber maintained at 37 degrees Celsius, 5 % Carbon Dioxide (CO_2). At 80 % cell surface confluency, cells were washed two times with 1X Phosphate Buffered Saline (PBS) and passaged at a concentration of 4 % in media. Cells were passaged every five days with 0.25 % Trypsin-EDTA.

2.1.2 A549 Cell Culture

Human alveolar adenocarcinoma (A549) cells were cultured in Ham's F-12 K medium (F-12 K) supplemented with 10 % FBS. Cells were grown in an incubator chamber maintained 37 degrees Celsius, 5% CO_2. At 80 % cell surface confluence, cells were washed two times with 1X Phosphate Buffered Saline (PBS) and passaged at a concentration of 4 % in media. Cells were passaged every five days with 0.25 % Trypsin-EDTA.

2.1.3 SH-SY5Y Cell Culture

Human bone marrow neuroblastoma (SH-SY5Y) cells were cultured in a 1:1 mixture of F-12K and DMEM, supplemented with 10 % FBS. Cells were grown in an incubator chamber maintained at 37 degrees Celsius, 5 % CO_2. At 80% cell surface confluence, cells were washed two times with 1X Phosphate Buffered Saline (PBS) and passaged at a concentration of 4 % in media. Cells were passaged every ten days days with 0.25 % Trypsin-EDTA.

2.1.4 Growing Cells for Experimentation

At 80% cell surface confluence, 250 mL of cells were seeded onto 60 millimeter (mm) glass bottom dishes and maintained in a 37 degrees, 5 % CO_2 maintained incubator until 60 % cell confluency was reached for experimentation. 60 % cell surface confluency was achieved two days after cells were seeded onto glass bottom dishes.

2.2 Phospholipid Coated Gold Nanoparticles

2.2.1 Synthesis

Phospholipid coated gold nanoparticles were prepared by a "three step" seed growth mediated method described by Meijing Wang, MSc.[1] The first two steps of this method comprised the preparation of two separate solutions; the growth solution and the seed solution. The resultant gold nanoparticles were then prepared in the third step of the method by which the growth solution and seed solution were mixed in conjunction with a weak reducing agent. An example of the preparation is in the following text.

The growth solution was prepared in a 25 milliliter (mL) round bottom flask. First, potassium gold (III) chloride ($KAuCl_4$) was dissolved in water to a final concentration of 0.48 millimolar (mM). This was stirred in the 25 mL round bottom flask for five minutes. Next, 0.114 grams of 1-stearoyl-2-oleoyl-sn-glycero-3-phospho-(1'-rac-glycerol) (sodium salt) (SOPG) phospholipid, was added to the flask. Last, a nitro-benzoxadiazol conjugated SOPG lipid (NBD-SOPG), 1-oleoyl-2-{12-[(7-nitro-2-1,3-benzoxadiazol-4-yl)amino]dodecanoyl}-sn-glycero-3-[phospho-rac-(1-glycerol)] (ammonium salt), was added to the flask at a concentration of 8.8 % (w/w). NBD-SOPG is thus a lipid capable of fluorescence upon excitation by a 488 nm laser. The solution was then left to stir for an additional thirty minutes.

The seed solution was prepared in a separate 50 mL round bottom flask. First, $KAuCl_4$ was dissolved in water to a final concentration of 0.64 mM. This was stirred in the flask for five minutes. Second, 10 mL of a 3.8 mM solution of trisodium citrate ($Na_3C_6H_5O_7$) in water was added to the flask and stirred for an additional ten minutes. Last, 3 mL of a 2.9 mM solution of sodium borohydride ($NaBH_4$) in water was added to the flask. The solution was then stirred for five minutes to produce gold "seeds" between 2-3 nanometers (nm) in size.

As previously discussed, the phospholipid coated gold nanoparticles were prepared by combining both the growth and seed solutions in conjunction with a weak reducing agent. Thus, 5 mL of growth solution was first stirred in a separate 25 mL round bottom flask. Second, 0.3 mL of the seed solution was added to the flask and stirred for an additional ten minutes. Last, 0.25 mL of a 9.0 mM solution of ascorbic acid ($C_6H_8O_6$) in water was added to the flask to produce phospholipid coated gold nanoparticles (GNPs) of approximately 20 nm in size. To ensure monodispersity, the GNPs were stirred for one hour prior to being placed in a 4 degrees Celsius fridge. The GNPs were maintained in the fridge at 4 degrees Celsius prior to experimental use.

2.2.2 Characterization

Phospholipid coated gold nanoparticles prepared in this manner were *fully* characterized previously by Meijing Wang via transmission electron microscopy (TEM), scanning electron microscopy (SEM), dynamic light scattering, and ultraviolet/visible (UV Vis) Absorption.[2]

For the work presented in Chapter 4, dynamic light scattering (DLS) was performed to re-confirm the GNPs were monodisperse in solution and also of 20 nm in diameter for Clathrin Mediated Endocytosis.

2.2.2.1 Dynamic Light Scattering

DLS is a widely used technique to determine the size and monodispersity of nanoparticles in solution at the nanoscale.[78] Monodispersity is particularly important for cellular uptake experiments to ensure the particles are of the desired size are separated and equally distributed in the solution prior to cells for uptake.

Particles in solution undergoing Brownian motion in solution will scatter light in a time dependent manner relative to each other within a focused laser beam. The fluctuating scattered light is detected at a particular angle by a photomultiplier tube as an intensity as a function of time $I(t)$. Larger particles scatter light to a larger extent but move more slowly so the intensity fluctuates less rapidly. On the contrary, smaller particles scatter less light; however cause the intensity to fluctuate more rapidly.

The normalized auto correlation function is used to describe the persistence of the intensity fluctuations, where $I(t)$ is the intensity of scattered light at time t and $I(t+\tau)$ represents the intensity of scattered light at a later time, $t+\tau$, whereby τ is delay time;[79]

$$g_n(\tau) = \langle \delta_n\big(I(t)\big)\delta_n\big(I(t+\tau)\big)\rangle \quad (1)$$

The decay of the auto correlation function for a diffusive system is an exponentially decaying function that depends on q.and D, the diffusion coefficient of the particle;

$$g(\tau) = Aexp(-2q^2D\tau)$$

The hydrodynamic radius can be derived via the Stokes-Einstein Equation, where R_H is the hydrodynamic radius, k is the Boltzman constant, T is the temperature of the system, η is the refractive index of the species, and D is the diffusion coefficient;[80]

$$R_H = \frac{kT}{6\pi\eta D}$$

Additionally, the scattered light intensity is related to the cube of the number or distribution of particles, and the intensity is related to the square of the volume of the particle.

The number, volume, and intensity distributions of GNPs were measured through the use of a Malvern Nano-S Dynamic Light Scattering instrument. 1 mL of gold nanoparticles were placed in a cuvette and measured in the instrument, three records obtained per sample.

2.3 Internalization of Nanomaterial Systems with Time

2.3.1 Continuous Exposure of Nanomaterial Systems to Cells

Four samples were required for each experiment.

At 60% cell surface confluency, cell culture media was replaced with 1 mL of fresh media. Next, 100 microliters (μL) of nanomaterial system was added to each sample. Samples were placed in a 37 degrees Celsius, 5 % CO_2 maintained incubator. Each sample was removed from the incubator at different time points; one, two, four, or twenty-four hours after addition. Samples were washed at room temperature with 1X PBS, and then exposed to 1 mL of 4%

Paraformaldehyde (PFA) at room temperature for ten minutes to fix the cells. Samples were washed with 1X PBS for a final time and used for imaging.

2.3.2 Fixed Exposure, Variable Uptake of Nanomaterial Systems in Cells

Four samples were required for each experiment.

At 60% cell surface confluency, cell culture media was replaced with 1 mL of fresh media. Next, 100 μL of nanomaterial system was added to each sample. Samples were placed in a 37 degrees Celsius, 5 % CO_2 maintained incubator. Each sample was removed from the incubator after two hours had elapsed. Media was removed from each sample, and subsequently washed with 1X PBS. 1 mL of fresh media was added to samples prior to being placed back into the 37 degree Celsius, 5% CO_2 maintained incubator. Each of the samples was removed from the incubator at different time points; after one, two, four, or twenty-four hours elapsed, respectively. Samples were washed at room temperature with 1X PBS and then exposed to 1 mL of 4% PFA at room temperature for ten minutes for cell fixation. Samples were then washed with 1X PBS for a final time and used for imaging.

2.4 Immunofluorescent Labelling of Single Endocytic Compartments

2.4.1 Primary & Secondary Antibody labelling

Labeling of the various endocytic compartments was accomplished through the use antibodies specific for Rab and LAMP-1 protein endocytic markers of endosomes in the Clathrin Mediated Endocytic Pathway. Rab11, Rab5, Rab7, and LAMP-1 were used to label the recycling endosome (RE), early endosome (EE), late endosome (LE), and lysosome (Lys), respectively [81]. The primary antibodies used were monoclonal and originated from three different species (mouse, rabbit, and rat) to avoid potential crosslinking in subsequent experiments. Polyclonal secondary antibodies labeled with different fluorescent probes were added to bind with primary antibodies. The fluorescent probes of the polyclonal antibodies were labelled and identified by the manufacture as Cy3, Alexa Fluor 488 nm, Alexa Fluor 555 nm, and Alexa Fluor 647 nm.

As previously discussed, samples were prepared by seeding cells onto 60 mm glass bottom dishes and maintained in a 37 degrees Celsius, 5% CO_2 incubator until 60% cell surface

confluency was reached. At 60% cell surface confluency, samples were exposed to 1mL of 4 % PFA at room temperature for ten minutes for cell fixation. Samples were then washed with 1X PBS and exposed to 1 mL of a 0.3% solution of Triton X-100 detergent in 1x PBS for fifteen minutes in a 37 degrees Celsius, 5% CO_2 incubator to permeabilize the cell membrane so that antibodies can access the intracellular compartments. Samples were then removed from the incubator, washed with 1X PBS, and exposed to 100 μL of a 3 % solution of Bovine Serum Albumin (BSA) in 1X PBS. BSA served to prevent non-specific intracellular binding of antibodies upon labelling.

Next, samples were washed with 1X PBS and labelled with the primary antibody of interest. Primary antibodies used for experimentation were prepared at a concentration of 1% in 1X PBS. 100 μL of the primary antibody was added to samples, and samples were maintained overnight in a 4 degrees Celsius fridge. The next day, cells were washed with 1X PBS and labelled with the secondary antibody for ninety minutes at room temperature. Cells were then washed with 1X PBS for the last time and used for imaging.

The optimal secondary antibody concentration in 1X PBS was determined via a concentration dependent experiment; five samples were prepared for one endosomal marker of interest, each varying with secondary antibody concentration. Concentration dependent curves were obtained by plotting emission intensity as a function of secondary antibody concentration. Secondary antibodies used for further use and experimentation were identified based on the position in the titration curve indicating optimal binding specificity. Optimal binding specificity was determined based on the point for which the maximum amount of fluorescence was observed for the smallest concentration of secondary antibody.

2.4.2 Primary Antibody Labelling

As a control for background fluorescence in cells, a separate sample was prepared as described in Chapter 2.4.1 without the labelling of a secondary antibody.

2.4.3 Secondary Antibody Labelling

As a control for non-specific binding of the secondary antibody, a separate sample was prepared as described in Chapter 2.4.1 without the labelling of a primary antibody.

2.5 Considerations for Immunofluorescent Labelling of Two or Three Species

For experiments involving the labelling of two or three species, the excitation and emission profiles of the markers for each species were selected so that there was minimal spectral overlap. This experimental design was done to ensure the emission intensity from each channel when imaged was unique to a specific species being measured.

An important point to keep to consideration is the actual *color* of images one can select for analysis or set-up for imaging on a computer does not matter, however the *probe used* in the experiment does matter. Thus, images in this thesis pertaining to *all* two color species in a double labelling experiment are shown in red and green. This was done because yellow is reflected when red and green are overlaid, thus we felt it was clearer to the eye to observe yellow to mean two species are interacting. However, although red and green were chosen for images, these colors may *not* pertain to the actual probe used in the experiment. For example; let's take an experiment in which two species are present in cells, one fluorescent species excited with a 561 nm laser and the other fluorescent species excited with a 633 nm laser; the image corresponding to the species excited by the 561 nm laser may be shown in red and the image corresponding to the species excited by the 633 nm laser may be shown in green.

For three color species, images for each species will be shown in red, green, and blue; likewise, the actual *probe* used may not necessarily correspond to the color of the image shown in the figure in this thesis.

2.6 Immunofluorescent Labelling of Two species

2.6.1 Two Endocytic Compartments

The combinations of probes used for immunofluorescent labelling of two endocytic compartments were the following; Cy3 and Alexa Fluor 647 nm, Cy3 and Alexa Fluor 488 nm, Alexa Fluor 488 nm and Alexa Fluor 647 nm, Alexa Fluor 488 nm and Alexa Fluor 555 nm, and Alexa Fluor 555 nm and Alexa Fluor 647 nm.

The extent of co-localization between two markers of endocytic compartments of the Clathrin Mediated Endocytic pathway was studied. Specifically, the following four combinations

were studied, each constituting one sample; Rab5 and Rab7 markers, Rab7 and LAMP-1 markers, Rab5 and Rab11 markers, and Rab5 and LAMP-1 markers.

The following table summarizes the various combinations of experiments used with an antibody.

For each combination studied, labelling was performed in a sequential fashion. The first antibody primary and secondary pair were added to samples as specified in Chapter 2.4.1. Once samples were labelled with one antibody primary and secondary pair, samples were washed with 1X PBS at room temperature, and then exposed to the second antibody primary and secondary pair of interest as specified in Chapter 2.4.1. Samples were washed with 1X PBS and used for imaging.

Rab5	**Rab7**	**Rab11**	**LAMP-1**
Mouse Anti-Rab5 Goat Anti-Mouse Cy3	Rabbit Anti-Rab7 Goat Anti-Rabbit Alexa Fluor 647	X	
Mouse Anti-Rab5 Goat Anti-Mouse Cy3			Rat Anti-LAMP-1 Goat Anti-Rat Alexa Fluor 647
Mouse Anti-Rab5 Goat Anti-Mouse Cy3	X	Rabbit Anti-Rab11 Goat Anti-Rabbit Alexa Fluor 647	
	Rabbit Anti-Rab7 Goat Anti-Rabbit Alexa Fluor 647		Rat Anti-LAMP-1 Goat Anti-Rat Alexa Fluor 555
Mouse Anti-Rab5 Goat Anti-Mouse Cy3	Rabbit Anti-Rab7 Goat Anti-Rabbit Alexa Fluor 647		Rat Anti-LAMP-1 Goat Anti-Rat Alexa Fluor 488

Figure 2.1 Antibodies used for two and three color excitation

Each antibody used for labelling of two or three species originated from a different animal to prevent cross reactivity of antibodies. In addition, each secondary antibody used in two or three color experiments contained different fluorescent probes to be excited by the following wavelengths of lasers (in nm); 488, 561, and 633. 633 nm laser excites probes identified as Alexa Fluor 647 nm and laser excitation of 561 nm excites probes identified as Alexa Fluor 555 nm. The colors red, green, and blue are not necessarily indicative of the color of the actual probe, but to imply that each *emission profile* in two and three color images is *different* and not overlapping.

2.6.1.1 Control Experiment for Two Endocytic Compartments

This experiment was performed as specified in Chapter 2.6.1 without the labelling of *one* primary or secondary antibody. For example; a control experiment for Rab7 & LAMP-1 would be the following; Rab7 Primary and Secondary and LAMP-1 primary (without secondary). Thus, a total of *four* controls were prepared for an experiment to study the co-localization of two markers for endocytic compartments.

2.6.2 Nanomaterial System with an Endocytic Compartment

The following experiment was completed to determine the extent of co-localization between a nanomaterial system (GNPs or oligomers of $\alpha-$ Syn) and a marker of an endocytic compartment of the clathrin mediated endocytic pathway. Nanomaterial systems in relation to the early, late, recycling, and lysosomal endosomes were studied.

The combinations of probes used for immunofluorescent labelling of GNPs with endocytic marked compartments were the following; 488 nm and Alexa Fluor 647 nm, 488 nm and Cy3, 488 nm and Alexa Fluor 555 nm.

The combinations of probes used for immunofluorescent labelling of oligomers of $\alpha-$ Syn with endocytic marked compartments were the following; 488 nm and Alexa Fluor 647 nm, 488 nm and Cy3, 488 nm and Alexa Fluor 555 nm, Cy3 and Alexa Fluor 647 nm, Cy5 and Alexa Fluor 488 nm, Cy5 and Cy3, and Cy5 and Alexa Fluor 555 nm.

Samples were maintained in a 37 degrees Celsius, 5% CO_2 incubator with 1 mL of media and 100 microliters (μL) of a nanomaterial system. After two hours commenced, samples were washed with 1X PBS and fixed with 1 mL of 4% PFA. Samples were then labelled with primary and secondary antibodies specific for an endocytic compartment, as discussed in Chapter 2.4.1.

2.7 Immunofluorescent Labelling of Three Species; Extent of Ternary Complex Formation

2.7.1 Three Endocytic Compartments

This experiment involved the labelling of one sample with the early, late, and lysosomal markers to determine the extent of co-localization amongst these marked compartments in the clathrin mediated endocytic pathway. The combination of probes used for immunofluorescent labelling of three endocytic compartments was Cy3 and Alexa Fluor 647 nm and Alexa Fluor 488 nm .

Samples were first prepared with the labelling of Rab5 and Rab7 marked compartments, as previously discussed in Chapter 2.6.1. The samples were then washed with 1X PBS, and labelled with LAMP-1 as discussed in Chapter 2.4.1.

2.7.2 Phospholipid Coated Gold Nanoparticles with Endocytic Compartments

The following three color experiments, each constituting one sample, were completed to quantify the association of gold nanoparticle vesicles with two endocytic marked compartments to understand the transfer of nanoparticles between two compartments; GNPs & Rab5 & Rab7 marked compartments, GNPs & Rab5 & Rab11 marked compartments, and GNPs & Rab7 & LAMP-1 marked compartments.

The combinations of probes used for immunofluorescent labelling of GNPs with two endocytic marked compartments were the following; 488 nm and Cy3 and Alexa Fluor 647 nm, 488 nm and Alexa Fluor 555 nm and Alexa Fluor 647 nm.

Samples were exposed to 100 μL of GNPs and 1 mL of cell culture media and placed in a 37 degrees Celsius, 5% CO_2 maintained incubator. After two hours commenced, samples were washed with 1x PBS then fixed with 1 mL of 4% PFA for ten minutes at room temperature. Samples were then labelled with antibodies specific for two endocytic compartments as previously discussed in Chapter 2.6.1.

2.8 α-Synuclein Oligomers

Each oligomer used in cellular uptake experiments were diluted in 1X PBS to a desired concentration.

2.8.1 Development

Oligomers of α −synuclein genes were developed as described elsewhere.[82] Oligomers were functionalized with 488 nm, Cy3, and Cy5 probes for all imaging experiments.

2.8.2 Simultaneous Labelling of Two Oligomers

Samples were exposed to 100 μL of one oligomer of interest, 100 μL of a second oligomer of interest, 1 mL of cell culture media and placed in a 37 degrees Celsius, 5% CO_2 maintained incubator. After two hours commenced, samples were washed with 1x PBS then fixed with 1 mL of 4% PFA for ten minutes at room temperature. Monomers, dimers, and tetramers used for these experiments were functionalized with Cy3 and Cy5 probes.

2.8.3 Binding specificity and efficiency of α-Synuclein in cells

2.8.3.1 Titration Curves of α-Synuclein; Determining the Specific Concentration of Oligomers for Cellular Uptake Studies

Concentration curves were obtained for monomers, dimers, and tetramers of α −Synuclein in order to determine a concentration of each oligomer to use for cell uptake that ensured specific binding in cells. Five concentrations for each oligomer functionalized with Cy5 probes were compared to identify a specific concentration. The average intensity corresponding to each concentration of an oligomer was plotted as a function of respective concentration of the oligomer.

Five samples were prepared by seeding SH-SY5Y cells onto 60 mm glass bottom dishes and maintained in a 37 degrees Celsius, 5% CO_2 maintained incubator until 60% cell surface confluency was reached. At 60% cell surface confluency, each sample was exposed to 1 mL of fresh media and 100 μL of a specific concentration of oligomer in 1X PBS for two hours in a 37 degrees Celsius, 5 % CO2 maintained incubator. The concentrations used for each sample were 1,2,4,8, and 10 μM. After two hours had commenced, samples were then washed with 1X PBS, fixed with 1 mL of 4% PFA for ten minutes at room temperature, and then washed with 1X PBS a final time and ready for imaging.

As a result, the monomer, dimer, and tetramer concentrations used for cell uptake studies were 8, 4, and 2 μM respectively.

2.8.3.2 Exposure of α-Synuclein Post Cell Fixation

This experiment was completed for the monomers and tetramers with Cy5 probes. Four samples were required for each oligomer in this experiment.

SH-SY5Y cells were seeded onto 60 mm glass bottom dishes and maintained in a 37 degrees Celsius, 5% CO_2 maintained incubator until 60% cell surface confluency was reached. At 60% cell surface confluency, samples were exposed to 1 mL of 4% PFA at room temperature for ten minutes for cell fixation. Samples were then washed with 1X PBS, and exposed to 100 uL of a 3% solution of Bovine Serum Albumin (BSA) in 1X PBS. BSA served to prevent non-specific intracellular binding of antibodies upon labelling.

Each sample was then exposed to an oligomer for a specific time interval; 1, 2, 4, and 24 hours. Samples were washed with 1X PBS after the specific time had commenced, and ready to be imaged.

2.8.3.3 Exposure of Pre-Aggregated α-Synuclein Post Cell Fixation

This experiment was completed for the monomers and tetramers with Cy5 probes. Four samples were required for each oligomer in this experiment.

Samples were prepared by seeding SH-SY5Y cells onto 60 mm glass bottom dishes and maintained in a 37 degrees Celsius, 5% CO2 maintained incubator until 60% cell surface confluency was reached. At 60% cell surface confluency, samples were exposed to 1mL of PFA at room temperature for ten minutes for cell fixation. Samples were then washed with 1X PBS, and exposed to 100 μL of a 3% solution of Bovine Serum Albumin (BSA) in PBS. BSA served to prevent non-specific intracellular binding.

Prior to exposure of $\alpha-$Synuclein oligomers to fixed cells, $\alpha-$Synuclein oligomers were maintained in a temperature controlled shaking device. The concentrations of oligomers prepared for the shaking device were twelve-fold greater than their respective concentrations used for cellular uptake, to ensure aggregation in solution. Specifically, 100 μL of 96 μM monomer and 24 μM tetramer in 1X PBS were prepared, then placed into the temperature controlled shaking device overnight. The temperature controlled shaker was set to a temperature of 37 degrees Celsius and shaken at 150 revolutions per minute (rpm).

The next day, the pre-aggregated oligomers were diluted to their appropriate concentrations for cellular uptake, 8 μM and 2 μM for the Monomer and Tetramer, respectively. Each sample was then exposed to pre-aggregated oligomers for a specific time interval; 1, 2, 4, and 24 hours. Samples were washed with 1x PBS after the specific time had commenced, and ready to be imaged.

2.9 Real Time (Live Cell) Imaging

2.9.1 Individually Labelled Oligomers

The monomers, dimers, and tetramers with Cy5 probes were each studied individually, one sample required for each for experimentation.

Samples were prepared by seeding SH-SY5Y cells onto 60 mm glass bottom dishes and maintained in a 37 degrees Celsius, 5% CO_2 maintained incubator until 60% cell surface confluency was reached. At 60% cell surface confluency, samples were exposed to 100 µL of oligomer of interest and 1 mL of cell culture media and placed in a 37 degrees Celsius, 5% CO_2 maintained incubator. After two hours commenced, samples were washed with 1X PBS and replaced with 1 mL of fresh media. Samples were then imaged within thirty minutes of washing.

2.10 Laser Scanning Confocal Microscopy

As illustrated in Figure 2.1, the laser passes through an excitation pinhole and enters the excitation filter. The excited light is then reflected by a dichroic mirror and galvanometer mirror scan compartment to enter through the rear side of the objective lens. The specimen is then exposed to the scanning laser beam in an xy raster fashion. As a result, emitted light passes back through the objective lens and dichroic mirror. Any emitted light out of focus in the z plane for imaging is rejected, and the focused light is passed through the pinhole for detection.

A laser scanning confocal microscope combines the useful features of both a *scanning* laser beam and an emission pinhole for a more resolved, in focus image compared to typical widefield microscopes. This scanning feature of the apparatus is advantageous to achieve both detection of fluorescent intensity at each pixel position, but also allows for potential measurements and analysis of intensity fluctuation, which will be further discussed in Chapter 2.11. The implementation of a pinhole in this set up prevents out of focus intensity in the z plane

of the image from being detected. Thus, the pinhole allows for accurate sampling and precise measurement of intensity of species.

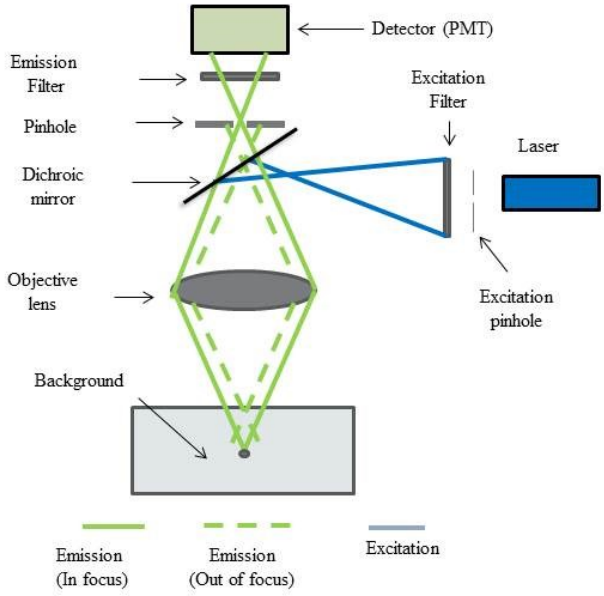

Figure 2.2 Schematic of the Laser Scanning Confocal Microscope

For all experiments completed in this study, the intensity measurements obtained from images was done in a fashion such that oversampling of pixels was accomplished. We define oversampling in which the diameter of the laser beam is *greater* than the size of the pixel. In this thesis, the laser beam diameter was at least twenty-four times larger than the pixel size (pixel size was approximately 20 nm, laser beam diameter approximately 480 nm). Therefore, pixels in the image are correlated as the large laser beam scans the sample. Figure 2.3 is an example to illustrate the definition of oversampling; in the figure, a laser beam (represented as a circle) scans a specimen from left to right. The specimen in this example consists of green squares to represent pixels.

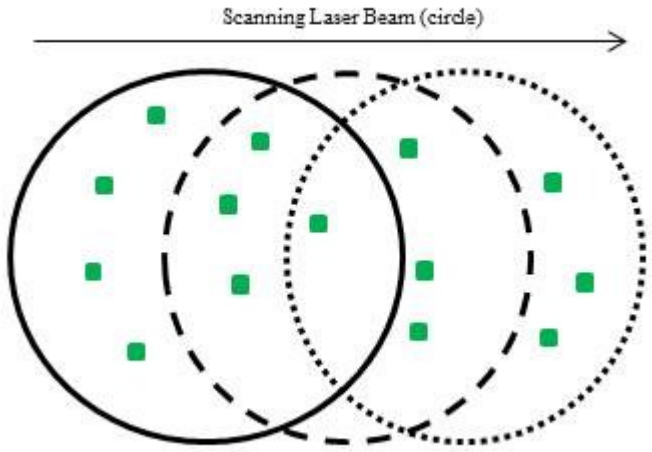

Figure 2.3 Laser beam relative to position in cell as it scans across a specimen

The laser beam is represented in a circle as it scans across a specimen; the diameter of the beam is much larger in comparison to the pixel. In all experiments in this thesis, the pixel size is at least 24 times less in comparison to the *diameter* of the laser beam. The green squares are representative of pixels in the image; thus, as the laser scans across the specimen, the intensity emitted and detected from each pixel is correlated.

An intensity is recorded for *each pixel* in which the location of the center of the laser beam (maximum of its Gaussian profile) is located with respect to the pixel. However, the recorded intensity at that specific pixel position will be a sum of intensities from all the molecules or surrounding pixels within the area of the beam when the center of that beam is at that pixel location. Thus, intensities recorded for each pixel can be used for correlation analysis.

More information in regard to intensity and fluctuation analysis will be discussed in Chapter 2.11.

2.10.1 Lasers

Lasers used for image acquisition were Argon for Fluorescein Isothiocyanite (FITC) configuration (488 nm excitation of 488 nm and Alexa Fluor 488 nm probes), Solid State for Cyanine-3 (Cy3) Configuration (561 nm excitation of Cy3 and Alexa Fluor 555 nm probes), and HeNe for Cyanine-5 (Cy5) Configuration (633 nm excitation of Cy5 and Alexa Fluor 647 nm probes).

2.10.2 Image Acquisition

Images of the cells in a sample were obtained via a Carl Zeiss 710 Laser Scanning Confocal Microscope with a 63 x 1.4 Numerical Aperture Oil DIC Plan-Apochromatic lens. ZEN 2011 was the software used to adjust and select parameters for image acquisition.

2.10.3 Image Acquisition for fixed samples

2.10.3.1 Image Acquisition for Fixed Samples with One Species

The pixel dwell time was set to 3.15 microseconds (μs) with an average of 2 line scans, and the pinhole was set to 1 airy-unit (AU). A Zoom factor of 14 was used to achieve a pixel size of approximately 20 nanometers. Each image comprised a square of 512 x 512 pixels, resulting with a 10 x 10 micron image for image correlation spectroscopy analysis. For each experiment, 25-40 images were obtained; each image corresponding to a different cell in the sample.

Samples labelled with one species were illuminated with FITC (488 nm), Cy3 (561 nm), or Cy5 (633 nm) laser configurations, respectively, and complementary DIC for focusing.

2.10.3.2 Image Acquisition for Fixed Samples with Two Species

The pixel dwell time was set to 3.15 microseconds (μs) with an average of 2 line scans, and the pinhole was set to 1 airy-unit (AU). A Zoom factor of 14 was used to achieve a pixel size of approximately 20 nanometers. Each image comprised a square of 512 x 512 pixels, resulting with a 10 x 10 micron image for image correlation spectroscopy analysis. For each experiment, 25-40 images were obtained; each image corresponding to a different cell in the sample.

For samples labelled with two species, each of different fluorescent emission profiles, samples were excited with one of the three possible configurations; FITC/Cy3, FITC/Cy5, or Cy3/Cy5. The detectors for each configuration were adjusted in such a way that the emission from each channel was unique to a specific wavelength range. In addition, as a control measure, samples labelled with one fluorescent probe, such as Cy3, were illuminated with the FITC configuration, and then with the Cy5 configuration separately, to inquire about any potential cross talk.

2.10.3.3 Image Acquisition for Fixed Samples with Three Species

The pixel dwell time was set to 3.15 microseconds (μs) with an average of 2 line scans, and the pinhole was set to 1 airy-unit (AU) for the Cy5 channel. A Zoom factor of 14 was used to achieve a pixel size of approximately 20 nanometers. Each image comprised a square of 512 x 512 pixels, resulting with a 10 x 10 micron image for image correlation spectroscopy. For each experiment, 25-40 images were obtained; each image corresponding to a different cell in the sample. FITC/Cy3/Cy5 combination was used to excite fixed samples with three different fluorescent probes.

2.10.3.4 Image Acquisition Cross-Talk Control

As a control measure, a sample labelled with all three species of different fluorescent emission profiles was prepared. All detection channels were opened, but the sample was excited with only one laser at a time. The intensity was then quantified from each channel to determine if any intensity was detected in the channels not corresponding to the appropriate excitation laser. As with all positive controls in this thesis, the detectors were carefully set to detect wavelengths within a specific range; 489-564 nm for FITC (488 nm) channel, 561-620 nm for Cy3 (561 nm channel), and 633-697 nm for Cy5 (633 nm) channel.

2.10.4 Image Acquisition for Samples with Live Cell Labelling

For live cell imaging, one experiment constituted the collection of 50-100 images as a function of time on one region of one cell.

2.10.4.1 Image Acquisition for Live Samples Labelled with One Species

The pixel dwell time was set to 1.58 μs with an average of 2 line scans, and the pinhole was set to 1 airy-unit (AU). A Zoom factor of 14 was used to achieve a pixel size of approximately 20 nanometers. Each image comprised a square of 512 x 512 pixels, resulting with a 10 x 10 micron image for image correlation spectroscopy analysis. For each experiment, 80-100 images were obtained; each image corresponding to the same region of a cell in the sample, image acquisition every 2-15 seconds, depending on the species of interest. Eight experiments were performed for each species of interest. Cy5 channel was used to excite species for real time experiments.

2.10.5 Summary and Definitions of Species based on excitation profile of LSCM

In this work, dyes and probes identified by manufacturers as 488 nm were excited using the 488 nm laser in the LSCM. Dyes and probes identified by manufacturers as Cy3 and 555 nm were excited using the 561 nm laser in the LSCM. Dyes and probes identified by manufacturers as Cy5 and 647 nm were excited using the 633 nm laser in the LSCM. Thus, species (GNPs, markers, and oligomers) are represented in Chapters 3, 4, 5, and 6 in the following format; *species-excitation laser wavelength (nm).* For example; an image corresponding to the immunofluorescent labelling of Rab7 markers in cells excited by either 488 or 633 nm lasers will be represented in this work as Rab7-488 or Rab7-633, respectively. The following table is a summary of species with their respective laser used for excitation and the definition for reference.

Table 2.1 Summary of Species with laser excitation wavelength and definition

Species-Excitation Laser Wavelength (nm)	Definition
GNPs[1]	Phospholipid coated gold nanoparticles with 488 nm fluorescent lipid probe.
Rab5-561	Rab5 with a Cy3 fluorescent probe
Rab11-633	Rab11 with an Alexa Fluor 647 nm fluorescent probe
Rab7-488	Rab7 with an Alexa Fluor 488 nm fluorescent probe
Rab7-633	Rab7 with an Alexa Fluor 647 nm fluorescent probe
LAMP-1-488	Lysosomal Associated Membrane Protein 1 with an Alexa Fluor 633 nm fluorescent probe
LAMP-1-561	Lysosomal Associated Membrane Protein 1 with an Alexa Fluor 555 nm fluorescent probe
LAMP-1-633	Lysosomal Associated Membrane Protein 1 with an Alexa Fluor 647 nm fluorescent probe
Ms-488	Monomers with a 488 nm fluorescent probe
Ms-561	Monomers with a Cy3 fluorescent probe
Ms-633	Monomers with a Cy5 fluorescent probe
Ds-488	Dimers with a 488 nm fluorescent probe
Ds-561	Dimers with a Cy3 fluorescent probe
Ds-633	Dimers with a Cy5 fluorescent probe
Ts-488	Tetramers with a 488 nm fluorescent probe
Ts-561	Tetramers with a Cy3 fluorescent probe
Ts-633	Tetramers with a Cy5 fluorescent probe

1 All GNPs used in this work were excited with a 488 nm laser. No other fluorescent lipids were used in this synthesis of phospholipid coated gold nanoparticles.

2.11 Image Correlation Spectroscopy Family

Image correlation spectroscopy (ICS) is a quantitative analysis method to analyze the fluorescent intensity fluctuations in an image obtained from a laser scanning confocal microscope. This analysis allows one to retrieve a number of pieces of information; average intensity of a species, number of clusters, number of clusters per square micron, the relative degree of aggregation of species, and the extent of co-localization between two or three species of interest.

2.11.1 Image Correlation Spectroscopy Theory

As previously discussed, the laser beam in a laser scanning confocal apparatus scans across a specimen in a xy raster fashion. The observation volume is defined by a convolution of the laser beam itself and the point spread function for the image pinhole.[83] As the beam scans across a specimen, an intensity measurement is recorded for each pixel with respect to the laser maximum in the image.

Let the intensity detected at pixel position (x, y) in an image be represented as $i(x, y)$.

Let the intensity of the species in a pixel averaged over all pixels be represented as $\langle i(x, y)\rangle$, whereby the angular brackets denote the average over all pixel intensities.

The fluctuation in intensity is then defined in the following expression as the difference between the intensity at one pixel and the overall average intensity over all pixels in the image;

$$\delta\big(i(x, y)\big) = i(x, y) - \langle i(x, y)\rangle \tag{2}$$

Furthermore, expression (2) can be normalized by dividing the expression by the average intensity, where sub constant n indicates normalization;

$$\delta_n(i(x, y)) = \frac{i(x, y) - \langle i(x, y)\rangle}{\langle i(x, y)\rangle} \tag{3}$$

The normalized auto correlation function can then be derived by taking the product of two fluctuations in intensity, whereby α and β represent spatial lags in the x and y direction, respectively;

$$g(\alpha, \beta) = \langle \delta_n(x, y)\delta_n(x + \alpha, y + \beta)\rangle \tag{4}$$

In the limit α and β approach zero, the amplitude of the normalized auto correlation function, denoted by $g(0,0)$, gives rise to the variance of the normalized auto correlation function;[77]

$$g(0,0) = var(\delta_n i(x, y)) \tag{5}$$

When the intensity is a precise measurement of the concentration of clusters containing species, this variance also represents an inverse relationship to the average number of fluorescent clusters, N_C in the observation region, given in the following expression;

$$g(0,0) = var\big(\delta_n i(x,y)\big) = \frac{1}{\langle N_C \rangle} \tag{6}$$

The area of the observation volume can be represented as $\pi\omega^2$, where ω is the e^{-2} beam radius. Thus, the average number of fluorescent particles per square micron, defined as the Cluster Density (CD), can be calculated in the following expression;

$$CD = \frac{1}{g(0,0)\pi\omega^2} = \frac{\langle N_C \rangle}{\pi\omega^2} \tag{7}$$

Last, the average number of fluorescent molecules is proportional to the average intensity of fluorescent molecules, such that $\langle i(x,y) \rangle = c\langle N_M \rangle$, where c is a proportionality constant reflecting the limits of the optics such as emission collection efficiency, quantum yields, and molar adsorption coefficients.[83] Thus, a degree of aggregation can be defined as follows;

$$DA = \langle i(x,y) \rangle g(0,0) = c\frac{\langle N_M \rangle}{\langle N_C \rangle} \tag{8}$$

The constant c can be determined experimentally by measuring the intensity of one single molecule. In this this study, the constant c was determined in *some* cases to determine the number of antibodies per cluster. However, the DA is represented and discussed as a product of the intensity and autocorrelation amplitude for a measure of the relative degree of aggregation.

2.11.1.1 Laser Beam Width in Relation to Size of Cluster

In laser scanning confocal microscopy and image correlation spectroscopy analysis, there are three important laser beam widths to understand; the theoretically expected laser beam width, the "true" fitted measured laser beam width, and the experimental fitted laser beam width.

The theoretically expected width of the laser beam is diffraction limited. The magnitude of this width is expected to be measured for a single diffraction limited molecule. Thus, let a diffraction limited laser beam width be defined as ω_{DL}. This width is proportional to the wavelength of excitation light, λ and inversely proportional to the numerical aperture of the lens, $N.A$;

$$\omega_{DL} = \frac{\lambda}{2 * N.A} \tag{9}$$

In this thesis, we assume the "true" fitted laser beam width, ω_O, can be measured from a sample labelled with only secondary antibodies. The secondary antibodies are fluorescent and meant to be specific for *one molecule* and provide us with the actual width of the laser beam. The results to be shown in Chapter 3 in this work suggest that the beam measured from the secondary antibodies is *not* diffraction limited as the "true" width is usually slightly larger in magnitude in comparison to the theoretical diffraction limited width of the laser beam.

The experimental fitted laser beam width, ω_{Exp}, corresponds to a measurement of endosomes, the fitted width of the laser beam measured for a sample labelled with both primary and secondary antibodies for one marker of an endosome. In this thesis, ω_{Exp} is always larger than ω_O. Thus, the greater magnitude of the experimental fitted laser beam width indicates that the laser beam has been *convoluted with an object of finite size.* If the ω_{Exp} arises from convolution of the Gaussian laser beam with a uniformly labeled fluorescent object, it is possible to determine the extent of the distortion of the final correlation function with which the ω_{Exp} can be determined.

With that in mind, assume that each endosome has a uniform labelling and is circular with diameter, d. When d=0, there is no convolution or distortion of the Gaussian profile of the laser beam. As d increases, the distortion arising from the convolution increases as shown in Figure 2.4 for convolution of objects that have diameters equal to 0.75, 1.25, 1.75, and 2.25 times the value of ω_O. For smaller values, the functions maintain a near Gaussian shape, but for the larger values, the functions are broader.

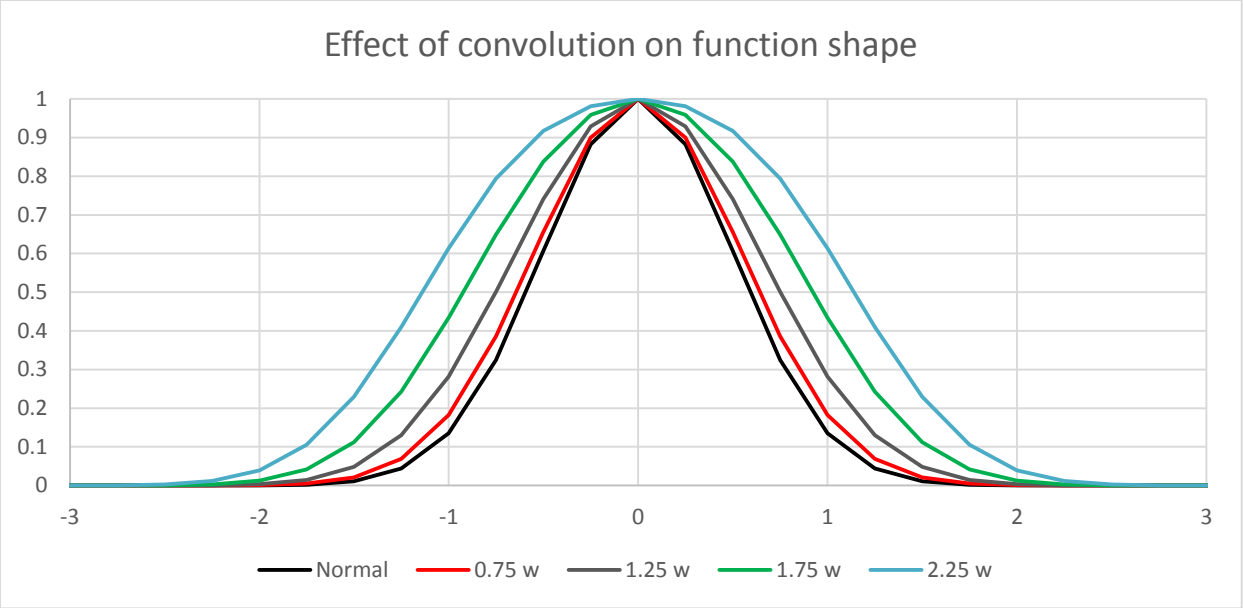

Figure 2.4 Effect of Convolution on Function Shape

The normal curve corresponding to the "true" fitted beam width is shown in black. For objects of a certain diameter, the laser beam is convoluted with an object of finite size, and as a result, the shape of the function is distorted. The larger the object, the greater the distortion. The "true" fitted laser beam width, ω_O is represented as w in figure.

To determine how much the distortion arises from these objects or endosomes affects the fits, the curves in Figure 2.4 were fit as if the function were a Gaussian profile given by the function;

$$f(x) = Aexp\frac{-2x^2}{{\omega_c}^2} \tag{10}$$

Where A is the amplitude of the function and ω_c arising from the fit to the width for the convoluted curve.

Figure 2.5 shows an example for a profile corresponding to a laser beam that has been convoluted with an object of diameter $1.25\omega_0$. The experimental profile is compared to its fit to a Gaussian profile.

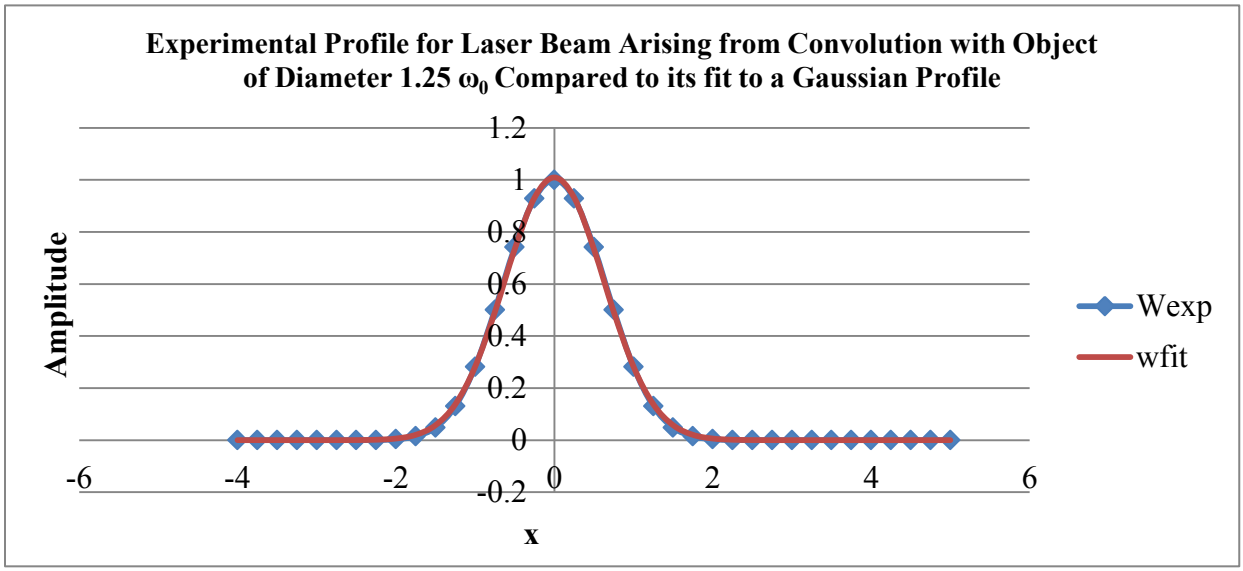

Figure 2.5 An Experimental Profile Arising from Convolution Plotted with Respect to its fit to a Gaussian Profile

There is significant distortion of the profile for objects in which the object size, d, is greater than 1.25 ω_O.

The fit and experimental profiles are overlaid, indicating the experimentally measured profile of the laser beam fits to a Gaussian profile. For all work presented in this thesis, although the experimentally measured laser beam width arises from convolution, the profile is not distorted to a large extent for endosomes and nanomaterials studied.

Figure 2.6 shows the case where $\omega_O = 240\,nm$ and the object sizes ranges from $d = 0\,nm$ to $d = 540\,nm$. The dotted curve corresponds to a quadratic fit to the points, however the choice of a quadratic is arbitrary; the quadratic fit allows for extrapolation.

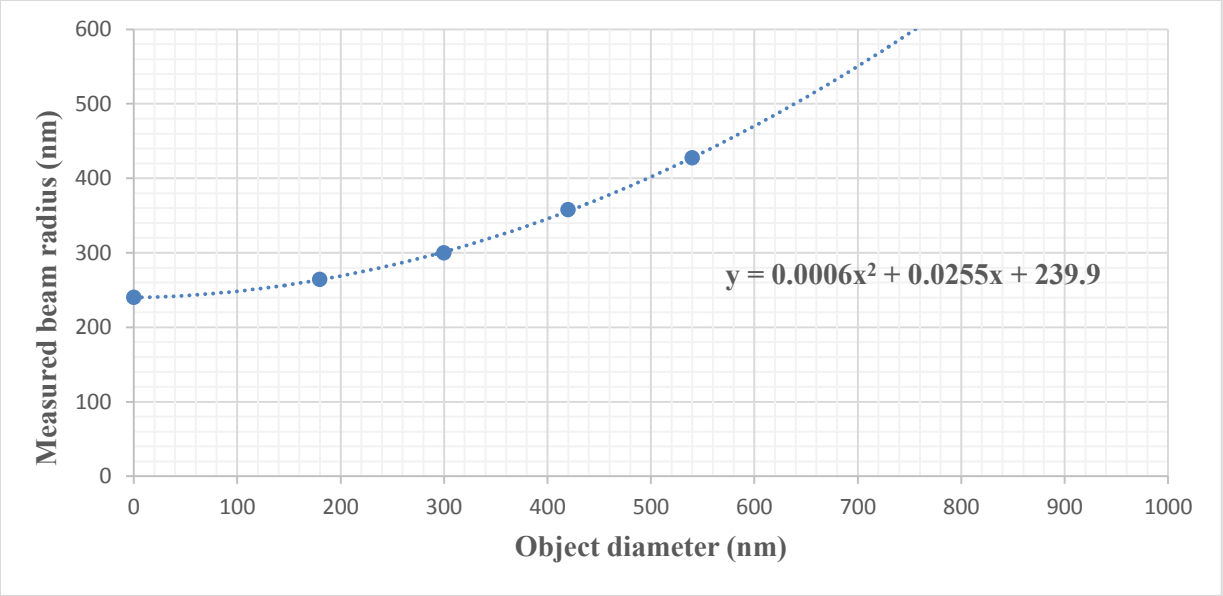

Figure 2.6 Experimental Fitted Laser Beam Width as a Function of Object Size

Curves similar to that in Figure 2.6 can then be used to estimate the average diameter of the objects that are distorting the value of the beam size as estimated from the correlation functions in the image correlation spectroscopy measurements. For example, if the average beam radius is found to be 600 nm, the average object size would be estimated to be about 780 nm in diameter. This logic is used to estimate the various endosomes in Chapter 3.

2.11.2 Image Cross Correlation Spectroscopy Theory

Image cross correlation spectroscopy (ICCS) is an extension of ICS such that it enables the analysis of images collected from two species labelled with two different colors.

Let's assume the first image of interest is green and the second image is red. The normalized cross correlation function reflects the product of the fluctuations occurring in both green and red channels;

$$g_{gr}(\alpha,\beta) = \langle \delta i_g(x,y)\delta i_r(x+\alpha, y+\beta)\rangle \qquad (11)$$

By the same convention as expression (6), the normalized cross correlation function amplitude provides quantitative information in regard to the number of clusters containing a

specific species in the observation region of the laser beam. This is reflected in the following expression;

$$g_{gr}(0,0) = \lim_{\alpha \to 0, \beta \to 0} = \frac{\langle N_{gr} \rangle}{\langle N_g \rangle \langle N_r \rangle} \tag{12}$$

The average number of clusters that consist of both green *and* red species is represented as $\langle N_{gr} \rangle$. The average number of clusters containing only green and only red species are each represented as $\langle N_g \rangle$ and $\langle N_r \rangle$ respectively.

Expression (12) can be re-expressed to isolate the $\langle N_{gr} \rangle$ in the following expression, whereby $g_g(0,0)$ and $g_r(0,0)$ are the auto correlation amplitudes corresponding to the green and red channels, respectively.

$$\langle N_{gr} \rangle = \frac{g_{gr}(0,0)}{g_g(0,0) g_r(0,0)} \tag{13}$$

The extent of co-localization can be inferred with the following two expressions;

$$F(g|r) = \frac{\langle N_{gr} \rangle}{\langle N_g \rangle} = \frac{g_{gr}(0,0)}{g_r(0,0)} \tag{14}$$

$$F(r|g) = \frac{\langle N_{gr} \rangle}{\langle N_r \rangle} = \frac{g_{gr}(0,0)}{g_g(0,0)} \tag{15}$$

Expression (14) is a representation of the fraction of clusters containing green species that also have red species. Conversely, expression (15) is a representation of the fraction of clusters containing red species that also have green species.

2.11.3 Triple Image Cross Correlation Spectroscopy

Triple Image Cross Correlation Spectroscopy (TRICCS) is an extension of ICCS such that it enables the analysis of images of species labeled with *three colors* to provide a means to understand the extent of formation of a ternary complex.

Let's assume the first image of interest is green, the second image of interest is red, and the third image of interest is blue. The normalized triple cross correlation function reflects the product of the fluctuations occurring in green, red, and blue channels;

$$g_{grb}(\alpha,\beta,\theta,\rho) = \langle \delta i_g(x,y)\delta i_r(x+\alpha,y+\beta)\delta i_b(x+\theta,y+\rho)\rangle \quad (16)$$

The spatial lag variables for x and y in the red channel is represented by α and β and those in the blue channel are represented by θ and ρ, respectively.

By similar convention to expression (13), the average number of clusters that consist of green, red, and blue species can be represented as $\langle N_{grb}\rangle$The average number of clusters containing only green, only red, and only blue species are each represented as $\langle N_g\rangle$ and $\langle N_r\rangle$, and $\langle N_b\rangle$ respectively.

$$\langle N_{grb}\rangle = \frac{g_{gr}(0,0,0,0)}{g_g(0,0)g_r(0,0)g_b(0,0)} \quad (17)$$

The association of one color with a binary complex of two colors can be determined with the following expressions;

$$F(g|rb) = \frac{\langle N_{grb}\rangle}{\langle N_g\rangle} = \frac{g_{grb}(0,0,0,0)}{g_r(0,0)g_b(0,0)} \quad (18)$$

$$F(r|gb) = \frac{\langle N_{grb}\rangle}{\langle N_r\rangle} = \frac{g_{grb}(0,0,0,0)}{g_g(0,0)g_b(0,0)} \quad (19)$$

$$F(b|rg) = \frac{\langle N_{grb}\rangle}{\langle N_b\rangle} = \frac{g_{grb}(0,0,0,0)}{g_r(0,0)g_g(0,0)} \quad (20)$$

Likewise, the association of a binary complex of two colors with one color can also be determined with the following expressions;

$$F(gr|b) = \frac{\langle N_{grb}\rangle}{\langle N_{gr}\rangle} = \frac{g_{grb}(0,0,0,0)}{g_b(0,0)g_{gr}(0,0)} \quad (21)$$

$$F(gb|r) = \frac{\langle N_{grb}\rangle}{\langle N_{gb}\rangle} = \frac{g_{grb}(0,0,0,0)}{g_r(0,0)g_{gb}(0,0)} \quad (22)$$

$$F(rb|g) = \frac{\langle N_{grb}\rangle}{\langle N_{rb}\rangle} = \frac{g_{grb}(0,0,0,0)}{g_g(0,0)g_{rb}(0,0)} \quad (23)$$

As an example, the following figure illustrates a distribution of various complexes;

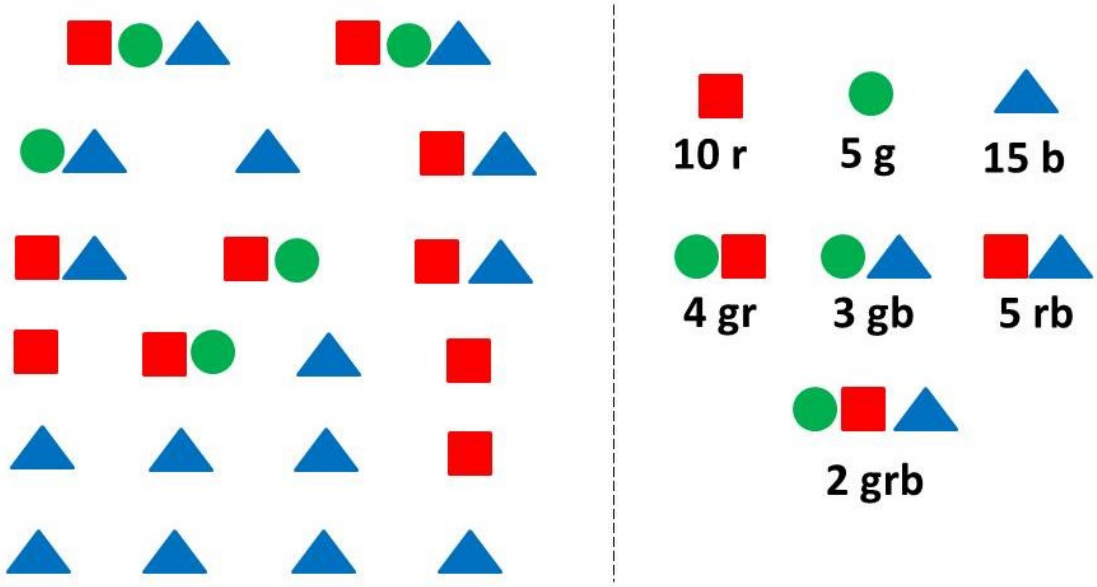

Figure 2.7 Exemplary Distribution of Clusters Containing One, Two, and Three Colored Species

This is an example of a distribution of red, green, blue, red-green, red-blue, green-blue, and red-green-blue complexes. Thus, there are clusters that have just *one* colored species, some in which there are clusters containing *two* colored species, and some clusters that contain *three* colored species.

The figure shows that there are clusters in which one, two, and three colors are present. The total number of clusters that have one color reflect individual, binary, and ternary complexes that contain that one color. For example, there are a total of 10 red clusters (10r) in the figure; there are 3 clusters with only red, 5 clusters of red with another color, and 2 clusters of red with two other colors. Thus, 10 clusters in this distribution are labelled with red species. Likewise, there are four green-red clusters (4 gr); 2 clusters contain green and red species, 2 clusters contain green, red, *and* blue species.

The following table of fractions reflects the extent of association of one color with a binary complex of two colors, and vice versa;

Table 2.2 Exemplary Table of Fractions for TRICCS Analysis

Association of one color with a binary complex	Association of a binary complex with one color
$F(g\|rb)$ = 2/5	$F(gr\|b)$ = 2/4
$F(r\|gb)$ = 2/10	$F(gb\|r)$ = 2/3
$F(b\|rg)$ =2/15	$F(rb\|g)$ = 2/5

The fractions correspond to the distribution shown in Figure 2.7. As an example, $F(gr|b)$ = 2/5 means that of the 5 clusters containing green species, two have red and blue species as well. $F(gr|b)$ = 2/4 means that of the 4 clusters that have green and red, 2 have blue as well.

2.11.4 Temporal Image Correlation Spectroscopy Theory

Temporal Image Correlation Spectroscopy (TICS) is an extension of ICS in which the spatial fluctuation in intensity for one species of interest is determined as a function of *time*. Thus, TICS is useful to obtain information regarding the dynamics of a system of interest.[84]

Let's assume an image is collected at time t and an image of the same single species of interest in the *same observation region* is collected at a later time point, $t + \tau$, where τ is delay time. The expression for the normalized auto correlation function takes the following form;

$$g(\alpha, \beta, \tau) = \langle \delta_n(x, y, t)\delta_n(x + \alpha, y + \beta, t + \tau)\rangle \tag{24}$$

In TICS, the shape & rate of decay of the auto correlation function reveals specific dynamic processes that give rise to the fluctuation in fluorescence between the images such as diffusion, flow, diffusion & flow, and chemical reactions. The work completed for this study is in relation to clathrin mediated endocytosis, thus all experiments completed in this study assume a "diffusive" process.

The decay of the amplitude of the auto correlation function as a function of delay time, τ, is then fit to a three parameter hyperbolic decay expression;

$$g(0,0,t) = \frac{A}{1 + \frac{\tau}{\tau_d}} + C \tag{25}$$

In expression (25), A represents the extrapolated amplitude of the correlation function, τ is the delay time, τ_d is the diffusion time, and C is a constant added to allow for incomplete

decay of the correlation function. This is the characteristic time for diffusion of a particle over the distance of the beam.

Last, the diffusion coefficient can be determined with τ_d and , the $1/e^2$ radius of the focused laser beam;

$$D = \frac{\omega^2}{4\tau_d} \tag{26}$$

Figure 2.8 shows an example of the temporal auto correlation function of monomers of α −syn fitted to the hyperbolic decay shown in equation (24).

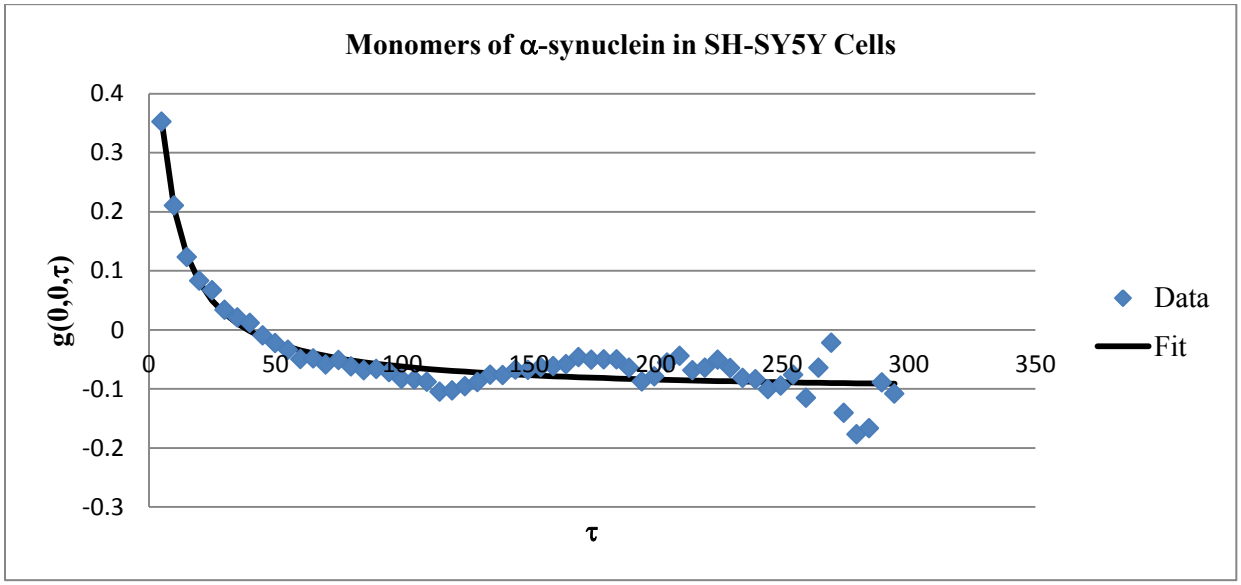

Figure 2.8 Exemplary Temporal Auto Correlation Function for Monomers of α-synuclein in SH-SY5Y Cells

In Figure 2.8, the fit is relatively good; in this particular example, the diffusion time is 5.20 seconds and the experimentally measured beam width is 0.33 microns. Thus, the diffusion coefficient can be calculated as 5.23E-3 square microns per second using equation (25)

2.12 Image J & ICS Software for ICS Family Analysis

In this study, the following pieces of information were obtained from images using ImageJ software; the normalized auto and cross correlation function amplitudes, average image intensity, and laser beam width in microns. Regions of interest were selected to 256x256 of the

512x512 image, merely to reduce the number of dark regions of the image where there is no cell. This is done so intensity from regions that are not representative of the sample are collected, otherwise the average intensity will be affected adversely. The Image Correlation Toolkit was utilized. Depending on the type of action required (ICS, TICS, TICCS, etc) the following fit parameters were estimated to obtain the previously mentioned desired pieces of information; distance for fit in microns, x & y resolution in microns, beam radius, and delay time for temporal image correlation experimental analysis.

For TRICCS measurements, images were analyzed using Image Correlation Spectroscopy software. Parameters for the range of data points, triple cross correlation amplitude, laser beam radius, and correlation value at infinite limits were estimated to obtain the auto, cross, and triple correlation functions amplitudes, and intensities for single, double, and triple color images, in various combinations. For analysis with Image Correlation Spectroscopy Software, images were converted with the help from Dr. Nick Smisdom, from .lsm to .bmp.

To obtain hyperbolic decay fits for temporal image correlation experimental analysis, Igor Pro software was used. The extrapolated autocorrelation function amplitude, diffusion time, and the value for an incomplete correlation function decay fits were obtained, after being prompted to enter in estimations of said parameters. Igor Pro was also utilized to obtain global fits, where necessary.

Microsoft excel was utilized for data storage and statistical analysis. For each experiment, the following calculations were obtained for an entire set of images in one experiment; average, standard deviation, and standard error. Distributions of various parameters were plotted and analyzed and to be discussed in subsequent chapters of this thesis. T-tests were also calculated with the use of excel for two data sets of interest.

Data sets were reviewed for any caveats or discrepancies. The following table of values summarizes the criteria for which a data point for a respective image in an experiment was rejected from analysis;

Table 2.3 Criteria for Data Rejection

Experiment	Beam fit ω (μm)	F(r|g) and F(g|r)
One Color	$\omega > 1.5$	N.A
Two colors	$\omega > 1.5$	$F(r\|g)$ and $F(g\|r) > 1.2$
Three colors	$\omega > 1.5$	$F(r\|g)$ and $F(g\|r) > 1.2$

Live cell experiments for the study of individual oligomers of α-synuclein in cells were analyzed in varying batches of total number of images; 20, 40, 50, 60, and 80 images. This was done to determine if there was a parameter dependence on the number of images in an experiment. Little difference and error in measurement was observed between experiments analyzed in batches of 20-50 images. Thus, the results reported in this study for live cell imaging experiments in TICCS were based on an analysis of 50 images in one experiment; this will be discussed further in Chapter 6. The following graph is a representation of the distribution of diffusion times in various image batches for the α-synuclein tetramer labelled with 633, with error bars reflecting standard error.

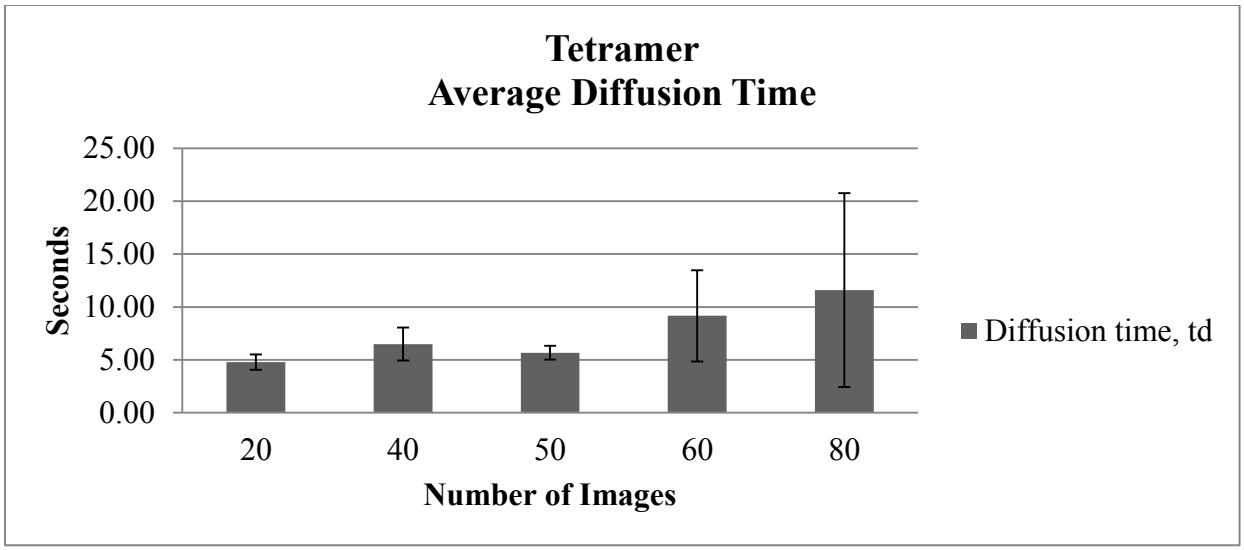

Figure 2.9 Diffusion Time Distribution for Tetramer 633

2.13 Materials

C2C12 cells were obtained from American Type Culture Collection™. Dulbecco's modified eagle medium (DMEM), fetal bovine serum (FBS), and 0.25% Trypsin-EDTA were obtained from Invitrogen Life Technologies™.

A549 cells were obtained from American Type Culture Collection™. DMEM, FBS, and 0.25% Trypsin-EDTA were obtained from Invitrogen Life Technologies™.

SH-SY5Y cells were obtained from American Type Culture Collection™. DMEM, F-12K, FBS, and 0.25% Trypsin-EDTA were obtained from Invitrogen Life Technologies™.

SOPG and NBD-SOPG powders were obtained from Avanti® Polar Lipids, Inc. $KAuCl_4$ and $Na_3C_6H_5O_7$ were obtained from Sigma Aldrich®. $NaBH_4$ was obtained from EMD Millipore®. $C_6H_8O_6$ was obtained from EM Science®, Div EM Industries Inc®. MilliQ water was used for this synthesis.

PFA was obtained from EMD®.

Primary antibodies specific for Rab5 and LAMP-1 were obtained from Abcam®. Primary antibodies specific for Rab7 and Rab11 were obtained from Cell Signaling Technology®. All primary antibodies used were monoclonal. Secondary antibodies for Rab7, Rab11, and LAMP-1 were obtained from Cell Signaling Technology®.

Chapter 3

Study of Endocytic Marked Compartments in C2C12 and A549 Cells

3 Study of Endocytic Marked Compartments in C2C12 and A549 Cells

Antibodies directed for endocytic marker proteins, such as Rab5, Rab7, Rab11, and LAMP-1 can be used to image the location of the respective endocytic compartments. Therefore, it is possible to determine the location of these compartments within cells.

Specifically, presuming that the early endosomes mature into late endosomes and ultimately fuse with lysosomes, Rab5 and Rab7 would be expected to co-exist on the same portion of the endosomes during the maturation process and Rab7 and LAMP-1 would be expected to co-exist during the fusion process. To understand how nanoparticles interact with each of these compartments and are processed in cells, it is important to quantitatively know the extent to which these markers co-exist in various compartments.

The purpose of the work presented in Chapter 3 is to determine the extent to which endocytic marker proteins co-exist in the same compartment. The distribution of each marker was first characterized separately. The pairwise co-localization of two markers was then characterized and the extent to which three markers simultaneously co-exist was determined. To achieve these results, image correlation spectroscopy analysis was performed on laser scanning confocal microscopy images of cells immunofluorescently labelled with antibodies specific for Rab5, Rab7, Rab11, and LAMP-1 to visualize the early, late, recycling, and lysosomal endocytic markers, respectively.

To determine if marker distribution was cell type specific, this study was conducted on two different cell types, C2C12 and A549 cells. C2C12 cells are a mouse muscle myoblast cell line.[85] A549 cells are human lung carcinoma epithelial cells.[86]

3.1 Individually Labelled Endocytic Marked Compartments in C2C12 Cells

The data and analysis in Chapter 3.1 pertains to confocal fluorescence microscopy images of C2C12 cells singly labelled with primary antibodies specific for markers of clathrin mediated endocytic compartments and fluorescent secondary antibodies specific for the corresponding primary antibodies. Primary and secondary antibody pairs corresponding to Rab5,

Rab7, Rab11, and LAMP-1 were used to study markers specific for early, late, recycling, and lysosomal endocytic compartments in C2C12 cells, respectively.

Materials and methods corresponding to labelling of markers in cells can be found in Chapter 2.4. Laser scanning confocal microscopy imaging of one marker can be found in Chapter 2.10.3.1. Image Correlation Spectroscopy can be found in Chapter 2.11.1.

3.1.1 Rab5-561 Marked Early Endocytic Compartments in C2C12 Cells

To study the marker associated with early endocytic compartments in C2C12 cells, cells were immunofluorescently labelled with primary antibodies specific for Rab5 markers and fluorescent secondary antibodies specific for the primary Rab5 antibodies.

Figure 3.1 shows 10 μm x10 μm confocal fluorescence microscopy images of antibodies targeting Rab5 endocytic markers in four different cells in a sample. In each image, there are a number of regions corresponding to the location of individual or groups of endosomes. The four images show that the distributions of endosomes are heterogeneous but still similar between the four different cells.

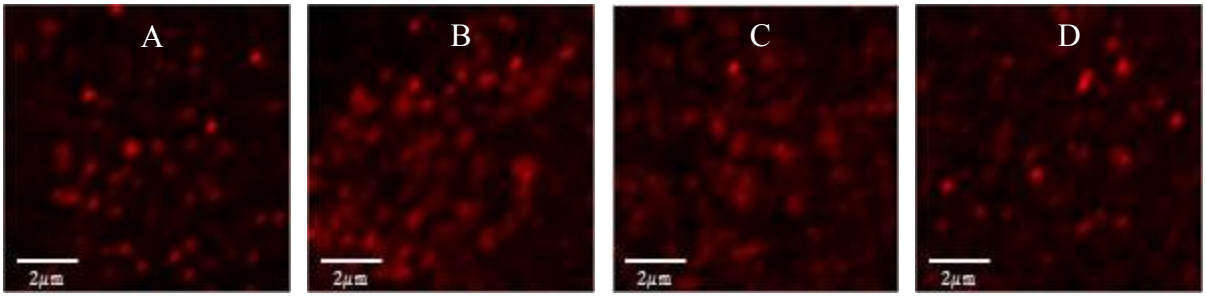

Figure 3.1 Images of Rab5-561 Marked Early Endocytic Compartments in C2C12 Cells

Panels A, B, C and D are representative of confocal fluorescence microscopy images of four different cells in the same sample labelled with primary antibodies specific for Rab5-561 markers and secondary antibodies specific for Rab5-561 primary antibodies to visualize early endocytic marked compartments.

Figure 3.1 shows the reproducibility of the sampling of images of early endocytic marked compartments. Although the images represented in panels A, B, C and D are visually similar, they are not exactly the same due to the heterogeneity of cells. It is critical to obtain a large

number of images, specifically 30-40 images if possible, to ensure accurate sampling of the system of interest. Due to the fact that the distribution of fluorescence is heterogeneous, fluctuations in intensity across the images will occur, allowing for analysis by ICS.

Recall that ICS will provide three important parameters; the amplitude of the auto correlation function, the fit for the width of the correlation function corresponding to the laser beam (μm), and the average intensity. Each of these parameters corresponding to the four images presented in Figure 3.1 is listed in Table 3.1.

Table 3.1 ICS Paramaters for Images of Rab5-561 Marked Early Endocytic Compartments in C2C12 Cells

Image	A (Cell 1)	B (Cell 2)	C (Cell 3)	D (Cell 4)
g(0,0)	0.49	0.42	0.23	0.38
ω (μm)	0.24	0.28	0.35	0.26
$I_{avg.}$	521	576	702	618

The autocorrelation amplitude,$g(0,0)$, fitted laser beam width, ω, and average intensity, $I_{avg.}$, were obtained for each image represented in Figure 3.1.

The data obtained for each cell represented in Table 3.1 show the variability between cells among the auto correlation amplitude, fitted laser beam width, and average intensity. The auto correlation amplitude obtained for each cell ranges between approximately 0.23-0.49. The fitted value for ω obtained for each cell ranges between approximately 0.24-0.35 microns. Lastly, the average intensity of Rab5 markers ranges from approximately 521-702. Because the values vary, it is important to obtain a large data set to get reliable estimates of each parameter.

Due to the quantitative nature of this study, control experiments are critical. Thus, images of cells labelled with both primary and secondary antibodies corresponding to Rab5 markers were compared to images of control samples in which cells were labelled with only primary antibodies or only secondary antibodies.

In Figure 3.2, images A and B correspond to images of two control samples; image A corresponds to one cell from a sample labelled with only the primary antibodies specific for Rab5-561 markers. Image B corresponds to one cell from a sample labelled with only the

secondary antibodies specific for the primary antibodies for Rab5-561 markers. Image C is representative of one cell from a sample labelled with primary and secondary antibodies for Rab5-561 markers. Image D is a contrast enhanced image of image C for clearer visualization of the range of labelling efficiencies.

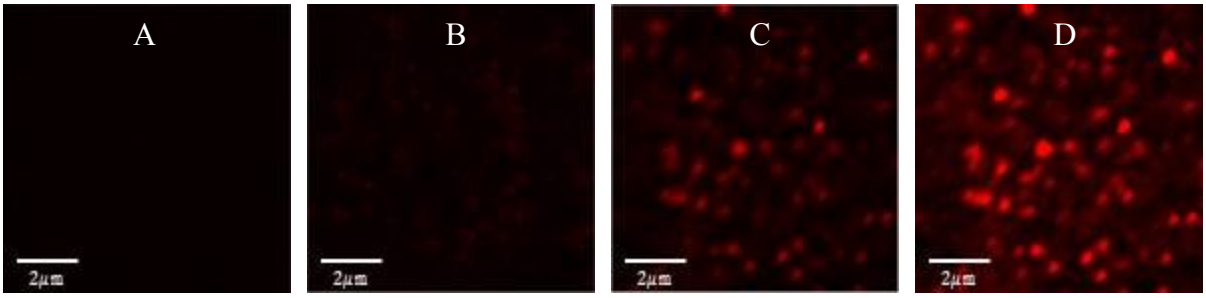

Figure 3.2 Images of Antibody Controls and Rab5 Marked Early Endocytic Compartments in C2C12 Cells

Image A corresponds to a sample labelled with only the primary antibodies specific for Rab5-561 markers. Image B corresponds to a sample labelled with only the secondary antibodies specific for the primary antibodies for Rab5-561 markers. Image C is representative of a cell sample labelled with primary and secondary antibodies for Rab5-561 markers. Image D is a contrast enhanced image of Image C for clearer visualization of the range of labelling efficiencies.

Images A and B in Figure 3.2 show that there is minimal fluorescence emitted from the primary and secondary antibodies in the cell, respectively. Image A appears to show less fluorescence emitted from the primaries in the cell in comparison to Image B; the presence of the red regions in image B is due to the minimal fluorescence emitted from the secondary Rab5-561 antibodies. This type of fluorescence emission arises from non-specific binding of secondary Rab5-561 antibodies. Therefore, the minimal fluorescence emitted from the controls in the cell as shown in images A and B means that the fluorescence emitted from Rab5-561 marked compartments in the cell as shown in image C is specific.

The contrast enhanced Image D is shown for comparison and to provide a better visualization of Rab5-561 marked compartments. However, contrast enhancement can be misleading and imply that Rab5-561 markers have been saturated by the laser upon illumination. This is not the case as shown in image C, which is the original image of Rab5-561 marked compartments. Therefore, ICS analysis was not completed on contrast enhanced images.

Table 3.2 ICS Parameters for Images of Antibody Controls and Rab5-561 Marked Early Endocytic Compartments in C2C12 Cells

Image	g(0,0)	ω (μm)	$I_{avg.}$
A (Primary Control)	0.0007	0.39	5.70
B (Secondary Control)	0.04	0.23	7.65
C (Rab5-561)	0.49	0.24	521

This table is representative of the data obtained for a set of controls, a sample labelled with antibodies specific for Rab5 marked endocytic compartments and the original image.

In Table 3.2, the average intensity corresponding to a cell labelled with primary antibodies is consistent with the "black" image A. Similar to a blank control, (a cell that has not been labelled with *any* antibodies), there are no fluorescent molecules added if labelling with only primary antibodies. The auto correlation amplitude for the primary control is 0.0007 which is expected as this amplitude compares to a blank control not shown in this work.

The intensity corresponding to Rab5-561 marked compartments in image C is approximately 521; this intensity measurement is approximately one-hundred-fold greater in comparison to the intensity of fluorescence emission from the secondary control. Additionally, the amplitude of the autocorrelation function is approximately 0.49, which is at least twelve-fold greater than the amplitude of the secondary control. Thus, the measured intensity and auto correlation amplitude measured for image C are a specific representation of Rab5-561 marked compartments in one cell.

Recall, in Chapter 2.11.1.1, the width of the laser beam measured for secondary antibodies can be represented as the true fit for the laser beam width, ω_O. The width of the laser beam measured for endosomes can be represented by ω_{Exp}. Based on the logic presented in Chapter 2.11.1.1, we can ultimately determine if the experimental laser beam width has been convoluted with an endosome of a certain diameter. If the measured experimental width does arise from convolution, the diameter of the endosome can be extrapolated using Figure 2.6 when the true fit of the beam is approximately 240 nm.

Thus, the true fit for the laser beam width based on this data suggests the width of the laser beam is approximately 0.23 microns. The fit obtained for Rab5 marked compartments is approximately the same, 0.24 microns. This is an implication that clusters or endosomes containing Rab5-561 markers have a diameter that is comparable to the size of the laser beam

width.

The primary control reflects the background of the system; thus, the measurement obtained for the fit of laser beam width is not reliable because there is no fluorescence.

As previously discussed, it is important to obtain a large number of images, preferably 30-40 images if possible, in an experiment for representative sampling and better estimates of the parameters. Table 3.3 shows the averages of the autocorrelation amplitude, fitted laser beam width, and average intensity from a data set of 10 images of the primary control, 5 images of the secondary control, and 38 images of Rab5-561. The values for each parameter are shown with the standard error.

Table 3.3 Averages of ICS Parameters for Images of Antibody Controls and Rab5-561 Markd Early Endocytic Compartments in C2C12 Cells

Species	n_{images}	$\langle \mathbf{g(0,0)} \rangle$	$\langle \boldsymbol{\omega}\ (\boldsymbol{\mu m}) \rangle$	$\langle I_{avg.} \rangle$
A (Primary Control)	10	0.0009 ± 0.0003[1]	0.37 ± 0.10	5.63 ± 0.03
B (Secondary Control)	5	0.05 ± 0.004	0.24 ± 0.01	7.76 ± 0.13
C (Rab5)	38	0.23 ± 0.02	0.32 ± 0.01	598 ± 24

[1] Standard error.

The average intensity of Rab5-561 markers in the observation region of the laser beam is approximately 598. The intensities corresponding to primary and secondary antibody controls are approximately one hundred-fold less in comparison to images labelled with primary and secondary antibodies. Thus, after obtaining several images, the measurement of the intensity of Rab5-561 markers in the observation area is specific, as it is far greater in magnitude in comparison to the controls.

The value for the auto correlation amplitude for clusters containing Rab5-561 markers is approximately 0.23. The values obtained for the primary and secondary control amplitudes are at least four-fold less than that of the auto correlation amplitude measurement for clusters containing Rab5-561 markers. This difference in magnitude among the controls and the measurement of Rab5-561 markers indicates that the magnitude of the auto correlation amplitude for Rab5-561 markers is a reliable measurement.

The fit for the laser beam width is approximately 0.32 microns. This is an indication that clusters containing Rab5-561 markers are larger in comparison to the laser beam width. Using Figure 2.6, the extrapolated measurement for the diameter of Rab5-561 marked endosomes is

approximately 0.34 microns. The fit for the secondary control is approximately 0.24 microns, which indicates the experimentally measured fit for the laser beam (0.32 microns) arises from convolution. The primary control represents the background of the system and does not provide specific information about Rab5-561 markers.

As previously mentioned, the intensity of fluorescence emitted from a sample labelled with secondary antibodies corresponds to the non-specific binding of secondary antibodies. Therefore, the non-specific binding of antibodies can ultimately be used to measure the number of individual antibodies per cluster.

Equation 28 shows that the degree of aggregation, $\langle DA \rangle$, is related to the product of the amplitude of the correlation function and the intensity;

$$DA = g(0,0) * \langle I_{avg.} \rangle = \text{c} * \langle N_M \rangle / \langle N_C \rangle \tag{27}$$

Assuming that the secondary antibodies bind as individual molecules;

$$\langle N_m \rangle = \langle N_C \rangle \tag{28}$$

The calculated value for the degree of aggregation for the secondary control yields an estimate of the proportionality constant,c;

$$\begin{aligned} c &= \langle g_{sec}(0,0) \rangle * \left[\langle I_{avg.}(secondary) \rangle - \langle I_{avg.}(primary) \rangle \right] \\ &= 0.05 * (7.76 - 5.63) = 0.11 \end{aligned} \tag{29}$$

Since all of these experiments were conducted under identical conditions, we can use this estimate of the constant to calculate the average number of secondary antibodies per cluster;

$$DA = \frac{0.23 * (598 - 7.76)}{0.11} = 1{,}234\ antibodies \tag{30}$$

Thus, using the intensities and auto correlation amplitudes for primary, secondary, and Rab5, the data suggest that there are 1,234 Rab5 antibodies per cluster. Since the secondary antibody is polyclonal, there may be more than one bound polyclonal antibody per Rab5, so this is an upper limit of the number of Rab5 antibodies per cluster.

3.1.2 Rab7-633 Marked Late Endocytic Compartments in C2C12 Cells

Rab7-633 was used to study the distribution and location of late endocytic compartments in C2C12 cells. Labelling and imaging of Rab7-633 marked compartments in cells was accomplished by the same methods as previously shown for Rab5-561 marked compartments in Chapter 3.1.1.

In Figure 3.3, image A corresponds to a sample labelled with only the primary antibodies specific for Rab7 markers. Image B corresponds to a sample labelled with only the secondary antibodies specific for the primary antibodies for Rab7 markers. Image C is representative of a cell sample labelled with both primary and secondary antibodies for Rab7-633 markers. Image D is a contrast enhanced image of image C for clearer visualization of the range of labelling efficiencies.

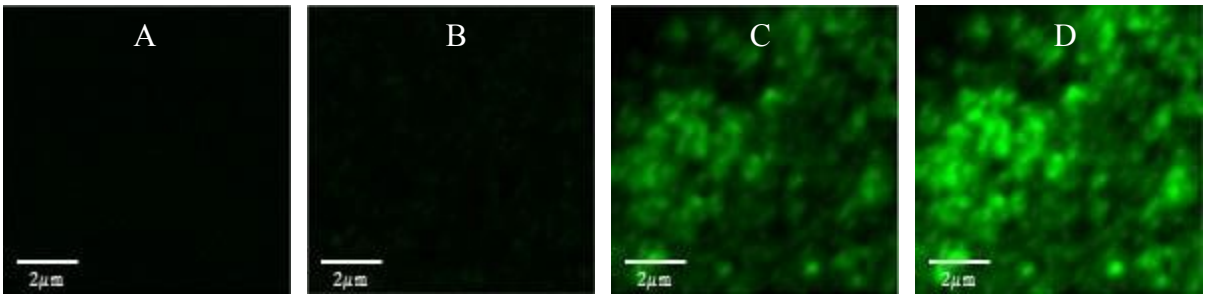

Figure 3.3 Rab7-633 Marked Late Endocytic Compartments in C2C12 Cells

Image A corresponds to a sample labelled with only the primary antibodies specific for Rab7 markers. Image B corresponds to a sample labelled with only the secondary antibodies specific for the primary antibodies for Rab7 markers. Image C is representative of a cell sample labelled with primary and secondary antibodies for Rab7-633 markers. Image D is a contrast enhanced image of Image C for clearer visualization of the range of labelling efficiencies.

As with Rab5-561 markers, images A and B in Figure 3.3 show there is very minimal fluorescence emitted from the primary and secondary controls in both cells, respectively. However, there appears to be a greater amount of fluorescence emitted by the secondary control in the cell as shown in image B due to the faint green regions that reflect non-specific binding of Rab7-633 antibodies. However, images A and B show fewer fluorescent regions in the cells in comparison to the Rab7-633 marked compartments shown in image C. Thus, the minimal fluorescence emitted from the controls in the cells as shown in images A and B imply that the

fluorescence emitted from Rab7-633 markers shown in image C is specific. The contrast enhanced image D is shown for better visualization of Rab7-633 marked compartments.

Table 3.4 shows the averages of the auto correlation amplitude, fitted laser beam width, and average intensity from a data set of 10 images of the primary, 10 images of the secondary, and 37 images of Rab7-633. The values for each parameter are shown with the standard error.

Table 3.4 Averages of ICS Parameters for Images of Antibody Controls of Rab7-633 Marked Late Endocytic Compartments in C2C12 Cells

Species	n_{images}	$\langle \mathbf{g(0,0)} \rangle$	$\langle \boldsymbol{\omega}\ (\boldsymbol{\mu m}) \rangle$	$\langle I_{avg.} \rangle$
Primary Control	10	0.0003 ± 0.0001[1]	0.22 ± 0.09	13.2 ± 0.03
Secondary Control	10	0.02 ± 0.001	0.23 ± 0.01	18.1 ± 0.3
Rab7-633	37	0.31 ± 0.03	0.48 ± 0.01	312 ± 15

[1] Standard error.

The averaged data in Table 3.4 correspond to cells labelled with respect to Rab7-633 markers on late endocytic compartments. The averaged parameters each reflect a similar error with respect to the experiments corresponding to cells labelled with primary and secondary antibodies corresponding to Rab5-561 in Chapter 3.1.1. The average intensity of Rab7-633 marked compartments is approximately 312, more than seventeen-fold larger in comparison to the controls. In addition, the auto correlation amplitude for clusters containing Rab7-633 markers is approximately 0.31. The auto correlation amplitudes corresponding to the primary and secondary controls are much less in magnitude than the measurement of Rab7-633 markers; the secondary control amplitude is at least fifteen-fold-less than the amplitude for clusters containing Rab7 markers.

The fit for ω corresponding to Rab7-633 marked compartments is approximately 0.48 microns and the fit corresponding to the secondary control is approximately 0.23 microns. These measurements indicate the experimentally calculated fit for the laser beam (0.48 microns) arises from convolution. Using Figure 2.6, the diameter of Rab7 endosomes is approximately 0.62 microns. Similar to Rab5 marked compartments, the primary control is a representation of background noise.

As discussed and shown previously in Equation 28, one can infer and calculate the estimate for the average number of antibodies per cluster from the intensities and auto correlation amplitudes of the controls; the data for this experiment suggests that on average, there are approximately 930 antibodies of Rab7-633 per cluster.

3.1.3 Rab11-633 Marked Recycling Endocytic Compartments in C2C12 Cells

Rab11-633 was used to study the distribution and location of recycling endocytic compartments in C2C12 cells. Labelling and imaging of Rab11-633 marked compartments in cells was accomplished in the same fashion as shown in Chapters 3.1.1 and 3.1.2 with Rab5-561 and Rab7-633 markers.

In Figure 3.4, image A corresponds to a sample labelled with only the primary antibodies specific for Rab11 markers. Image B corresponds to a sample labelled with only the secondary antibodies specific for the primary antibodies for Rab11 markers. Image C is representative of a cell sample labelled with primary and secondary antibodies for Rab11-633 markers. Image D is a contrast enhanced image of image C for clearer visualization of the range of labelling efficiencies.

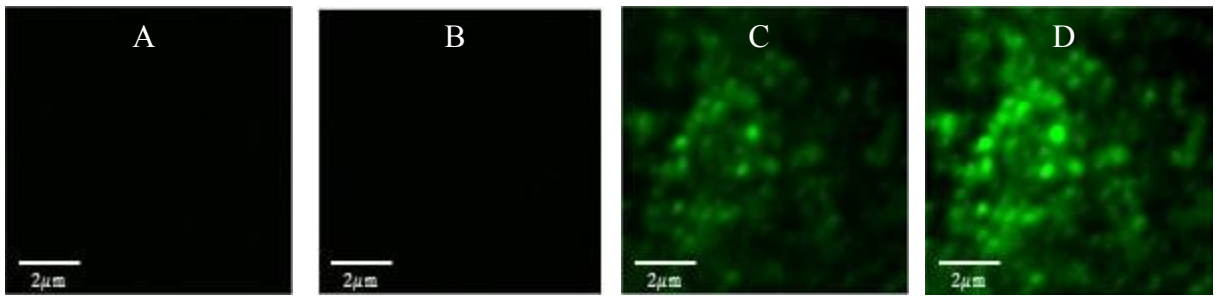

Figure 3.4 Rab11-633 Marked Recycling Endocytic Compartments in C2C12 Cells

Image A corresponds to a sample labelled with only the primary antibodies specific for Rab11 markers. Image B corresponds to a sample labelled with only the secondary antibodies specific for the primary antibodies for Rab11 markers. Image C is representative of a cell sample labelled with primary and secondary antibodies for Rab11-633 markers. Image D is a contrast enhanced image of Image C for clearer visualization of the range of labelling efficiencies.

Images A and B in Figure 3.4 shows the minimal fluorescence that is emitted from the primary and secondary controls in the cells, respectively. In contrast to Rab5-561 and Rab7-633 non-specific labelling, there appears to be no fluorescence emitted by the secondary control in

the cell shown in image B. Thus, judging from image B, there may be no non-specific binding of Rab11-633 in C2C12 cells. Images A and B show fewer fluorescent regions in the cells in comparison to Rab7-633 marked compartments shown in image C. Thus, the minimal fluorescence emitted from the controls in cells shown in images A and B indicates that the fluorescence in cells shown in image C is a specific representation of Rab11-633 compartments. The contrast enhanced image D is shown for better visualization of Rab11-633 marked compartments.

Table 3.5 shows the averages of the auto correlation amplitude, fitted laser beam width, and average intensity from a data set of 3 images of the primary, 5 images of the secondary, and 34 images of Rab11-633. The values for each parameter are shown with the standard error.

Table 3.5 Averages of ICS Paramaters for Images of Antibody Controls and Rab11-633 Marked Recycling Endocytic Compartments in C2C12 cells

Species	n_{images}	$\langle \mathbf{g(0,0)} \rangle$	$\langle \boldsymbol{\omega}\ (\boldsymbol{\mu m}) \rangle$	$\langle I_{avg.} \rangle$
Primary Control	3	0.002 ± 0.001 [1]	0.28 ± 0.07	7.16 ± 0.28
Secondary Control	5	0.003 ± 0.001	0.32 ± 0.05	7.22 ± 0.19
Rab11	34	0.18 ± 0.01	0.44 ± 0.01	511 ± 42

[1]Standard Error

The average intensity of Rab11-633 markers in the observation area of the laser beam is approximately 511. The intensities for the corresponding controls are approximately seventy-fold less than the measurement of Rab11-633 markers. However, as previously discussed in reference to Figure 3.4, there appears to be little difference between the secondary and primary control. This is quantitatively represented in Table 3.5, as the secondary intensity is only 0.06 units of intensity greater in comparison to the primary intensity. Due to the lack of non-specific binding of Rab11-633 antibodies, a value for c and hence the number of Rab11-633 antibodies observed per cluster cannot be estimated under these experimental conditions.

The auto correlation amplitude for clusters containing Rab11-633 markers is approximately 0.18. The amplitudes corresponding to the primary and secondary controls are approximately sixty-fold less in magnitude than the auto correlation amplitude for clusters containing Rab11-633 markers. This difference in magnitude is promising to indicate the measured auto correlation amplitude for clusters containing Rab11-633 markers is specific.

The average fit for ω is approximately 0.44 microns in comparison to the true fit for the laser beam measured by the secondary control, 0.32 microns. This true fit is 0.08 microns larger than 0.24 microns. With that in mind, the plot shown in Figure 2.6 can be slightly adjusted to account for this change for ω_0 to assume a true fit of the laser beam is 0.32 microns. Therefore, the diameter for Rab11 markers is approximately 0.56 microns.

3.1.4 LAMP-1 Marked Lysosomal Endocytic Compartments in C2C12 Cells

LAMP-1 marked lysosomal endocytic compartments were studied in three separate experiments using three secondary antibodies with different fluorescent probes. Different fluorescent probes were required for double labelling experiments to be discussed later in this chapter. The three LAMP-1 experiments used were Alexa Fluor 488, 555, and 633 secondary antibodies (labelled LAMP-1-488, LAMP-1-555, and LAMP-1-633).

3.1.4.1 LAMP-1-488 Marked Lysosomal Endocytic Compartments in C2C12 Cells

LAMP-1-488 was used to study the distribution and location of lysosomal endocytic compartments in C2C12 cells. Labelling and imaging of LAMP-1-488 marked compartments in cells was accomplished in the same fashion as previously shown for Rab5-561, Rab7-633, and Rab11-633 markers.

In Figure 3.5, image A corresponds to a sample labelled with only the primary antibodies specific for LAMP-1-488 markers. Image B corresponds to a sample labelled with only the secondary antibodies specific for the primary antibodies for LAMP markers. Image C is representative of a cell sample labelled with primary and secondary antibodies for LAMP-1-488 markers. Image D is a contrast enhanced image of image C for clearer visualization of the range of labelling efficiencies.

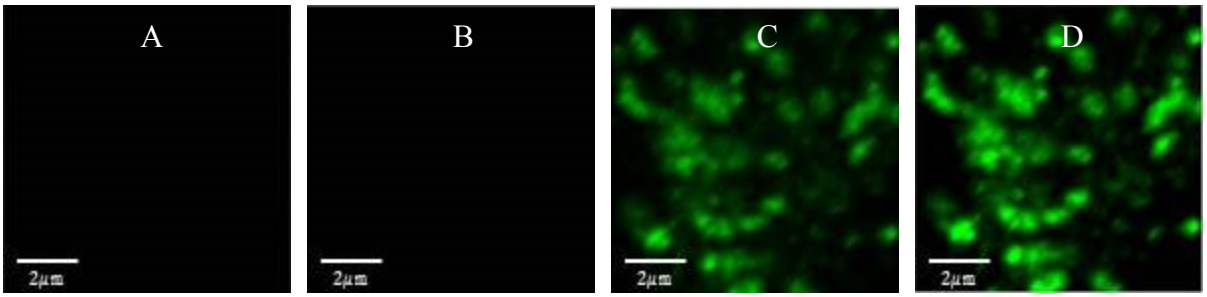

Figure 3.5 LAMP-1-488 Marked Lysosomal Endocytic Compartments in C2C12 Cells

Image A corresponds to a sample labelled with only the primary antibodies specific for LAMP-1 markers. Image B corresponds to a sample labelled with only the secondary antibodies specific for the primary antibodies for LAMP-1 markers. Image C is representative of a cell sample labelled with primary and secondary antibodies for LAMP-1 markers. Image D is a contrast enhanced image of Image C for clearer visualization of the range of labelling efficiencies.

Images A and B in Figure 3.5 show that there is minimal fluorescence emitted from the primary and secondary controls in the cells, respectively. This minimal fluorescence emitted from the controls in the cells means that the fluorescence emitted in the cell as shown in image C is a reliable representation of LAMP-1-488 marked lysosomal endocytic compartments that have not been saturated by the laser upon illumination. Image D is contrast enhanced for better visualization.

The data corresponding to Figure 3.5 is represented in Table 3.6. Table 3.6 is a representation of the averages of the auto correlation amplitude, fitted laser beam width, and average intensity of LAMP-1 markers from a data set of 3 images of the primary, 2 images of the secondary, and 35 images of LAMP-1-488. The values for each parameter are shown with the standard error.

Table 3.6 Averages of ICS Paramaters for Images of Antibody Controls of LAMP-1-488 Marked Lysosomal Endocytic Compartments in C2C12 Cells

Species	n_{images}	$\langle \mathbf{g(0,0)} \rangle$	$\langle \boldsymbol{\omega}\ (\boldsymbol{\mu m}) \rangle$	$\langle I_{avg.} \rangle$
Primary Control	3	0.002 ± 0.002[1]	0.13 ± 0.07	43.2 ± 0.4
Secondary Control	2	0.002 ± 0.001	0.06 ± 0.05	42.0 ± 0.0
LAMP-1 488	35	0.50 ± 0.03	0.47 ± 0.01	558 ± 23

[1] Standard Error

The average intensity of LAMP-1-488 markers in the observation region of the laser beam is approximately 558. The intensities for the corresponding controls are at least twelve-fold less than that of the intensity measurement of LAMP-1-488 markers. This *difference* in intensity among controls and markers is less in comparison to previous measured intensity controls for Rab5, Rab7, and Rab11 markers. Nonetheless, the intensities are a small fraction of the measured intensity of cells marked with LAMP-1-488 (558). The difference between the secondary and primary control intensities vary by 0.8 units of intensity; thus, a value for c and the number of LAMP-1-488 antibodies observed per cluster cannot be estimated under these experimental conditions.

The auto correlation amplitude for clusters containing LAMP-1-488 markers is approximately 0.50. The auto correlation amplitudes corresponding to the primary and secondary controls are 250 fold less in magnitude than the measurement of the auto correlation amplitude for LAMP-1-488 marked compartments. Thus although the measured intensities for the controls are large, the auto correlation amplitudes for the controls measured do not reflect specific LAMP-1-488 binding.

The fit for ω is approximately 0.47 microns. In contrast to fits for ω obtained for Rab5-561, Rab7-633, and Rab11-633 primary and secondary controls, the secondary antibody control corresponding to LAMP-1 markers is approximately 0.06 microns. This relatively small value of 0.06 microns indicates that the laser beam width cannot be fit to the width of the correlation function and is not a reliable estimate of the beam width. Likewise, the primary control reflects no specific binding of LAMP-1-488 antibodies.

3.1.4.2 LAMP-1-561 Marked Lysosomal Endocytic Compartments in C2C12 Cells

LAMP-1-561 was used to study the distribution and location of lysosomal endocytic compartments in C2C12 cells. Labelling and imaging of LAMP-1-555 marked compartments in cells was accomplished in the same fashion as previously shown for Rab5-561, Rab7-633, Rab11-633, and LAMP-1 488 markers.

In Figure 3.6, image A corresponds to a sample labelled with only the primary antibodies specific for LAMP-1-561 markers. Image B corresponds to a sample labelled with only the secondary antibodies specific for the primary antibodies for LAMP-1 markers. Image C is

representative of a cell sample labelled with primary and secondary antibodies for LAMP-1-561 markers. Image D is a contrast enhanced image of image C for clearer visualization of the range of labelling efficiencies.

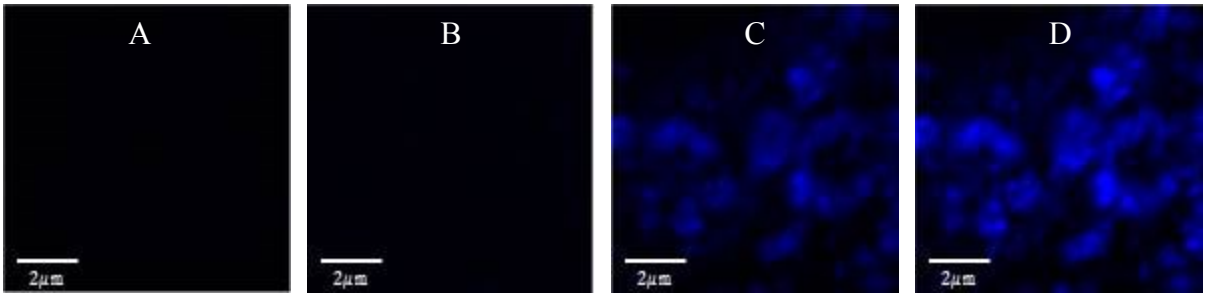

Figure 3.6 LAMP-1 555 Marked Lysosomal Endocytic Compartments in C2C12 Cells

Image A corresponds to a sample labelled with only the primary antibodies specific for LAMP-1 markers. Image B corresponds to a sample labelled with only secondary antibodies specific for the primary antibodies for LAMP-1 markers. Image C is representative of a cell sample labelled with primary and secondary antibodies for LAMP-1 markers. Image D is a contrast enhanced image of image C for clearer visualization of the range of labelling efficiencies.

Images A and B in Figure 3.6 shows minimal fluorescence emitted from the primary and secondary controls in cells, respectively. This minimal fluorescence emitted from the controls in cells indicates the fluorescence emitted in the cell as shown in image C is a specific representation of LAMP-1 marked lysosomal endocytic compartments.

The data corresponding to Figure 3.6 is represented in Table 3.7. The averages of the auto correlation amplitude, fitted laser beam width, and average intensity of LAMP-1-561 markers are shown.

Table 3.7 Averages of ICS Paramaters for Images of Antibody Controls of LAMP-1 561 Marked Lysosomal Endocytic Compartments in C2C12 Cells

Species	n_{images}	$\langle \mathbf{g(0,0)} \rangle$	$\langle \boldsymbol{\omega}\ (\boldsymbol{\mu m}) \rangle$	$\langle I_{avg.} \rangle$
Primary Control	10	0.002 ± 0.001[1]	0.34 ± 0.06	5.45 ± 0.04
Secondary Control	10	0.02 ± 0.004	0.24 ± 0.01	6.05 ± 0.05
LAMP-1-561	41	0.48 ± 0.05	0.50 ± 0.01	633 ± 30

1 Standard error.

This data closely resembles the data obtained for LAMP-1-488 lysosomal marked endocytic compartments to validate reproducible labelling of LAMP-1-555 marked compartments.

Last, the intensity of LAMP-1-561 markers in the observation region of the laser beam is approximately 633. As with Rab5-561 markers, the intensities for the corresponding primary and secondary controls are approximately one hundred fold less than the true measurement of LAMP-1 markers. There is some minor non-specific binding occurring due to the greater fluorescent intensity measured for the secondary controls. Thus, the data for this experiment suggests that on average there are approximately 25,078 antibodies of LAMP-1-561 per cluster. This measurement is greater in magnitude in comparison to other markers due to the fact the intensity is only 10% above the background.

The auto correlation amplitude corresponding to clusters containing LAMP-1-561 is approximately 0.48. The auto correlation amplitudes corresponding to the primary and secondary controls are at least twenty-four-fold less in magnitude than the measurement of the auto correlation amplitude for LAMP-1-561 marked compartments. This difference in magnitude between the auto correlation amplitudes for the controls and LAMP-1-561 compartments means 0.48 is a reliable representation for the auto correlation amplitude corresponding to clusters containing LAMP-1-561 markers.

The fit for ω is approximately 0.50 microns. This is one of the largest fits observed for clusters containing a specific marker. Additionally, this fit for the laser beam corresponding to LAMP-1-561 markers is approximately 2.5 fold larger in magnitude than the fits obtained for the secondary controls which is approximately 0.20 microns. Using Figure 2.6, the diameter of LAMP-1 marked endosomes can be extrapolated to be approximately 0.64 microns.

3.1.4.3 LAMP-1-633 Marked Lysosomal Endocytic Compartments in C2C12 Cells

LAMP-1-633 was used to study the distribution and location of lysosomal endocytic compartments in C2C12 cells. Labelling and imaging of LAMP-1-647 marked compartments in cells was accomplished in the same fashion as previously shown for Rab5-561, Rab7-633, Rab11-633, LAMP-1 488, and LAMP-1 555 markers.

In Figure 3.7, image A corresponds to a sample labelled with only the primary antibodies specific for LAMP-1-633 markers. Image B corresponds to a sample labelled with only the secondary antibodies specific for the primary antibodies for LAMP-1 markers. Image C is representative of a cell sample labelled with primary and secondary antibodies for LAMP-1-633 markers. Image D is a contrast enhanced image of image C for clearer visualization of the range of labelling efficiencies.

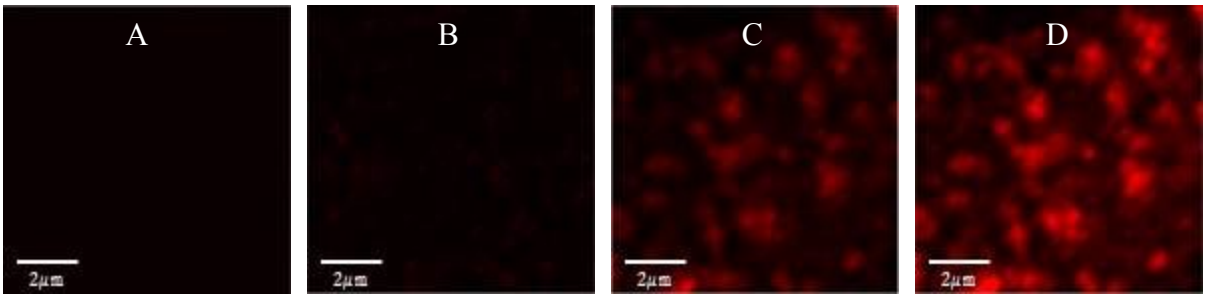

Figure 3.7 LAMP-1-633 Marked Lysosomal Endocytic Compartments in C2C12 Cells

Image A corresponds to a sample labelled with only the primary antibodies specific for LAMP-1-633 markers. Image B corresponds to a sample labelled with only the secondary antibodies specific for the primary antibodies for LAMP-1 markers. Image C is representative of a cell sample labelled with primary and secondary antibodies for LAMP-1 markers. Image D is a contrast enhanced image of image C for clearer visualization of the range of labelling efficiencies.

Images A and B in Figure 3.7 illustrate the minimal fluorescence emitted from the primary and secondary controls in cells, respectively, however there is some fluorescence of light emitted from the secondary antibodies in cells as shown in image B due to the faint red spots observed. Image C is a clear representation of specific binding of LAMP-1-633 markers. Image D is shown for contrast enhancement and better visualization.

The data corresponding to Figure 3.7 is represented in Table 3.8. Table 3.8 is a representation of the averages of the auto correlation amplitude, fitted laser beam width, and average intensity of LAMP-1-633 markers from a data set of 10 images of the primary, 5 images of the secondary, and 41 images of the LAMP-1-633 positive controls. The values for each parameter are shown with the standard error.

Table 3.8 Averages of ICS Paramaters for Images of Antibody Controls of LAMP-1-633 Marked Lysosomal Endocytic Compartments in C2C12 Cells

Species	n_{images}	$\langle \mathbf{g(0,0)} \rangle$	$\langle \boldsymbol{\omega}\ (\boldsymbol{\mu m}) \rangle$	$\langle I_{avg.} \rangle$
Primary Control	10	0.0001 ± 0.0000[1]	0.27 ± 0.08	14.4 ± 1.2
Secondary Control	5	0.008 ± 0.001	0.34 ± 0.06	12.0 ± 0.3
LAMP-1-633	41	0.43 ± 0.03	0.51 ± 0.01	419 ± 18

[1] Standard error.

The averaged parameters each reflect a similar error with respect to the experiments corresponding to cells labelled with primary and secondary antibodies specific for Rab5-561, Rab7-633, and Rab11-633. More importantly, the data closely resemble the data obtained for LAMP-1-488 and LAMP-1-561 Marked Lysosomal Endocytic Marked Compartments to validate reproducible labelling of LAMP-1 compartments.

The average intensity of LAMP-1-633 markers in the observation region of the laser beam is approximately 419. The average intensities for the corresponding controls are approximately thirty-fold less than the intensity measurement of LAMP-1-633 markers. The intensity, however, the secondary intensity is 1.6 units of intensity *less* than the primary intensity. Thus, there is no non-specific LAMP-1-633 antibody binding under these experimental conditions and the number of LAMP-1 antibodies per cluster cannot be estimated.

The auto correlation amplitude corresponding to clusters containing LAMP-1-633 is approximately 0.43. The auto correlation amplitudes corresponding to the primary and secondary controls are at least fifty-three-fold less in magnitude than the measurement for the auto correlation amplitude for clusters containing LAMP-1-633 markers. This is a promising measurement to indicate a reliable representation for the auto correlation amplitude corresponding to clusters containing LAMP-1-633 markers.

The fit for ω is approximately 0.51. This fit for the laser beam corresponding to LAMP-1-633 markers is approximately 2 fold larger in magnitude than the fits obtained for the secondary control, which is 0.34 microns. As with Rab11 marked compartments, the true fit for the laser beam is slightly larger in comparison; therefore, by adjusting Figure 2.6 to have a ω_O value of 0.34 microns, the diameter of Rab11 endosomes can be extrapolated to approximately 0.60 microns.

3.1.5 Comparisons of Marked Endocytic Compartments in C2C12 Cells

The purpose of this section is to quantitatively compare each species from all data obtained. Each of the data discussed in Chapter 3.1 is summarized below in Table 3.9 for further interpretation and comparison.

Table 3.9 Summary of Averaged ICS Parameters for Cells Labelled with Markers of Endocytic Compartments

Species	n_{images}	$\langle \mathbf{g(0,0)} \rangle$	$\langle \boldsymbol{\omega}\ (\boldsymbol{\mu m}) \rangle$	$\langle I_{avg.} \rangle$
Rab5-561	38	0.23 ± 0.02[1]	0.32 ± 0.01	598 ± 24
Rab7-633	37	0.31 ± 0.03	0.48 ± 0.06	312 ± 15
Rab11-633	34	0.18 ± 0.01	0.44 ± 0.01	511 ± 42
LAMP-1-488	35	0.50 ± 0.03	0.47 ± 0.01	558 ± 23
LAMP-1-561	41	0.48 ± 0.05	0.50 ± 0.01	633 ± 30
LAMP-1-633	41	0.43 ± 0.03	0.51 ± 0.01	419 ± 18

This data has been previously shown; the purpose is to compare and contrast each of the averaged parameters obtained. [1] Standard error.

In Table 3.9, the autocorrelation amplitude ranges between 0.23-0.50. Specifically, the auto correlation amplitude increases with the progression of endosomes in the clathrin mediated endocytic pathway.

The resolution of the microscope is dependent on the wavelength of light; therefore, the longer the wavelength of light, a slightly larger fit for the laser beam is expected for species labelled with different fluorescent probes. For example; the fits for the laser beam width for each LAMP-1 marker increases with fluorescent probe.

In addition, the fit for ω ranges between 0.32-0.51 microns. Based on this data, one would observe that the fit obtained for each associated marker increases with progression of endosomes in the clathrin mediated endocytic pathway. In all cases, the measured fit for each cluster containing markers reflects a convolution of the laser beam with the endosome. On average, the endosomes have a diameter ranging approximately between 0.34-0.60 microns.

The average intensity for each species of interest ranges between 300–600. There is no absolute trend with the intensity; however, it must be remembered that the intensity of

fluorescence emission from a species will vary with experiments and is dependent on the intensity of light at the sample and gain of detection of the intensity.

As discussed in Chapter 2, one can use the data obtained to calculate the average number of clusters that contain a specific species, $\langle N_{Species} \rangle$, the number of clusters that contain a particular species per square micron, ⟨CD⟩, and the *relative* degree of aggregation for the number of species per cluster, ⟨DA⟩. The averaged calculations are in reference to the data obtained and are represented in Table 3.10.

Table 3.10 Averages of Derived Paramaters for Cells Labelled with Markers for Endocytic Compartments in C2C12 Cells

Species	$\langle N_{Species} \rangle$	⟨CD⟩	⟨DA⟩
Rab5-561	5.70 ± 0.45[1]	18.0 ± 1.4	127 ± 10
Rab7-633	4.22 ± 0.35	6.51 ± 0.67	91.3 ± 7.6
Rab11-633	6.06 ± 0.31	10.9 ± 0.8	92.2 ± 10.0
LAMP-1-488	2.19 ± 0.10	3.54 ± 0.29	268 ± 13
LAMP-1-561	2.87 ± 0.23	4.22 ± 0.49	259 ± 17
LAMP-1-633	2.61 ± 0.13	3.49 ± 0.27	175 ± 10

Calculations are based on the data represented in Table 3.9. [1]Standard error.

In Table 3.10, the number of clusters that contain a marker of an endocytic compartment is on the order of 2-6 clusters. Due to the increasing trend of the auto correlation amplitudes for each cluster containing markers, a decrease in the number of clusters that contain marker species is expected as the number of clusters is calculated by taking the reciprocal of the auto correlation amplitude. There are a greater number of clusters observed to contain either Rab5 or Rab11 markers than there are to contain Rab7 and LAMP-1 markers. Also, there is similarity in the number of species containing LAMP-1 markers as measured by the differently labelled secondary antibody probes.

In addition, the cluster density appears to be largest in magnitude for Rab5 and Rab11 marked endocytic compartments than for Rab7 and LAMP-1 marked compartments. The cluster density depends on the number of clusters and the fit obtained for the laser beam; the number of clusters fluctuates to a greater extent than the average fit for the beam in these experiments. Therefore, the values measured for the cluster density are weighed by the number of clusters.

This study has provided a means to understand the distribution of markers and that there are in fact differences exhibited; there appear to be fewer clusters of larger size observed as the clathrin mediated endocytic pathway progresses.

3.2 Co-Localization of Marked Endocytic Compartments in C2C12 Cells

In the previous section, each marker was characterized separately. In this section, the pairwise co-localization of markers will be discussed.

As discussed in the introduction, markers are replaced at the various stages of the endocytic pathway. Specifically, Rab7 markers have been studied and shown to replace Rab5 markers when early endosomes mature into late endosomes. LAMP-1 markers are known to replace Rab7 markers when late endosomes fuse with lysosomes. Thus, there markers are known to co-localize at some point during these replacement stages for maturation and fusion of endosomes. Thus, this study was performed to explore the extent to which two markers may simultaneously co-exist during maturation and fusion steps. This study will provide information in regard to whether each marker previously studied in Chapter 3.1 is unique for one endosomal compartment.

Recall, it is important to understand that the colors chosen for visualization for imaging or analysis in ImageJ is not relevant. Red and green were chosen to visualize the extent of interaction among two species because when overlaid, red and green reflect the color yellow. Thus, for a high degree of co-localization between pairwise interaction of red and green species in an image, one would expect to see yellow regions in the overlaid image to confirm the presence of two markers occupying the same cluster. Image Cross Correlation Spectroscopy is then important to provide the quantitative means to interpret the extent of co-localization of two markers and a better interpretation of how much yellow is truly observed.

In this section, the following experimental combinations were studied; Rab5-561 & Rab7-633, Rab5-561 & Rab11-633, Rab5-561 & LAMP-1-633, and Rab7-633 & LAMP-1-561. The experimental procedure for immunofluorescent labelling of two markers in cells can be found in Chapter 2.6.1. Laser scanning confocal microscopy imaging of two markers can be found in Chapter 2.10.3.2. Image Cross Correlation Spectroscopy analysis can be found in Chapter 2.11.2.

In Chapter 3.8, data is shown to reflect no cross reactivity or cross talk with species.

3.2.1 Rab5-561 & Rab7-633 Marked Endocytic Compartments in C2C12 Cells

Cells were doubly labelled for Rab5-561 and Rab7-633 markers; these markers are specific for early and late endosomes, respectively. Figure 3.8 shows contrast enhanced images of Rab5-561, in red, and Rab7-633, in green, marked compartments in one cell. The Merge image is an overlay of the Rab5-561 and Rab7-633 contrast enhanced images. The Original Merge is an overlay of the Rab5-561 and Rab7-633 images that were *originally obtained* in the experiment without contrast enhancement. Thus, the Original Merge image is shown for comparison to that of the Merge image.

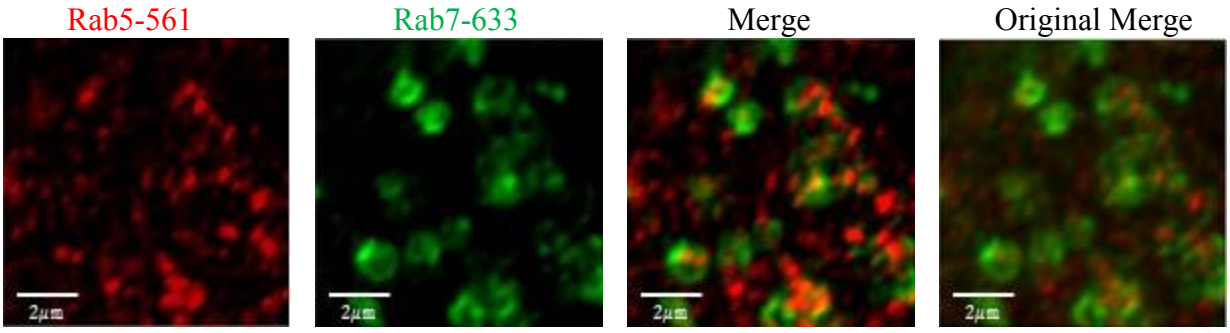

Figure 3.8 Rab5-561 & Rab7-633 Marked Endocytic Compartments in C2C12 Cells

In Figure 3.8, very few yellow regions are observed in the overall Merge image. Therefore, the few yellow clusters in the Merge image imply that there is a small degree of co-localization of Rab5-561 and Rab7-633 markers occupying the same cluster.

Table 3.11 reflects the calculations obtained via Image Cross Correlation Spectroscopy analysis. Specifically, the number of clusters containing markers, $\langle N_{Species} \rangle$ and the average fractions of co-localization of Rab5-561 and Rab7-633 markers are represented. The average fraction of clusters containing Rab5-561 markers that also contain Rab7-633 markers is denoted by $\langle F(Rab5|Rab7) \rangle$. Likewise, the average fraction of clusters containing Rab7-633 markers that also contain Rab5-561 markers is denoted by $\langle F(Rab7|Rab5) \rangle$.

Table 3.11 Average Number of Clusters Containing Species and Fractions of Co-Localization of Rab5 & Rab7 Markers in C2C12 Cells

Species	$\langle N_{Species} \rangle$	$\langle F(Rab5\|Rab7) \rangle$	$\langle F(Rab7\|Rab5) \rangle$
Rab5-561	5.39 ± 0.50[1]		
Rab7-633	5.49 ± 0.86		
Rab5-561 & Rab7-633	2.16 ± 0.26	0.46 ± 0.05	0.53 ±0.06

[1] Standard error.

The calculations for the average number of clusters of species represented in Table 3.11 reflect that there are approximately 5.39 clusters that contain Rab5-561 markers and approximately 5.49 clusters containing Rab7-633 markers. Lastly, there are approximately 2.16 clusters that contain both Rab5-561 and Rab7-633 markers.

The calculations for the average fractions of co-localization represented in Table 3.11 reflect on average approximately 46% of clusters that contain Rab5-561 markers also contain Rab7-633 markers and approximately 53% of the clusters containing Rab7-633 markers also contain Rab5-561 markers. Thus, half of the clusters containing Rab7-633 have Rab5-561, and half of the clusters containing Rab5-561 have Rab7-633.

It is important to keep to consideration the fractions shown in Table 3.11 are not a direct calculation of the average number of pairwise labelled clusters to the individual number of clusters. In addition, the fractions of co-localization are perhaps larger than one might have expected from the images. To ensure that this is not an artifact of the cross-correlation function of random or coincidental fluctuations, random images of Rab5-561 and Rab7-633 obtained from *different* cells were cross correlated. This data showed that the cross correlation amplitudes obtained from 55 images ranged from 0.00-0.10, with an average of 0.02. So, the cross correlated values could be systematically overestimated by 16% on average. Thus, a fraction of 0.46 may be as low as 0.40 because of coincidental cross correlation.

Thus, this is a very important calculation to do for two color experiments in which the markers are quite dense in the region of observation to ensure that two species of interest being measured are in fact measuring the estimate of clusters and fractions of co-localization.

3.2.2 Rab5-561 & Rab11-633 Marked Endocytic Compartments in C2C12 Cells

Cells were doubly labelled for Rab5 and Rab11 markers to study the pairwise co-localization of the early and recycling endocytic markers, respectively.

Figure 3.9 shows contrast enhanced images of Rab5-561, in red, and Rab11-633, in green, marked compartments in one cell. The Merge image is an overlay of the Rab5-561 and Rab11-633 contrast enhanced images. The Original Merge is an overlay of the Rab5-561 and Rab11-633 images that were *originally obtained* in the experiment without contrast enhancement. Thus, the Original Merge image is shown for comparison to that of the Merge image.

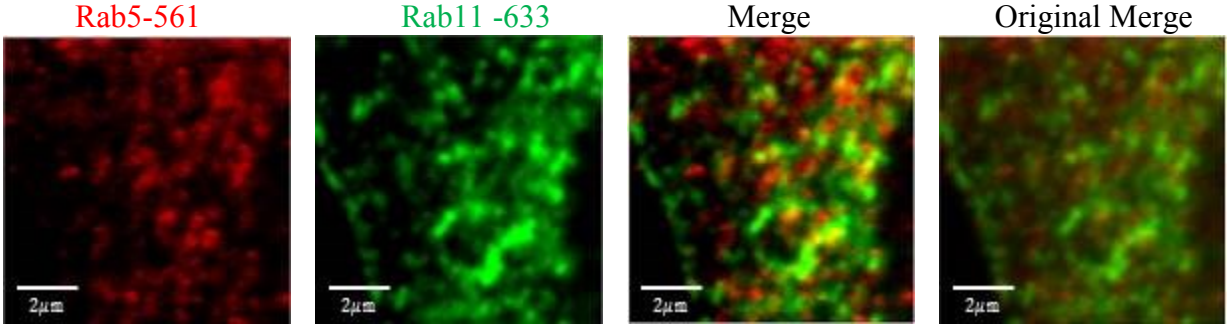

Figure 3.9 Rab5-561 & Rab11-633 Marked Endocytic Compartments in C2C12 Cells

The Merge image in Figure 3.9, there are few yellow regions to indicate some co-localization among Rab5-561 and Rab11-633 markers occupying the same cluster,.

Table 3.12 reflects the average calculations obtained using Image Cross Correlation Spectroscopy analysis. Specifically, the number of clusters containing markers, $\langle N_{Species} \rangle$ and the average fractions of co-localization of Rab5-561 and Rab11-633 markers are represented. The average fraction of clusters containing Rab5-561 markers that also contain Rab11-633 markers is denoted by $\langle F(Rab5|Rab11) \rangle$. Likewise, the average fraction of clusters containing Rab11-633 markers that also contain Rab5-561 markers is denoted by $\langle F(Rab11|Rab5) \rangle$.

Table 3.12 Average Number of Clusters Containing Species and Fractions of Co-Localization of Rab5-561 & Rab11-633 Markers in C2C12 Cells

Species	$\langle N_{Species} \rangle$	$\langle F(Rab5 \mid Rab11) \rangle$	$\langle F(Rab11 \mid Rab5) \rangle$
Rab5-561	13.4 ± 0.8[1]		
Rab11-633	6.75 ± 0.38		
Rab5-561 & Rab11-633	2.85 ± 0.27	0.23 ± 0.02	0.44 ± 0.04

[1] Standard error.

The calculations for the average number of clusters of species represented in Table 3.12 reflect that there are approximately 13.4 clusters containing Rab5-561 markers and approximately 6.75 clusters containing Rab11-633 markers. Lastly, there are approximately 2.86 clusters that contain both Rab5-561 and Rab11-633 markers.

The calculations for the average fractions of co-localization represented in Table 3.12 reflect on average approximately 23% of clusters that contain Rab5-561 markers also contain Rab11-633 markers and approximately 44% of the clusters containing Rab11-633 markers also contain Rab5-561 markers.

The images obtained in Figure 3.9 and the averaged values calculated in Table 3.12 are in agreement; visually speaking, a small fraction of clusters containing Rab5-561 also contain Rab11-633 markers than do clusters containing Rab5-561 also contain Rab11-633.

3.2.3 Rab5-561 & LAMP-1-633 Marked Endocytic Compartments in C2C12 Cells

Cells were doubly labelled for Rab5-561 and LAMP-1-633 markers to study the pairwise co-localization of the early and lysosomal endocytic markers, respectively.

Figure 3.10 shows contrast enhanced images of Rab5-561, in red, and LAMP-1-633, in green, marked compartments in one cell. The Merge image is an overlay of the Rab5-561 and LAMP-1-633 contrast enhanced images. The Original Merge is an overlay of the Rab5-561 and LAMP-1-633 images that were *originally obtained* in the experiment without contrast enhancement. Thus, the Original Merge image is shown for comparison to that of the Merge image.

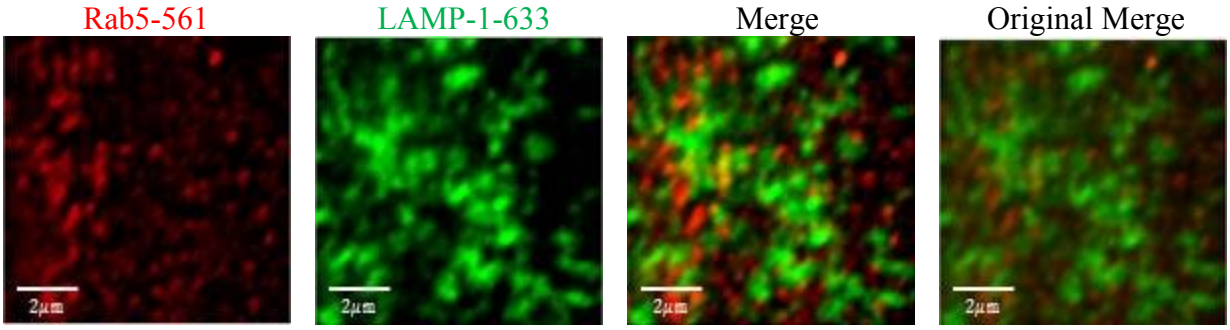

Figure 3.10 Rab5-561 & LAMP-1-561 Marked Endocytic Compartments in C2C12 Cells

Similar to the co-localization of Rab5-561 with Rab7-633 and Rab11-633 markers, the Merge image in Figure 3.10 shows some presence of yellow in the Merge image thus reflecting co-localization among Rab5-561 and LAMP-1-633 markers.

Table 3.13 reflects the average calculations obtained using Image Cross Correlation Spectroscopy analysis. Specifically, the number of clusters containing markers, $\langle N_{Species} \rangle$ and the average fractions of co-localization of Rab-5-561 and LAMP-1-633 markers are represented. The average fraction of clusters containing Rab5-561 markers that also contain LAMP-1-633 markers is denoted by $\langle F(Rab5|LAMP-1) \rangle$. Likewise, the average fraction of clusters containing LAMP-1-633 markers that also contain Rab5-561 markers is denoted by $\langle F(LAMP-1|Rab5) \rangle$.

Table 3.13 Average Number of Clusters Containing Species and Fractions of Co-Localization of Rab5-561 & LAMP-1-633 Markers in C2C12 Cells

Species	$\langle N_{Species} \rangle$	$\langle F(Rab5\|LAMP-1) \rangle$	$\langle F(LAMP-1\|Rab5) \rangle$
Rab5-561	5.66 ± 0.65[1]		
Lamp-1-633	4.96 ± 0.51		
Rab5-561 & LAMP-1-633	1.58 ± 0.31	0.32 ± 0.05	0.31 ± 0.04

[1] Standard error.

The calculations for the average number of clusters of species represented in Table 3.13 reflect that there are approximately 5.66 clusters containing Rab5-561 markers and

approximately 4.96 clusters containing LAMP-1-633 markers. Lastly, there are approximately 1.58 clusters that contain both Rab5-561 and LAMP-1-633 markers.

The calculations for the average fractions of co-localization represented in Table 3.13 reflect on average approximately 32% of clusters that contain Rab5-561 markers also contain LAMP-1-633 markers. Additionally, approximately 31% of the clusters containing LAMP-1-633 markers also contain Rab5-561 markers.

The images obtained in Figure 3.10 and the averaged values calculated in Table 3.13 are in agreement; visually speaking, a very small fraction of each species is located on another cluster consisting of another species. This finding, however, is very surprising. According to the literature, Rab5-561 compartments are meant to be specific for early endosomes and LAMP-1-633 compartments specific for lysosomes. Thus, the presence of Rab5 early endocytic markers on lysosomal endosomes was an unexpected result.

3.2.4 Rab7-633 & LAMP-1-561 Marked Endocytic Compartments in C2C12 Cells

Cells were doubly labelled for Rab7-633 and LAMP-1-561 markers to study the pairwise co-localization of the late and lysosomal endocytic markers, respectively.

Figure 3.11 shows contrast enhanced images of Rab7-633, in red, and LAMP-1-561, in green, marked compartments in one cell. The Merge image is an overlay of the Rab7-633 and LAMP-1-561 contrast enhanced images. The Original Merge is an overlay of the Rab7-633 and LAMP-1-561 images that were *originally obtained* in the experiment without contrast enhancement. Thus, the Original Merge image is shown for comparison to that of the Merge image.

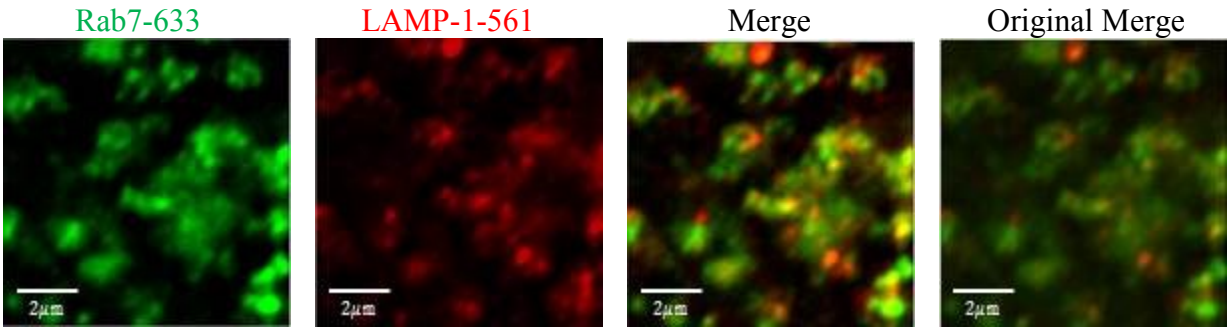

Figure 3.11 Rab7-633 & LAMP-1-561 Marked Endoyctic Compartments in C2C12 Cells

There are a large number of yellow regions in the Merge image in Figure 3.11. Thus, this reflects a very high degree of co-localization of Rab7-633 and LAMP-1-561 markers.

Table 3.14 reflects the average calculations obtained via Image Cross Correlation Spectroscopy analysis. Specifically, the number of clusters containing markers, $\langle N_{Species} \rangle$ and the average fractions of co-localization of Rab7-633 and LAMP-1-561 markers are represented. The average fraction of clusters containing Rab7-633 markers that also contain LAMP-1-561 markers is denoted by $\langle F(Rab7|LAMP-1) \rangle$. Likewise, the average fraction of clusters containing LAMP-1-561 markers that also contain Rab7-633 markers is denoted by $\langle F(LAMP-1|Rab7) \rangle$.

Table 3.14 Average Number of Clusters Containing Species and Fractions of Co-Localization of Rab7-633 & LAMP-1-561 Markers in C2C12 Cells

Species	$\langle N_{Species} \rangle$	$\langle F(Rab7\|LAMP-1) \rangle$	$\langle F(LAMP-1\|Rab7) \rangle$
Rab7-633	1.95 ± 0.14[1]		
LAMP-1-561	1.81 ± 0.20		
Rab7-633 & LAMP-1-561	1.46 ± 0.14	0.74 ± 0.04	0.86 ± 0.03

[1] Standard error.

3.2.5 Summary of Fractions & Comparison in C2C12

Table 3.15 is a summarized table of each of the averaged fractions of co-localization obtained for two species in C2C12 cells previously discussed.

Table 3.15 Summary of fractions of co-localization with Standard Error in C2C12 Cells

$\langle F(Red \mid Green) \rangle$	Rab5	Rab7	Rab11	LAMP-1
Rab5	-	0.46 ± 0.05	0.23 ± 0.02	0.32 ± 0.05
Rab7	0.53 ± 0.06[1]	-	N.D	0.74 ± 0.04
Rab11	0.44 ± 0.04	N.D	-	N.D
LAMP-1	0.31 ± 0.04	0.86 ± 0.03	N.D	-

N.D refers to "No Data". [1]Standard error

The results presented in Table 3.15 reflect the following; each cluster consisting of one marker for an endocytic compartment contains at least one other marker for another endocytic compartment.

The extent to which Rab5 markers associate with Rab7 markers is largest in magnitude in comparison to the association of Rab5 markers with LAMP-1 and Rab11 markers. This is a reasonable estimate as early endosomes mature into late endosomes thus some degree of co-existence is expected to occur among Rab5 and Rab7 markers occupying the same cluster. Additionally, the co-existence of Rab11 markers on compartments marked with Rab5 is expected as there may be some recycling of receptors occurring from the early endosome onto the recycling endosome to be recycled back to the plasma membrane. However, given there is some degree of co-existence of Rab5 and LAMP-1 markers on the same cluster, this measurement implies that Rab5 markers are not fully displaced on endosomes during the maturation step of early to late endosomes; Rab5 markers are still present on lysosomes.

The extent to which Rab7 markers associate with LAMP-1 markers is greater in comparison to the association of Rab7 markers with Rab5 markers. Consistent with the hypothesized claim that late endosomes fuse with lysosomes, perhaps a higher co-localization of Rab7 and LAMP-1 markers than Rab7 with Rab5 markers is expected.

The extent to which LAMP-1 markers associate with Rab7 markers is largest in magnitude in comparison to the association of LAMP-1 with Rab5 markers. This is promising such that co-localization among lysosomes and early endosome markers is not fully expected.

However, as previously mentioned, there is some degree of co-existence of Rab5 and LAMP-1 markers on the same cluster.

In summary, these results support the hypothesis for this thesis for markers in terms of their maturation and fusion steps. Additionally, this study has provided additional information that although these markers associate with appropriate endosomes as known in the literature, it has been inferred that these markers are not specifically unique to one endocytic compartment, and that they can be simultaneously present on one endosome, or cluster.

3.3 Co-localization of One Endocytic Marker with Two Other Endocytic Markers in C2C12 Cells

The previous section discussed the extent to which two markers are simultaneously found in one endosome or compartment. Chapter 3.3 focusses on the co-localization of three markers to determine if one cluster could have three markers present. Results show the co-localization of markers for the early, late, and lysosomal endocytic compartments are expected to associate to a lesser extent than the association of two markers.

As with the two color experiments, each of the secondary antibodies used for labelling their respective compartments consisted of an emission profile that did not overlap. The experimental procedure for immunofluorescent labelling of three markers in cells can be referred to Chapter 2.7.1. Laser scanning confocal microscopy imaging of two markers can be referred to in Chapter 2.10.3.3. Triple Image Cross Correlation Spectroscopy analysis can be referred to in Chapter 2.11.3.

3.3.1 Rab5-561, Rab7-633, & LAMP-1-488 Marked Compartments in C2C12 Cells

Figure 3.12 is a visual representation of contrast enhanced images of a cell labelled with Rab5 (in red), Rab7 (in green), and LAMP-1 (in blue). The Merge image is all three individual images merged.

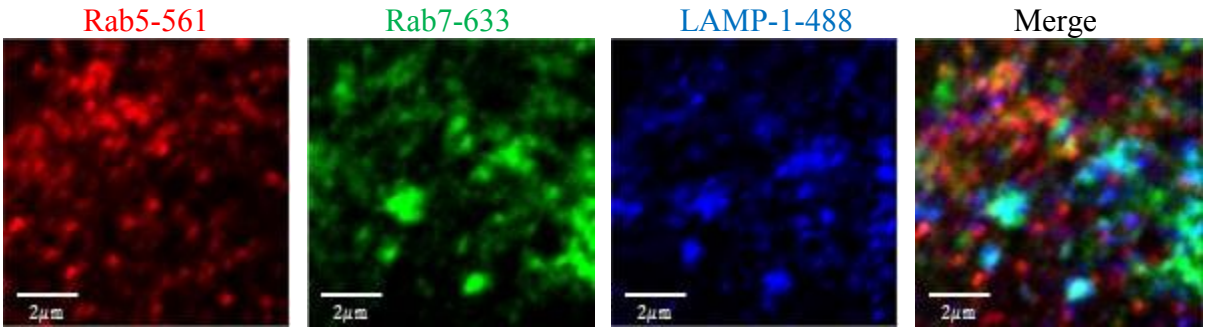

Figure 3.12 Rab5-561 & Rab7-633 & LAMP-1-488 Marked Endocytic Compartments in C2C12 Cells

In Figure 3.12, there appear to be some "yellow" spots observed to reflect Rab5-561 and Rab7-633 co-localization. Additionally, the observed purple spots in the image reflect the co-localization of Rab5-561 and LAMP-1-488 markers. Rab7-633 and LAMP-1-488 co-localize by the apparent "cyan" color observed due to the overlapping green and blue images.

In a three-color labelling experiment, one would observe the color white with 100% overlap of red, green, and blue. This is not immediately obvious, thus triple image cross correlation spectroscopy (TRICCS) is done to extract a quantitative representation for the association of three species.

Table 3.16 shows the number of images, n_{images} obtained in one experiment with the corresponding average number of clusters observed containing markers, $\langle N_{Species} \rangle$. Seventeen images were used for analysis; thirty images were obtained for this experiment, thus thirteen were rejected for analysis. These images reflect that of the measurements obtained for one and two color experiments, for which a much greater amount of images were obtained.

Table 3.16 Averaged Number of Clusters Containing Markers in C2C12 cells

Species	n_{images}	$\langle N_{Species} \rangle$
Rab5-561	17	2.80 ± 0.33[1]
Rab7-633	17	3.91 ± 0.44
LAMP-1-488	17	5.85 ± 0.43
Rab5-561 & Rab7-633	17	0.66 ± 0.14
Rab5-561 & LAMP-1-633	17	0.43 ± 0.09
Rab7-633 & LAMP-1-488	17	1.56 ± 0.25
Rab5-561 & Rab7-633 & LAMP-1-488	17	1.72 ± 0.41

[1] Standard error.

The most important observation to note is the similarities observed in comparison to one and two color experiments. The relative number of clusters containing individual species and number of clusters containing two species compare with previous results for two color experiments and shown in Table 3.11, Table 3.12, Table 3.13, and Table 3.14.

Table 3.16 reflects the numbers of clusters containing one marker ranges between 2.80-5.85. Additionally, the number of clusters in which two markers are observed simultaneously is also in agreement with previous experiments, such that the number of clusters of markers observed ranges between 0.43-1.56. There is slight variation with each individual measurement; however it must be remembered that this is a different sample for which these measurements were calculated. For further validation, the 10% standard error reflected in the measurement is in agreement with the 10% errors reflected in previous experiments.

In contrast to previous experiments, the number of clusters containing Rab5-561, Rab7-633, and LAMP-1-488 markers is 1.72. To fully understand this value, fractions of co-localization were calculated and are represented in Table 3.17.

Table 3.17 Average Fractions of Co-Localization of Endocytic Markers in C2C12 Cells

$\langle F(Rab5 \mid Rab7\ LAMP-1) \rangle$	$\langle F(Rab7 \mid Rab5\ LAMP-1) \rangle$	$\langle F(LAMP-1 \mid Rab5\ Rab7) \rangle$
0.56 ± 0.06[1]	0.42 ± 0.06	0.28 ± 0.05

[1] Standard error.

According to Table 3.17, approximately 56% of the clusters containing Rab5 markers also contain Rab7 and LAMP-1 markers. Approximately 42% of clusters containing Rab7 markers contain Rab5 and LAMP-1 markers. Lastly, approximately 28% of clusters containing LAMP-1 markers contain Rab5 and Rab7 markers.

In reference to Table 3.15, approximately 46% of clusters containing Rab5 markers also contain Rab7 markers and approximately 32% of clusters containing Rab5 markers also contain LAMP-1 markers. Thus, the 56% fraction of Rab5 clusters that contain Rab7 and LAMP-1 markers is an implication that there are a large number of complexes in which three species are present and possibly fewer compartments in which only two markers are present. In addition, this finding suggests that the population measured to contain Rab5 and Rab7 also contain LAMP-1.

In reference to Table 3.15, approximately 53% of clusters containing Rab7 markers also contain Rab5 markers and 74% of clusters containing Rab7 markers also contain LAMP-1 markers. Therefore, a 42% extent of co-localization of Rab7 with two markers is 20% less in comparison to Rab7/LAMP-1 association.

Lastly, as shown in Table 3.15, approximately 31% of clusters containing LAMP-1 markers contain Rab5 markers and approximately 86% of clusters containing LAMP-1 markers also contain Rab7 markers. Therefore, the 28% association of Rab5 with each of the other two markers makes sense and a small fraction of the clusters that contain LAMP-1 and Rab5 markers must also contain Rab7 markers.

This supports that compartments contain markers known to be specific for the early, late and lysosomal endocytic compartments in C2C12 cells. In addition, this data suggests that not only can one compartment contain all three markers, but Rab5 markers are present on late and lysosomal endocytic compartments and not displaced at the end of the endocytic pathway. Pairwise *and* three marker clusters are potentially observed in C2C12 cells. However, the complexes which are marked by two markers may also take into account a complex in which *one* other marker is also present.

3.4 Individually Labelled Endocytic Marked Compartments in A549 Cells

The data and analysis in Chapter 3.4 refer to confocal fluorescence microscopy images of A549 cells singly labelled with primary antibodies specific for markers of clathrin mediated endocytic compartments and fluorescent secondary antibodies specific for the corresponding primary antibodies. Primary and secondary antibody pairs corresponding to Rab5, Rab7, Rab11, and LAMP-1 were used to study markers specific for early, late, recycling, and lysosomal endocytic compartments in A549 cells, respectively.

Materials and methods corresponding to labelling of markers in cells can be found in Chapter 2.4. Laser scanning confocal microscopy imaging of one marker can be found in Chapter 2.10.3.1. Image Cross Correlation Spectroscopy can be referred to in Chapter 2.11.1.

3.4.1 Rab5-561 Marked Early Endocytic Compartments in A549 Cells

Rab5-561 was used to study the distribution and location of early endocytic compartments in A549 cells.

In Figure 3.13, images A and B correspond to images of two control samples; image A corresponds to one cell from a sample labelled with only the primary antibodies specific for Rab5 markers. Image B corresponds to one cell from a sample labelled with only the secondary antibodies specific for the primary antibodies for Rab5 markers. Image C is representative of one cell from a sample labelled with primary and secondary antibodies for Rab5-561 markers. Image D is a contrast enhanced image of image C for clearer visualization of the range of labelling efficiencies.

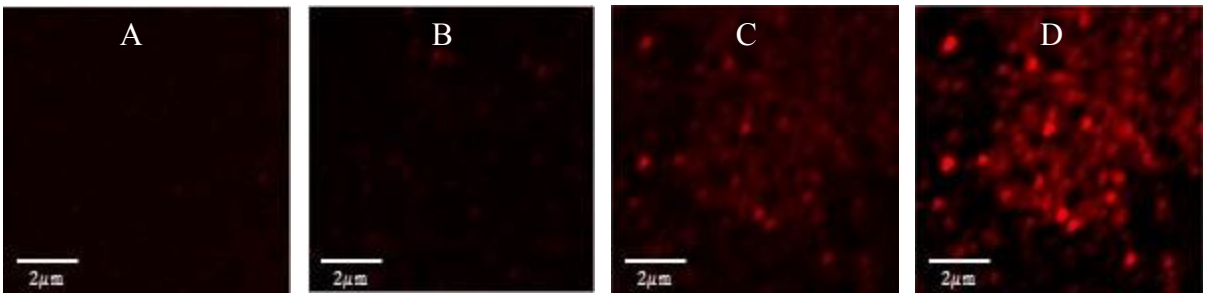

Figure 3.13 Images of Antibody Controls and Rab5-561 Marked Early Endocytic Compartments in A549 Cells

Image A corresponds to a sample labelled with only the primary antibodies specific for Rab5-561 markers. Image B corresponds to a sample labelled with only the secondary antibodies specific for the primary antibodies for Rab5 markers. Image C is representative of a cell sample labelled with primary and secondary antibodies for Rab5-561 markers. Image D is a contrast enhanced image of Image C for clearer visualization of the range of labelling efficiencies.

Images A and B in Figure 3.13 show very little fluorescence emitted the primary and secondary controls in cells, respectively. However, image B shows few red regions to indicate non-specific binding of Rab5-561 secondary antibodies. Thus, the minimal fluorescence emitted from the controls in cells shown in images A and B, validates the fluorescence emitted from Rab5-561 marked compartments shown in image C. Image C is thus a specific visual representation of Rab5-561 marked compartments that have not been saturated by the laser upon illumination, unlike some of the regions that appear to be saturated in image D due to contrast enhancement.

The data corresponding to Figure 3.13 is represented in Table 3.18. Table 3.18 is a representation of the averages of the auto correlation amplitude, fitted laser beam width, and average intensity of Rab5-561 markers from a data set of 10 images of the primary, 10 images of the secondary, and 26 images of Rab5-561. The values for each parameter are shown with the standard error.

Table 3.18 Averages of ICS Parameters for Images of Antibody Controls and Rab5-561 Marked Early Endocytic Compartments in A549 cells

Species	n_{images}	$\langle \mathbf{g}(\mathbf{0},\mathbf{0}) \rangle$	$\langle \boldsymbol{\omega}\ (\boldsymbol{\mu}\mathbf{m}) \rangle$	$\langle I_{avg.} \rangle$
Primary Control	10	0.003 ± 0.001[1]	0.33 ± 0.07	11.6 ± 0.2
Secondary Control	10	0.07 ± 0.01	0.28 ± 0.02	15.2 ± 0.8
Rab5-561	26	0.27 ± 0.03	0.31 ± 0.01	337 ± 12

[1] Standard error.

The average intensity of Rab5-561 markers in the observation region of the laser beam is approximately 337. After obtaining several images, the measurement of the intensity of Rab5-561 markers in the observation area is at least twenty-one-fold greater in comparison to the intensity of the controls. However, as shown in Figure 3.13, there is non-specific binding of the Rab5-561 secondary antibodies, which is based on the difference in intensity for the primary and secondary control. Thus, using the intensities and auto correlation amplitudes for primary, secondary, and positive controls for Rab5, there are approximately 345 Rab5-561 antibodies per cluster.

The value for the auto correlation amplitude for clusters containing Rab5-561 markers is approximately 0.27. The values obtained for the primary and secondary control amplitudes are at least three-fold less in magnitude than that of the measurement for the auto correlation amplitude for clusters containing Rab5-561 markers. This difference in magnitude is promising to reflect a specific estimate of the auto correlation amplitude corresponding to clusters containing Rab5-561 markers.

The fit for the true measurement of the laser beam is approximately 0.28 microns; therefore, the experimentally measured width for the laser beam for Rab5-561 marked endosomes arises from convolution. However, the endosomes are larger than approximately 0.31 microns in diameter.

3.4.2 Rab7-633 Marked Late Endocytic Compartments in A549 Cells

Rab7-633 was used to study the distribution and location of late endocytic compartments in A549 cells.

In Figure 3.14, image A corresponds to a sample labelled with only the primary antibodies specific for Rab7 markers. Image B corresponds to a sample labelled with only the secondary antibodies specific for the primary antibodies for Rab7 markers. Image C is representative of a cell sample labelled with primary and secondary antibodies for Rab7-633 markers. Image D is a contrast enhanced image of Image C for clearer visualization of the range of labelling efficiencies.

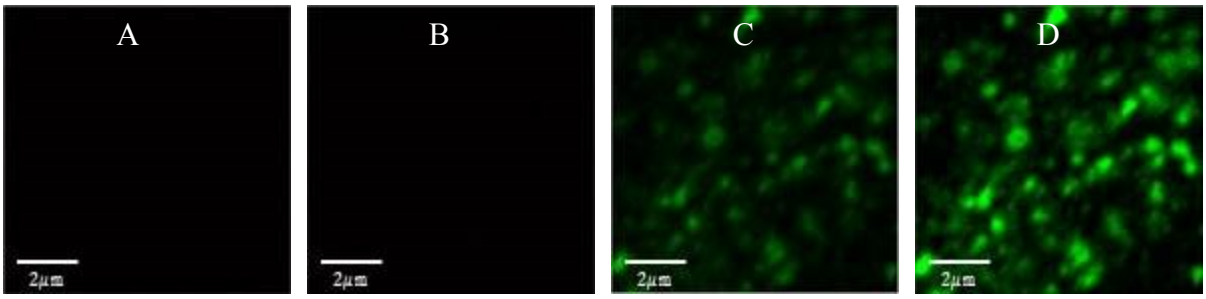

Figure 3.14 Rab7 Late Endocytic Markers in A549 Cells

Image A corresponds to a sample labelled with only the primary antibodies specific for Rab7 markers. Image B corresponds to a sample labelled with only the secondary antibodies specific for the primary antibodies for Rab7 markers. Image C is representative of a cell sample labelled with primary and secondary antibodies for Rab7 markers. Image D is a contrast enhanced image of image C for clearer visualization of the range of labelling efficiencies.

Images A and B in Figure 3.14 show minimal fluorescence emitted from the primary and secondary controls in cells, respectively. This minimal fluorescence emitted from the controls in cells in comparison to the fluorescence emitted as shown in image C means that the fluorescence in the cell shown in image C is a specific representation of Rab7-633 marked late endocytic compartments. Image D is shown for contrast enhancement.

The data corresponding to Figure 3.14 is represented in Table 3.19. In Table 3.19, the averages of the auto correlation amplitude, fitted laser beam width, and average intensity of Rab7-633 markers from a data set of primary, secondary, and Rab7-633 are shown. The values for each parameter are shown with the standard error.

Table 3.19 Averages of ICS Parameters for Images of Antibody Controls and Rab7-633 Marked Late Endocytic Compartments in A549 cells

Species	n_{images}	$\langle \mathbf{g(0,0)} \rangle$	$\langle \boldsymbol{\omega}\ (\boldsymbol{\mu m}) \rangle$	$\langle I_{avg.} \rangle$
Primary Control	10	0.08 ± 0.03[1]	0.33 ± 0.22	13.4 ± 0.1
Secondary Control	10	0.06 ± 0.0006	0.26 ± 0.01	20.0 ± 0.7
Rab7-633	26	0.80 ± 0.21	0.43 ± 0.01	344 ± 26

[1] Standard error.

The average intensity of Rab7-633 markers in the observation area of the laser beam is approximately 344. This intensity is at least ten-fold greater in comparison to the intensity corresponding to the primary and secondary controls. As discussed and shown previously in Equation 28, one can infer and calculate the estimate for the average number of antibodies per cluster from the intensities and auto correlation amplitudes of the controls; the data for this experiment suggests that there are approximately 654 antibodies of Rab7 per cluster.

The auto correlation amplitude for clusters containing Rab7 markers is approximately 0.80. The average auto correlation amplitudes corresponding to the primary and secondary controls are at least 13 fold less in magnitude than the measurement of the auto correlation amplitude for clusters containing Rab7 markers; which is indicative based on the low intensity of fluorescence emitted from primary and secondary antibodies.

Lastly, the fit for ω corresponding to Rab7-633 marked compartments is approximately 0.43 microns and the fit corresponding to the secondary control is 0.26 microns. Like Rab5-561 marked compartments, this experimental value also arises from convolution. Using Figure 2.6, the extrapolated diameter of Rab11 marked compartments is approximately 0.52 microns.

3.4.3 Rab11-633 Marked Recycling Endocytic Compartments in A549 Cells

Rab11-633 was used to study the distribution and location of recycling endocytic compartments in A549 cells.

In Figure 3.15, image A corresponds to a sample labelled with only the primary antibodies specific for Rab11 markers. Image B corresponds to a sample labelled with only the secondary antibodies specific for the primary antibodies for Rab11 markers. Image C is representative of a cell sample labelled with primary and secondary antibodies for Rab11-633

markers. Image D is a contrast enhanced image of Image C for clearer visualization of the range of labelling efficiencies.

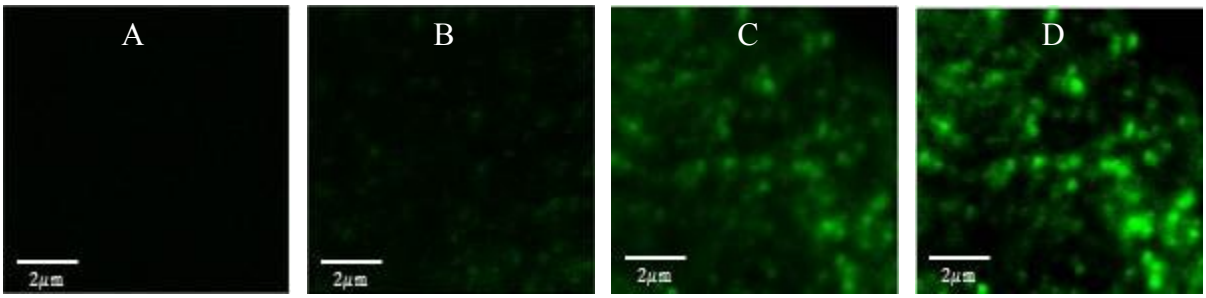

Figure 3.15 Rab11-633 Marked Recycling Endocytic Marked Compartments in A549 Cells.

Image A corresponds to a sample labelled with only the primary antibodies specific for Rab11 markers. Image B corresponds to a sample labelled with only the secondary antibodies specific for the primary antibodies for Rab11 markers. Image C is representative of a cell sample labelled with primary and secondary antibodies for Rab11-633 markers. Image D is a contrast enhanced image of Image C for clearer visualization of the range of labelling efficiencies.

Images A and B in Figure 3.15 show the minimal fluorescence emitted from the primary and secondary controls in cells, respectively. However, there is non-specific binding occurring as shown in image B, due to the presence of faint green regions. However, image C reflects specific labelling of Rab11-633 compartments. This minimal fluorescence emitted from the primary and secondary controls in cells validates the fluorescence emitted as shown from an image labeled with primary antibodies specific for Rab11 markers and secondary antibodies specific for the primary antibodies, in image C. Image C is a specific representation of Rab11 marked recycling endocytic compartments that have not been saturated by the laser upon illumination. Image D is shown for contrast enhancement.

Table 3.20 shows the averages of the auto correlation amplitude, fitted laser beam width, and average intensity from a data set for 4 images of primary, 10 images of secondary, and 31 images of Rab11 positive controls. The values for each parameter are shown with the standard error.

Table 3.20 Averages of ICS Parameters for Images of Antibody Controls and Rab11-633 Marked Recycling Endocytic Compartments in A549 cells

Species	n_{images}	$\langle g(0,0) \rangle$	$\langle \omega\ (\mu m) \rangle$	$\langle I_{avg.} \rangle$
Primary Control	4	0.002 ± 0.001[1]	0.43 ± 0.11	35.9 ± 0.2
Secondary Control	10	0.08 ± 0.01	0.33 ± 0.03	71.7 ± 4.0
Rab11-633	31	0.34 ± 0.03	0.36 ± 0.01	499 ± 28

[1]Standard Error

The average intensity of Rab11-633 markers in the observation area of the laser beam is approximately 499. The intensities for the corresponding primary and secondary controls are approximately seven-fold less in magnitude compared to the intensity of Rab11-633 markers but none the less are still a fraction of the overall intensity emitted from clusters of Rab11-633 markers. As shown in Figure 3.15, image B has some non-specific binding given the intensity is measured to be on average 71.7. Thus, on average, the number of Rab11 antibodies per fluorescent cluster is approximately 51 antibodies per cluster. This is a small number of antibodies observed per cluster, smallest in magnitude than what has been observed in previous experiments.

The auto correlation amplitude for clusters containing Rab11-633 markers is approximately 0.34. The amplitudes corresponding to the primary and secondary controls are at least four-fold less in magnitude than the measurement of the auto correlation amplitude for clusters containing Rab11-633 markers. Specifically, the secondary control auto correlation amplitude is 0.08, which is encouraging that although there is non-specific binding occurring, there is little correlation of the intensity fluctuation to contribute to the true measurement of Rab11 clusters.

Lastly, the fit for ω is approximately 0.36 microns which is approximately the same size of the secondary control. However, this value reflects *slight* convolution, similar to Rab7 marked compartments. In this case, the true ω_0 is larger than 0.24 microns. Thus, Figure 2.6 can be adjusted accordingly to calculate a diameter of approximately the same size as 0.30 microns.

3.4.4 LAMP-1 Marked Lysosomal Endocytic Compartments in A549 Cells

LAMP-1 Marked Lysosomal Endocytic Compartments were studied in three separate experiments using three secondary antibodies with different fluorescent probes. Different fluorescent probes were required for double labelling experiments to be discussed later in this chapter. The three LAMP-1 experiments used were Alexa Fluor 488, 555, and 633 secondary antibodies (labelled LAMP-1-488, LAMP-1-555, and LAMP-1-633).

3.4.4.1 LAMP-1 488 Marked Lysosomal Endocytic Compartments in A549 Cells

LAMP-1 488 was used to study the distribution and location of lysosomal endocytic compartments in A549 cells.

In Figure 3.16, image A corresponds to a sample labelled with only the primary antibodies specific for LAMP-1 markers. Image B corresponds to a sample labelled with only the secondary antibodies specific for the primary antibodies for LAMP-1 markers. Image C is representative of a cell sample labelled with primary and secondary antibodies for LAMP-1-488 markers. Image D is a contrast enhanced image of image C for clearer visualization of the range of labelling efficiencies.

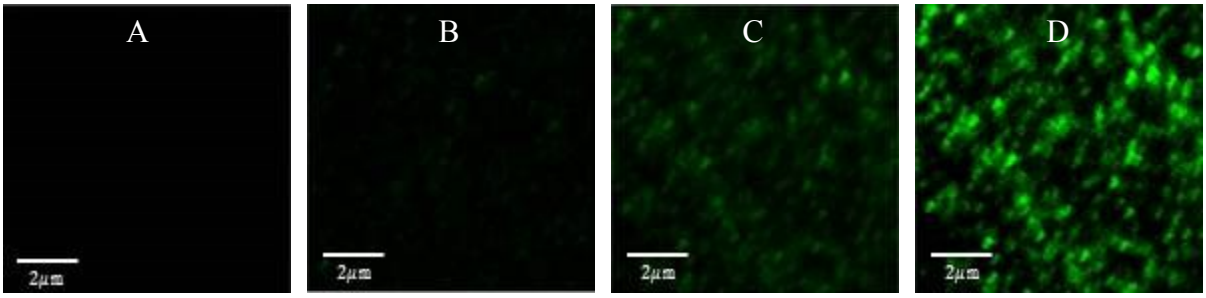

Figure 3.16 LAMP-1-488 Marked Lysosomal Endocytic Compartments in A549 Cells

Image A corresponds to a sample labelled with only the primary antibodies specific for LAMP-1 markers. Image B corresponds to a sample labelled with only secondary antibodies specific for the primary antibodies for LAMP-1 markers. Image C is representative of a cell sample labelled with primary and secondary antibodies for LAMP-1-488 markers. Image D is a contrast enhanced image of Image C for clearer visualization of the range of labelling efficiencies.

Images A and B in Figure 3.16 illustrate the minimal fluorescence emitted from the primary and secondary controls in cells, respectively. The minimal amount of fluorescence emitted from the controls in cells validates the fluorescence emitted the cell shown in image C

for LAMP-1-488 markers. Image C is a clear representation of LAMP-1-488 marked lysosomal endocytic compartments that have not been saturated by the laser upon illumination. Image D is shown for better visualization.

The data corresponding to Figure 3.16 is represented in Table 3.21. Table 3.21 is a representation of the averages of the auto correlation amplitude, fitted laser beam width, and average intensity of LAMP-1-488 markers from a data set of 4 images of primary, 10 images of secondary, and 31 images of LAMP-1-488 positive controls. The values for each parameter are shown with standard error.

Table 3.21 Averages of ICS Parameters for Images of Antibody Controls and LAMP-1 488 Marked Lysosomal Endocytic Compartments in A549 Cells

Species	n_{images}	$\langle \mathbf{g(0,0)} \rangle$	$\langle \boldsymbol{\omega}\ (\boldsymbol{\mu m}) \rangle$	$\langle I_{avg.} \rangle$
Primary Control	4	0.001 ± 0.000[1]	0.45 ± 0.07	16.0 ± 0.18
Secondary Control	10	0.09 ± 0.02	0.28 ± 0.02	27.9 ± 1.7
LAMP-1 488	31	0.30 ± 0.07	0.28 ± 0.01	200 ± 6

[1] Standard error.

The average intensity of LAMP-1 markers in the observation region of the laser beam is approximately 200. The intensities for the corresponding controls are at least seven-fold less than the intensity measurement of LAMP-1 markers. On average, there are approximately 51 LAMP-1-488 antibodies per cluster.

The auto correlation amplitude for clusters containing LAMP-1-488 markers is approximately 0.30. The average auto correlation amplitudes corresponding to the primary and secondary controls are at least one-hundred-fold less in magnitude than the measurement of the auto correlation amplitude for clusters containing LAMP-1-488 marked compartments. This is a promising measurement to indicate a specific representation for the auto correlation amplitude corresponding to clusters containing LAMP-1-488 markers.

The fit for ω corresponding to LAMP-1 488 marked compartments is approximately 0.28 microns, which is the same size for the true beam width as measured by the secondary control. These results suggest the measurement of the beam width of LAMP-1-488 clusters does not arise from convolution. In addition, the approximate size of LAMP-1 marked endosomes is 0.28 microns in diameter.

3.4.4.2 LAMP-1 -561 Marked Lysosomal Endocytic Compartments in A549 Cells

LAMP-1-561 was used to study the distribution and location of lysosomal endocytic compartments in C2C12 cells.

In Figure 3.17, Image A corresponds to a sample labelled with only the primary antibodies specific for LAMP-1 markers. Image B corresponds to a sample labelled with only the secondary antibodies specific for the primary antibodies for LAMP-1 markers. Image C is representative of a cell sample labelled with primary and secondary antibodies for LAMP-1-561 markers. Image D is a contrast enhanced image of Image C for clearer visualization of the range of labelling efficiencies.

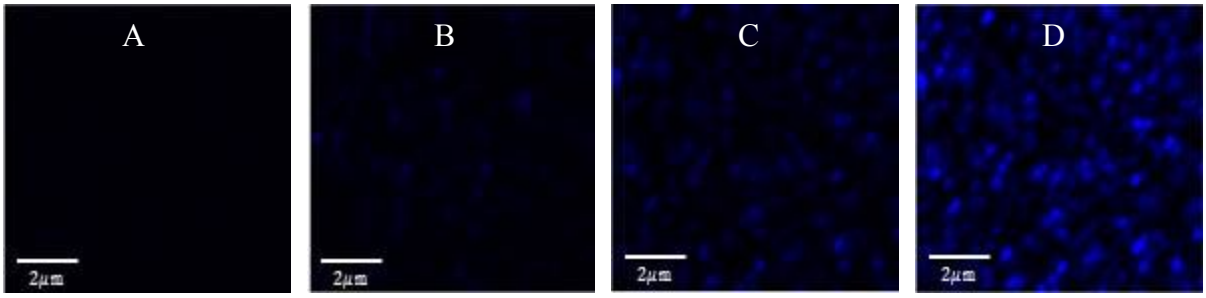

Figure 3.17 LAMP-561 Marked Late Endocytic Compartments in A549 Cells

Image A corresponds to a sample labelled with only the primary antibodies specific for LAMP-1 markers. Image B corresponds to a sample labelled with only the secondary antibodies specific for the primary antibodies for LAMP-1 markers. Image C is representative of a cell sample labelled with primary and secondary antibodies for LAMP-1 markers. Image D is a contrast enhanced image of image C for clearer visualization of the range of labelling efficiencies.

Images A and B in Figure 3.17 illustrate the minimal fluorescence emitted from the primary and secondary controls in cells, respectively. However, there is some fluorescence emitted from the secondary control in the cell, shown by the presence of faint blue regions in image B. Nonetheless, this minimal fluorescence emitted from the controls implies the fluorescence emitted from the cell as shown in image C is representative of LAMP-1-561 markers.

The data corresponding to Figure 3.17 is represented in Table 3.22. Table 3.22 is a representation of the averages of the auto correlation amplitude, fitted laser beam width, and

average intensity of LAMP-1 markers from a data set of multiple images of the primary, secondary, and LAMP-1 positive controls. The values for each parameter are shown along with the standard error.

Table 3.22 Averages of ICS Parameters for Images of Antibody Controls and LAMP-1-561 Marked Lysosomal Endocytic Compartments in A549 cells

Species	n_{images}	$\langle \mathbf{g(0,0)} \rangle$	$\langle \boldsymbol{\omega}\ (\boldsymbol{\mu m}) \rangle$	$\langle I_{avg.} \rangle$
Primary Control	10	0.02 ± 0.02[1]	0.40 ± 0.14	12.7 ± 0.22
Secondary Control	10	0.46 ± 0.14	0.24 ± 0.01	30.0 ± 1.4
LAMP-1-561	32	0.53 ± 0.04	0.36 ± 0.01	453 ± 32

[1] Standard error.

The intensity of LAMP-1-561 markers in the observation region of the laser beam is approximately 453. The intensities for the corresponding controls are at least fifteen-fold less than the intensity of LAMP-1-561 markers. The intensity of the secondary control is at least two-fold greater than the intensity of the primary control; therefore, although the intensity due to this non-specific binding will impact the intensity measurement of LAMP-1-561 markers, the intensity measurement of LAMP-1-561 markers is specific.

The precise estimate for the average number of antibodies per cluster from the intensities and auto correlation amplitudes of the controls; as such, the data for this experiment suggests that there are approximately 28 LAMP-1 antibodies per cluster.

The auto correlation amplitude corresponding to clusters containing LAMP-1-561 is approximately 0.53. The auto correlation amplitudes corresponding to the primary controls are less in magnitude than the measurement of LAMP-1-561 marked compartments. However, the amplitude for the secondary control is only 0.07 units less than the amplitude of LAMP-1-561 clusters. Thus, this observation also provides some indication that the non-specific binding may have some influence on the measurement of the auto correlation amplitude for LAMP-1 561 marked clusters.

The fit for ω is approximately 0.36 microns and the true fit of the laser beam is 0.24 microns. Using Figure 2.6, the extrapolated diameter for LAMP-1 marked compartments is approximately 0.42 microns.

3.4.4.3 LAMP-1 -633 Marked Lysosomal Endocytic Compartments in A549 Cells

LAMP-1-633 was used to study the distribution and location of lysosomal endocytic compartments in A549 cells.

In Figure 3.18, image A corresponds to a sample labelled with only the primary antibodies specific for LAMP-1 markers. Image B corresponds to a sample labelled with only the secondary antibodies specific for the primary antibodies for LAMP-1 markers. Image C is representative of a cell sample labelled with primary and secondary antibodies for LAMP-1-633 markers. Image D is a contrast enhanced image of image C for clearer visualization of the range of labelling efficiencies.

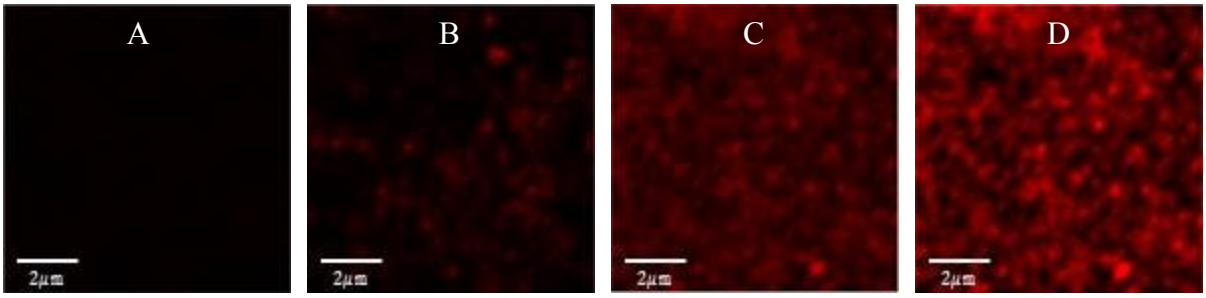

Figure 3.18 LAMP-1-633 Endocytic Marked Compartments in A549 Cells

Image A corresponds to a sample labelled with only the primary antibodies specific for LAMP-1 markers. Image B corresponds to a sample labelled with only the secondary antibodies specific for the primary antibodies for LAMP-1 markers. Image C is representative of a cell sample labelled with primary and secondary antibodies for LAMP-1 markers. Image D is a contrast enhanced image of Image C for clearer visualization of the range of labelling efficiencies.

Images A and B in Figure 3.18 illustrate the minimal fluorescence emitted from the primary and secondary controls in cells, respectively. However, there is definitely some fluorescence emitted from the secondary control in the cell to indicate some non-specific binding as shown in image B. Nonetheless, this minimal fluorescence emitted from the controls validates the fluorescence emitted from a cell image labeled with primary antibodies specific for LAMP-1 markers and secondary antibodies specific for the primary antibodies. Image C is a clear representation of LAMP-1-633 marked lysosomal endocytic compartments that have not been saturated by the laser upon illumination. Image D is shown for clear visualization.

The data corresponding to Figure 3.7 is represented in Table 3.23. Table 3.23 is a representation of the averages of the auto correlation amplitude, fitted laser beam width, and average intensity of LAMP-1 markers from a data set of multiple images of the primary, secondary, and LAMP-1-633. The values for each parameter are shown along with the standard error.

Table 3.23 Averages of ICS Parameters for Images of Antibody Controls and LAMP-1-633 Marked Lysosomal Endocytic Compartments in A549 cells

Species	$\langle \mathbf{g(0,0)} \rangle$	$\langle \boldsymbol{\omega}\ (\boldsymbol{\mu m}) \rangle$	$\langle I_{avg.} \rangle$
Primary Control	0.004 ± 0.003[1]	0.33 ± 0.04	13.3 ± 0.4
Secondary Control	0.25 ± 0.04	0.37 ± 0.03	39.8 ± 4.6
LAMP-1-633	0.10 ± 0.01	0.33 ± 0.01	468 ± 29

[1] Standard error.

Last, the average intensity of LAMP-1-633 markers in the observation region of the laser beam is approximately 468 .The intensities for the corresponding controls are at least eleven-fold less in comparison to that of the measurement of LAMP-1-633 markers. This low intensity is promising and indicates that although there is some small degree of non-specific binding, it does not dominate the system and the positive LAMP-1-633 measurement is reliable.

One can infer and calculate the estimate for the average number of antibodies per cluster from the intensities and auto correlation amplitudes of the controls; thus the number of LAMP-1 antibodies per cluster as it pertains to the data obtained in this experiment is approximately 6 antibodies per cluster.

The auto correlation amplitude corresponding to clusters containing LAMP-1-633 is approximately 0.10. The auto correlation amplitudes corresponding to the primary control is at least sixty-two-fold less in magnitude than the measurement of LAMP-1 marked compartments. However, there is a relatively large auto correlation amplitude corresponding to the secondary antibody to potentially indicate non-specific binding, as was shown with LAMP-1-555 secondary non-specific binding.

The fit for ω is approximately 0.33 microns. The fit obtained for LAMP-1 633 marked compartments indicates the diameter of clusters containing LAMP-1 633 markers is approximately the same size of the laser beam width.

3.4.5 Comparisons of Endocytic Marked Compartments in A549 Cells

The purpose of this section is to quantitatively compare each species from the data obtained. Each of the data discussed in Chapter 3.4 is summarized below in Table 3.24 for further interpretation and comparison.

Table 3.24 Summary of Averages of ICS Parameters for Cells Labelled with Markers of Endocytic Compartments

Species	n_{images}	$\langle g(0,0) \rangle$	$\langle \omega\ (\mu m) \rangle$	$\langle I_{avg.} \rangle$
Rab5-561	31	0.27 ± 0.03[1]	0.31 ± 0.01	337 ± 12
Rab7-633	26	0.80 ± 0.21	0.43 ± 0.01	344 ± 26
Rab11-633	31	0.34 ± 0.03	0.36 ± 0.01	499 ± 28
LAMP-1-488	30	0.30 ± 0.07	0.28 ± 0.01	200 ± 6
LAMP-1-561	32	0.53 ± 0.04	0.36 ± 0.01	453 ± 32
LAMP-1 633	26	0.10 ± 0.01	0.33 ± 0.01	468 ± 29

This data has been previously shown; the purpose is to compare and contrast each of the averaged parameters obtained. [1] Standard error.

In Table 3.24, the autocorrelation amplitude ranges between 0.20-0.50. The auto correlation amplitude does not reflect any obvious trend associated with the progression of the clathrin mediated endocytic pathway, as shown with C2C12 cells. One key feature one may observe from this data is the relatively large auto correlation amplitude observed for Rab7 markers.

Additionally, the fit for ω ranges between 0.31-0.43 microns. Similarly with the auto correlation amplitude, the fit for the laser beam is constant, reflecting no specific trend. As shown, the corresponding extrapolated diameter for each endosome ranges in size of approximately 0.30-0.50 microns.

The average intensity for each species of interest ranges between 300–600.There is no absolute trend in terms of the intensity as the intensity of fluorescence emission from a species

can vary with experiments and is dependent on transmittance of light to the sample and gain of intensity.

As shown earlier in this Chapter corresponding to markers in C2C12 cells, one can derive expressions from the data obtained to calculate the average number of clusters that contain a specific species, , $\langle N_{Species} \rangle$, the number of clusters that contain species per square micron, ⟨CD⟩, and the relative degree of aggregation for the number of species per cluster, ⟨DA⟩. The averaged calculations are in reference to the data obtained and represented in Table 3.25.

Table 3.25 Averages of Derived ICS Parameters for Cells Labelled with Markers for Endocytic Compartments in A549 Cells

Species	$\langle N_{Species} \rangle$	$\langle CD \rangle$	$\langle DA \rangle$
Rab5-561	4.83 ± 0.56[1]	17.1 ± 1.8	89.8 ± 9.7
Rab7-633	1.94 ± 0.20	4.02 ± 0.68	227 ± 29
Rab11-633	3.56 ± 0.65	9.09 ± 0.75	163 ± 13
LAMP-1-488	4.88 ± 0.42	20.1 ± 1.8	57.1 ± 11
LAMP-1-561	2.24 ± 0.16	5.57 ± 0.49	221 ± 16
LAMP-1-633	11.1 ± 0.8	3.86 ± 0.38	43.6 ± 2.0

Calculations are based on the data represented in Table 3.24. [1] Standard error.

In Table 3.25, the average number of clusters and clusters per square micron that contain a marker of an endocytic compartment reveals no specific trend with the progression of the clathrin mediated endocytic pathway.

3.5 Co-localization of Endocytic Marked Compartments in A549 Cells

In this section, as with C2C12 cells, the pairwise co-localization of markers was studied in A549 cells.

In this section, the following experimental combinations were studied; Rab5-561 & Rab7-633, Rab5-561 & Rab11-633, Rab5-561 & LAMP-1-631, and Rab7-631 & LAMP-1-561.

3.5.1 Rab5-561 & Rab7-631 Marked Endocytic Compartments in A549 Cells

Cells were doubly labelled for Rab5-561 and Rab7-633 markers; these markers are known to be specific for early and late endosomes, respectively. Figure 3.19 shows contrast enhanced images of Rab5-561, in red, and Rab7-633, in green, marked compartments in one cell.

The Merge image is an overlay of the Rab5-561 and Rab7-631 contrast enhanced images. The Original Merge is an overlay of the Rab5-561 and Rab7-631 images that were *originally obtained* in the experiment without contrast enhancement. Thus, the Original Merge image is shown for comparison to that of the Merge image.

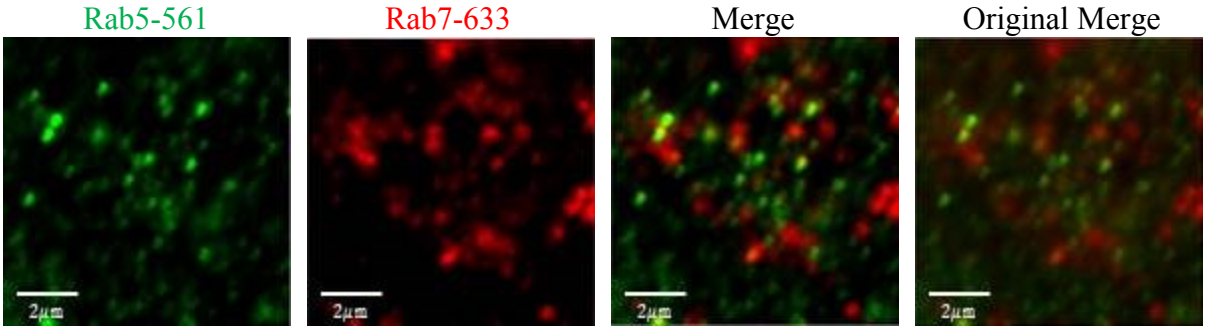

Figure 3.19 Rab5-561 & Rab7-633 Marked Endocytic Compartments in A549 Cells

The Merge image in Figure 3.8 reflects few regions of yellow clusters to imply some co-localization of Rab5-561 and Rab7-633 markers.

Table 3.26 reflects the average calculations obtained via Image Cross Correlation Spectroscopy analysis. Specifically, the number of clusters containing markers, $\langle N_{Species} \rangle$ and the average fractions of co-localization of Rab5-561 and Rab7-631 markers are represented. The average fraction of clusters containing Rab5-561 markers that also contain Rab7-631 markers is denoted by $\langle F(Rab5|Rab7) \rangle$. Likewise, the average fraction of clusters containing Rab7-631 markers that also contain Rab5-561 markers is denoted by $\langle F(Rab7|Rab5) \rangle$.

Table 3.26 Average Number of Clusters Containing Species and Fractions of Co-Localization of Rab5-561 & Rab7-633 Marked Endocytic Compartments in A549 Cells

Species	$\langle N_{Species} \rangle$	$\langle F(Rab5\|Rab7) \rangle$	$\langle F(Rab7\|Rab5) \rangle$
Rab5-561	4.44 ± 0.40[1]		
Rab7-633	5.44 ± 0.46		
Rab5-561 & Rab7-633	2.09 ± 0.21	0.50 ± 0.03	0.39 ± 0.03

[1] Standard error.

The calculations for the average number of clusters of species represented in Table 3.26 reflect that there are approximately 4.44 clusters contain Rab5-561 markers and there are approximately 5.44 clusters containing Rab7-633 markers. Lastly, there are approximately 2.09 clusters of that contain both Rab5-561 and Rab7-633 markers.

The calculations for the average fractions of co-localization represented in Table 3.26 reflect on average approximately 50% of clusters that contain Rab5-561 markers also contain Rab7-633 markers and approximately 39% of the clusters containing Rab7-633 markers also contain Rab5-561 markers.

3.5.2 Rab5-561 & Rab11-633 Marked Compartments in A549 Cells

Cells were doubly labelled for Rab5-561 and Rab11-633 markers to study the pairwise co-localization of the early and recycling endocytic markers, respectively.

Figure 3.20 shows contrast enhanced images of Rab5-561, in red, and Rab11-633, in green, marked compartments in one cell. The Merge image is an overlay of the Rab5-561 and Rab11-633 contrast enhanced images. The Original Merge is an overlay of the Rab5-561 and Rab11-633 images that were *originally obtained* in the experiment without contrast enhancement. Thus, the Original Merge image is shown for comparison to that of the Merge image.

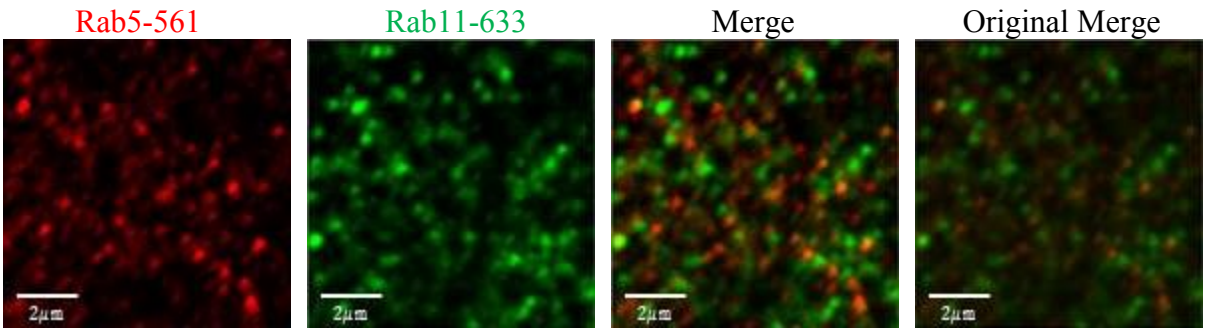

Figure 3.20 Rab5-561 & Rab11-633 Marked Endocytic Compartments in A549 Cells

From a visual perspective, the Merge image in Figure 3.20 shows a small degree of co-localization among Rab5-561 and Rab11-633 markers occupying the same cluster.

Table 3.27 reflects the average calculations obtained via Image Cross Correlation Spectroscopy analysis. Specifically, the number of clusters containing markers, $\langle N_{Species} \rangle$ and the average fractions of co-localization of Rab5-561 and Rab11-633 markers are represented. The average fraction of clusters containing Rab5-561 markers that also contain Rab11-633 markers is denoted by $\langle F(Rab5|Rab11) \rangle$. Likewise, the average fraction of clusters containing Rab11-633 markers that also contain Rab5-561 markers is denoted by $\langle F(Rab11|Rab5) \rangle$.

Table 3.27 Average Number of Clusters Containing Species and Fractions of Co-Localization of Rab5-561 & Rab11-633 Markers in A549 Cells

Species	$\langle N_{Species} \rangle$	$\langle F(Rab5\|Rab11) \rangle$	$\langle F(Rab11\|Rab5) \rangle$
Rab5-561	4.01 ± 0.43		
Rab11-633	2.57 ± 0.32		
Rab5-561 & Rab11-633	0.85 ± 0.07	0.28 ± 0.04	0.37 ± 0.03

[1] Standard error.

The calculations for the average number of clusters of species represented in Table 3.27 reflect that there are approximately 4.01 clusters containing Rab5-561 markers and there are approximately 2.57 clusters containing Rab11-633 markers. Lastly, there are approximately 0.85 clusters that contain both Rab5-561 and Rab11-633 markers.

The calculations for the average fractions of co-localization represented in Table 3.27 reflect on average approximately 28% of clusters that contain Rab5-561 markers also contain Rab11-633 markers and approximately 37% of the clusters containing Rab11-633 markers also contain Rab5-561 markers.

3.5.3 Rab5-561 & LAMP-1-633 Marked Compartments in A549 Cells

Cells were doubly labelled for Rab5-561 and LAMP-1-633 markers to study the pairwise co-localization of the early and lysosomal endocytic markers, respectively.

Figure 3.21 shows contrast enhanced images of Rab5-561, in red, and LAMP-1-633, in green, marked compartments in one cell. The Merge image is an overlay of the Rab5-561 and

LAMP-1-633 contrast enhanced images. The Original Merge is an overlay of the Rab5-561 and LAMP-1-633 images that were *originally obtained* in the experiment without contrast enhancement. Thus, the Original Merge image is shown for comparison to that of the Merge image.

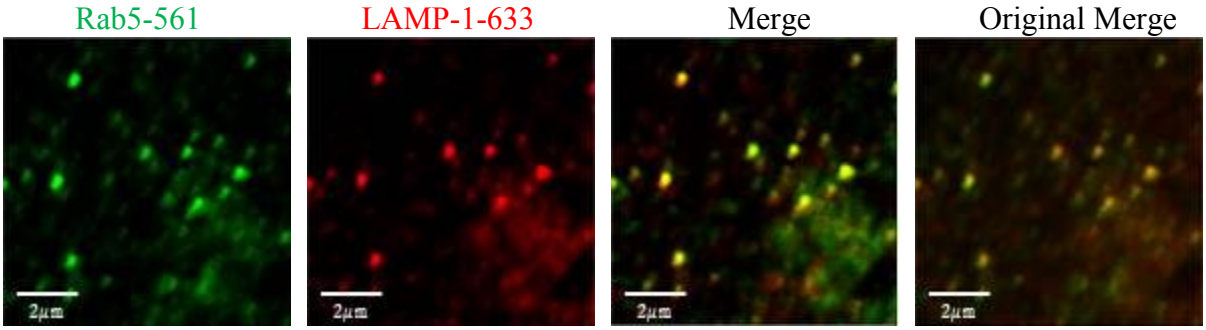

Figure 3.21 Rab5-561 & LAMP-1-633 Marked Endocytic Compartments in A549 Cells.

From a visual perspective, the Merge image in Figure 3.21 there appears to be a large number of yellow clusters. Thus, there is a very high co-localization among Rab5-561 and LAMP-1-633 markers.

Table 3.28 reflects the average calculations obtained via Image Cross Correlation Spectroscopy analysis. Specifically, the number of clusters containing markers, $\langle N_{Species} \rangle$ and the average fractions of co-localization of Rab5-561 and LAMP-1-633 markers are represented. The average fraction of clusters containing Rab5-561 markers that also contain LAMP-1-633 markers is denoted by $\langle F(Rab5|LAMP-1) \rangle$. Likewise, the average fraction of clusters containing LAMP-1-633 markers that also contain Rab5-561 markers is denoted by $\langle F(LAMP-1|Rab5) \rangle$.

Table 3.28 Average Number of Clusters Containing Species and Fractions of Co-Localization of Rab5-561 & LAMP-1-633 Markers in A549 Cells

Species	$\langle N_{Species} \rangle$	$\langle F(Rab5 \mid LAMP-1) \rangle$	$\langle F(LAMP-1 \mid Rab5) \rangle$
Rab5-561	4.59 ± 0.69[1]		
Lamp-1-633	4.69 ± 0.59		
Rab5-561 & Lamp-1-633	3.55 ± 0.47	0.82 ± 0.04	0.80 ± 0.05

[1] Standard error.

The calculations for the average number of clusters of species represented in Table 3.28 reflect that there are approximately 4.59 clusters containing Rab5-561 markers and there are also approximately 4.69 clusters containing LAMP-1-633 markers. Lastly, there are approximately 3.55 clusters that contain both Rab5-561 and LAMP-1-633 markers.

The calculations for the average fractions of co-localization represented in Table 3.28 reflect on average approximately 82% of clusters that contain Rab5-561 markers also contain LAMP-1-633 markers and approximately 80% of the clusters containing LAMP-1-633 markers also contain Rab5-561 markers.

3.5.4 Rab7-633 & LAMP-1-561 Marked Compartments in A549 Cells

Cells were doubly labelled for Rab7-633 and LAMP-1-561 markers to study the pairwise co-localization of the late and lysosomal endocytic markers, respectively.

Figure 3.22 shows contrast enhanced images of Rab7-633, in red, and LAMP-1-561, in green, marked compartments in one cell. The Merge image is an overlay of the Rab7-633 and LAMP-1-561 contrast enhanced images. The Original Merge is an overlay of the Rab7-633 and LAMP-1-561 images that were *originally obtained* in the experiment without contrast enhancement. Thus, the Original Merge image is shown for comparison to that of the Merge image.

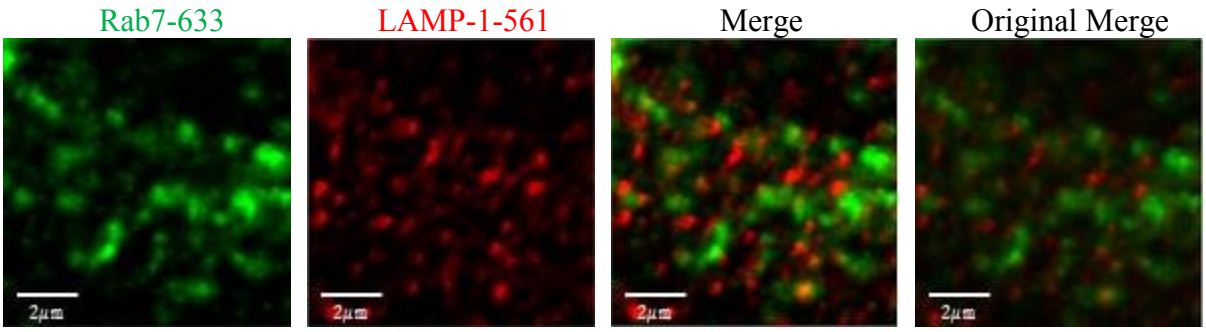

Figure 3.22 Rab7-633 & LAMP-1-561 Marked Endocytic Compartments in A549 Cells

From a visual perspective, the Merge image in Figure 3.22 small degree of co-localization, if any, due to few "yellow regions" one can observe in the Merge image.

Table 3.29 reflects the average calculations obtained via Image Cross Correlation Spectroscopy analysis. Specifically, the number of clusters containing markers, $\langle N_{Species} \rangle$ and the average fractions of co-localization of Rab7-633 and LAMP-1-561 markers are represented. The average fraction of clusters containing Rab7-633 markers that also contain LAMP-1-561 markers is denoted by $\langle F(Rab7|LAMP-1) \rangle$. Likewise, the average fraction of clusters containing LAMP-1 markers that also contain Rab7 markers is denoted by $\langle F(LAMP-1|Rab7) \rangle$.

Table 3.29 Average Number of Clusters Containing Species and Fractions of Co-Localization of Rab7-633 & LAMP-1-561 Markers in A549 Cells

Species	$\langle N_{Species} \rangle$	$\langle F(Rab7\|LAMP-1) \rangle$	$\langle F(LAMP-1\|Rab7) \rangle$
Rab7-633	3.95 ± 0.44[1]		
LAMP-1-561	2.43 ± 0.24		
Rab7-633 & LAMP-1-561	0.84 ± 0.15	0.26 ± 0.06	0.37 ± 0.06

[1] Standard error.

The calculations for the average number of clusters of species represented in Table 3.29 reflect that there are approximately 3.95 clusters containing Rab7-633 markers with and there are

also approximately 2.43 clusters containing LAMP-1-561 markers. Lastly, there are approximately 0.84 clusters that contain both Rab7-633 and LAMP-1-561 markers.

The calculations for the average fractions of co-localization represented in Table 3.29 reflect on average approximately 26% of clusters that contain Rab7-633 markers also contain LAMP-1-561 markers and approximately 37% of the clusters containing LAMP-1-561 markers also contain Rab7-633 markers.

3.5.5 Summary of Fractions of Co-localization in A549 Cells

Table 3.30 is a summary of each of the averaged fractions of co-localization obtained for two species in A549 cells previously discussed.

Table 3.30 Summary of Averaged Fractions of co-localization in A549 Cells with error reflecting Standard Error

$\langle F(Red\|Green)\rangle$	Rab5	Rab7	Rab11	LAMP-1
Rab5	-	0.50 ± 0.03	0.28 ± 0.04	0.82 ± 0.04
Rab7	0.39 ± 0.03	-	N.D	0.26 ± 0.06
Rab11	0.37 ± 0.03	N.D	-	N.D
LAMP-1	0.80 ± 0.05	0.37 ± 0.06	N.D	-

N.D refers to "No Data".

The results presented in Table 3.30 reflect the following; each cluster consisting of one marker for an endocytic compartment contains at least one other marker for another endocytic compartment. Thus, the hypothesized theory of Rab7 markers fully replacing Rab5 markers does not seem to be the case implied with these studies; although this process may be occurring, but Rab5 markers are not specifically unique to one compartment, as are Rab7 markers.

The extent to which Rab5 markers associate with LAMP-1 markers is largest in magnitude in comparison to the association of Rab5 markers with Rab7 and Rab11 markers. Since Rab5 compartments are meant to be specific for early endosomes and LAMP-1 compartments specific for lysosomes, 80% co-localization among the two markers is very significant and unusual.

The extent to which Rab7 markers associate with Rab5 markers is largest in magnitude in comparison to the association of Rab7 markers with LAMP-1 markers. Although few clusters contain both markers, a much higher fraction of co-localization was expected due to the fusion between late endosomes and lysosomes hypothesis.

The extent to which LAMP-1 markers associate with Rab5 markers is largest in magnitude in comparison to the association of LAMP-1 with Rab7 markers.

In summary, these results do not fully support the hypothesized claim for markers by means of the expected interactions meant to occur with other markers for maturation and fusion steps in Figure 1.2. Specifically, the larger association between early and lysosome markers compared to late and lysosome markers is unusual.

This study has also provided additional information that it has been inferred that these markers are not specifically unique to one endocytic compartment, and that they are in fact simultaneously present on one endosome, or cluster.

3.6 Co-localization of One Endocytic Marked Compartment with two other Endocytic Marked Compartments in A549 Cells

The previous section discussed the extent to which two markers are simultaneously found on one endosome or compartment. Chapter 3.6 focusses on the co-localization of three markers to determine if one cluster could have three markers present. Results show the co-localization of markers for the early, late, and lysosomal endocytic compartments are expected to associate to a lesser extent than the association of two markers.

As with the two color experiments, each of the secondary antibodies used for labelling their respective compartments consisted of an emission profile that did not overlap. The experimental procedure for immunofluorescent labelling of three markers in cells can be referred to Chapter 2.7.1. Laser scanning confocal microscopy imaging of two markers can be referred to in Chapter 2.10.3.3. Triple Image Cross Correlation Spectroscopy analysis can be referred to in Chapter 2.11.3.

3.6.1 Rab5-561, Rab7-633, & LAMP-1-488 Marked Compartments in A549 Cells

Figure 3.23 is a visual representation of contrast enhanced images of a cell labelled with Rab5-561 (red), Rab7-633 (blue), and LAMP-1-488 (green). The Merge image is all three individual images merged.

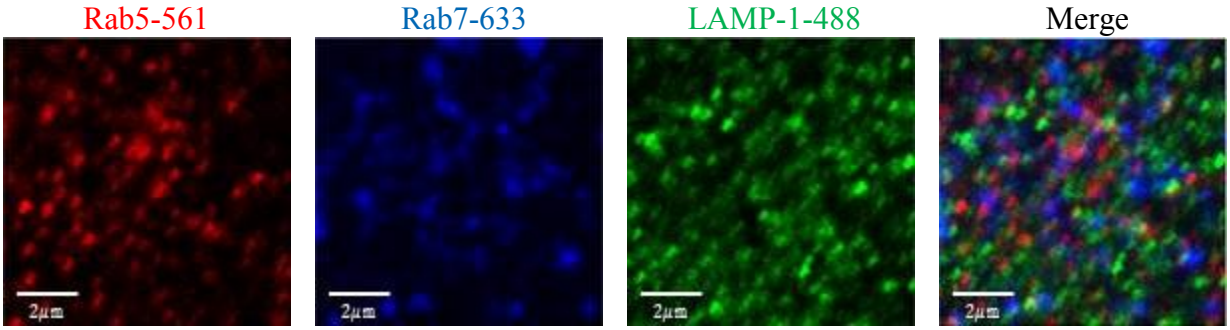

Figure 3.23 Rab5-561, Rab7-633, and LAMP-1-488 Marked Endocytic Compartments in A549 Cells

Table 3.31 shows the number of images, n_{images} obtained in one experiment with the corresponding average number of fluorescent clusters of species observed, $\langle N_{Species} \rangle$. These images precisely reflected that of the measurements obtained for one and two color experiments, for which a much greater amount of images were obtained.

Table 3.31 Averaged Number of Clusters Containing Markers in A549 cells

Species	n_{images}	$\langle N_{Species} \rangle$
LAMP-1-488	14	5.20 ± 0.31[1]
Rab5-561	14	2.55 ± 0.26
Rab7-633	14	3.74 ± 0.33
LAMP-1-488 & Rab5-561	14	0.40 ± 0.09
LAMP-1-488 & Rab7-633	14	0.33 ± 0.08
Rab5-561 & Rab7-633	14	0.35 ± 0.04
LAMP-1-488 & Rab5-561 & Rab7-633	14	0.43 ± 0.14

[1] Standard error.

The most important observation to note is the similarities observed in comparison to one and two color experiments. The relative number of clusters containing individual species and number of clusters containing two species compare with previous results for two color experiments in A549 cells.

Table 3.31 reflects there are between 2.55-5.20 clusters containing one marker in the observation region defined by the laser beam point spread function. Additionally, the number of clusters in which two markers are observed simultaneously is also in agreement with previous experiments, such that the number of clusters of markers observed ranges between 0.33-0.40. There is slight variation with each individual measurement, however it must be kept to consideration that this is a different sample for which these measurements were calculated.

In contrast to previous experiments, the number of clusters containing Rab5-561, Rab7-633, and LAMP-1-488 markers is 0.43. To fully understand this value, fractions of co-localization were calculated and are represented in Table 3.32.

Table 3.32 Averaged Fractions of Co-localization of Endocytic Marked Compartments in A549 Cells

$\langle F(LAMP-1 \mid Rab5\ Rab7)\rangle$	$\langle F(Rab5 \mid LAMP-1\ Rab7)\rangle$	$\langle F(Rab7 \mid LAMP-1\ Rab5)\rangle$
0.08 ± 0.03[1]	0.16 ± 0.05	0.11 ± 0.03

[1] Standard error.

According to Table 3.32, approximately 8% of the clusters containing LAMP-1 markers contain Rab5 and Rab7 markers. Approximately 16% of clusters containing Rab5 markers contain LAMP-1 and Rab7 markers. Lastly, approximately 11% of clusters containing Rab7 markers contain LAMP-1 and Rab5 markers. These fractions are very small, thus indicate that of the total clusters specific for one marker, *very* few clusters have two markers simultaneously present in a cluster.

As shown in Table 3.30, approximately 80% of clusters containing LAMP-1 markers contain Rab5 markers and approximately 37% of clusters containing LAMP-1 markers also contain Rab7 markers. Therefore, although LAMP-1 is likely to be found on clusters containing either Rab5 or Rab7, very few clusters of LAMP-1 also contain the other two markers. This is supported by the small fraction of clusters of LAMP-1 clusters that contain Rab7 markers.

In reference to Table 3.30, approximately 50% of clusters containing Rab5 markers also contain Rab7 markers and approximately 82% of clusters containing Rab5 markers also contain

LAMP-1 markers. Thus, this low 16% fraction of Rab5 clusters that contain Rab7 and LAMP-1 markers is an implication that there are also very few clusters that consist of all three markers; in particular, the low fraction may in fact be strongly affected by the association of Rab5 markers with Rab7 markers.

Also in reference to Table 3.30, approximately 39% of clusters containing Rab7 markers also contain Rab5 and 26% of clusters containing Rab7 markers also contain LAMP-1 markers. Thus, 11% co-localization among Rab7 with two other markers may also be slightly effected by the Rab7/LAMP-1 interaction.

There are clusters with binary and ternary complexes; but there may be few clusters containing three markers out of the total distribution of complexes. In addition, the complexes which are marked by two markers may also take into account a complex in which *one* other marker is also present.

3.7 Chapter Conclusions

The purpose of this chapter was to understand the distribution of markers in endocytic compartments in addition to the association of two and three markers in C2C12 and A549 cells as a means to either support or argue previous findings of how these markers truly associate during clathrin mediated endocytosis. Thus, the distribution and association of Rab proteins and LAMP-1 markers are important for the understanding of membrane trafficking in cells.

Contrary to the proposed hypothesis for this thesis that markers are thought to behave similarly in cells, this study has ultimately shown three main points; 1) markers are not unique to one particular endosome, 2) the distribution of markers on endosomes and sizes of endosomes vary with cell type, and 3) the association or interaction of multiple markers varies with cell type.

This work has shown that on average, the lower limit for association of one marker with another is approximately 20%. As discussed in the introduction, this provides some additional information to the understanding of “marker replacement” that is supposed to occur when an endosome is either maturing into another endosome or fusing with another endosome. This data has shown that two markers can be present on one endosome and markers are not fully displaced on endosomes as the pathway progresses.

The distribution of markers between cells lines is different. Specifically, the number of clusters containing markers decreases and the relative size of these clusters increases with the progression of the clathrin mediated endocytic pathway in C2C12 cells. In contrast, there are no variations observed for the distribution of clusters containing markers and the relative size of these clusters with the progression of endocytosis in A549 cells. Therefore, this is an interesting finding that exhibits the truly different nature of cells and that markers specific for endocytosis vary with cell type.

The association of multiple markers between both cells is different. The maturation and fusion steps of endosomes and the associated markers are supported based on the results obtained for C2C12 studies. On the contrary, the maturation and fusion steps of endosomes and the associated markers are not *fully* supported based on the results obtained for A549 studies. Although similarities are observed among the early/recycling and early/late endosome interactions, there is a difference among early/lysosome interaction between cells.

Likewise, the extent to which three species occupy one cluster or endosome is different among C2C12 and A549 cells; the results obtained for C2C12 cells indicate that there are a large number of clusters containing three species within a distribution of markers in comparison to A549 cells; specifically, there are fewer three-marker complexes observed in the total distribution of one, two, and three marker complexes in A549 cells. These findings also suggest that the fraction of complexes in which three markers are present are counted in the distribution of binary complexes.

Differences in the distribution and association of multiple markers may arise due to the origins and functions of C2C12 and A549 cells. C2C12 cells are mouse muscle myoblastoma cells and A549 cells are human lung adenocarcinoma cells.[85,86] Thus, both cell lines originate from different tissues *and* mammals which explain the differences in distribution and association of markers presented in this work. With respect to cell function, the purpose of muscles is to contract to produce force.[87] C2C12 muscle cells in particular are interesting because they can be differentiated from myobloasts to osteoblasts (bone cells).[88] Studies have shown C2C12 cells to be effective models for studying bone morphogenetic proteins due to their importance for regulating skeletal formation and embryonic development, to name a few.[89] A549 cells are type II lung epithelial cells, responsible for the diffusion and transport of nutrients across the alveoli

of the lungs in the body.[90] In addition, type II cells are responsible for the synthesis and secretion of pulmonary surfactant from cells to reduce surface tension in the lungs for ease in breathing.[91] Therefore, both cells are very important for the proper functioning of tissues (muscles and lungs), but they have different *origins and functions* which may explain the differences observed for the distribution and extent of association of markers in both cell types.

These results are interesting findings that reflect the differences (with some similarities) of marker localization on clusters and the extent to which markers are able to co-exist in the same cluster. Based on the results from this chapter, the distribution and association of proteins responsible for membrane trafficking varies with cell type. This study has provided a useful, further understanding of membrane trafficking, and the roles for which markers are responsible for associating with endosomes to permit membrane trafficking in cells. This study has also shown the effectiveness for ICS analysis to understand intracellular behavior of endocytosis and inquire about the relative size of endosomes.

3.8 Control Experiments in C2C12 Cells

Chapter 3.8 is an analysis of the various control experiments completed to test for cross reactivity and cross talk of antibodies.

3.8.1 Control for Cross Reactivity of Antibodies in C2C12 Cells

For any study involving the use of fluorescent antibodies in multi-color experiments, cross reactivity experiments must be done to ensure that each antibody used is unique for one specific species; in this work, the primary antibody must be specific for one marker, and the secondary antibody must be specific for that particular primary antibody.

To ensure cross reactivity of antibodies was avoided, primary antibodies originate from different hosts; for example, in these two and three color experiments as shown in table primary antibodies originated from a rat, mouse, or rabbit. Despite this claim, it is recommended for immunofluorescence studies to do a cross reactivity experiment if in the event the manufacturer's claim is not reliable.

To test for cross reactivity of antibodies in this work, C2C12 cells were labelled with Rab7 and LAMP-1 as discussed previously in 3.2.4 and compared to four other samples prepared

without the addition of one primary or secondary antibody, in various combinations. Figure 3.24 is a representation of this experiment.

Experiment #	Green Species	Red Species
1	Rab7 P&S	LAMP-1 P&S
2	Rab7 P&S	LAMP-1 P
3	Rab7 P&S	LAMP-1 S
4	Rab7 P	LAMP-1 P&S
5	Rab7 S	LAMP-1 P&S

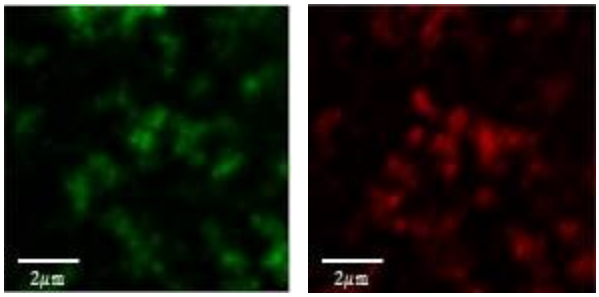

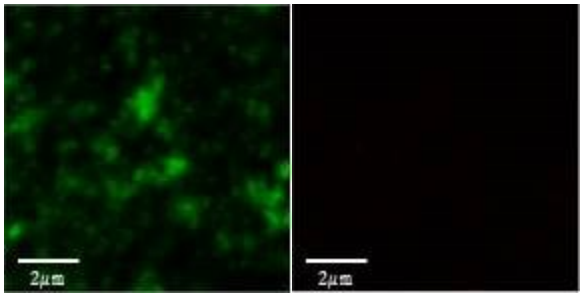

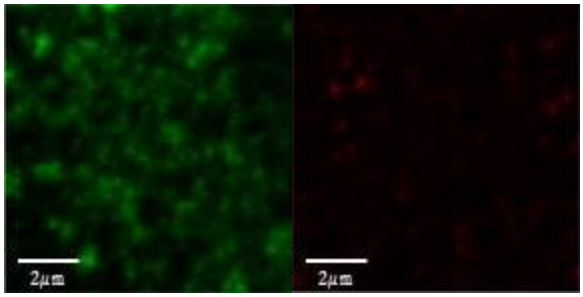

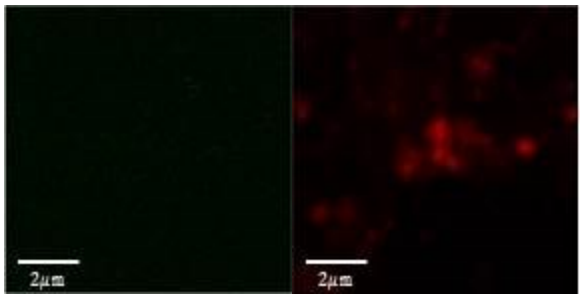

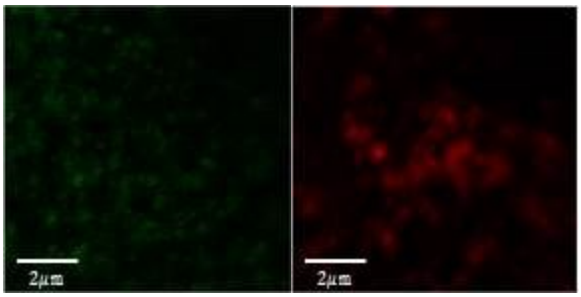

Figure 3.24 Control for Cross Reactivity of Antibodies in C2C12 Cells

By inspection, images with only primary antibody, such as Rab7 P or LAMP1 P appear to be "black" in color. Similarly, images with only secondary antibody, such as Rab7 S or LAMP-1 S, little fluorescence is observed to be emitted from antibodies but not a significant amount in comparison to images in which both primary and secondary antibodies were used as shown with experiment 1 in Figure 3.24.

Image Cross Correlation Spectroscopy was then performed and the results are shown in Table 3.33.

Table 3.33 Cross Reactivity Data in C2C12 Cells

Experiment #	Experiment	Species	$\langle g(0,0)\rangle$	$\langle \omega\ (\mu m)\rangle$	$\langle I_{avg.}\rangle$
1	Rab7 P&S and LAMP-1 P&S	Rab7 P&S	0.62 ± 0.07[1]	0.58 ± 0.05	173 ± 14
1	Rab7 P&S and LAMP-1 P&S	LAMP-1 P&S	0.86 ± 0.06	0.49 ± 0.03	509 ± 92
2	Rab7 P&S and LAMP-1 P	Rab7 P&S	0.40 ± 0.09	0.45 ± 0.03	116 ± 11
2	Rab7 P&S and LAMP-1 P	LAMP-1 P	0.03 ± 0.01	0.31 ± 0.03	9.34 ± 0.2
3	Rab7 P&S and LAMP-1 S	Rab7 P&S	0.36 ± 0.09	0.44 ± 0.05	108 ± 13
3	Rab7 P&S and LAMP-1 S	LAMP-1 S	0.22 ± 0.06	0.30 ± 0.02	15.4 ± 0.7
4	Rab7 P and LAMP-1 P&S	Rab7 P	0.01 ± 0.01	0.41 ± 0.08	8.58 ± 0.12
4	Rab7 P and LAMP-1 P&S	LAMP-1 P&S	0.46 ± 0.13	0.48 ± 0.05	563 ± 74
5	Rab7 S and LAMP-1 P&S	Rab7 S	0.12 ± 0.02	0.35 ± 0.03	20.9 ± 1.5
5	Rab7 S and LAMP-1 P&S	LAMP-1 P&S	0.37 ± 0.07	0.47 ± 0.03	622 ± 60

[1]Standard error.

In some cases, antibodies can cross react. This experiment was performed to ensure the antibodies were specific for each species of interest. The data obtained for species of single primary and secondary antibodies reflect auto correlation amplitudes on the order of 0.01 and the intensity is at most 20 which is a representation of background. One would expect to have a greater magnitude in secondary control intensity than primary control intensity due to non-specific binding of secondary antibodies.

3.8.2 Control for Cross-Talk of Antibodies in C2C12 Cells

Another potential issue with fluorescent imaging is cross talk. Cross talk is defined as the onset of emission resulting from excitation of molecules in which the fluorescent emission profile does not match that of the emission profile range of detection expected. For example; cross talk would ensue if a molecule with a 488 fluorescent tag emitted light upon excitation of a 561 nm wavelength laser. Although this is highly unlikely, it is a good control to check.

Additionally, simple overlap of emission profiles of two species being excited in the same detection volume will give rise to cross talk.

Thus as a control measure, a sample labelled with all three species of different fluorescent emission profiles was prepared. All detection channels were opened, but the sample was excited with only one laser at a time. The intensity was then quantified from each channel to determine if any intensity was detected in the channels not corresponding to the appropriate excitation laser. As with all imaging experiments in this thesis, the detectors were carefully set to detect wavelengths within a specific range; 489-564 for 488 channel, 561-620 for 561 channel, and 633-697 for 633 channel.

Figure 3.25 represents the images obtained for a cross talk experiment in C2C12 cells where by a sample was labelled with Rab5, Rab7, and LAMP-1 488 as done previously in Chapter 3.3.1.

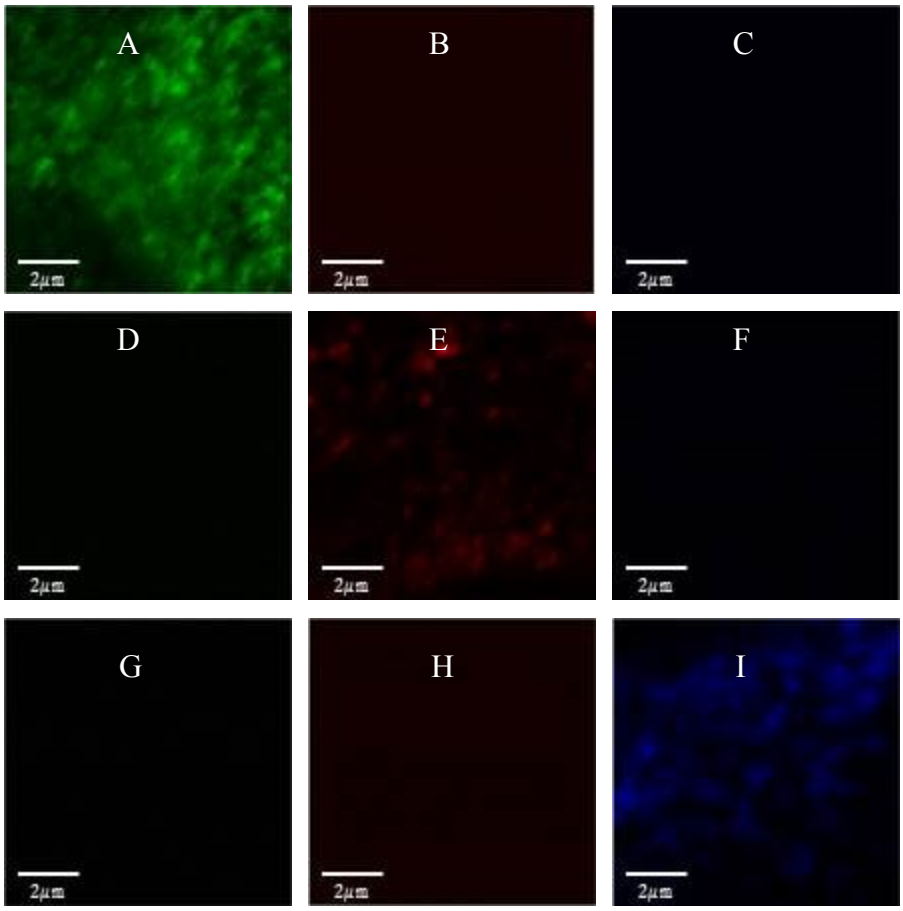

Figure 3.25 Control for Cross Talk of Antibodies in C2C12 Cells

C2C12 cells labelled with Rab5, Rab7, and LAMP-1 488 as previously done in subsection 3.3.1.
Images A-C Correspond to images obtained by excitation with only a 488 nm laser.
Images D-F Correspond to images obtained by excitation with only a 561 nm laser.
Images G-I Correspond to images obtained by excitation with only a 633 nm laser.

By visual inspection, Images A, E, and I are each the positive controls. All other images show little fluorescence which validates there is little to no-cross talk in these experiments. Image correlation spectroscopy was then completed on a set of images to obtain average values of data in Table 3.34.

Table 3.34 Average Data Obtained for Cross Talk Control Experiments in C2C12 Cells

Panel	Laser Excitation	Detection Channel	$\langle \mathbf{g(0,0)} \rangle$	$\langle \boldsymbol{\omega}\ (\boldsymbol{\mu m}) \rangle$	$\langle I_{avg.} \rangle$
A	488	488	0.10 ± 0.02[1]	0.45 ± 0.04	**940 ± 130**
B	488	561	0.001 ± 0.000	0.40 ± 0.02	13.7 ± 0.3
C	488	633	0.002 ± 0.000	0.35 ± 0.09	10.4 ± 0.1
D	561	488	0.001 ± 0.000	0.34 ± 0.17	8.89 ± 4.20
E	561	561	0.31 ± 0.16	0.24 ± 0.12	**191 ± 104**
F	561	633	0.001 ± 0.001	0.04 ± 0.04	7.82 ± 3.69
G	633	488	0.01 ± 0.01	0.11 ± 0.08	12.5 ± 0.13
H	633	561	0.01 ± 0.01	0.21 ± 0.11	12.6 ± 0.19
I	633	633	0.41 ± 0.11	0.50 ± 0.04	**439 ± 41.4**

1 Standard error.

Based on the averages of data obtained in Table 3.34, the auto correlation amplitudes for Images excited with a different wavelength than their respective emission profiles are at least ten percent less than the auto correlation amplitude obtained for species excited with wavelengths matching that of their emission profile. Most importantly, the intensities reflect the positive controls for each of the three antibodies used. These intensities are at least ten times larger than that of Images excited with a different wavelength then their respective emission profiles. In previous experiments involving image cross correlation spectroscopy, experiments involved in two color samples were excited individually to avoid this issue. However, based on the results reported in this cross talk control experiment, fluorescence corresponding to each species of interest measured in two and three color experiments are unique to one species. Thus, it is encouraged to do two and/or three color experiments and excite two species of interest simultaneously with care paid attention to the wavelength range at which the detector is set.

3.9 Control Experiments in A549 Cells

Chapter 3.9 is an analysis of the various control experiments completed to test for cross reactivity and cross talk of antibodies.

3.9.1 Cross Reactivity Control Experiment

To test for cross reactivity of antibodies in this work, A549 cells were labelled with Rab7 and LAMP-1 and compared to four other samples prepared without the addition of one primary or secondary antibody, in various combinations, as done with C2C12 cells in 3.8.1. Figure 3.26 is a representation of this experiment.

Experiment #	Green Species	Red Species
1	Rab7 P&S	LAMP-1 P&S
2	Rab7 P&S	LAMP-1 P
3	Rab7 P&S	LAMP-1 S

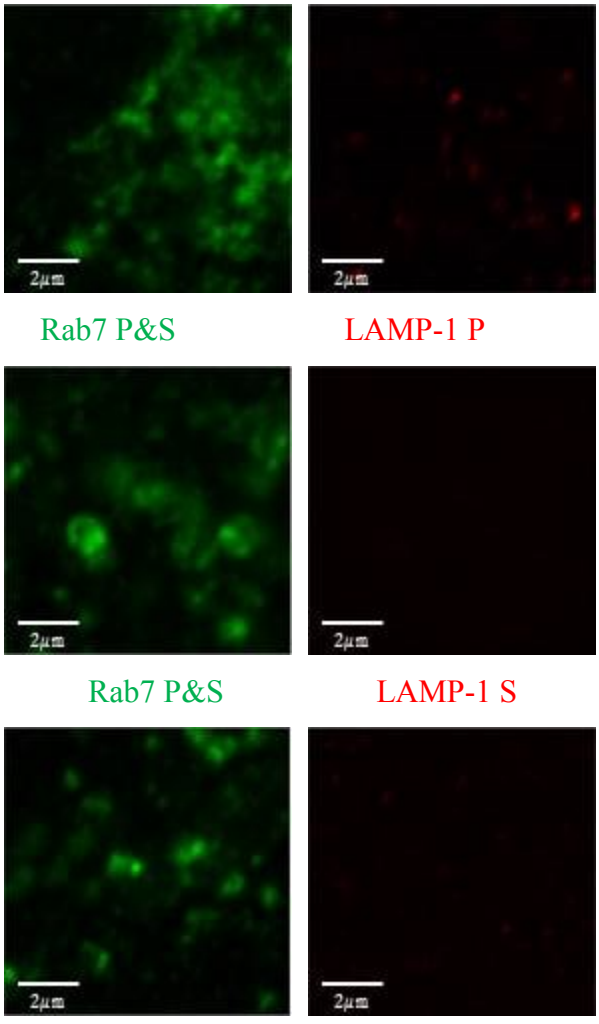

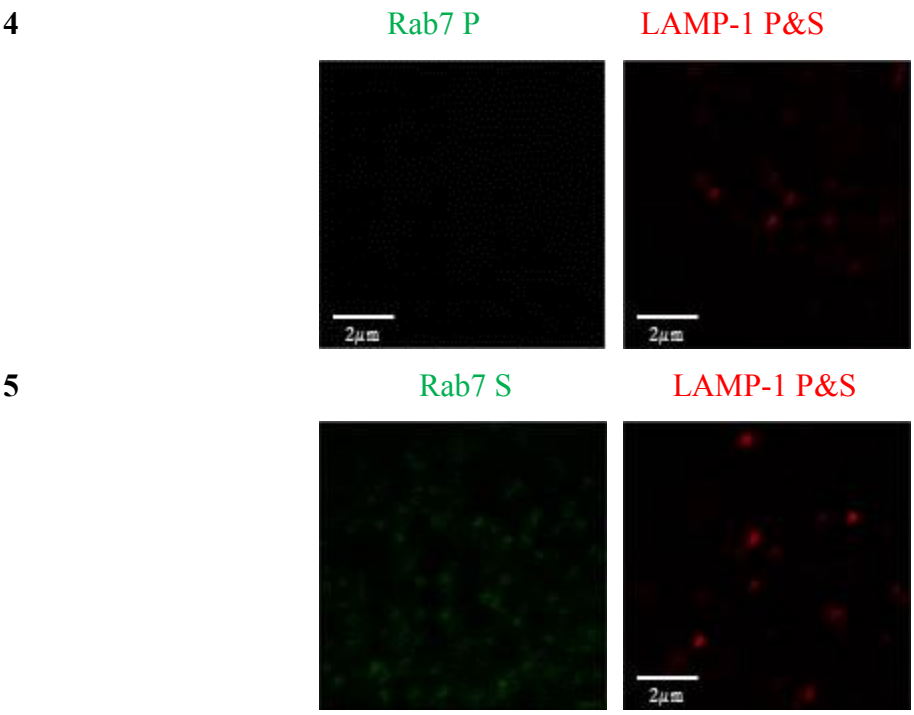

Figure 3.26 Cross Reactivity Control Experiment in A549 Cells

By inspection, images with only primary antibody, such as Rab7 P or LAMP1-P, the images appear to be "black" in color. Similarly, images with only secondary antibody, such as Rab7 S or LAMP-1 S, little fluorescence is observed but not a significant amount.

Image Cross Correlation Spectroscopy was then performed and the results are shown in Table 3.35.

Table 3.35 Cross Reactivity Control in A549 Cells

Experiment #	Experiment	Channel	$\langle g(0,0) \rangle$	$\langle \omega\ (\mu m) \rangle$	$\langle I_{avg.} \rangle$
1	Rab7 P&S and LAMP-1 P&S	Rab7 P&S	0.62 ± 0.07	0.58 ± 0.05	173 ± 14
1	Rab7 P&S and LAMP-1 P&S	LAMP1 P&S	0.86 ± 0.06	0.49 ± 0.03	509 ± 92
2	Rab7 P&S and LAMP-1 P	Rab7 P&S	0.40 ± 0.09	0.45 ± 0.03	116 ± 11
2	Rab7 P&S and LAMP-1 P	LAMP1 P	0.03 ± 0.01	0.31 ± 0.03	9.34 ± 0.2
3	Rab7 P&S and LAMP-1 S	Rab7 P&S	0.36 ± 0.09	0.44 ± 0.05	108 ± 13
3	Rab7 P&S and LAMP-1 S	LAMP1 S	0.22 ± 0.06	0.30 ± 0.02	15.4 ± 0.7
4	Rab7 P and LAMP-1 P&S	Rab7 P	0.01 ± 0.01	0.41 ± 0.08	8.58 ± 0.12
4	Rab7 P and LAMP-1 P&S	LAMP1 P&S	0.46 ± 0.13	0.48 ± 0.05	563 ± 74
5	Rab7 S and LAMP-1 P&S	Rab7 S	0.12 ± 0.02	0.35 ± 0.03	20.9 ± 1.5
5	Rab7 S and LAMP-1 P&S	LAMP1 P&S	0.37 ± 0.07	0.47 ± 0.03	622 ± 60

This experiment was performed as with C2C12 cells to ensure the antibodies were accurately specific for each species of interest. As such, the data obtained for species of single primary and secondary antibodies reflect auto correlation amplitudes on the order of 0.01 and the intensity is at most 20 which is a representation of background. One would expect to have a greater magnitude in secondary control intensity than primary control intensity.

3.9.2 Cross Talk Experiment in A549 Cells

As shown in Chapter 3.8.2, cross talk control was also studied for A549.

A sample labelled with all three species of different fluorescent emission profiles was prepared. All detection channels were opened, but the sample was excited with only one laser at a time. As such, the intensity was then quantified from each channel to determine if any intensity was detected in the channels not corresponding to the appropriate excitation laser. As with all experiments in this thesis, the detectors were carefully set to detect wavelengths within a specific

range; 489-564 for 488 nm channel, 561-620 for 561 nm channel, and 633-697 for 633 nm channel.

Figure 3.25 represents the images obtained for a cross talk experiment in C2C12 cells where by a sample was labelled with Rab5, Rab7, and LAMP-1 488 as done previously.

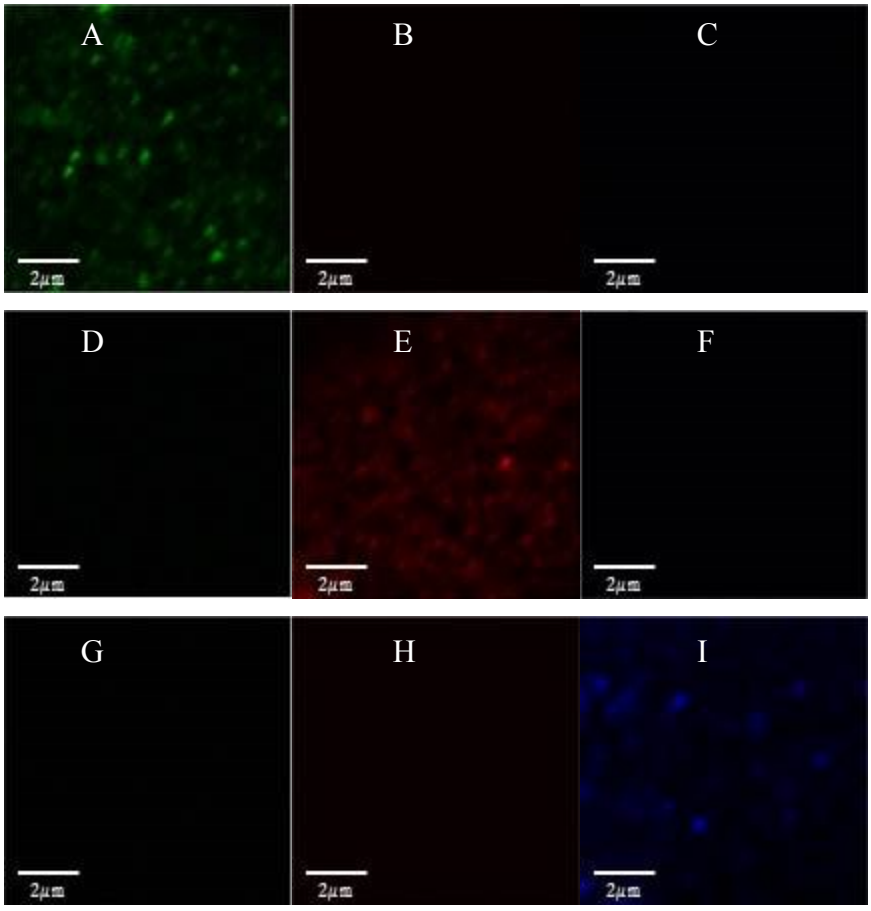

Figure 3.27 Control for Cross Talk of Antibodies in A549 Cells

A549 cells labelled with Rab5, Rab7, and LAMP-1 488 as previously done in subsection
Images A-C Correspond to images obtained by excitation with only 488 laser.
Images D-F Correspond to images obtained by excitation with only 561 laser.
Images G-I Correspond to images obtained by excitation with only 633 laser.

By visual inspection, Images A, E, and I are each the positive controls. All other images show little fluorescence which validates there is little to no-cross talk in these experiments. Image correlation spectroscopy was then completed on a set of images to obtain average values of data in Table 3.36.

Table 3.36 Control for Cross Talk of Antibodies in A549 Cells

Panel	Laser Excitation	Detection Channel	$\langle g(0,0) \rangle$	$\langle \omega\ (\mu m) \rangle$	$\langle I_{avg.} \rangle$
A	488	488	0.31 ± 0.18	0.27 ± 0.16	**108 ± 63**
B	488	561	0.00004 ± 0.00002	0.36 ± 0.21	30.6 ± 3.8
C	488	633	0.001 ± 0.001	0.52 ± 0.30	6.54 ± 3.78
D	561	488	0.004 ± 0.004	0.66 ± 0.43	15.4 ± 0.1
E	561	561	0.10 ± 0.02	0.33 ± 0.06	**328 ± 17**
F	561	633	0.001 ± 0.003	0.70 ± 0.33	6.84 ± 0.08
G	633	488	0.00001 ± 0.00010	0.38 ± 0.01	15.7 ± 0.0
H	633	561	0.00002 ± 0.00000	0.32 ± 0.02	30.9 ± 0.1
I	633	633	0.40 ± 0.06	0.38 ± 0.04	**392 ± 43**

1 Standard error.

Based on the averages of data obtained in Table 3.36, the auto correlation amplitudes for images excited with a different wavelength then their respective emission profiles are at least ten percent less than the auto correlation amplitude obtained for species excited with wavelengths matching that of their emission profile. Most importantly, the intensities reflect the positive controls for each of the three antibodies used. These intensities are at least ten times larger than that of images excited with a different wavelength then their respective emission profiles.

Chapter 4

Study of Endocytic Compartments Containing Phospholipid Coated Gold Nanoparticles in C2C12 and A549 Cells

4 Study of Endocytic Compartments Containing Phospholipid Coated Gold Nanoparticles in C2C12 and A549 Cells

In the previous chapter, we showed that imaging and ICS analysis provide a useful means to study three species of interest and the extent to which they co-exist in one compartment of a cell. As a result, we determined that; 1) markers are not unique to one particular endosome, 2) the distribution of markers on endosomes and sizes of endosomes vary with cell type, and 3) the association or interaction of multiple markers varies between cell types.

This understanding of marker distribution among cells allows us to study whether the internalization of a specific nanoparticle system undergoes clathrin mediated endocytosis. As discussed in the introduction, it is understood that gold nanoparticles undergo clathrin mediated endocytosis. Phospholipid coated gold nanoparticles are prepared in the Petersen lab, but the ultimate fate and pathway of these nanoparticles in cells was undetermined. Therefore, it was of interest to determine the extent to which phospholipid coated gold nanoparticles synthesized in our lab were able to undergo clathrin mediated endocytosis based on their association with endocytic marked compartments.[39]

First, we studied the internalization of phospholipid coated gold nanoparticles by exposing cells to phospholipid coated gold nanoparticles for 1, 2, 4 and 24 hours followed by fixation. This experiment is called variable exposure, fixed uptake. The internalization of phospholipid coated gold nanoparticles was also studied by exposing cells to phospholipid coated gold nanoparticles, washing the cells, and allowing uptake for 1, 2, 4, and 24 hours before fixation. This experiment is called fixed exposure, variable uptake. In addition, pairwise interaction between phospholipid coated gold nanoparticles and a marker of an endosome was studied to quantitatively determine the extent to which phospholipid coated gold nanoparticles associate with one marker of an endocytic compartment. Lastly, the three-way co-localization of phospholipid coated gold nanoparticles and two markers were studied to determine the extent to which these three species simultaneously co-existed in one compartment.

Thus, this chapter focusses on determining the extent to which compartments contain phospholipid coated gold nanoparticles. This chapter will also discuss and determine if

phospholipid coated gold nanoparticle internalization and association with endocytic markers is cell type specific, by using both C2C12 and A549 cells.

4.1 Internalization of Phospholipid Coated Gold Nanoparticles in C2C12 Cells

The focus of Chapter 4.1 is the study of the internalization of phospholipid coated gold nanoparticles in C2C12 cells. Two different experiments were performed to study the internalization of phospholipid coated gold nanoparticles in C2C12 cells; variable exposure, fixed uptake and fixed exposure, variable uptake. The images were adjusted to greyscale in Chapter 4.1 for better contrast. The experimental procedure required for variable exposure, fixed uptake of phospholipid coated gold nanoparticles is discussed in Chapter 2.3.1. The experimental procedure required for fixed exposure, variable uptake of phospholipid coated gold nanoparticles is discussed in Chapter 2.3.2. Laser scanning confocal microscopy of images is discussed Chapter 2.11.1. For all images containing GNPs, 488 nm laser was used to excite GNPs. Lastly, image cross correlation spectroscopy analysis is discussed Chapter 2.11.2.

4.1.1 Variable Exposure, Fixed Uptake of Phospholipid Coated Gold Nanoparticles in C2C12 Cells

C2C12 cells were exposed to phospholipid coated gold nanoparticles by a variable exposure, fixed uptake experiment.

In Figure 4.1, images A, B, C, and D each correspond to one confocal fluorescence microscopy image of one cell from each of the four samples prepared in the experiment in which the cells in each sample were exposed to phospholipid coated gold nanoparticles for 1, 2,4 and 24 hours, respectively, prior to fixation.

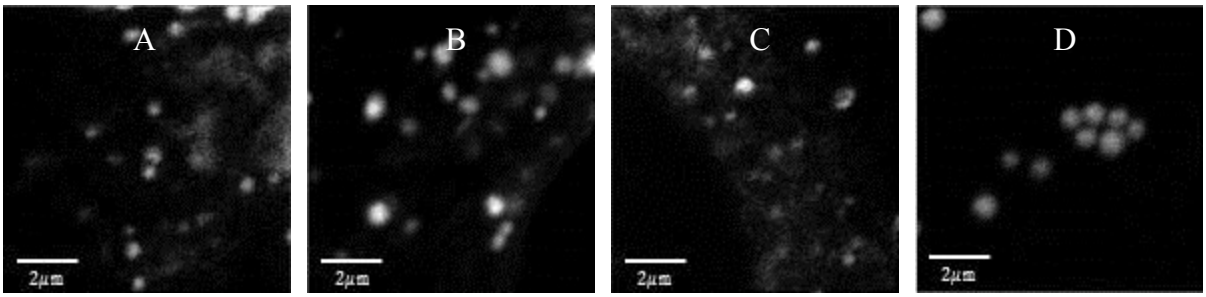

Figure 4.1 Images of Phospholipid Coated Gold Nanoparticles after Variable Exposure, Fixed Uptake in C2C12 Cells

Images A, B, C, and D each correspond to one confocal fluorescence microscopy image of one cell from each of the four samples prepared in the experiment in which the cells in each sample were exposed to phospholipid coated gold nanoparticles for 1, 2,4 and 24 hours, respectively, prior to fixation.

The images shown in Figure 4.1 reflect differences from exposing C2C12 cells to phospholipid coated gold nanoparticles for different times. For example; there appear to be a fewer clusters containing GNPs in the cell in image D after 24 hours of exposure then one would observe in the cell in image A after 1 hour of GNP exposure.

Table 4.1 shows the averages of the auto correlation amplitude, fitted laser beam width, and average intensity for 20-30 images of each sample of C2C12 cells exposed to phospholipid coated gold nanoparticles for 1, 2, 4, and 24 hours.

Table 4.1 ICS Parameters Corresponding for Phospholipid Coated Gold Nanoparticles after Variable Exposure, Fixed Uptake in C2C12 Cells

Variable Exposure Time (hours)	$\langle \mathbf{g(0,0)} \rangle$	$\langle \boldsymbol{\omega}\ (\boldsymbol{\mu m}) \rangle$	$\langle I_{avg.} \rangle$
1	0.36 ± 0.05[1]	0.40 ± 0.02	154 ± 11
2	0.62 ± 0.11	0.47 ± 0.02	197 ± 28
4	0.30 ± 0.08	0.42 ± 0.03	110 ± 9
24	0.56 ± 0.05	0.43 ± 0.01	326 ± 29

[1] Standard error.

The average intensity measured for phospholipid coated gold nanoparticles in the observation region of the laser beam appears to be consistent between 1-4 hours of continuous exposure, however there is a two to three fold increase in the average intensity after cells have

been continuously exposed to phospholipid coated gold nanoparticles for 24 hours. Even by visual observation of image D, this is quite evident.

The auto correlation amplitudes obtained for each time interval of variable exposure are between 0.30-0.60, however there is no obvious trend observed with time of exposure. In addition, the average fitted laser beam width for each time interval of exposure is approximately 0.40 microns. As discussed in Chapter 3, the fitted laser beam width is a convolution of the size of the species in the observation region of the laser beam and the size of the laser beam itself. Thus, this measurement provides some indication that these gold nanoparticle compartments may be larger than 0.40 microns in diameter.

Table 4.2 shows the average number of clusters containing phospholipid coated gold nanoparticles, the average number of clusters containing phospholipid coated gold nanoparticles per square micron, and the average relative degree of aggregation of phospholipid coated gold nanoparticles per cluster were calculated for a set of 20-30 images per sample time interval. The calculations presented in Table 4.2 correspond to data shown in Table 4.1.

Table 4.2 Derived Paramaters for Phospholipid Coated Gold Nanoparticles after Variable Exposure, Fixed Uptake in C2C12 Cells

Variable Exposure Time (hours)	$\langle N_{GNPs} \rangle$	$\langle CD \rangle$	$\langle DA \rangle$
1	4.31 ± 1.09[1]	7.99 ± 1.30	52.0 ± 6.5
2	2.40 ± 0.42	3.76 ± 0.85	137 ± 37
4	5.64 ± 1.57	13.3 ± 5.6	33.1 ± 10.2
24	2.18 ± 0.19	4.15 ± 0.48	160 ± 12

[1] Standard error.

The average number of clusters containing phospholipid coated gold nanoparticles, $\langle N_{GNPs} \rangle$, and average clusters per square micron, $\langle CD \rangle$, show no specific trend with varying times of continuous exposure to C2C12 cells. The cluster density fluctuates relative to the number of phospholipid coated gold nanoparticles because the laser beam width does not change with time.

4.1.2 Fixed Exposure, Variable Uptake of GNPs in C2C12 Cells

C2C12 cells were exposed to GNPs by a fixed exposure, variable uptake experiment.

In Figure 4.2, images A, B, C, and D each correspond to one confocal fluorescence microscopy image of one cell from each of the four samples exposed to phospholipid coated gold nanoparticles for 2 hours, washed, and re-incubated for 1, 2, 4, and 24 hours, respectively, then fixed.

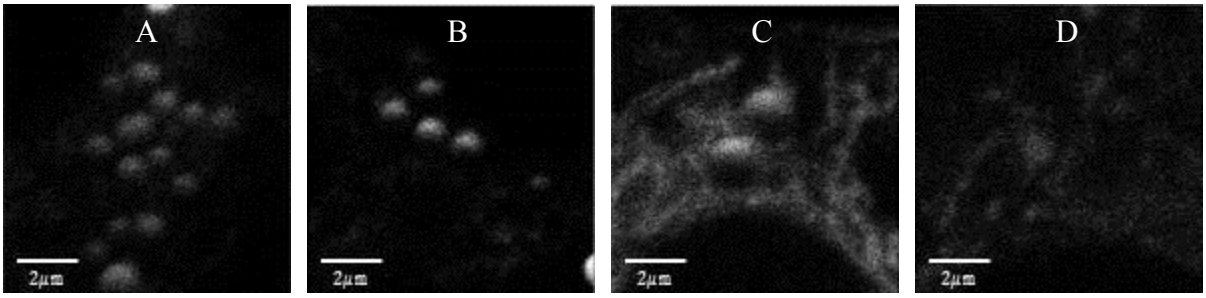

Figure 4.2 Images of Phospholipid Coated Gold Nanoparticles after Fixed Exposure, Variable Uptake in C2C12 Cells

Images A, B, C, and D each correspond to one confocal fluorescence microscopy image of one cell from each of the four samples exposed to phospholipid coated gold nanoparticles for 2 hours, washed, and re-incubated for 1, 2, 4, and 24 hours, respectively, then fixed.

In Figure 4.2, images A and B show distinct clusters containing phospholipid coated gold nanoparticles in cells after 1 and 2 hours but images C and D show mostly diffuse fluorescence emitted in cells after 4 and 24 hours.

Table 4.3 shows the averages of the auto correlation amplitude, fitted laser beam width, and average intensity for 20-30 images of each sample of C2C12 cells exposed to phospholipid coated gold nanoparticles for 2 hours, then re-incubated for 1, 2, 4, and 24 hours for uptake. The average values for each parameter is shown with standard error.

Table 4.3 ICS Paramaters for Phospholipid Coated Gold Nanoparticles after Fixed Exposure, Variable Uptake in C2C12 Cells

Variable Uptake Time (hours)	$\langle \mathbf{g(0,0)} \rangle$	$\langle \boldsymbol{\omega}\ (\boldsymbol{\mu m}) \rangle$	$\langle I_{avg.} \rangle$
1	0.23 ± 0.05[1]	0.53 ± 0.07	117 ± 9
2	0.13 ± 0.03	0.48 ± 0.02	91.4 ± 4.7
4	0.08 ± 0.01	0.46 ± 0.02	97.6 ± 3.2
24	0.05 ± 0.01	0.43 ± 0.01	42.6 ± 1.1

[1] Standard error.

The average intensity measured for phospholipid coated gold nanoparticles in the observation region of the laser beam appears to be nearly constant between 1-4 hours of uptake, however there is a two-fold decrease in the average intensity after phospholipid coated gold nanoparticles have been present in cells for 24 hours. By visual observation, this is quite evident as the image reflects possible background noise.

The auto correlation amplitude obtained for 24 hours of phospholipid coated gold nanoparticle uptake in C2C12 cells is less than 0.10 and approaches the lower limit of significance of measuring any system of interest by ICS. In contrast, the auto correlation amplitudes obtained for 1-4 hours of gold nanoparticle uptake in C2C12 cells is greater than 0.10, if not approximately 0.10, which is specifically measuring the presence of phospholipid coated gold nanoparticles in cells and not background noise.

The fitted laser beam width for each time interval of uptake ranges between 0.40-0.50 microns. The size of these gold nanoparticle compartments are in very good agreement with the fitted laser beam width obtained for each marker of a clathrin mediated endosome as discussed in Chapter 3; each of these compartments similarly range in diameter of 0.50-0.60 microns.

Table 4.4 shows the average number of clusters containing phospholipid coated gold nanoparticles, $\langle N_{GNPs} \rangle$, the average number of clusters containing phospholipid coated gold nanoparticles per square micron, $\langle CD \rangle$, and the average relative degree of aggregation of phospholipid coated gold nanoparticles per cluster, $\langle DA \rangle$, corresponding to the data shown in Table 4.3. The average values for each parameter are represented with respect to standard error.

Table 4.4 Averages of Derived Parameters for Phospholipid Coated Gold Nanoparticles Undergoing Fixed Exposure, Variable Uptake in C2C12 Cells

Variable Uptake Time (hours)	$\langle N_{GNPs} \rangle$	$\langle CD \rangle$	$\langle DA \rangle$
1	10.5 ± 2.0[1]	20.9 ± 4.4	28.7 ± 7.9
2	11.0 ± 1.7	17.5 ± 3.6	11.9 ± 2.6
4	16.7 ± 1.8	28.5 ± 4.6	7.4 ± 1.1
24	29.4 ± 3.0	59.2 ± 8.8	2.2 ± 0.6

[1] Standard error.

On average, there are about 20 clusters per square micron containing phospholipid coated gold nanoparticles at earlier times. After 4 hours have elapsed for uptake, there are approximately 28.5 clusters containing phospholipid coated gold nanoparticles and then approximately 59.2 clusters per square micron containing phospholipid coated gold nanoparticles. However, the number of clusters per square micron after 24 hours of uptake reflects that of the background noise in the system.

The relative degree of aggregation for phospholipid coated gold nanoparticles with the progression of uptake time decreases; this decrease is dependent on the intensity as the measurements of the derived parameters and data are representative of the background noise.

4.2 Co-Localization of Endocytic Marked Compartments with Phospholipid Coated Gold Nanoparticles in C2C12 Cells

This section focusses on the study of the co-localization of endocytic markers with phospholipid coated gold nanoparticles in C2C12 cells. This particular co-localization measures the extent to which an endocytic marked compartment contains phospholipid coated gold nanoparticles and the extent for which phospholipid coated gold nanoparticle clusters contain markers.

The following experimental combinations were studied; Rab5-561 & GNPs, Rab11-633 & GNPs, Rab7-633 & GNPs, and LAMP-1-561 & GNPs. Recall, GNPs contain a 488 fluorescent probe, thus GNPs were excited with a 488 nm laser. GNPs are colored in green and markers for endocytic compartments are colored red in images, respectively. Recall, the color of the images does not represent the wavelength of excitation as specified in Chapter 2.5; colors of images

were chosen merely for analysis and visualization. The double labelling procedure of phospholipid coated gold nanoparticles and primary and secondary antibodies required for labelling of one marker can be referred in Chapter 2.6.2.

Procedure required for obtaining images via laser scanning confocal microscopy can be referred to in Chapter 2.10.3.2. Lastly, Image cross correlation spectroscopy analysis can be referred to in Chapter 2.11.2.

4.2.1 Rab5-561 Marked Early Endocytic Compartments Containing Phospholipid Coated Gold Nanoparticles in C2C12 Cells.

The extent to which phospholipid coated gold nanoparticles associate with Rab5 marked early endocytic compartments was studied first.

Figure 4.3 is shows contrast enhanced images of GNPs and Rab5-561 marked compartments in one cell. The Merge image is an overlay of the GNPs and Rab5-561 images. The Original Merge is an overlay of the GNPs and Rab5-561 images that were obtained originally in the experiment without contrast enhancement. Thus, the Original Merge image is shown for purpose of comparison to that of the Merge image.

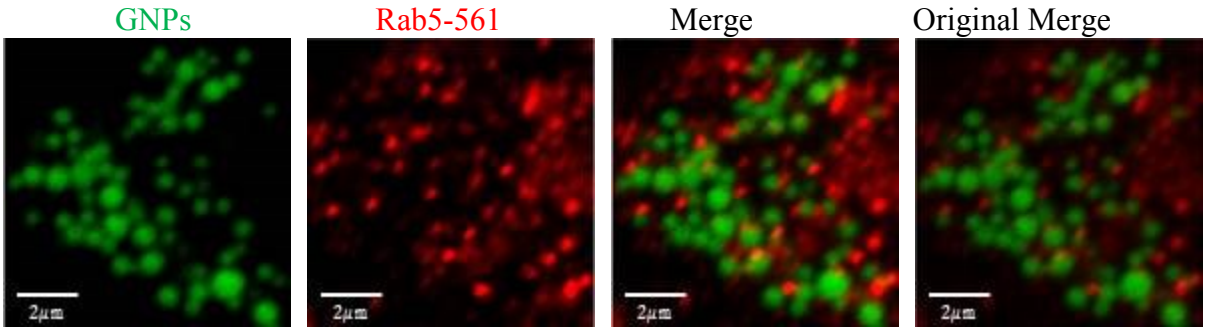

Figure 4.3 Rab5-561 Marked Early Endocytic Compartments Containing Phospholipid Coated Gold Nanoparticles in C2C12 Cells

A visual representation of contrast enhanced confocal fluorescence microscopy images of GNPs and Rab5-561 marked compartments in one cell. The Merge image is an overlay of the GNPs-488 and Rab5-561 images. The Original Merge is an overlay of the GNPs and Rab5-561 images that were obtained originally in the experiment without contrast enhancement. Thus, the Original Merge image is shown for purpose of comparison to that of the Merge image.

There are few yellow regions or clusters observed in the Merge Image in Figure 4.3, suggesting little co-localization of among phospholipid coated gold nanoparticles and Rab5-561 marked compartments in C2C12 cells.

Table 4.5 shows the average number of clusters denoted by $\langle N_{Species} \rangle$ and the average fractions of co-localization of GNPs and Rab5-561 marked compartments. The average fraction of clusters containing phospholipid coated gold nanoparticles that contain Rab5-561 markers is denoted by $\langle F(GNPs|Rab5) \rangle$. Likewise, the average fraction of clusters containing Rab5 markers that contain phospholipid coated gold nanoparticles is denoted by $\langle F(Rab5|GNPs) \rangle$.

Table 4.5 Average Number of Clusters of Species and Fractions of Co-Localization of GNPs & Rab5-561 Marked Early Endocytic Compartments in C2C12 Cells

Species	$\langle N_{Species} \rangle$	$\langle F(GNPs\|Rab5) \rangle$	$\langle F(Rab5\|GNPs) \rangle$
GNPs	1.84 ± 0.30[1]		
Rab5-561	1.68 ± 0.24		
GNPs & Rab5-561	0.35 ± 0.07	0.21 ± 0.03	0.21 ± 0.03

[1] Standard error.

In Table 4.5, the average number of clusters containing phospholipid coated gold nanoparticles is consistent with the number of observed clusters after 2 hours of variable exposure, as previously shown in Table 4.2. There are approximately 1.84 clusters containing phospholipid coated gold nanoparticles. In addition, there are approximately 1.68 clusters marked by Rab5-561 and 0.35 clusters that contain both phospholipid coated gold nanoparticles and Rab5 markers.

The calculations for the average fractions of co-localization represented in Table 5.5 reflect approximately 21% of clusters containing phospholipid coated gold nanoparticles contain Rab5 and approximately 21% of the clusters marked by Rab5 contain phospholipid coated gold nanoparticles.

The images obtained in Figure 4.3 and the averaged values calculated in Table 4.5 are in agreement; a very small fraction of each species, specifically 20% of early endocytic clusters contain gold nanoparticles and 20% of clusters with gold nanoparticles contain Rab5-561 markers.

4.2.2 Rab11-633 Marked Recycling Endocytic Compartments Containing Phospholipid Coated Gold Nanoparticles in C2C12 Cells

The extent to which phospholipid coated gold nanoparticles associate with Rab11-633 marked recycling endocytic compartments was studied.

Figure 4.4 shows contrast enhanced images of GNPs and Rab11-633 marked compartments in one cell. The Merge image is an overlay of the GNPs and Rab11-633 images. The Original Merge is an overlay of the GNPs and Rab11-633 images that were obtained originally in the experiment without contrast enhancement. Thus, the Original Merge image is shown for purpose of comparison to that of the Merge image.

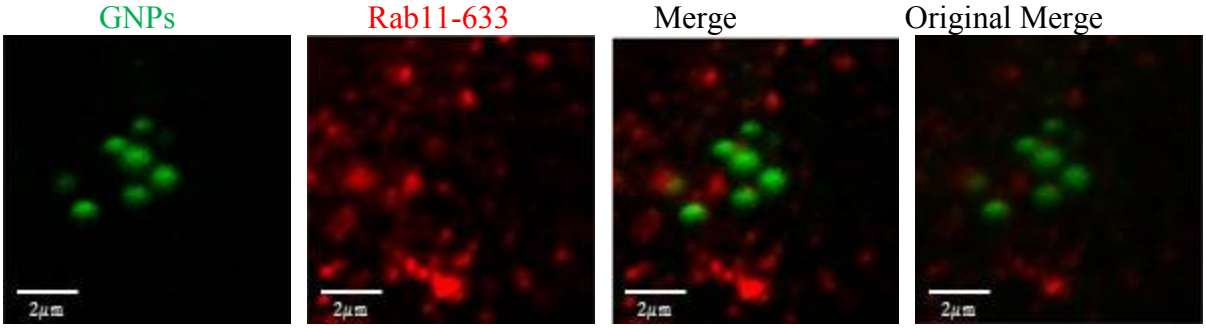

Figure 4.4 Rab11-633 Marked Recycling Endocytic Compartments Containing Phospholipid Coated Gold Nanoparticles in C2C12 Cells

Contrast enhanced confocal fluorescence microscopy images of GNPs and Rab11-633 marked compartments in one cell. The Merge image is an overlay of the GNPs and Rab11-633 images. The Original Merge is an overlay of the GNPs and Rab11-633 images that were obtained originally in the experiment without contrast enhancement. Thus, the Original Merge image is shown for purpose of comparison to that of the Merge image.

Similar to that of Rab5-561 and GNPs in Figure 4.3, from a visual perspective, there are few, if any, yellow regions in the Merge image in Figure 4.4 thus reflecting little degree of co-localization among phospholipid coated gold nanoparticles and Rab11-633 markers.

Table 4.6 shows the average number of clusters denoted by $\langle N_{Species} \rangle$ and the average fractions of co-localization of GNPs and Rab11-633 marked compartments. The average fraction of clusters containing phospholipid coated gold nanoparticles that contain Rab11-633 markers is

denoted by $\langle F(GNPs|Rab11)\rangle$. Likewise, the average fraction of clusters containing Rab11-633 markers that contain phospholipid coated gold nanoparticles is denoted by $\langle F(Rab11|GNPs)\rangle$.

Table 4.6 Average Number of Clusters and Fractions of Co-Localization of GNPs & Rab11-633 Marked Recycling Endocytic Compartments in C2C12 Cells

Species	$\langle N_{Species}\rangle$	$\langle F(GNPs\|Rab11)\rangle$	$\langle F(Rab11\|GNPs)\rangle$
GNPs	2.44 ± 0.44[1]		
Rab11-633	2.46 ± 0.19		
GNPs & Rab11-633	0.42 ± 0.09	0.25 ± 0.07	0.18 ± 0.04

[1] Standard error.

In Table 4.6, the average number of clusters containing phospholipid coated gold nanoparticles is consistent with the number of observed clusters for 2 hours of variable exposure, as previously shown in Table 4.2. There are approximately 2.44 clusters containing phospholipid coated gold nanoparticles and approximately 2.46 clusters containing Rab11-633 markers. There are also approximately 0.42 clusters that contain both phospholipid coated gold nanoparticles and Rab11-633 markers.

The calculations for the average fractions of co-localization represented in Table 4.6 reflect approximately 25% of the clusters containing phospholipid coated gold nanoparticles associate with Rab11-633 markers and approximately 18% of the clusters containing Rab11-633 markers contain phospholipid coated gold nanoparticles.

The images obtained in Figure 4.4 and the averaged values calculated in Table 4.6 are in agreement; visually speaking, a very small fraction of each species associate with one another in an observation area which suggests that very few clusters labelled to be recycling endosomes have phospholipid coated gold nanoparticles. Meanwhile, a slightly higher percentage of clusters containing gold nanoparticles have some recycling markers on them.

4.2.3 Rab7-633 Marked Late Endocytic Compartments Containing Phospholipid Coated Gold Nanoparticles in C2C12 Cells.

The extent to which phospholipid coated gold nanoparticles associate with Rab7-633 marked late endocytic compartments was studied.

Figure 4.5 shows contrast enhanced images of GNPs and Rab7-633 marked compartments in one cell. The Merge image is an overlay of the GNPs and Rab7-633 images. The Original Merge is an overlay of the GNPs and Rab7-633 images that were obtained originally in the experiment without contrast enhancement. Thus, the Original Merge image is shown for purpose of comparison to that of the Merge image.

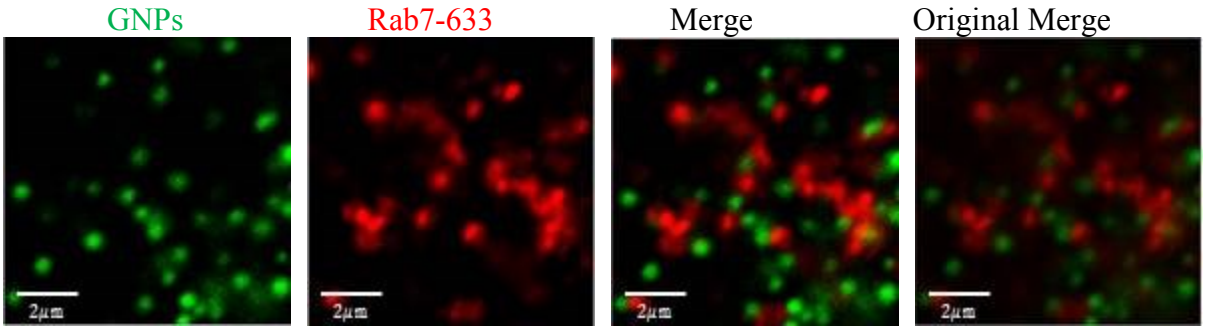

Figure 4.5 Rab7-633 Marked Late Endocytic Compartments Containing Phospholipid Coated Gold Nanoparticles in C2C12 Cells

Contrast enhanced confocal fluorescence microscopy images of GNPs and Rab7-633 marked compartments in one cell. The Merge image is an overlay of the GNPs and Rab7-633 images. The Original Merge is an overlay of the GNPs and Rab7-633 images that were obtained originally in the experiment without contrast enhancement. Thus, the Original Merge image is shown for purpose of comparison to that of the Merge image.

Similar to that of Rab5-561 and GNPs and Rab11-633 and GNPs in Figure 4.3 and Figure 4.4, the Merge Image in Figure 4.5 reflects little if any degree of co-localization among phospholipid coated gold nanoparticles and Rab7 marked late endocytic compartments in C2C12 cells.

Table 4.7 shows the average number of clusters denoted by $\langle N_{Species} \rangle$ and the average fractions of co-localization of GNPs and Rab7 marked compartments. The average fraction of clusters containing phospholipid coated gold nanoparticles that contain Rab7-633 markers is denoted by $\langle F(GNPs|Rab7) \rangle$. Likewise, the average fraction of clusters containing Rab7-633 markers that contain phospholipid coated gold nanoparticles is denoted by $\langle F(Rab7|GNPs) \rangle$.

Table 4.7 Average Number of Clusters and Fractions of Co-Localization of GNPs & Rab7-633 Marked Late Endocytic Compartments in C2C12 Cells

Species	$\langle N_{Species} \rangle$	$\langle F(GNPs \mid Rab7) \rangle$	$\langle F(Rab7 \mid GNPs) \rangle$
GNPs	1.20 ± 0.13[1]		
Rab7-633	2.13 ± 0.14		
GNPs & Rab7	0.34 ± 0.03	0.33 ± 0.04	0.17 ± 0.02

[1] Standard error.

In Table 4.7, the average number of clusters of phospholipid coated gold nanoparticles is consistent with the number of observed clusters for 2 hours of variable exposure, as previously shown in Table 4.2. There are approximately 1.20 clusters containing phospholipid coated gold nanoparticles and approximately 2.13 clusters marked by Rab7. Lastly, there are approximately 0.34 clusters that contain both phospholipid coated gold nanoparticles and Rab7-633 markers.

The calculations for the average fractions of co-localization represented in Table 4.7 reflect approximately 33% of the clusters of phospholipid coated gold nanoparticles contain Rab7-633 markers and approximately 17% of the clusters marked by Rab7 contain phospholipid coated gold nanoparticles.

The images obtained in Figure 4.5 and the averaged values calculated in Table 4.7 are in agreement; visually speaking, a very small fraction of each species associate with one another in an observation area. Specifically, there are a greater fraction of clusters of GNPs associate with Rab7-633 markers than do clusters marked with Rab7-633 contain GNPs.

4.2.4 LAMP-1-633 Marked Lysosomal Endocytic Compartments Containing Phospholipid Coated Gold Nanoparticles in C2C12 Cells.

The extent to which phospholipid coated gold nanoparticles associate with LAMP-1-633 marked lysosomal endocytic compartments was studied.

Figure 4.5 shows contrast enhanced images of GNPs and LAMP-1-633 marked compartments in one cell. The Merge image is an overlay of the GNPs and LAMP-1-633 images. The Original Merge is an overlay of the GNPs and LAMP-1-633 images that were obtained

originally in the experiment without contrast enhancement. Thus, the Original Merge image is shown for purpose of comparison to that of the Merge image.

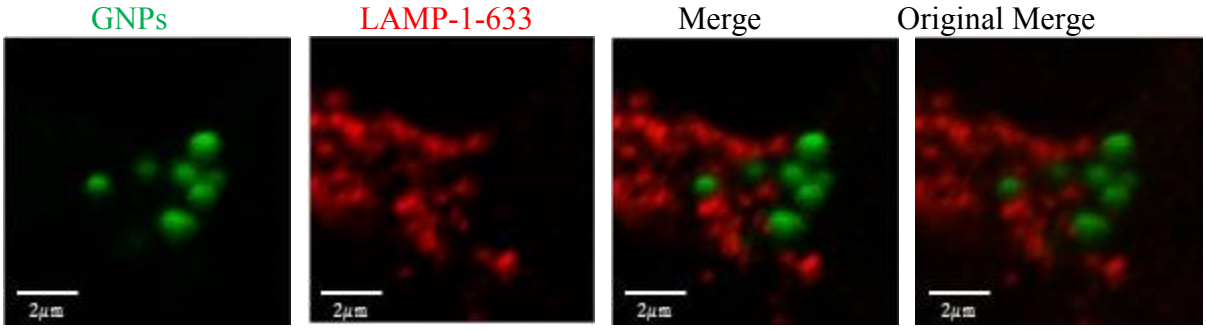

Figure 4.6 LAMP-1 Marked Lysosomal Endocytic Compartments Containing Phospholipid Coated Gold Nanoparticles in C2C12 Cells.

Contrast enhanced fluorescence microscopy images of GNPs-633 and LAMP-1 marked compartments in one cell. The Merge image is an overlay of the GNPs-633 and LAMP-1 images. The Original Merge is an overlay of the GNPs-633 and LAMP-1 images that were obtained originally in the experiment without contrast enhancement. Thus, the Original Merge image is shown for purpose of comparison to that of the Merge image.

Similar to that of Figure 4.3, Figure 4.4, and Figure 4.5, from a visual perspective, the Merge image Figure 4.6 reflects little degree of co-localization among phospholipid coated gold nanoparticle and LAMP-1-633 marked compartments in C2C12 cells.

Table 4.8 reflects the average number of clusters denoted by $\langle N_{Species} \rangle$ and the average fractions of co-localization of GNPs and LAMP-1-633 marked compartments. The average fraction of clusters containing phospholipid coated gold nanoparticles that contain LAMP-1-633 markers is denoted by $\langle F(GNPs|LAMP-1) \rangle$. Likewise, the average fraction of clusters containing LAMP-1 markers that contain phospholipid coated gold nanoparticles is denoted by $\langle F(LAMP-1|GNPs) \rangle$.

Table 4.8 Average Number of Clusters and Fractions of Co-Localization of GNPs & LAMP-1-633 Marked Lysosomal Endocytic Compartments in C2C12 Cells

Species	$\langle N_{Species} \rangle$	$\langle F(GNPs \mid LAMP-1) \rangle$	$\langle F(LAMP-1 \mid GNPs) \rangle$
GNPs	1.66 ± 0.38[1]		
LAMP-1-633	1.71 ± 0.21		
GNPs & LAMP-1-633	0.29 ± 0.05	0.25 ± 0.04	0.22 ± 0.04

[1] Standard error.

In Table 4.8, the average number of clusters of phospholipid coated gold nanoparticles is consistent with the number of observed clusters for 2 hours of variable exposure, as previously shown in Table 4.2. There are approximately 1.66 clusters of phospholipid coated gold nanoparticles. There are also approximately 1.71 clusters marked with LAMP-1-633 and approximately 0.29 clusters that contain both phospholipid coated gold nanoparticles and LAMP-1-633 markers.

The calculations for the average fractions of co-localization represented in Table 4.8 reflect approximately 25% of the clusters containing phospholipid coated gold nanoparticles contain LAMP-1 markers and approximately 22% of the clusters marked with LAMP-1contain phospholipid coated gold nanoparticles.

The images obtained in Figure 4.5 and the averaged values calculated in Table 4.8 are in agreement; visually speaking, a very small fraction of each species associate with one another in an observation area.

4.3 Summary of Fractions of Co-localization in C2C12 Cells

Table 4.9 and Table 4.10 are summarized tables of each of the averaged fractions of co-localization of phospholipid coated gold nanoparticles with an endocytic compartment.

Table 4.9 Extent of co-localization of GNPs with Endocytic Marked Compartments in C2C12 Cells

$\langle F(Green\|Red)\rangle$	Rab5	Rab7	Rab11	LAMP1
GNPs	0.21 ± 0.03[1]	0.33 ± 0.04	0.25 ± 0.07	0.25 ± 0.04

[1] Standard error.

Table 4.10 Extent of co-localization of Endocytic Marked Compartments with GNPs in C2C12 Cells

$\langle F(Red\|Green)\rangle$	GNPs
Rab5	0.21 ± 0.03[1]
Rab7	0.17 ± 0.02
Rab11	0.18 ± 0.04
LAMP1	0.22 ± 0.04

[1] Standard error.

The fractions of co-localization in Table 4.9 reflect the following; on average, between 20-30% of clusters containing phospholipid coated gold nanoparticles also contain markers associated with one endocytic compartment. The results indicate that although a low fraction of clusters containing gold nanoparticles also contain a marker, this is a significant interaction. Thus, clathrin mediated endocytosis of this nanomaterial system is occurring.

Table 4.10 reflects the following; on average, approximately 20% of clusters containing one marker also contain phospholipid coated gold nanoparticles. Likewise, although this is a small fraction, on average, 20% of clusters containing a marker of an endocytic compartment contain phospholipid coated gold nanoparticles, thus endocytosis of phospholipid coated gold nanoparticles is occurring.

4.4 Co-Localization of Phospholipid Coated Gold Nanoparticles with Two Other Endocytic Compartments in C2C12 Cells

The previous section discussed the co-localization of phospholipid coated gold nanoparticles with markers specific for endocytic compartments. Chapter 4.4 discusses the extent to which phospholipid coated gold nanoparticles associate with two markers and the extent to which one marker associates with another marker and phospholipid coated gold nanoparticles. This tells us the co-existence of phospholipid coated gold nanoparticles with two endocytic

markers for further inquiry of the transfer of gold nanoparticles between two endocytic marked compartments.

In this section, the following experimental combinations were studied; GNPs & Rab5-561 & Rab11-633, GNPs & Rab5-561, & Rab7-633, GNPs & Rab5-561 & LAMP-1-633, and GNPs & Rab7-633 & LAMP-1-633. As with one and two color studies, GNPs are always excited with a 488 nm laser. GNPs are colored green in images, markers colored in red and blue. Recall, the coloring of the images does not represent the wavelength of excitation; the colors green, red, and blue were chosen for image analysis to visualize pairwise and three-way interaction, as mentioned in Chapter 2.5. The triple labelling procedure of phospholipid coated gold nanoparticles and primary and secondary antibodies required for labelling of two markers can be referred in Chapter 2.7.2. Procedure required for obtaining images via laser scanning confocal microscopy can be referred to in Chapter 2.10.3.3. Lastly, triple image cross correlation spectroscopy analysis can be referred to in Chapter 2.11.3.

4.4.1 GNPs & Rab5-561 & Rab11-633 in C2C12 Cells

The association of phospholipid coated gold nanoparticles with Rab5-561 and Rab11-633 markers was studied in C2C12 cells.

Figure 4.7 shows contrast enhanced images of a cell labelled with phospholipid coated gold nanoparticles, Rab5-561, and Rab11-633.

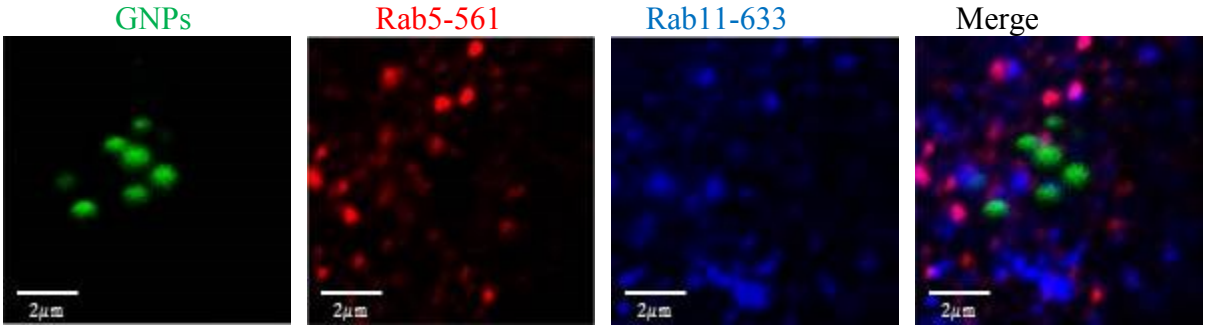

Figure 4.7 GNPs & Rab5-561 & Rab11-633 in C2C12 Cells

In Figure 4.7, the observed purple spots in the image reflect the co-localization of Rab5-561 and Rab11-631.

In a three-color labelling experiment, one would observe the color white with 100% overlap of red, green, and blue. This is not immediately obvious, thus triple image cross correlation spectroscopy (TRICCS) is implemented to extract a quantitative representation of three color co-localization.

Table 4.11 shows the number of images, n_{images} obtained in one experiment with the corresponding average number of clusters containing one, two, or three species, $\langle N_{Species} \rangle$.

Table 4.11 Average Number of One, Two, and Three Labelled Clusters of GNPs, Rab5-561, and Rab11-633 Marked Endocytic Compartments in C2C12 Cells

Species	n_{images}	$\langle N_{Species} \rangle$
GNPs	9	3.81 ± 1.39[1]
Rab5-561	9	1.79 ± 0.48
Rab11-633	9	1.83 ± 0.35
GNPs & Rab5-561	9	0.41 ± 0.18
GNPs & Rab11-633	9	0.20 ± 0.08
Rab-5615 & Rab11-633	9	0.41 ± 0.10
GNPs & Rab5-561 & Rab11-633	9	0.47 ± 0.15

[1] Standard error.

The most important observation to take from these experiments is the similarities observed in a two color and one color experiments. Table 4.11 reflects the averages of the numbers of clusters of species observed containing one specific marker and phospholipid coated gold nanoparticles ranges between 1.83-3.81 clusters. Additionally, the number of clusters in which two markers are observed simultaneously is also in agreement with previous experiments, such that the number of clusters containing markers ranges between 0.20-0.41. There is some variation with each individual measurement; however it must be considered that this is a different experiment for which these measurements were calculated.

In contrast to previous experiments, the average number of clusters containing GNPs, Rab5-561, and Rab11-633 were observed and calculated to be approximately 0.47. To fully understand this value, fractions of co-localization were calculated and represented in Table 4.12.

Table 4.12 Average Fractions of Co-Localization in a GNPs, Rab5-561, and Rab11-633 Experiment in C2C12 Cells

⟨F(GNPs|Rab5 Rab11)⟩	⟨F(Rab5 | GNPs Rab11)⟩	⟨F(Rab11| GNPs Rab5)⟩
0.18 ± 0.05[1]	0.31 ± 0.12	0.23 ± 0.07

[1] Standard error.

In Table 4.12, approximately 18% of clusters containing GNPs contain Rab5-561 and Rab11-633 markers. In reference to Table 4.9, this calculation compares to that of the association GNPs and Rab5 markers and GNPs and Rab11 markers, such that all pairwise associations likely have a third marker.

Approximately 31% of clusters containing Rab5 markers contain Rab11 markers and GNPs with a standard error of 0.12 that of the measured value. In reference to Table 4.9, this calculation compares to that of the association of Rab5 markers and GNPs. This calculation also compares to that of the association of Rab5 clusters with Rab11 clusters, although about 10% greater, in reference to.

Approximately 23% of clusters containing Rab11 markers contain Rab5 markers and GNPs with a standard error of 0.07 that of the measured value. In Table 4.10, this calculation compares to that of the association of Rab11 markers and GNPs. This calculation is approximately 20% less in comparison to that of the association of Rab11 and Rab5 markers.

Granted there is an approximate 20% co-localization for pairwise interactions between GNPs and markers in addition to markers and GNPs, this fraction implies that the binary fractions also take into account some clusters that have three species.

4.4.2 GNPs & Rab5-561 & Rab7-633 in C2C12 Cells

The association of phospholipid coated gold nanoparticles with Rab5 and Rab7 markers was studied in C2C12 cells.

Figure 4.8 shows contrast enhanced images of a cell labelled with phospholipid coated gold nanoparticles, Rab5-561, and Rab7-633.

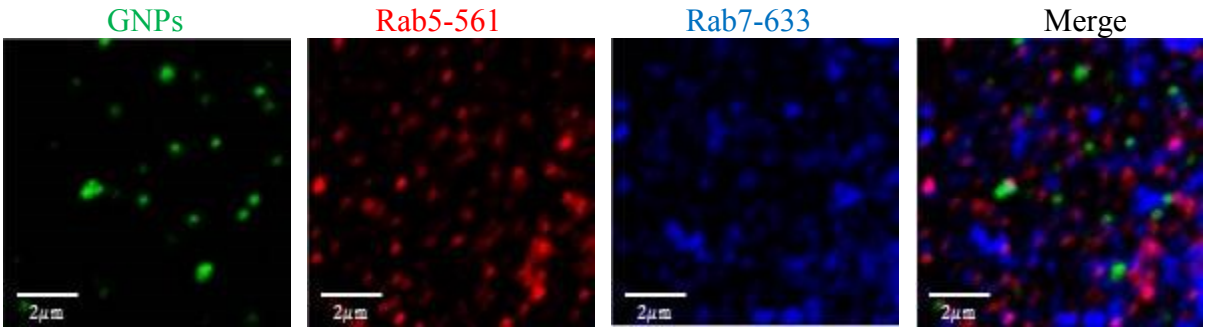

Figure 4.8 GNPs & Rab5-561 & Rab7-633 in C2C12 Cells

In Figure 4.8, the observed purple spots in the image reflect the co-localization of Rab5-561 and Rab7-633. GNPs and Rab7-633 co-localize by the apparent "cyan" color observed due to the overlapping green and blue images.

Table 4.13 shows the number of images, n_{images}obtained in one experiment with the corresponding average number of clusters of species observed, $\langle N_{Species} \rangle$.

Table 4.13 Average Number of One, Two, and Three Labelled Clusters of GNPs, Rab5-561, and Rab7-633 Marked Endocytic Compartments in C2C12 Cells

Species	n_{images}	$\langle N_{Species} \rangle$
GNPs	14	2.77 ± 0.93[1]
Rab5-561	14	1.92 ± 0.18
Rab7-633	14	1.52 ± 0.16
GNPs & Rab5-561	14	0.33 ± 0.10
GNPs & Rab7-633	14	0.46 ± 0.14
Rab5 & Rab7-633	14	0.27 ± 0.13
GNPs & Rab5-561 & Rab7-633	14	0.30 ± 0.09

[1] Standard error.

Table 4.13 reflects the number of clusters of species observed for each individual marked compartment and phospholipid coated gold nanoparticles ranges between 1.52-2.77. Additionally, the number of clusters in which two markers are observed simultaneously is also in agreement with previous experiments, such that the number of clusters of containing two species ranges between approximately 0.27-0.46. There is slight variation with each individual

measurement, however it must be kept to consideration that this is a different sample for which these measurements were calculated.

In contrast to previous experiments, the number of clusters containing GNPs, Rab5-561, and Rab7-633 markers were observed and calculated to be approximately 0.30. To fully understand this value, fractions of co-localization were calculated and represented in Table 4.14.

Table 4.14 Average Fractions of Co-Localization in a GNPs, Rab5, and Rab7 Experiment in C2C12 Cells

⟨F(GNPs|Rab5 Rab7)⟩	⟨F(Rab5 | GNPs Rab7)⟩	⟨F(Rab7| GNPs Rab5)⟩
0.16 ± 0.05[1]	0.13 ± 0.03	0.20 ± 0.07

[1] Standard error.

In Table 4.14, approximately 16% of clusters containing GNPs contain Rab5-561 and Rab11 markers with a standard error of ± 0.05 that of the measured value. As presented in Table 4.9, this calculation compares to that of the association of GNPs with Rab5-561 markers and the association of GNPs and Rab7 markers.

Approximately 13% of clusters containing Rab5 markers contain Rab7 markers and GNPs with a standard error of ± 0.03 that of the measured value. As shown in Table 4.10, this calculation is approximately 10% less in comparison to that of the association of Rab5-561 with GNPs. Additionally, this calculation is approximately 40% less in comparison to that of the association of Rab5-561 markers with Rab7-633 markers, in reference to Table 3.17.

Approximately 20% of clusters containing Rab7-633 markers contain Rab5-561 markers and GNPs with a standard error of 0.07 that of the measured value. As shown in Table 4.10, this calculation compares to that of the association of Rab7-633 markers and GNPs. Additionally, this calculation is 30% less in comparison to that of the association of Rab7-633 markers with Rab5-561 markers, in reference to Table 3.17.

Granted there is an approximate 20% co-localization for pairwise interactions between GNPs and markers in addition to markers and GNPs, this fraction implies that the extent of pairwise co-localization takes also take into account some clusters that have three species,

similarly to the experiment involving the association GNP, Rab5-561, and Rab11-561 compartments.

4.4.3 GNPs & Rab5-561 & LAMP-1-633 in C2C12 Cells

The association of phospholipid coated gold nanoparticles with Rab5-561 and LAMP-1-633 markers was studied in C2C12 cells.

Figure 4.9 shows contrast enhanced images of a cell labelled with phospholipid coated gold nanoparticles, Rab5-561, and LAMP-1-633.

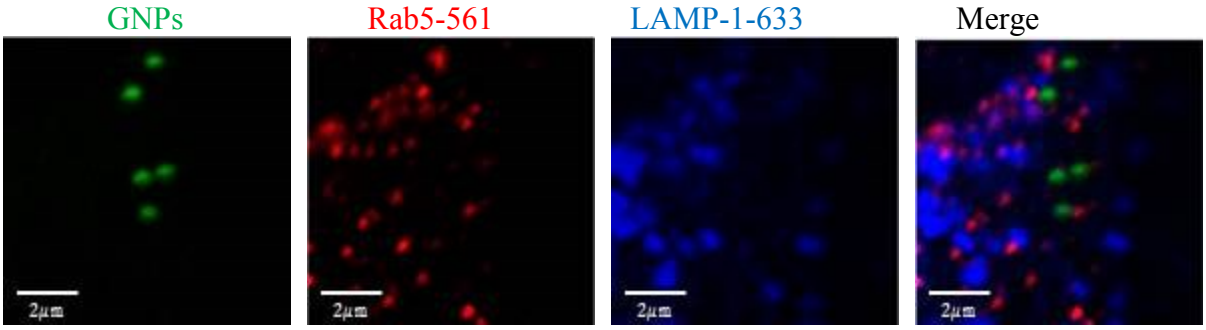

Figure 4.9 GNPs & Rab5-561 & LAMP-1-633 in C2C12 Cells

In Figure 4.9, the observed purple spots in the image reflect the co-localization of Rab5-561 and LAMP-1-633. GNPs and LAMP-1-633 co-localize by the apparent "cyan" color observed due to the overlapping green and blue images.

Table 4.15 shows the number of images, n_{images}obtained in one experiment with the corresponding average number of clusters of species observed, $\langle N_{Species} \rangle$.

Table 4.15 Average Number of One, Two, and Three Labelled Clusters of GNPs, Rab5-561, and LAMP-1-633 Marked Endocytic Compartments in C2C12 Cells

Species	n_{images}	$\langle N_{Species} \rangle$
GNPs	10	3.71 ± 0.67[1]
Rab5-561	10	2.14 ± 0.42
LAMP-1	10	2.31 ± 0.45
GNPs & Rab5-561	10	0.21 ± 0.07
GNPs & LAMP-1-633	10	0.67 ± 0.32
Rab5-561 & LAMP-1-633	10	0.29 ± 0.07
GNPs & Rab5-561 & LAMP-1-633	10	0.28 ± 0.07

[1] Standard error.

Table 4.15 reflects the numbers of clusters of species observed for each individual marked compartment and phospholipid coated gold nanoparticles ranges between 2.14-3.71. Additionally, the number of clusters in which two markers are observed simultaneously is also in agreement with previous experiments, such that the number of clusters of species observed ranges between 0.21-0.67. There is slight variation with each individual measurement, however it must be remembered that this is a different sample for which these measurements were calculated.

In contrast to previous experiments, the number of clusters containing GNPs, Rab5-561, and LAMP-1-633 were observed and calculated to be approximately 0.28. To fully understand this value, fractions of co-localization were calculated and represented in Table 4.16.

Table 4.16 Averaged Fractions of co-localization of GNPs, Rab5, and LAMP-1

$\langle F(GNPs \mid Rab5\ LAMP-1) \rangle$	$\langle F(Rab5 \mid GNPs\ LAMP-1) \rangle$	$\langle F(LAMP-1 \mid GNPs Rab5) \rangle$
0.08 ± 0.02[1]	0.14 ± 0.03	0.12 ± 0.01

[1] Standard error.

In Table 4.16, approximately 8% of clusters containing GNPs contain Rab5-561 and LAMP-1-633 markers. As presented in Table 4.9, this calculation is 10% less than that of the association of clusters of GNPs with Rab5-561 markers. This calculation is also 10% less than that of the association of clusters of GNPs with LAMP-1-561 markers.

Approximately 14% of clusters containing Rab5-561 contain GNPs and LAMP-1-633 markers. As shown in Table 4.10, this calculation is 10% less than that of the association of Rab5 markers with GNPs. Additionally, this calculation is approximately 20% less in comparison to that of the association of Rab5 markers with LAMP-1 markers, in reference to Table 3.17.

Approximately 12% of clusters containing LAMP-1-633 markers contain Rab5-561 markers and GNPs. As shown in Table 4.10, this calculation is 10% less in comparison to that of association LAMP-1-633 markers with GNPs. Additionally, this calculation is 20% less in comparison to that of the association of LAMP-1-633 clusters with Rab5-561 clusters, in reference to Table 3.17.

This data strongly imply that although each species has a 20% probability of residing on the same cluster or endosome as one other marker or phospholipid coated gold nanoparticles, fewer clusters have phospholipid coated gold nanoparticles, Rab5 markers, *and* LAMP-1 markers residing on the same endosome.

4.4.4 GNPs & Rab7-633 & LAMP-1-561 in C2C12 Cells

The association of phospholipid coated gold nanoparticles with Rab7-633 and LAMP-1-561 markers was studied in C2C12 cells.

Figure 4.10 is a visual representation of contrast enhanced images of a cell labelled with phospholipid coated gold nanoparticles, Rab7-633, and LAMP-1-561.

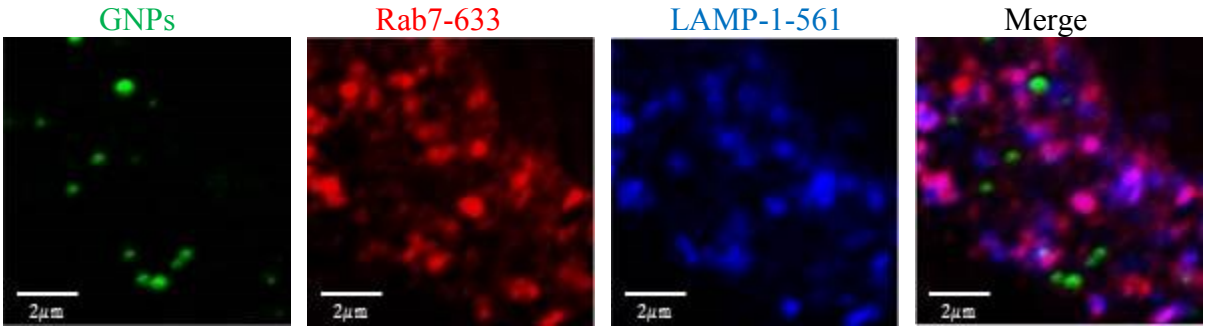

Figure 4.10 GNPs & Rab7-633 & LAMP1-561 in C2C12 Cells

In Figure 4.10, there are purple regions observed in the image to reflect the co-localization of Rab7-633 and LAMP-1-561. GNPs and LAMP-1 co-localize by the apparent "cyan" color observed due to the overlapping green and blue images.

Table 4.17 shows the number of images, n_{images}obtained in one experiment with the corresponding average number of clusters of species observed, $\langle N_{Species} \rangle$.

Table 4.17 Averaged Number of One, Two, and Three Clusters of GNPs, Rab7, and LAMP-1 Endocytic Marked Compartments in C2C12 Cells

Species	n_{images}	$\langle N_{Species} \rangle$
GNPs	5	1.35 ± 0.09[1]
Rab7	5	0.95 ± 0.21
LAMP-1	5	1.30 ± 0.15
GNPs & Rab7	5	0.18 ± 0.11
GNPs & LAMP1	5	0.17 ± 0.05
Rab7 & LAMP1	5	0.74 ± 0.08
GNPs & Rab7 & LAMP1	5	0.54 ± 0.11

[1] Standard error.

Table 4.17 reflects the numbers of clusters of species observed for each individual marked compartment and phospholipid coated gold nanoparticle cluster ranges between 0.95-1.35. Additionally, the number of clusters by which two markers are observed simultaneously is also in agreement with previous experiments, such that the number of clusters of markers species observed ranges between 0.17-0.74. There is slight variation with each individual measurement, however it must be kept to consideration that this is a different experiment for which these measurements were calculated.

In contrast to previous experiments, the number of clusters containing GNPs, Rab7-633, and LAMP-1-561 markers were observed and calculated to be approximately 0.54. To fully understand this value, fractions of co-localization were calculated and represented in Table 4.18.

Table 4.18 Averaged Fractions of Co-localization of GNPs with Late and Lysosomal Endocytic Marked Compartments in C2C12 Cells

$\langle F(GNPs \mid Rab7 \;\; LAMP-1) \rangle$	$\langle F(Rab7 \mid GNPs \; LAMP-1) \rangle$	$\langle F(LAMP-1 \mid GNPs \; Rab7) \rangle$
0.40 ± 0.08[1]	0.65 ± 0.17	0.45 ± 0.23

[1] Standard error.

In Table 4.18, approximately 40% of clusters containing GNPs also contain Rab7-633 and LAMP-1 markers. As presented in Table 4.9, this calculation is 20% greater than that of the association of GNPs with Rab7 markers. This calculation is also 20% greater than that of the association of GNPs with LAMP-1 markers, which is a bit unusual.

Approximately 65% of clusters containing Rab7 markers contain LAMP-1-561 markers and GNPs. As shown in Table 4.10, this calculation is 50% greater than that of the association of Rab7-633 markers with GNPs. Additionally, this calculation is in comparison to that of the association of Rab7-633 markers with LAMP-1-561 markers, in reference to Table 3.17.

Approximately 50% of clusters containing LAMP-1-561 markers contain Rab7-633 markers and GNPs. As shown in Table 4.10, this calculation is 30% greater in comparison to that of association LAMP-1-561 markers with GNPs. Additionally, this calculation is 40% less in comparison to that of the association of LAMP-1-561 markers with Rab7-633 markers, in reference to Table 3.17.

As previously shown in this section, the fraction of complexes containing two markers may also contain one other marker.

4.5 Internalization of Phospholipid Coated Gold Nanoparticles in A549 Cells

The internalization of GNPs and the association of GNPs with clathrin mediated endocytic compartments in A549 cells will be discussed as previously shown in Chapters 4.1, 4.2, and 4.4.

4.5.1 Variable Exposure, Fixed Uptake of Phospholipid Coated Gold Nanoparticles in A549 Cells

A549 cells were exposed to phospholipid coated gold nanoparticles via a variable exposure, fixed uptake experiment.

In Figure 4.11, images A, B, C, and D each correspond to one confocal fluorescence microscopy image of one cell from each of the four samples prepared in the experiment in which the cells in each sample were exposed to phospholipid coated gold nanoparticles for times of 1, 2, 4 and 24 hours, respectively, prior to fixation.

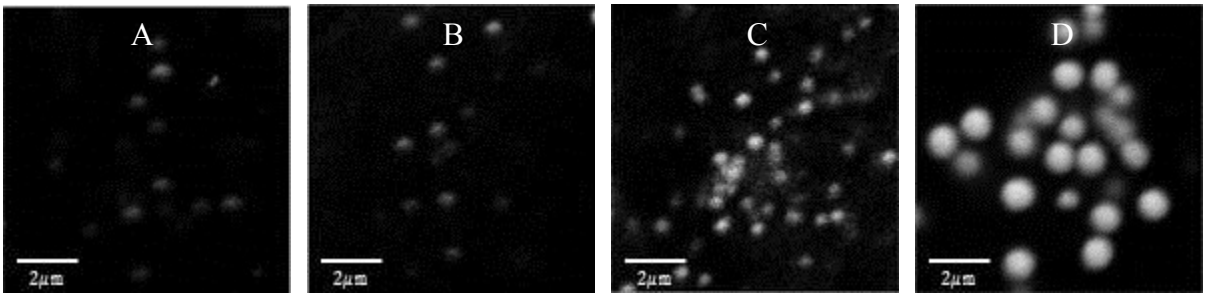

Figure 4.11 Images of Phospholipid Coated Gold Nanoparticles after Variable Exposure, Fixed uptake in A549 Cells

Images A, B, C, and D each correspond to one confocal fluorescence microscopy image of one cell from each of the four samples prepared in the experiment in which the cells in each sample were exposed to phospholipid coated gold nanoparticles for 1, 2,4 and 24 hours, respectively, prior to fixation.

The images shown in Figure 4.11 show that there appear to be fewer clusters of phospholipid coated gold nanoparticles in larger compartments with the progression of time in A549 cells.

Table 4.19 is a reflection of the averages of the auto correlation amplitude, average fitted laser beam width, and average intensity from a data set of 20-30 images of A549 cells exposed to phospholipid coated gold nanoparticles for 1, 2, 4, and 24 hours.

Table 4.19 Averages of ICS Paramaters for Phospholipid Coated Gold Nanoparticles after Variable Exposure, Fixed Uptake in A549 Cells

Time (hours)	$\langle \mathbf{g(0,0)} \rangle$	$\langle \boldsymbol{\omega}\ (\boldsymbol{\mu m}) \rangle$	$\langle I_{avg.} \rangle$
1	0.21 ± 0.04[1]	0.41 ± 0.01	82.8 ± 8.3
2	0.27 ± 0.07	0.39 ± 0.02	131 ± 15
4	0.65 ± 0.17	0.38 ± 0.01	138 ± 10
24	1.61 ± 0.18	0.48 ± 0.01	527 ± 43

[1] Standard error.

The data obtained as represented in Table 4.19 reflects an increasing trend of the auto correlation amplitude with time. The fit for the laser beam width ranges between 0.38-0.41 microns, which is quite similar in magnitude to the fits of the laser beam width corresponding to for markers observed in the observation area in A549 cells in Chapter 3. The fitted laser beam width corresponding to the measurement of markers of clathrin mediated endosomes is also approximately 0.40 microns. Thus, simply from this observation, one can assume phospholipid coated gold nanoparticles may be contained in endocytic compartments as shown in Chapter 3, or are at the very least undergoing clathrin mediated endocytosis. Additionally, the average intensity of phospholipid coated gold nanoparticles increases with time of phospholipid coated gold nanoparticle exposure to A549 cells.

Table 4.20 shows the derived parameters corresponding to the average number of clusters containing phospholipid coated gold nanoparticles, the average number of clusters containing phospholipid coated gold nanoparticles per square micron, and the average relative degree of aggregation for phospholipid coated gold nanoparticles per cluster; calculated for a set of 20-30 images per sample. The calculations presented in Table 4.20 are in reference to the data obtained in Table 4.19. The average values for each parameter are represented with respect to standard error.

Table 4.20 Averages of Derived Parameters for Phospholipid Coated Gold Nanoparticles Undergoing Variable Exposure, Fixed Uptake in A549 Cells

Variable Exposure Time (hours)	$\langle N_{GNPs} \rangle$	$\langle CD \rangle$	$\langle DA \rangle$
1	11.4 ± 2.1[1]	21.4 ± 3.6	16.4 ± 4.6
2	6.96 ± 1.33	14.8 ± 2.5	40.2 ± 15.8
4	3.73 ± 0.62	8.91 ± 1.70	71.2 ± 15.8
24	0.93 ± 0.16	1.49 ± 0.38	700 ± 49

[1] Standard error.

The data presented in Table 4.20 implies the number of clusters containing phospholipid coated gold nanoparticles in the observation region of the beam decreases with time but a larger relative degree of aggregation of these phospholipid coated gold nanoparticles per cluster is observed with the progression of exposure time in A549 cells. Likewise, the number of clusters containing phospholipid coated gold nanoparticles observed per square micron also decreases with time. Thus, phospholipid coated gold nanoparticles aggregate in fewer clusters but to a larger extent of aggregation within clusters when continuously exposed to A549 cells.

4.5.2 Fixed Exposure, Variable Uptake of GNPs in A549 Cells

A549 cells were exposed to phospholipid coated gold nanoparticles by a fixed exposure, variable uptake experiment.

In Figure 4.12, images A, B, C, and D each correspond to one confocal fluorescence microscopy image of one cell from each of the four samples exposed to phospholipid coated gold nanoparticles for 2 hours, washed, and re-incubated for 1,2,4,and 24 hours, respectively, then fixed.

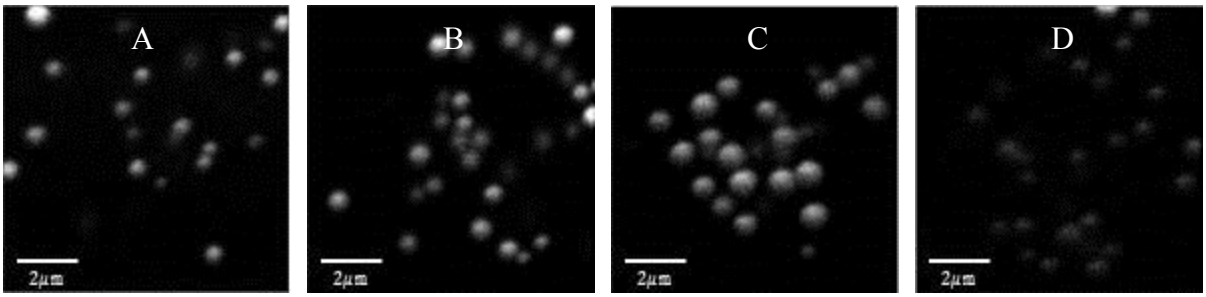

Figure 4.12 Images of Phospholipid Coated Gold Nanoparticles after Fixed Exposure, Variable Uptake in A549 Cells

Images A, B, C, and D each correspond to one confocal fluorescence microscopy image of one cell from each of the four samples exposed to phospholipid coated gold nanoparticles for 2 hours, washed, and re-incubated for 1,2,4,and 24 hours, respectively, then fixed.

Based on the images shown in Figure 4.12, the phospholipid coated gold nanoparticles appear to be taken up similarly over time in A549 cells.

Table 4.21 shows the averages of the auto correlation amplitude, fitted laser beam width, and average intensity for 20-30 images of each sample of A549 cells exposed to phospholipid coated gold nanoparticles for 2 hours, then re-incubated for 1, 2, 4, and 24 hours for uptake. The average values for each parameter are represented with respect to standard error.

Table 4.21 Averages of ICS Parameters for Phospholipid Coated Gold Nanoparticles after Fixed Exposure, Variable Uptake in A549 Cells

Variable Uptake Time (hours)	$\langle \mathbf{g(0,0)} \rangle$	$\langle \boldsymbol{\omega}\ (\boldsymbol{\mu m}) \rangle$	$\langle I_{avg.} \rangle$
1	2.98 ± 0.38[1]	0.36 ± 0.01	78.8 ± 6.9
2	1.24 ± 0.12	0.38 ± 0.01	65.3 ± 6.1
4	0.85 ± 0.10	0.37 ± 0.01	97.3 ± 9.9
24	0.31 ± 0.05	0.39 ± 0.01	29.8 ± 2.1

[1] Standard error.

The average intensity of phospholipid coated gold nanoparticles is more or less constant within the first four hours of uptake, however one can argue the intensity decreases after 24 hours of variable uptake has progressed.

The obtained fit for the laser beam width is consistent and on average approximately 0.40 microns. Therefore, the size of the compartments is also in very good agreement with the averaged fitted laser beam width obtained for markers in Chapter 3.

The auto correlation amplitude decreases with time based on the data shown in Table 4.21. Given that all auto correlation amplitudes for each time interval of variable uptake are greater than 0.10, the measured values of the auto correlation amplitude reflect specific uptake of phospholipid coated gold nanoparticles, such that there is no reflection of fluorescence arising from diffusion.

Table 4.22 is a representation of the average values of the calculations corresponding to phospholipid coated gold nanoparticles after fixed exposure, variable uptake in C2C12 cells. The average number of clusters containing phospholipid coated gold nanoparticles, $\langle N_{GNPs} \rangle$, the number of clusters containing phospholipid coated gold nanoparticles per square micron, $\langle CD \rangle$, and the relative degree of aggregation of phospholipid coated gold nanoparticles per cluster, $\langle DA \rangle$, were calculated for 20-30 images per sample. The calculations presented in Table 4.22 are in reference to the data obtained in Table 4.21. The average values for each parameter are shown with standard error.

Table 4.22 Derived Parameters for Phospholipid Coated Gold Nanoparticles in A549 Cells after Fixed Exposure, Variable Uptake

Variable Uptake Time (hours)	$\langle N_{GNPs} \rangle$	$\langle CD \rangle$	$\langle DA \rangle$
1	0.68 ± 0.08[1]	1.76 ± 0.23	201 ± 51
2	1.01 ± 0.12	2.26 ± 0.24	85.5 ± 14.5
4	1.60 ± 0.21	3.77 ± 0.47	77.3 ± 10.2
24	4.48 ± 0.62	10.3 ± 1.78	10.1 ± 2.3

[1] Standard error.

The number of clusters containing phospholipid coated gold nanoparticles increases with the progression of time allowed for A549 cells to uptake nanoparticles. Likewise, in Table 4.22, due to the minor change in magnitude corresponding to the fit for the laser beam width, the cluster density of phospholipid coated gold nanoparticles increases with time of uptake. The relative degree of aggregation decreases with the progression of time.

These calculations indicate that one would observe a greater number of clusters containing phospholipid coated gold nanoparticles with the progression of time but with a lesser relative degree of aggregation with time. This is a complete opposite trend in comparison to phospholipid coated gold nanoparticles after continuous exposure, variable uptake in A549 cells.

4.6 Co-Localization of Endocytic Compartments Containing Phospholipid Coated Gold Nanoparticles in A549 Cells

This section focusses on the study of the co-localization of endocytic markers with phospholipid coated gold nanoparticles in A549 cells. This particular co-localization measures the extent to which an endocytic marked compartment contains phospholipid coated gold nanoparticles and the extent for which phospholipid coated gold nanoparticle clusters contain markers.

In this section, the following experimental combinations were studied; Rab5-561 & GNPs, Rab11-633 & GNPs, Rab7-633 & GNPs, and LAMP-1-561 & GNPs. Recall, GNPs contain a 488 fluorescent probe, thus GNPs were excited with a 488 nm laser. GNPs are colored in green and markers for endocytic compartments are colored red in images, respectively. Recall, the color of the images does not represent the wavelength of excitation as specified in Chapter 2.5; colors of images were chosen merely for analysis and visualization. The double labelling procedure of phospholipid coated gold nanoparticles and primary and secondary antibodies required for labelling of one marker can be referred in Chapter 2.7.2.

Procedure required for obtaining images via laser scanning confocal microscopy can be referred to in Chapter 2.10.3.2. Lastly, Image cross correlation spectroscopy analysis can be referred to in Chapter 2.11.2.

4.6.1 Rab5-561 Marked Early Endocytic Compartments Containing Phospholipid Coated Gold Nanoparticles in A549 Cells

The extent to which phospholipid coated gold nanoparticles associate with Rab5-561 markers was studied.

Figure 4.13 is a visual representation of contrast enhanced images of GNPs and Rab5-561 marked compartments in one cell. The Merge image is an overlay of the GNPs and Rab5-561 images. The Original Merge is an overlay of the GNPs and Rab5-561 images that were obtained originally in the experiment without contrast enhancement. Thus, the Original Merge image is shown for purpose of comparison to that of the Merge image.

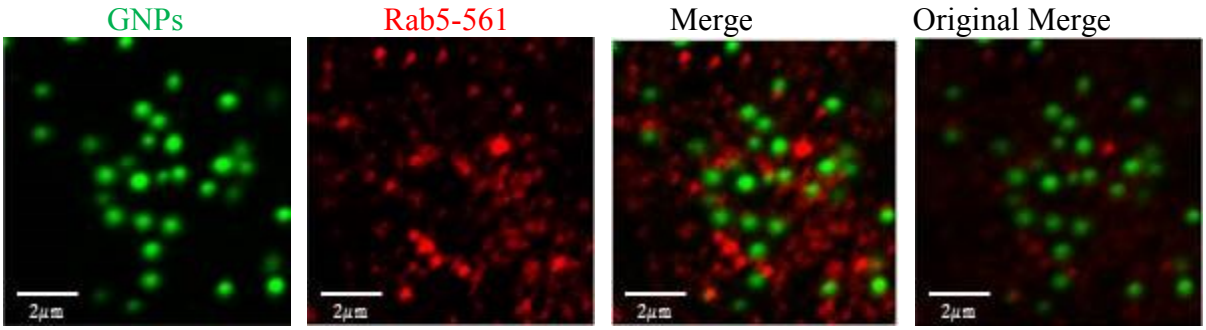

Figure 4.13 Rab5-561 Marked Early Endocytic Compartments Containing Phospholipid Coated Gold Nanoparticles in A549 Cells

A visual representation of contrast enhanced confocal fluorescence microscopy images of GNPs and Rab5-561 marked compartments in one cell. The Merge image is an overlay of the GNPs and Rab5-561 images. The Original Merge is an overlay of the GNPs and Rab5-561 images that were obtained originally in the experiment without contrast enhancement. Thus, the Original Merge image is shown for purpose of comparison to that of the Merge image.

The Merge image in Figure 4.13 shows no clear yellow regions to represent interaction between gold nanoparticles and Rab5 markers. Thus, there is little degree of co-localization among phospholipid coated gold nanoparticles Rab5 marked early endocytic compartments in A549 cells.

Table 4.23 reflects the average number of clusters denoted by $\langle N_{Species} \rangle$ and the average fractions of co-localization of GNPs and Rab5-561 marked compartments. The average fraction of clusters containing phospholipid coated gold nanoparticles that contain Rab5-561 markers is denoted by $\langle F(GNPs|Rab5) \rangle$. Likewise, the average fraction of clusters containing Rab5 markers that contain phospholipid coated gold nanoparticles is denoted by $\langle F(Rab5|GNPs) \rangle$.

Table 4.23 Average Number of Clusters Containing Species and Fractions of Co-Localization of GNPs & Rab5-561 Marked Early Endocytic Compartments in A549 Cells

Species	$\langle N_{Species} \rangle$	$\langle F(GNPs \mid Rab5) \rangle$	$\langle F(Rab5 \mid GNPs) \rangle$
GNPs	0.54 ± 0.09[1]		
Rab5-561	5.03 ± 0.32		
GNPs & Rab5-561	0.31 ± 0.05	0.64 ± 0.05	0.06 ± 0.01

[1] Standard error.

In Table 4.23, the average number of clusters containing phospholipid coated gold nanoparticles is less than the number of observed clusters after 2 hours of variable exposure, as previously shown in Table 4.20. There are approximately 0.54 clusters containing phospholipid coated gold and there are also approximately 5.03 clusters marked by Rab5-561. Lastly, there is approximately 0.31 cluster that contains both phospholipid coated gold nanoparticles and Rab5 markers.

The calculations for the average fractions of co-localization represented in Table 4.23 reflect approximately 64% of the clusters of phospholipid coated gold nanoparticles contain Rab5-561 markers and approximately 6% of the clusters marked by Rab5 contain phospholipid coated gold nanoparticles.

The images obtained in Figure 4.13 and the averaged values calculated in Table 4.23 are in agreement in terms of the small fraction of clusters marked with endosomal markers contain phospholipid coated gold nanoparticles; however, 60% co-localization of gold nanoparticles with Rab5-561 is quite high given the small amount of yellow color observed in the merge image of Figure 4.13.

4.6.2 Rab11-633 Marked Recycling Endocytic Compartments Containing Phospholipid Coated Gold Nanoparticles in A549 Cells

The extent to which phospholipid coated gold nanoparticles associate with Rab11-633 marked recycling endocytic compartments was studied.

Figure 4.14 shows contrast enhanced images of GNPs and Rab11-633 marked compartments in one cell. The Merge image is an overlay of the GNPs and Rab11-633 images. The Original Merge is an overlay of the GNPs and Rab11-633 images that were obtained originally in the experiment without contrast enhancement. Thus, the Original Merge image is shown for purpose of comparison to that of the Merge image.

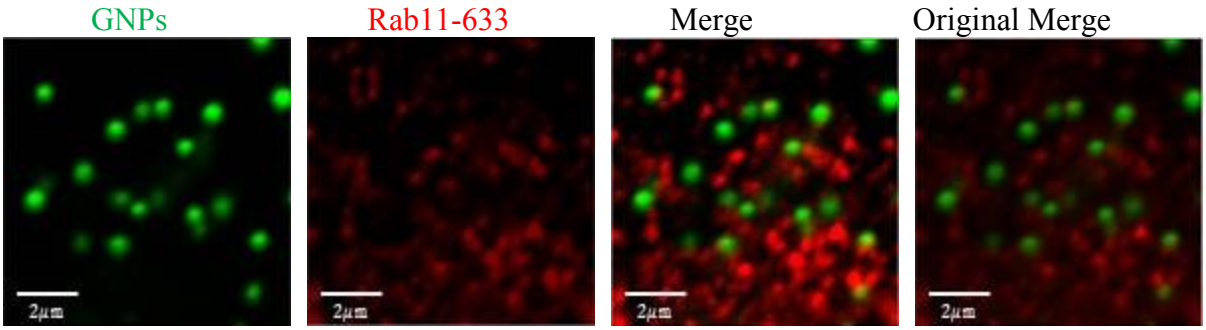

Figure 4.14 Rab11 Marked Recycling Endocytic Compartments Containing Phospholipid Coated Gold Nanoparticles in A549 Cells

Contrast enhanced confocal fluorescence microscopy images of GNPs and Rab11 marked compartments in one cell. The Merge image is an overlay of the GNPs and Rab11 images. The Original Merge is an overlay of the GNPs and Rab11 images that were obtained originally in the experiment without contrast enhancement. Thus, the Original Merge image is shown for comparison purposes to that of the Merge image.

Similar to that of Rab5-561 and GNPs in Figure 4.13, from a visual perspective, the Merge image in Figure 4.14 reflects little degree of co-localization of among phospholipid coated gold nanoparticles and Rab11 marked compartments in C2C12 cells.

Table 4.24 reflects the average number of clusters denoted by $\langle N_{Species} \rangle$ and the average fractions of co-localization of GNPs and Rab11 marked compartments. The average fraction of clusters containing phospholipid coated gold nanoparticles that contain Rab11 markers is denoted by $\langle F(GNPs|Rab11) \rangle$. Likewise, the average fraction of clusters containing Rab11 markers that contain phospholipid coated gold nanoparticles is denoted by $\langle F(Rab11|GNPs) \rangle$.

Table 4.24 Average Number of Clusters and Fractions of Co-Localization of GNPs & Rab11-633 Marked Recycling Endocytic Compartments in A549 Cells

Species	$\langle N_{Species} \rangle$	$\langle F(GNPs \mid Rab11) \rangle$	$\langle F(Rab11 \mid GNPs) \rangle$
GNPs	0.53 ± 0.07[1]		
Rab11-633	3.44 ± 0.40		
GNPs & Rab11-633	0.22 ± 0.03	0.49 ± 0.04	0.08 ± 0.01

[1] Standard error.

In Table 4.24, As such, there are approximately 0.53 clusters that contain phospholipid coated gold nanoparticles and there are approximately 3.44 of clusters marked with Rab11-633. Lastly, there is approximately 0.22 cluster that contains both phospholipid coated gold nanoparticles and Rab11-633 markers.

The calculations for the average fractions of co-localization represented in Table 4.24 reflect approximately 49% of the clusters of phospholipid coated gold nanoparticles contain Rab11-633 markers and approximately 8% of the Rab11-633 marked endocytic compartments contain phospholipid coated gold nanoparticles.

The images obtained in Figure 4.4 and the averaged values calculated in Table 5.24 are in agreement; visually speaking, a very small fraction of each species associate with one another in an observation region of the laser beam. Thus, although a fairly high fraction of clusters containing phospholipid coated gold nanoparticles contain recycling endocytic markers, fewer clusters of recycling markers contain phospholipid coated gold nanoparticles.

4.6.3 Rab7-633 Marked Late Endocytic Compartments Containing Phospholipid Coated Gold Nanoparticles in A549 Cells.

The extent to which phospholipid coated gold nanoparticles associate with Rab7-633 markers was studied.

Figure 4.15 shows contrast enhanced images of GNPs and Rab7-633 marked compartments in one cell. The Merge image is an overlay of the GNPs and Rab7-633 images. The Original Merge is an overlay of the GNPs and Rab7-633 images that were obtained

originally in the experiment without contrast enhancement. Thus, the Original Merge image is shown for purpose of comparison to that of the Merge image.

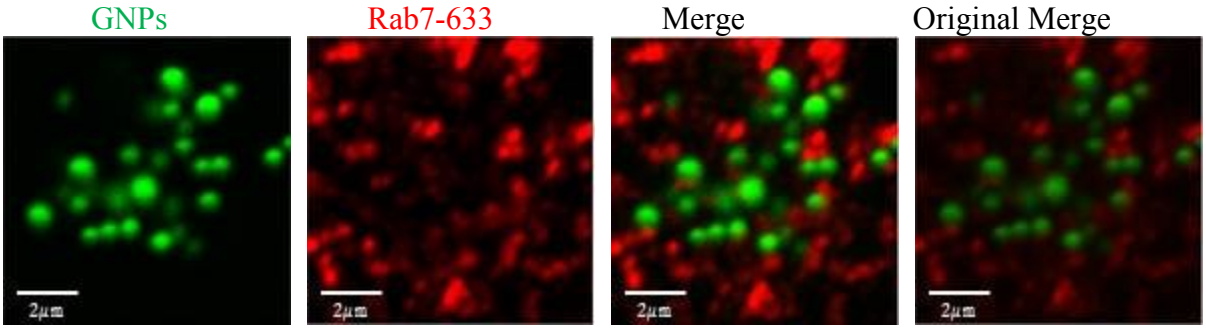

Figure 4.15 Rab7-633 Marked Late Endocytic Compartments Containing Phospholipid Coated Gold Nanoparticles in A549 Cells

Contrast enhanced fluorescence confocal microscopy images of GNPs and Rab7-633 marked compartments in one cell. The Merge image is an overlay of the GNPs and Rab7-633 images. The Original Merge is an overlay of the GNPs and Rab7-633 images that were obtained originally in the experiment without contrast enhancement. Thus, the Original Merge image is shown for purpose of comparison to that of the Merge image.

Similar to that of Rab5-561 and GNPs and Rab11-633 and GNPs in Figure 4.13 and Figure 4.14, from a visual perspective, the Merge image Figure 4.15 reflects little degree of co-localization among phospholipid coated gold nanoparticles and Rab7-633 marked late endocytic compartments in C2C12 cells.

Table 4.25 reflects the average number of clusters denoted by $\langle N_{Species} \rangle$ and the average fractions of co-localization of GNPs and Rab7-633 marked compartments. The average fraction of clusters containing phospholipid coated gold nanoparticles that contain Rab7-633 markers is denoted by $\langle F(GNPs|Rab7) \rangle$. Likewise, the average fraction of clusters containing Rab7 markers that contain phospholipid coated gold nanoparticles is denoted by $\langle F(Rab7|GNPs) \rangle$.

Table 4.25 Average Number of Clusters and Fractions of Co-Localization of GNPs & Rab7-633 Marked Late Endocytic Compartments in A549 Cells

Species	$\langle N_{Species} \rangle$	$\langle F(GNPs \mid Rab7) \rangle$	$\langle F(Rab7 \mid GNPs) \rangle$
GNPs	0.75 ± 0.15[1]		
Rab7-633	1.49 ± 0.25		
GNPs & Rab7	0.22 ± 0.04	0.38 ± 0.08	0.19 ± 0.04

[1] Standard error.

In Table 4.25, there are approximately 0.74 clusters containing phospholipid coated gold nanoparticles and there are also approximately 1.49 clusters containing Rab7-633 markers. Lastly, there are approximately 0.22 clusters that contain both phospholipid coated gold nanoparticles and Rab7-633 markers.

The calculations for the average fractions of co-localization represented in Table 4.25 reflect approximately 38% of the clusters of phospholipid coated gold nanoparticles contain Rab7-633 markers and approximately 19% of the clusters of Rab7-633 markers contain phospholipid coated gold nanoparticles with standard error ± 0.04 the average value.

The images obtained in Figure 4.15 and the averaged values calculated in Table 4.25 are in agreement; visually speaking, a very small fraction of each species associates with one another in an observation area.

4.6.4 LAMP-1-633 Marked Lysosomal Endocytic Compartments Containing Phospholipid Coated Gold Nanoparticles in A549 Cells

The extent to which phospholipid coated gold nanoparticles associate with LAMP-1-633 markers was studied.

Figure 4.16 is a visual representation of contrast enhanced images of GNPs and LAMP-1-633 marked compartments in one cell. The Merge image is an overlay of the GNPs and LAMP-1-633 images. The Original Merge is an overlay of the GNPs and LAMP-1-633 images that were obtained originally in the experiment without contrast enhancement. Thus, the Original Merge image is shown for purpose of comparison to that of the Merge image.

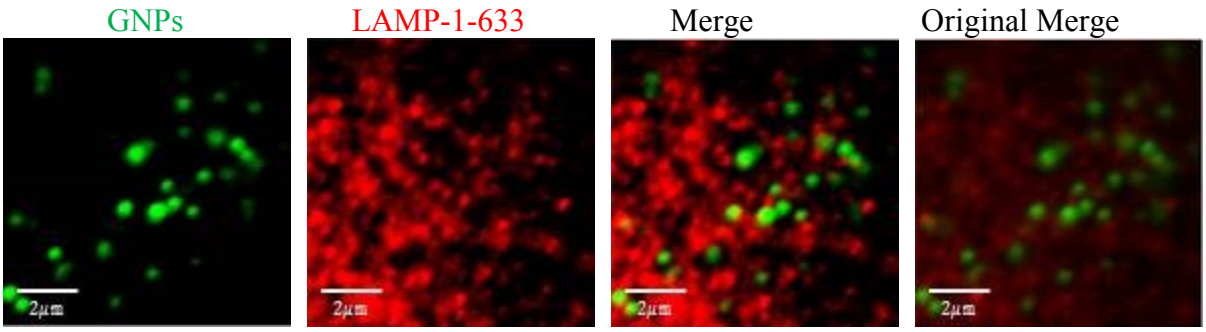

Figure 4.16 LAMP-1 Marked Lysosomal Endocytic Compartments Containing Phospholipid Coated Gold Nanoparticles in A549 Cells

Contrast enhanced fluorescence confocal microscopy images of GNPs and LAMP-1 marked compartments in one cell. The Merge image is an overlay of the GNPs and LAMP-1 images. The Original Merge is an overlay of the GNPs and LAMP-1 images that were obtained originally in the experiment without contrast enhancement. Thus, the Original Merge image is shown for purpose of comparison to that of the Merge image.

Similar to that of Figure 4.13, Figure 4.14, and Figure 4.15, from a visual perspective, the Merge image Figure 4.16 reflects little degree of co-localization among phospholipid coated gold nanoparticles and LAMP-1 marked late endocytic compartments in A549 cells.

Table 4.26 reflects the average number of clusters denoted by $\langle N_{Species} \rangle$ and the average fractions of co-localization of GNPs and LAMP-1 marked compartments. The average fraction of clusters containing phospholipid coated gold nanoparticles that contain LAMP-1-633 markers is denoted by $\langle F(GNPs|LAMP-1) \rangle$. Likewise, the average fraction of clusters containing LAMP-1-633 markers that contain phospholipid coated gold nanoparticles is denoted by $\langle F(LAMP-1|GNPs) \rangle$.

Table 4.26 Average Number of Clusters and Fractions of Co-Localization of GNPs & LAMP-1-633 Marked Lysosomal Endocytic Compartments in A549 Cells

Species	$\langle N_{Species} \rangle$	$\langle F(GNPs\|LAMP-1) \rangle$	$\langle F(LAMP-1\|GNPs) \rangle$
GNPs	0.46 ± 0.09[1]		
LAMP-1-633	9.67 ± 1.10		
GNPs & LAMP-1-633	0.25 ± 0.06	0.57 ± 0.08	0.03 ± 0.01

[1] Standard error.

In Table 4.26, there are approximately 0.46 clusters of phospholipid coated gold nanoparticles and there are also approximately 9.67 clusters marked with LAMP-1-633. Lastly, there are approximately 0.25 clusters that contains both phospholipid coated gold nanoparticles and LAMP-1 markers.

The calculations for the average fractions of co-localization represented in Table 4.26 reflect approximately 57% of the clusters that contain phospholipid coated gold nanoparticles contain LAMP-1 markers and approximately 3% of the clusters marked with LAMP-1 contain phospholipid coated gold nanoparticles.

The images obtained in Figure 4.16 and the averaged values calculated in Table 4.26 are in agreement; although a large percentage of gold nanoparticle containing clusters have LAMP-1-633 markers, few markers contain phospholipid coated gold nanoparticles. The high density of LAMP-1 markers may explain this low fraction.

4.7 Summary of Fractions of Co-localization in A549 Cells

Table 4.27 and Table 5.28 are summarized tables of each of the averaged fractions of co-localization of phospholipid coated gold nanoparticles with an endocytic compartment, and vice versa, in A549 cells previously discussed.

Table 4.27 Extent of co-localization of GNPs with Endocytic Marked Compartments in A549 Cells

$\langle F(Green\|Red)\rangle$	Rab5	Rab7	Rab11	LAMP-1
GNPs	0.64 ± 0.05[1]	0.38 ± 0.08	0.49 ± 0.04	0.57 ± 0.08

[1] Standard error.

Table 4.28 Extent of co-localization of Endocytic Marked Compartments with GNPs in A549 Cells

$\langle F(Red\|Green)\rangle$	GNPs
Rab5	0.06 ± 0.01[1]
Rab7	0.19 ± 0.04
Rab11	0.08 ± 0.01
LAMP-1	0.03 ± 0.01

[1] Standard error.

The fractions of co-localization in Table 4.27 reflect the following; on average, between 40-60% of clusters containing phospholipid coated gold nanoparticles contain markers associated with one endocytic compartment.

The fractions of co-localization in Table 4.28 reflect the following; on average, approximately 10-20% of clusters marked by one endocytic marker contain phospholipid coated gold nanoparticles.

4.8 Co-Localization of Phospholipid Coated Gold Nanoparticles with Two Endocytic Compartments in A549 Cells

The previous section discussed the co-localization of phospholipid coated gold nanoparticles with markers specific for endocytic compartments. Chapter 4.8 discusses the extent to which phospholipid coated gold nanoparticles associate with two markers and the extent to which one marker associates with another marker and phospholipid coated gold nanoparticles.

In this section, the following experimental combinations were studied; GNPs & Rab5-561 & Rab11-633, GNPs & Rab5-561, & Rab7-633, GNPs & Rab5-561 & LAMP-1-633, and GNPs & Rab7-633 & LAMP-1-633. As with one and two color studies, GNPs are always excited with

a 488 nm laser. GNPs are colored green in images, markers colored in red and blue. Recall, the coloring of the images does not represent the wavelength of excitation; the colors green, red, and blue were chosen for image analysis to visualize pairwise and three-way interaction, as mentioned in Chapter 2.5. The triple labelling procedure of phospholipid coated gold nanoparticles and primary and secondary antibodies required for labelling of two markers can be referred in Chapter 2.7.2. Procedure required for obtaining images via laser scanning confocal microscopy can be referred to in Chapter 2.10.3.3. Lastly, triple image cross correlation spectroscopy analysis can be referred to in Chapter 2.11.3.

4.8.1 GNPs & Rab5-561 & Rab11-633 in A549 Cells

The association of phospholipid coated gold nanoparticles with Rab5-561 and Rab11-633 markers was studied in A549 cells.

Figure 4.17 shows contrast enhanced images of a cell labelled with phospholipid coated gold nanoparticles, Rab5, and Rab11.

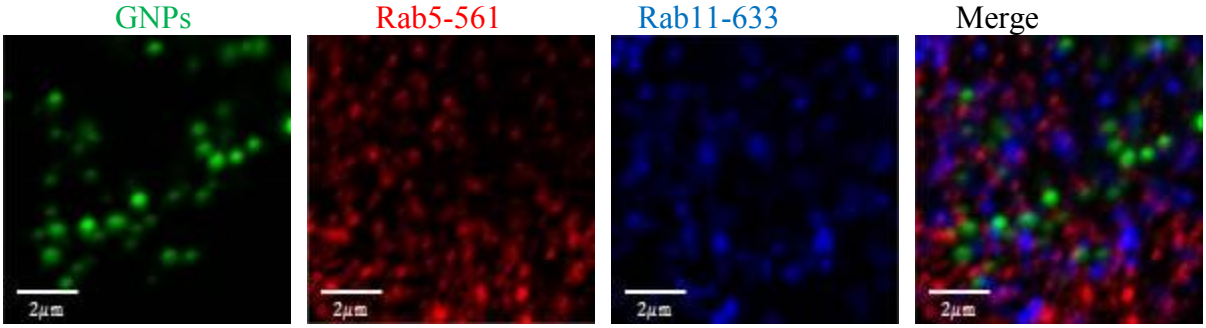

Figure 4.17 GNPs & Rab5-561 & Rab11-633 in A549 Cells

In Figure 4.17, there appear to be no yellow regions observed to reflect GNPs and Rab5 co-localization. Additionally, the observed purple regions in the image reflect the co-localization of Rab5-561 and Rab11-633. GNPs and Rab11-633 co-localize by the apparent "cyan" color observed due to the overlapping green and blue images.

Table 5.29 shows the number of images, n_{images} obtained in one experiment with the corresponding average number of clusters of species observed, $\langle N_{Species} \rangle$.

Table 4.29 Average Number of One, Two, and Three Labelled Clusters of GNPs, Rab5-561, and Rab11-633 Marked Endocytic Compartments in C2C12 Cells

Species	n_{images}	$\langle N_{Species} \rangle$
GNPs	14	0.38 ± 0.06[1]
Rab5-561	14	4.52 ± 0.37
Rab11-633	14	2.64 ± 0.32
GNPs & Rab5-561	14	0.10 ± 0.02
GNPs & Rab11-633	14	0.09 ± 0.03
Rab5-561 & Rab11-633	14	0.80 ± 0.08
GNPs & Rab5-561 & Rab11-633	14	0.11 ± 0.04

[1] Standard error.

Table 4.29 reflects the numbers of clusters of species observed for each individual marked compartment and phospholipid coated gold nanoparticles ranges between 0.38-5.00. Additionally, the number of clusters in which two markers are observed simultaneously is also in agreement with previous experiments, such that the number of clusters containing two markers ranges between 0.09-0.80. There is slight variation with each individual measurement, however it must be remembered that this is a different sample for which these measurements were calculated.

In contrast to previous experiments, the number of clusters of species of GNPs, Rab5-561, and Rab11-633 were observed and calculated to be approximately 0.11. To fully understand this value, fractions of co-localization were calculated and represented in Table 4.30.

Table 4.30 Average Fractions of Co-Localization in a GNPs, Rab5, and Rab11 Experiment in A549 Cells

$\langle F(GNPs \mid Rab5\ Rab11) \rangle$	$\langle F(Rab5 \mid GNPs\ Rab11) \rangle$	$\langle F(Rab11 \mid GNPs\ Rab5) \rangle$
0.33 ± 0.07[1]	0.03 ± 0.01	0.04 ± 0.01

[1] Standard error.

In Table 4.30, approximately 33% of clusters containing GNPs contain Rab5-561 and Rab11-633 markers. As presented in Table 4.27, this calculation is approximately 30% less in comparison to that of the association of GNPs with Rab5-561 markers. This calculation is about 20% less than that of the association of GNPs with Rab11-633 markers.

Approximately 3% of clusters containing Rab5-561 markers contain GNPs and Rab11-633 markers. As presented in Table 4.28, this calculation compares to that of the association of Rab5-561 markers with GNPs. On the contrary, this fraction is approximately 30% less than the calculation in Rab5-561 with Rab11-633 markers, as shown in Table 3.30.

Approximately 4% of clusters containing Rab11-633 markers contain GNPs and Rab5-561 markers. As presented Table 4.28 this calculation compares to that of the association of Rab11-633 markers with GNPs. On the contrary, this calculation is approximately 40% less in comparison to the association of Rab11-633 markers with Rab5-561 markers, in reference to Table 3.30.

Thus, although phospholipid coated gold nanoparticles contain Rab5-561 and Rab11-633 markers, very few clusters that contain one marker have gold nanoparticles and another marker. In addition, the pairwise interaction of phospholipid coated gold nanoparticles with either Rab5 or Rab11 markers may also take into account the second marker.

4.8.2 GNP & Rab5-561 & Rab7-633 in A549 Cells

The association of phospholipid coated gold nanoparticles with Rab5-561 and Rab7-633 markers was studied in A549 cells.

Figure 4.18 shows contrast enhanced images of a cell labelled with phospholipid coated gold nanoparticles, Rab5-561, and Rab7-633.

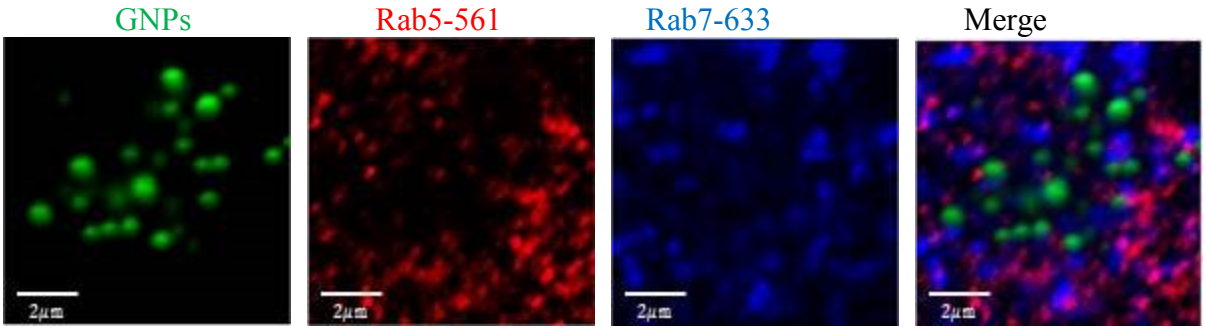

Figure 4.18 GNPs & Rab5 & Rab7 in A549 Cells

In Figure 4.18, there appear to be few yellow regions observed to reflect GNPs and Rab5-561 co-localization. Additionally, the observed purple spots in the image reflect the co-

localization of Rab5-561 and Rab7-633. GNPs and Rab7-633 co-localize by the apparent "cyan" color observed due to the overlapping green and blue images.

Table 5.31 shows the number of images, n_{images}obtained in one experiment with the corresponding average number of fluorescent clusters of species observed, $\langle N_{Species} \rangle$.

Table 4.31 Average Number of One, Two, and Three Labelled Clusters of GNPs, Rab5-561, and Rab7-633 Marked Endocytic Compartments in A549 Cells

Species	n_{images}	$\langle N_{Species} \rangle$
GNPs	20	0.42 ± 0.08[1]
Rab5-561	20	4.15 ± 0.35
Rab7-633	20	1.59 ± 0.13
GNPs & Rab5-561	20	0.11 ± 0.04
GNPs & Rab7-633	20	0.63 ± 0.40
Rab5-561 & Rab7-633	20	0.51 ± 0.05
GNPs & Rab5-561 & Rab7-633	20	0.09 ± 0.02

[1] Standard error.

Table 4.31 reflects the numbers of clusters of species marked with a specific marker or containing phospholipid coated gold nanoparticles to range between 0.42-4.15. Additionally, the number of clusters in which two markers are observed simultaneously is also in agreement with previous experiments, such that the number of clusters containing two markers ranges between 0.11-0.63. There is slight variation with each individual measurement; however it must be kept to consideration that this is a different sample for which these measurements were calculated.

In contrast to previous experiments, the number of clusters containing GNPs, Rab5-561, and Rab7-633 were observed and calculated to be approximately 0.09. To fully understand this value, fractions of co-localization were calculated and represented in Table 4.32.

Table 4.32 Averaged Fractions of Co-localization of GNPs with Early and Late Endocytic Marked Compartments in A549 Cells

⟨F(GNPs|Rab5 Rab7)⟩	⟨F(Rab5 | GNPs Rab7)⟩	⟨F(Rab7| GNPs Rab5)⟩
0.25 ± 0.04[1]	0.02 ± 0.00	0.05 ± 0.01

[1] Standard error.

In Table 4.32, approximately 25% of clusters containing GNPs contain Rab5-561 and Rab7-633 markers. As presented in Table 4.27 this calculation compares to that of the association of GNPs with Rab5-561 markers and the association of GNPs with Rab7-633 markers.

Approximately 2% of clusters containing Rab5-561 markers contain GNPs and Rab7-633 markers. As presented in Table 4.28 this calculation is approximately 18% less in comparison to that of the association of Rab5 markers with GNPs. Additionally, this calculation is approximately 48% less in comparison to that of the association of Rab5 markers with Rab7 markers, in reference to Table 3.30.

Approximately 5% of clusters containing Rab7-633 contain Rab5-561 markers. As presented in Table 4.28, this calculation 15% less in comparison to that of the association of Rab7-633 markers with GNPs. Additionally, this calculation is 38% less in comparison to that of the association of Rab7-633 markers with Rab5-561 markers, in reference to Table 3.30.

Likewise with the binary association of phospholipid coated gold nanoparticles with either Rab5 or Rab7 markers, very few clusters that contain one marker have gold nanoparticles and another marker. In addition, the pairwise interaction of phospholipid coated gold nanoparticles with either Rab5 or Rab7 markers may also take into account the other marker.

4.8.3 GNPs & Rab5-561 & LAMP-1-633 in A549 Cells

The association of phospholipid coated gold nanoparticles with Rab5-561 and LAMP-1-633 markers was studied in A549 cells.

Figure 4.19 is a visual representation of contrast enhanced images of a cell labelled with phospholipid coated gold nanoparticles and primary and secondary antibodies specific for Rab5 and LAMP-1.

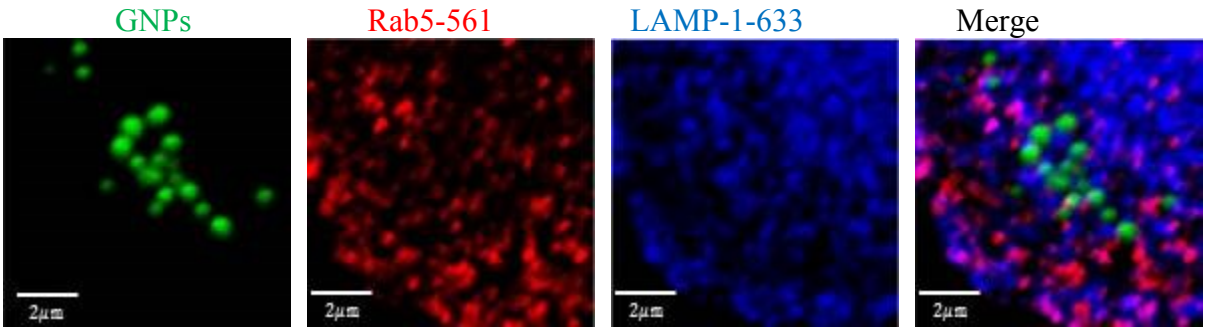

Figure 4.19 GNPs & Rab5 & LAMP-1 in A549 Cells.

In Figure 4.19, there appear to be few yellow regions observed to reflect GNPs and Rab5-561 co-localization. Additionally, the observed purple spots in the image reflect the co-localization of Rab5-561 and LAMP-1-633. GNPs and LAMP-1-633 co-localize by the apparent "cyan" color observed due to the overlapping green and blue images.

Table 4.33 shows the number of images, n_{images}obtained in one experiment with the corresponding average number of fluorescent clusters of species observed, $\langle N_{Species} \rangle$.

Table 4.33 Average Number of One, Two, and Three Labelled Clusters of GNPs, Rab5-561, and LAMP-1-633 Marked Endocytic Compartments in A549 Cells

Species	n_{images}	$\langle N_{Species} \rangle$
GNPs	13	0.41 ± 0.06[1]
Rab5-561	13	3.41 ± 0.40
LAMP-1-633	13	10.0 ± 1.00
GNPs & Rab5-561	13	0.08 ± 0.02
GNPs & LAMP-1-633	13	0.35 ± 0.09
Rab5 & LAMP-1-633	13	1.76 ± 0.17
GNPs & Rab5-561 & LAMP-1-633	13	0.14 ± 0.03

[1] Standard error.

Table 4.33 reflects the numbers of clusters of species observed for each individual marked compartment and phospholipid coated gold clusters ranges between 0.41-10.00. Additionally, the number of fluorescent clusters by which two markers are observed simultaneously is also in agreement with previous experiments, such that the number of clusters

of species observed ranges between 0.14-1.76. There is slight variation with each individual measurement, however it must be kept to consideration that this is a different sample for which these measurements were calculated.

In contrast to previous experiments, the number of clusters containing GNPs, Rab5-561, and LAMP-1-633 were observed and calculated to be approximately 0.14. To fully understand this value, fractions of co-localization were calculated and represented in Table 4.34.

Table 4.34 Averaged Fractions of co-localization of GNPs with Early and Lysosomal Endocytic Marked Compartments in A549 Cells

$\langle F(GNPs \mid Rab5\ LAMP-1) \rangle$	$\langle F(Rab5 \mid GNPs\ LAMP-1) \rangle$	$\langle F(LAMP-1 \mid GNPs Rab5) \rangle$
0.39 ± 0.08[1]	0.05 ± 0.01	0.02 ± 0.00

[1] Standard error.

In Table 4.34, approximately 39% of clusters containing GNPs contain Rab5-561 and LAMP-1-633 markers. In reference to Table 4.27, this calculation is 20% less than that of the association of GNPs with Rab5-561 markers. This calculation is also 10% less than that of the association of GNPs with LAMP-1-633 markers, in reference to Table 4.27.

Approximately 5% of clusters containing Rab5 markers contain LAMP-1-633 markers and GNPs. In reference to Table 4.28, this calculation matches that of the association of Rab5-561 markers with GNPs. Additionally, this calculation is approximately 75% less in comparison to that of the association of Rab5 markers with LAMP-1 markers, in reference to Table 3.30.

Approximately 2% of clusters containing LAMP-1-633 markers contain GNPs and Rab5-561 markers. In reference to Table 4.28, this calculation matches in comparison to that of the association of clusters of LAMP-1-633 markers and GNPs. Additionally, this calculation is 75% less in comparison to that of the association of LAMP-1-633 markers with Rab5-561 markers, in reference to Table 3.30.

This data strongly suggest that although there are very few clusters in which all three species are observed, the pairwise interaction of GNPs with either LAMP-1 or Rab7 reflect the some fraction of GNP clusters that also contain both LAMP-1 and Rab7.

4.8.4 GNPs & Rab7-633 & LAMP-1-561 in A549 Cells

The association of phospholipid coated gold nanoparticles with Rab7-633 and LAMP-1-561 markers was studied in A549 cells.

Figure 4.20 shows contrast enhanced images of a cell labelled with phospholipid coated gold nanoparticles, Rab7-633, and LAMP-1-561.

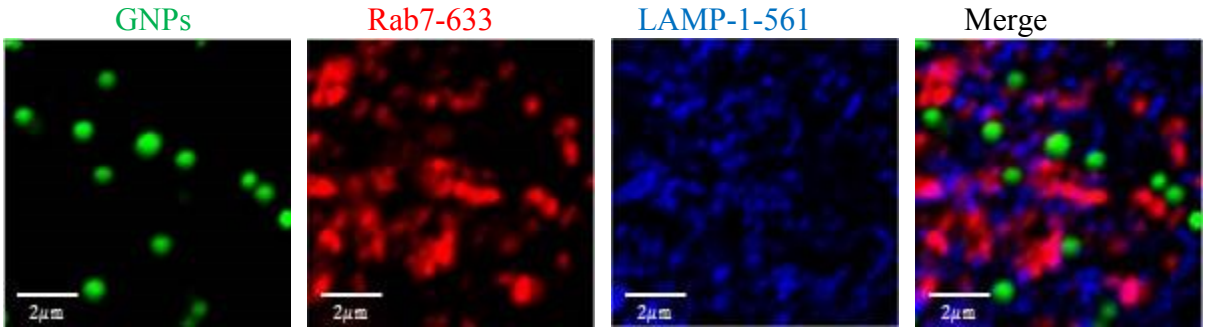

Figure 4.20 GNPs & Rab7-633 & LAMP-1-561 in A549 Cells

In Figure 4.20, there appear to be few yellow regions observed to reflect GNPs and Rab7-633 co-localization. Additionally, the observed purple spots in the image reflect the co-localization of Rab7-633 and LAMP-1-561. GNPs and LAMP-1-633 co-localize by the apparent "cyan" color observed due to the overlapping green and blue images.

Table 4.35 shows the number of images, n_{images}obtained in one experiment with the corresponding average number of clusters of species observed, $\langle N_{Species} \rangle$.

Table 4.35 Averaged Number of One, Two, and Three Clusters of GNPs, Rab7-633, and LAMP-1-561 Endocytic Marked Compartments in A549 Cells

Species	n_{images}	$\langle N_{Species} \rangle$
GNPs	20	0.50 ± 0.18[1]
Rab7-633	20	1.33 ± 0.16
LAMP-1-561	20	7.77 ± 0.54
GNPs & Rab7-633	20	0.14 ± 0.10
GNPs & LAMP-1-561	20	0.23 ± 0.10
Rab7-633 & LAMP-1-561	20	0.59 ± 0.24
GNPs & Rab7-633 & LAMP-1-561	20	0.07 ± 0.01

[1] Standard error.

Table 4.35 reflects the numbers of clusters containing one species ranges between 0.50-7.77. Additionally, the number of clusters in which two markers are observed simultaneously is also in agreement with previous experiments, such that the number of clusters of species observed is approximately 0.14-0.59 cluster. There is slight variation with each individual measurement, however it must be remembered that this is a different sample for which these measurements were calculated.

In contrast to previous experiments, the number of clusters containing GNPs, Rab7-633, and LAMP-1-561 were observed and calculated to be approximately 0.07. To fully understand this value, fractions of co-localization were calculated and represented in Table 4.36.

Table 4.36 Averaged Fractions of Co-localization of GNPs with Late and Lysosomal Endocytic Marked Compartments in A549 Cells

$\langle F(GNPs \mid Rab7\ \ LAMP-1) \rangle$	$\langle F(Rab7 \mid GNPs\ LAMP-1) \rangle$	$\langle F(LAMP-1 \mid GNPs\ Rab7) \rangle$
0.24 ± 0.05[1]	0.01 ± 0.00	0.06 ± 0.01

[1] Standard error.

In Table 4.36, approximately 24% of clusters containing GNPs contain Rab7-633 and LAMP-1 markers. In reference to Table 4.27, this calculation is 20% less than that of the association of GNPs with Rab7-633 markers. This calculation is also 40% less than that of the association of GNPs with LAMP-1 markers.

Approximately 1% of clusters containing Rab7 markers contain GNPs and LAMP-1 markers. In reference to Table 4.28Table 4.27, this calculation is 20% greater than that of the association of Rab7 markers with GNPs. Additionally, this calculation is 30% less in comparison to that of the association of Rab7 markers with LAMP-1 markers, as indicated in Table 3.30.

Approximately 6% of clusters containing LAMP-1 markers contain GNPs and Rab7 markers. In reference to Table 4.28, this calculation matches in comparison to that of association LAMP-1 markers with GNPs. Additionally, this calculation is 30% less in comparison to that of the association LAMP-1 markers with Rab7 markers.

Pairwise interaction of GNPs with Rab7 and LAMP-1 compare with the ternary complex formation; thus, these pairwise fractions may also take into account the third marker, Rab7 or LAMP-1.

4.9 Chapter Conclusions

The purpose of this chapter was to explore the extent to which phospholipid coated gold nanoparticles associate with markers of endosomes. This information was used to conclude whether or not the phospholipid coated gold nanoparticles undergo clathrin mediated endocytosis in C2C12 and A549 cells. Based on the results of this study, nanoparticles do undergo endocytosis. More specifically, three main conclusions can be drawn; 1) the internalization phenomena of phospholipid coated gold nanoparticles varies between cells, 2) pairwise interaction between phospholipid coated gold nanoparticles and endocytic markers varies between cells, and 3) three-way interaction between phospholipid coated gold nanoparticles and two endocytic markers also varies between cells.

Chapters 4.1 and 4.5 focused on the internalization of phospholipid coated gold nanoparticles in C2C12 and A549 cells, respectively. Phospholipid coated gold nanoparticles were always observed as C2C12 cells were continuously exposed to phospholipid coated gold nanoparticles in culture media; the number of clusters and degree of aggregation fluctuated with time. However, when phospholipid coated gold nanoparticles were no longer present in culture media after 24 hours progressed for uptake, phospholipid coated gold nanoparticles were no longer present in cells. Thus, C2C12 cells can be continuously exposed to nanoparticles for uptake; however there is a fixed amount of time in which these cells can withhold nanoparticles

in a gold nanoparticle free extracellular environment. On the contrary, A549 cells exhibit different behavior for gold nanoparticle internalization; *fewer* phospholipid coated gold nanoparticles with an increased relative degree of aggregation is observed with the progression of time of continuous exposure. When phospholipid coated gold nanoparticles are no longer present in the extracellular environment, a *greater* number of clusters (with a decrease in relative degree of aggregation) are observed. Thus, the internalization of phospholipid coated gold nanoparticles in a time dependent manner varies with cell type, specifically for A549 and C2C12 cells.

For binary complex formation in C2C12 cells; approximately 20-30% of each cluster containing phospholipid coated gold nanoparticles contains a marker for an endocytic compartment. Likewise, approximately 20% of each cluster containing a marker for an endocytic compartment also contains phospholipid coated gold nanoparticles. This approximate 20% pairwise co-localization between phospholipid coated gold nanoparticles with markers is promising to imply that the gold nanoparticles are present in endocytic marked compartments. In relation to the results obtained in Chapter 3, pairwise interaction among two markers was consistent with the proposed hypothesized theory of maturation and fusion of specific endosomes in C2C12 cells.

In regard to A549 cells, slightly different phenomena are observed for the binary complex formation; specifically, approximately 40-60% of clusters containing phospholipid coated gold nanoparticles also contain a marker for an endocytic compartment. Thus, gold nanoparticles are present in compartments. However, 3-8% of clusters containing one marker also contain phospholipid coated gold nanoparticles. Thus, very few clusters marked by a marker have phospholipid coated gold nanoparticles. These differences when compared to C2C12 cells are somewhat expected; in Chapter 3, it was shown that differences among pairwise interaction were observed and are somewhat inconsistent with the hypothesized maturation and fusion steps required of endocytosis. Thus, the extent to which phospholipid coated gold nanoparticles associate with markers in A549 cells is expected due to the extent of association of endocytic markers.

The extent of ternary complex formation of phospholipid coated gold nanoparticles with two markers is somewhat *similar* in C2C12 and A549 cells. Specifically, approximately 10-40%

of phospholipid coated gold nanoparticles associate with two markers in C2C12 cells and approximately 25-30% association is observed in A549 cells. In addition, these fractions for representing three-way interaction are slightly less in magnitude if not the same in comparison to pair-wise interactions which supports the analysis technique of ICS. These ternary fractions of gold nanoparticle association with two markers provide some indication that a fraction of the binary complexes in which there are phospholipid coated gold nanoparticles and one marker present may also consist of ternary complexes as well. For example; the total number of clusters observed that contain GNPs and Rab5 markers may account for clusters that have GNPs, Rab5, *and Rab7 markers* as well.

The extent of ternary interaction of markers associating with phospholipid coated gold nanoparticles and another marker *varies* with cell type. Approximately 12-65% of markers in C2C12 associate with GNPs and markers, whereas only 1-6% of markers in A549 cells associate with GNPs and markers, which implies few, perhaps one cluster in A549 cells containing a marker has GNPs and markers. The extent of binary complex formation in A549 cells also takes into account the extent of three species interacting, but fewer three-marker complexes are present out of the total distribution of complexes in A549 cells, compared to C2C12 cells. This observation is also consistent with the observed distribution of complexes containing three markers in C2C12 and A549 cells discussed in Chapter 3.

In addition, the average fit of the laser beam width for each time interval of exposure is consistent with average fit of the laser beam width corresponding to each marker of a clathrin mediated endosome as discussed in Chapter 3. Thus, simply from this observation, these gold nanoparticles possibly reside in endocytic compartments. To further inquire about the localization of phospholipid coated gold nanoparticles with endocytic compartments, coincidental fluorescence fluctuation analysis may be required for further analysis.

The ultimate *fate* of the phospholipid coated gold nanoparticles in these cell lines can be described by four different phenomena based on the results presented in this chapter; 1) the fluorescence of the NBD dye in the lipids has been quenched, 2) the gold nanoparticles potentially reside in compartments different from endosomes, 3) the cells eliminate the nanoparticles back into the extracellular environment via exocytosis, and/or 4) the cells degrade the nanoparticles. Quenching of NBD is a possibility and common quenchers of NBD include

molecular oxygen, iodide, acrylamide, and diothionite in solution.[92] However, previous studies in the Petersen lab have shown that the phospholipid bilayer surrounding the gold nanoparticles remains intact upon interaction with other membranes in cells.[2] Thus, the fluorescence arising from the gold nanoparticles after interaction with other membranes implies the bilayer membrane surrounding the gold is intact and quenching from other molecules (if any) is low. The second phenomena may also occur such that a small fraction of gold nanoparticles reside in compartments not studied; for this to be the case, live cell imaging would be useful but also deduction of pairwise fractions presented in Chapter 4 to determine if a small fraction of gold nanoparticles reside in other compartments. Preliminary work in the Petersen lab has also demonstrated that chemicals used to inhibit endocytosis prevented the internalization of these phospholipid coated gold nanoparticles. Thus, the location of phospholipid coated gold nanoparticles in compartments other than endosomes is perhaps unlikely. The third and fourth described phenomena are the most probable from these studies as the gold nanoparticles ultimately co-localize with lysosomes, which are acidic in nature for digestion, but at certain time points, the number of clusters of gold nanoparticles are low. Whether the gold nanoparticles re-enter cells after exocytosis (probable for A549 cells based on the time dependent *increase* in degree of aggregation with time) is a possible occurrence and real time imaging would be useful to address this question. In summary, results from this chapter suggest that the gold nanoparticles reside in acidic lysosomes for possible digestion but may be cleared from cells if not fully digested by the lysosomes.

Phospholipid coated gold nanoparticles are effectively taken up in C2C12 and A549 cells via clathrin mediated endocytosis, but associate with endocytic markers to various extents. This chapter has provided a useful means to show variability that exists among two cell types and to also provide additional information for how a particular type of gold nanoparticle material is processed and taken up in two different cell types. These phospholipid coated gold nanoparticles are an effective model to study in cells and based on their high degree of association with endocytic markers, they are a useful platform for pH sensitive drug delivery platforms. They are also biocompatible due the phospholipid bilayer coating and a useful system to study using fluorescence based techniques.

Chapter 5

α −Synuclein and Markers of Endocytic Compartments in Fixed SH-SY5Y Cells

5 α-Synuclein and Markers of Endocytic Compartments in Fixed SH-SY5Y Cells

Alpha Synuclein ($\alpha-$Syn) aggregation of fibrils in neurons is one of the causes of neurodegeneration in Parkinson's disease. In recent years, scientists have made great efforts to also study various oligomeric forms of the protein as the oligomers themselves have shown to be toxic prior to forming fibrils, thus may be a more accurate species to target for detection and diagnosis as opposed to fibrils.[93]Thus, an understanding of the aggregation and behavior of *oligomers* of $\alpha-$Syn is critical for the development of additional detection and treatment methods for Parkinson's disease.

The goal and motive for this study was to obtain quantitative information specific to the intracellular behavior of different oligomeric forms of $\alpha-$Syn as a means to compare and contrast the different oligomers. It is desired that the information specific to oligomers studied will provide scientists in the field with foundations to lead to the development of more effective detection and treatment methods for Parkinson's disease.

Oligomers of $\alpha-$Syn studied were monomers, engineered dimers, and engineered tetramers of the protein. [82] Monomers, dimers, and tetramers are abbreviated in tables and figures as Ms, Ds, and Ts, respectively.

In this work, first, the internalization of oligomeric forms of $\alpha-$Syn was studied by variable exposure, post cell fixation experiments in addition to a fixed exposure, variable uptake experiment, similar to the work completed for phospholipid coated gold nanoparticle studies in Chapter 4. Different from the work presented in Chapter 4, the passive diffusion of oligomers into cells was also studied to determine if passive transport was a possible mechanism of internalization. Based on the understanding of internalization, the pairwise interaction of oligomers was then studied to determine the extent to which two oligomers exist in the same cluster. The third study for this chapter focused on the association of oligomers with markers of endocytic compartments to determine if these oligomers do in fact undergo endocytosis.

5.1 Internalization of Oligomers of α −Syn

Chapter 5.1 focusses on the internalization of oligomers α −Syn in SH-SY5Y cells.

5.1.1 Internalization of oligomers of α −Syn after Variable Exposure, Post SH-SY5Y Cell Fixation

Cells were fixed first, blocked with BSA, and then exposed to monomers, dimers, and tetramers for 1, 2, 4, and 24 hours. Oligomers were able to diffuse through the fixed cell membranes of cells and internalize in SH-SY5Y cells. Therefore, the data and results obtained for this study is based on the passive diffusion of oligomers into cells and *not* endocytosis.

The experimental procedure can be found in Chapter 2.8.3.2. Laser scanning confocal microscopy imaging of one marker can be found in Chapter 2.10.3.1. Image Correlation Spectroscopy can be found in Chapter 2.11.1.

5.1.1.1 Internalization of Monomers after Variable Exposure, Post SH-SY5Y Cell Fixation

Monomers of α −syn were exposed to fixed SH-SY5Y cells to study the passive diffusion of monomers into cells.

Figure 5.1 shows original confocal fluorescence microscopy images of pre-fixed cells after being exposed to monomers. Images A, B, C, and D each correspond to one image of one SH-SY5Y cell with internalized monomers. Images vary based on exposure time of monomers to cells in a sample; 1, 2, 4, and 24 hours, respectively.

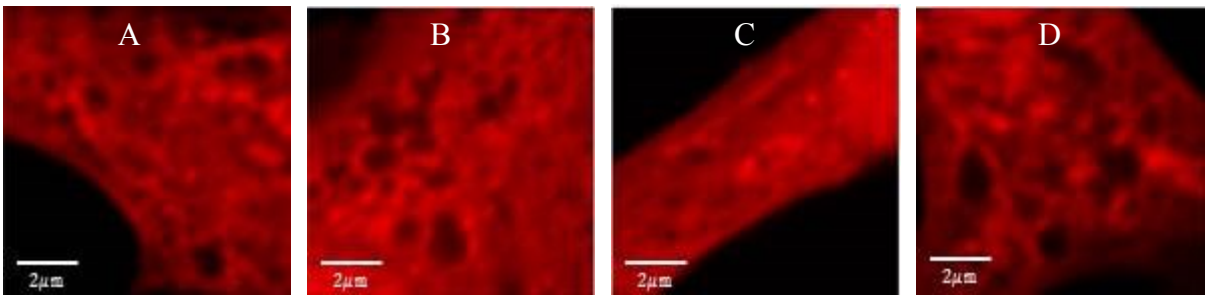

Figure 5.1 Images of Internalized Monomers after Variable Exposure to Pre-Fixed SH-SY5Y Cells

Confocal fluorescence microscopy images of pre-fixed cells after being exposed to monomers. Images A, B, C, and D each correspond to one image of one SH-SY5Y cell with internalized monomers. Images vary based on exposure time of monomers to cells in a sample; 1, 2, 4, and 24 hours, respectively.

In each image shown in Figure 5.1, monomers distribute over the entire cytoplasmic region in the image; this is different to experiments in which phospholipid coated gold nanoparticles were studied based on an assumed active transport pathway; with nanoparticles, clustering was observed as opposed to homogenously distributed species over the entire region of the cell.

Table 5.1 shows the averages of the auto correlation amplitude, fitted laser beam width, and average intensity of monomers after exposure to pre-fixed cells. Approximately 20-30 images were obtained for each exposure time of monomers to pre-fixed cells. The values are shown with standard error.

Table 5.1 Averages of ICS Parameters for Images of Monomers after Variable Exposure, Post SH-SY5Y Cell Fixation

Post Fix Variable Exposure Time (hours)	$\langle g(0,0) \rangle$	$\langle \omega\ (\mu m) \rangle$	$\langle I_{avg.} \rangle$
1	0.09 ± 0.02[1]	0.57 ± 0.02	723 ± 48
2	0.07 ± 0.01	0.53 ± 0.02	710 ± 33
4	0.09 ± 0.01	0.52 ± 0.01	880 ± 44
24	0.07 ± 0.01	0.51 ± 0.02	1224 ± 75

1 Standard error.

The average intensity of monomers ranges between 700-800 within the first four hours of exposure. The intensity of monomers then increases to 1224 after 24 hours has progressed.

The auto correlation amplitude for each time interval of post fixation exposure is constant for 1-24 hours, specifically 0.07 or 0.09. This autocorrelation amplitude is small in comparison to previous auto correlation amplitudes obtained for phospholipid coated gold nanoparticles and markers of endosomes in C2C12 and A549 cells. However, based on Figure 5.1, the monomers are fluorescent and the small auto correlation amplitude values do not reflect background noise. Because the monomers distribute over the majority of the entire cell, the small auto correlation amplitudes reflect this distribution of species.

The average fitted laser beam width ranges between 0.51-0.57 microns within 1-24 hours. As mentioned in previous chapters, the experimental average fitted laser beam width is a convolution of the laser beam width and the size of the species of interest being imaged. In Figure 5.1, there are a few presences of circular black spots that may give rise to in-homogeneities in the fluorescence distributions. Thus, this may be a reason for the larger width of the laser beam in comparison to previous studies (on average shown to be approximately 0.40 microns with markers and phospholipid coated gold nanoparticles). The magnitude of the measurement for the fit of the laser beam width arises from convolution.

Table 5.2 shows the averages of the number of clusters containing monomers, the average number of clusters containing monomers per square micron, and the average relative degree of aggregation of monomers per cluster after exposure to pre-fixed cells. The values are shown with standard error.

Table 5.2 Averages of Derived ICS Parameters for Images of Monomers after Variable Exposure, Post SH-SY5Y Cell Fixation

Post Fix Variable Exposure Time (hours)	$\langle N_{Ms} \rangle$	$\langle CD \rangle$	$\langle DA \rangle$
1	25.6 ± 5.1[1]	22.6 ± 5.1	59.4 ± 9.7
2	19.6 ± 2.3	24.8 ± 3.4	49.0 ± 5.1
4	22.0 ± 3.3	38.2 ± 9.2	67.7 ± 9.3
24	18.0 ± 2.2	23.4 ± 3.2	91.1 ± 10.3

1 Standard error.

The number of clusters containing monomers in the region of the laser beam ranges between 18-25 clusters after 1-24 hours of exposure to pre-fixed cells. The cluster density ranges between 22-38 clusters of monomers per square micron. This is a very large cluster density observed in this thesis, almost two fold greater than previous findings with phospholipid coated gold nanoparticles. Lastly, the relative degree of aggregation is on the order of 49-91 monomers per cluster. Given the number of clusters fluctuates with exposure time, the relative degree of aggregation is weighted more heavily on the intensity; thus, an increase in the relative degree of aggregation of monomers after 24 hours of exposure is expected because the intensity of monomers increased after 24 hours of exposure.

These results indicate that the number of clusters containing monomers is constant with exposure time, however the relative degree of aggregation of monomers in clusters increases with time.

5.1.1.2 Internalization of Dimers after Variable Exposure, Post SH-SY5Y Cell Fixation

Dimers of α −syn were exposed to fixed SH-SY5Y cells to study the passive diffusion of dimers into cells.

Figure 5.2 shows the original confocal fluorescence microscopy images of pre-fixed cells after being exposed to dimers. Images A, B, C, and D each correspond to one image of one SH-SY5Y cell with internalized dimers. Images vary based on exposure time of dimers to cells in a sample; 1, 2, 4, and 24 hours, respectively.

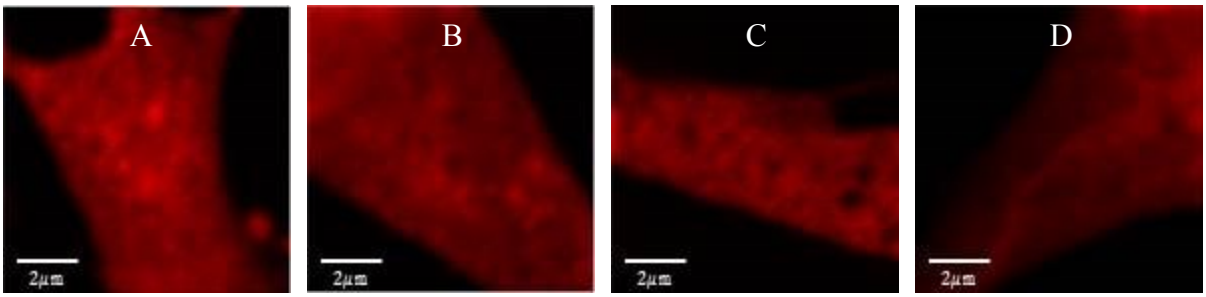

Figure 5.2 Images of Internalized Dimers after Variable Exposure, Post SH-SY5Y Cell Fixation

Confocal fluorescence microscopy images of pre-fixed after being exposed to dimers. Images A, B, C, and D each correspond to one image of one SH-SY5Y cell with internalized dimers. Images vary based on exposure time of dimers to cells in a sample; 1, 2, 4, and 24 hours, respectively.

As with the monomers in Figure 5.1, the dimers distribute homogenously throughout the cytoplasm.

Table 5.3 shows the averages of the auto correlation amplitude, fitted laser beam width, and intensity of dimers after exposure to pre-fixed cells. Data is shown with standard error. Approximately 20-30 images were obtained for each variable exposure time interval.

Table 5.3 Averages of ICS Parameters for Images of Dimers after Variable Exposure, Post SH-SY5Y Cell Fixation

Post Fix Variable Exposure Time (hours)	$\langle \mathbf{g(0,0)} \rangle$	$\langle \boldsymbol{\omega}\ (\boldsymbol{\mu}\mathbf{m}) \rangle$	$\langle I_{avg.} \rangle$
1	0.06 ± 0.01[1]	0.55 ± 0.01	177 ± 12
2	0.06 ± 0.01	0.58 ± 0.01	219 ± 12
4	0.09 ± 0.01	0.56 ± 0.02	158 ± 14
24	0.12 ± 0.02	0.63 ± 0.02	623 ± 44

1 Standard error.

Similar to monomers, there is an increase with the average intensity of dimers after 24 hours of exposure to pre-fixed cells. The auto correlation amplitude obtained for dimers ranges in magnitude of 0.06-0.12 with the progression of time. Additionally, the fit obtained for the width of the laser beam is between 0.55-0.63 microns. As with monomers upon exposure post SH-SY5Y cell fixation, the experimental fitted laser beam width arises from convolution.

Table 5.4 shows the average values of the calculations corresponding to dimers after variable exposure, post SH-SY5Y cell fixation. The average number of clusters containing dimers, the average number of clusters containing dimers per square micron, and the average relative degree of aggregation of dimers per cluster was calculated for 20-30 images per sample. The calculations correspond to data obtained in Table 5.3 and are shown with standard error.

Table 5.4 Averages of Derived ICS Parameters for Images of Dimers after Variable Exposure, Post SH-SY5Y Cell Fixation

Post Fix Variable Exposure Time (hours)	$\langle N_{Ds} \rangle$	$\langle CD \rangle$	$\langle DA \rangle$
1	16.8 ± 2.8[1]	18.0 ± 4.0	10.5 ± 1.2
2	24.9 ± 3.1	27.0 ± 4.4	12.3 ± 1.5
4	20.1 ± 3.0	25.6 ± 4.9	15.3 ± 3.1
24	18.7 ± 2.9	19.7 ± 4.2	76.7 ± 14.7

1 Standard error.

The number of clusters containing dimers in the observation region of the laser beam ranges between 16-24 clusters. Similarly, the number of clusters containing dimers observed per square micron ranges between18-27. In reference to Table 5.3, the increase in the degree of aggregation after 24 hours has elapsed is dependent on the increase in intensity, as the auto correlation amplitude is constant with time of exposure. Thus, these results indicate that the number of clusters containing dimers is constant with exposure time, however the relative degree of aggregation of dimers per cluster increases with exposure time. As with monomers, cells are able to continuously internalize dimers for long progressions of time.

5.1.1.3 Internalization of Tetramers after Variable Exposure, Post SH-SY5Y Cell Fixation

Tetramers of α −syn were exposed to fixed SH-SY5Y cells to study the passive diffusion of tetramers into cells.

Figure 5.3 shows confocal fluorescence microscopy images of pre-fixed cells after being exposed to tetramers. Images A, B, C, and D each correspond to one image of one SH-SY5Y cell

with internalized tetramers. Images vary based on exposure time of tetramers to cells in a sample; 1, 2, 4, and 24 hours, respectively.

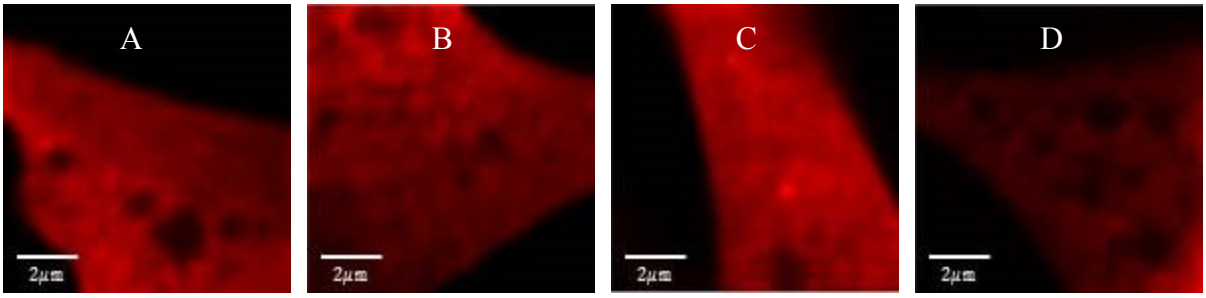

Figure 5.3 Images of Internalized Tetramers after Variable Exposure, Post SH-SY5Y Cell Fixation

Confocal fluorescence microscopy images of pre-fixed cells after being exposed to tetramers. Images A, B, C, and D each correspond to one image of one SH-SY5Y cell with internalized tetramers. Images vary based on exposure time of tetramers to cells in a sample; 1, 2, 4, and 24 hours, respectively.

Similar to the monomers and dimers, tetramers distribute amongst the surface of the cell to a very large extent. However, image D appears to be less bright in comparison to images A, B, and C.

Table 5.5 shows the averages of the auto correlation amplitude, fitted laser beam width, and average intensity of tetramers exposed to pre-fixed cells. Approximately 20-30 images were obtained for each variable exposure time interval. Data is shown with standard error.

Table 5.5 Averages of ICS Parameters for Images of Tetramers after Variable Exposure, Post SH-SY5Y Cell Fixation

Post Fix Variable Exposure Time (hours)	$\langle g(0,0) \rangle$	$\langle \omega\ (\mu m) \rangle$	$\langle I_{avg.} \rangle$
1	0.13 ± 0.02[1]	0.62 ± 0.02	830 ± 81
2	0.10 ± 0.02	0.57 ± 0.02	1108 ± 63
4	0.11 ± 0.02	0.61 ± 0.02	815 ± 64
24	0.17 ± 0.03	0.65 ± 0.02	599 ± 71

1 Standard error.

The average intensity of tetramers for each time interval of exposure to pre-fixed cells ranges between 500-1100. However, as shown with image D in Figure 5.3, the intensity is slightly lower in comparison to the intensities measured for 1-4 hours of post fix variable exposure. The auto correlation amplitude ranges between 0.10-0.17 for 1-24 hours of variable exposure to SH-SY5Y cells, which is greater in comparison to the monomers and dimers. The fit for the laser beam width ranges between 0.57-0.62 microns. Similar to monomers and dimers, the measured experimental fit for the laser beam width for tetramers arises from convolution.

Table 5.6 shows the average values of the calculations corresponding to tetramers after variable exposure, post SH-SY5Y cell fixation. The average number of clusters containing tetramers, the average number of clusters containing tetramers per square micron, and the average relative degree of aggregation of tetramers per cluster was calculated for 20-30 images per sample. The calculations correspond to the data obtained in Table 5.5 and are shown with standard error.

Table 5.6 Averages of Derived ICS Parameters for Images of Tetramers after Variable Exposure, Post SH-SY5Y Cell Fixation

Post Fix Variable Exposure Time (hours)	$\langle N_{Ts} \rangle$	$\langle CD \rangle$	$\langle DA \rangle$
1	14.3 ± 2.8[1]	15.6 ± 3.7	104 ± 16
2	19.9 ± 3.3	26.1 ± 6.3	108 ± 19
4	13.7 ± 1.8	14.0 ± 2.4	88.2 ± 10.6
24	9.92 ± 2.09	8.18 ± 1.74	95.6 ± 20.8

1 Standard error.

The number of clusters, number clusters per square micron, and relative degree of aggregation of tetramers fluctuates with time of exposure to pre-fixed SH-SY5Y cells. Each derived parameter does not depend on time of exposure of tetramers to pre-fixed cells.

5.1.1.4 Comparisons for Variable Exposure of Oligomers of α −Syn Post SH-SY5Y Cell Fixation

The purpose of this section is to compare the average number of clusters, average number of clusters per square micron, average intensity, and average relative degree of aggregation of

monomers, dimers, and tetramers in SH-SY5Y cells with the use of bar graphs. Bar graphs are based on data and calculations previously presented in Chapter 5.1.1.

Figure 5.4 is a bar graph for the average intensity of oligomers of α −syn after variable exposure, post SH-SY5Y cell fixation.

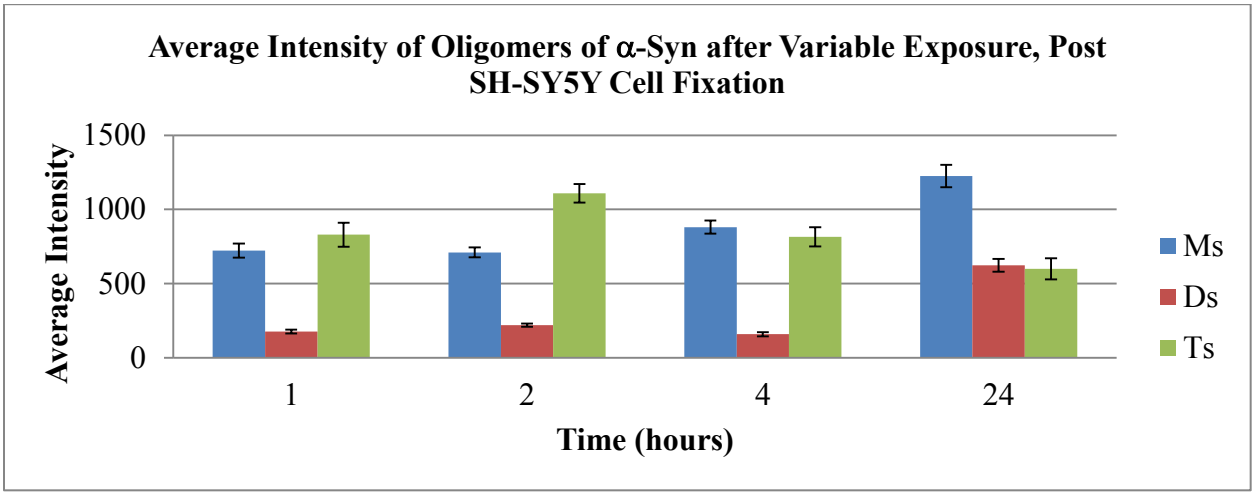

Figure 5.4 Bar graph of Average of Oligomers of α −Syn after Variable Exposure, Post SH-SY5Y Cell Fixation

The average intensity of each oligomer of α −syn after variable exposure, post SH-SY5Y cell fixation is plotted as a function of variable exposure time to SH-SY5Y cells.

The intensity of monomers and dimers is constant within 1-4 hours of exposure. The intensity of monomers and dimers then increases after 24 hours has progressed, more for dimers than monomers. The intensity for tetramers fluctuates within 1-4 hours of exposure, but decreases after 24 hours has progressed.

Figure 5.5 is a bar graph of the average number of clusters containing oligomers of α −Syn after variable exposure, post SH-SY5Y cell fixation.

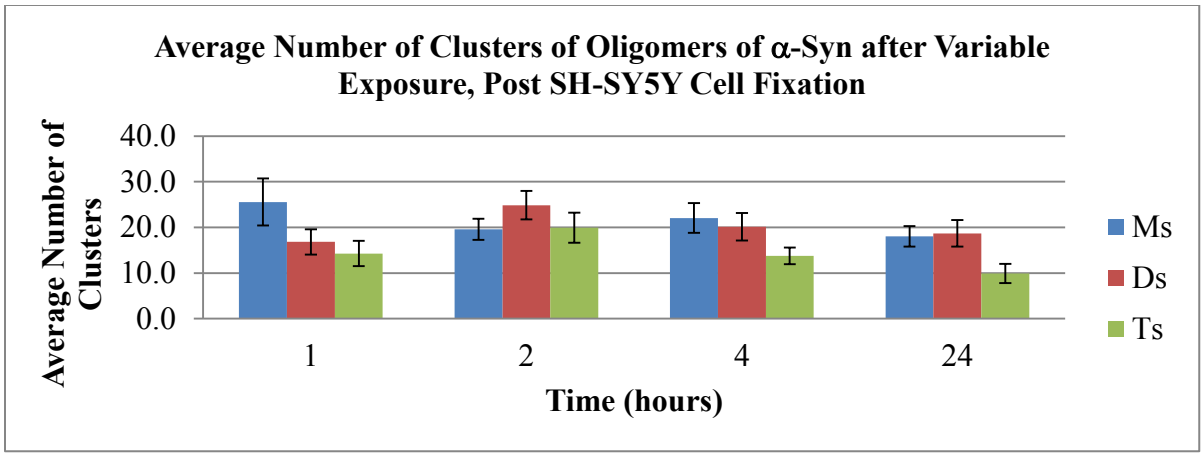

Figure 5.5 Bar graph of Average Number of Clusters Oligomers of α −Syn after Variable Exposure, Post SH-SY5Y Cell Fixation

The average number of clusters containing each oligomer of α −Syn per square micron after variable exposure, post SH-SY5Y cell fixation is plotted as a function of variable exposure time to SH-SY5Y cells.

This bar graph shows that the magnitude for the number of clusters containing oligomers does not depend on the size of the oligomer; the number of clusters containing oligomers observed at various times does not change. In addition, there are no specific trends for the number of clusters with time of exposure for each oligomer studied.

Figure 5.6 is a bar graph for the average cluster density of oligomers of α −Syn after variable exposure, post SH-SY5Y cell fixation.

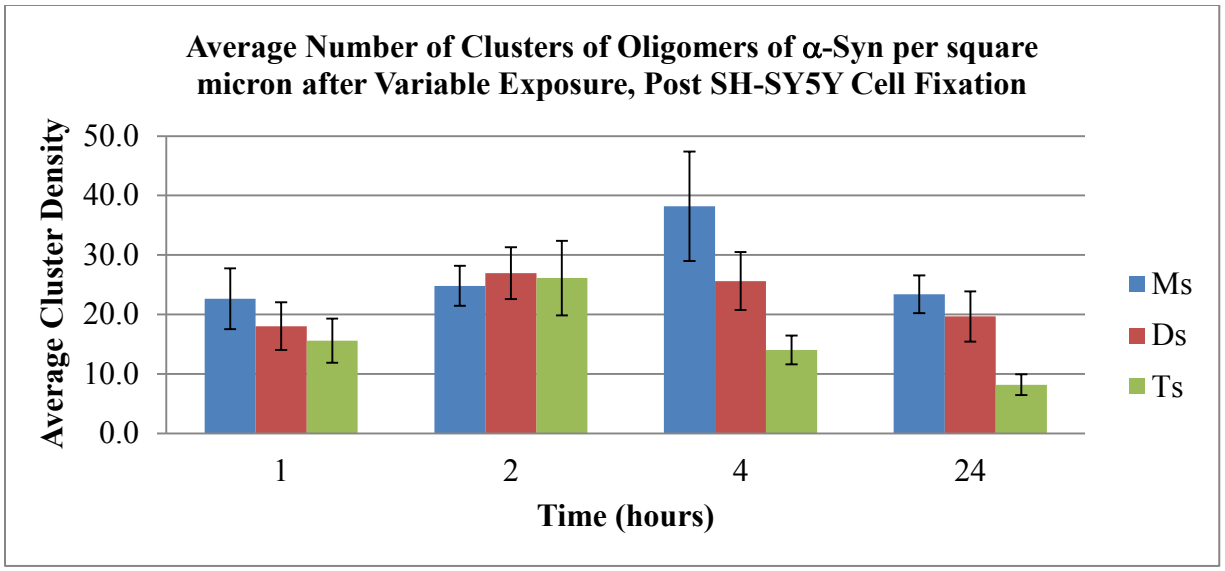

Figure 5.6 Bar graph of Average Number of Clusters of Oligomers of α −syn per square micron after Variable Exposure, Post SH-SY5Y Cell Fixation

The average number of clusters of oligomers of α −syn per square micron after variable exposure, post SH-SY5Y cell fixation is plotted as a function of variable exposure time to SH-SY5Y cells.

Because the experimentally fitted with of the laser beam does not change with time or oligomer, Figure 5.5 and Figure 5.6 are similar.

Figure 5.7 is a bar graph of the relative degree of aggregation of oligomers of α −Syn after variable exposure, post SH-SY5Y cell fixation.

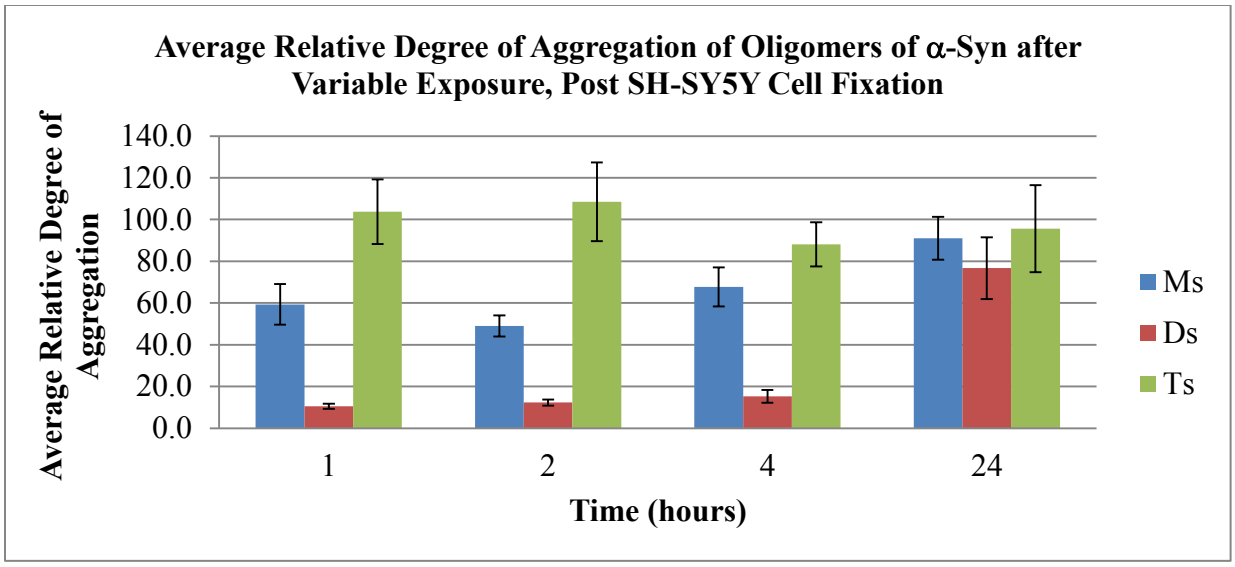

Figure 5.7 Bar graph of Average Relative Degree of Aggregation of Oligomers of α −Syn after Variable Exposure, Post SH-SY5Y Cell Fixation

The average relative degree of aggregation of oligomers of α −Syn per square micron after variable exposure, post SH-SY5Y cell fixation is plotted as a function of exposure time to SH-SY5Y cells.

In Figure 5.7, the relative degree of aggregation of monomers and dimers increases after 24 hours has progressed; this is expected because the relative degree of aggregation is weighted more heavily on the intensity of species at each time, as the auto correlation amplitudes do not change with exposure time. The relative degree of aggregation of tetramers is more or less constant with exposure time. However, after 24 hours has progressed, the relative degree of aggregation magnitude for each oligomer is similar. Thus, although monomers and dimers share a similar trend that the relative degree of aggregation increases after 24 hours has progressed and the relative degree of aggregation for tetramers does not change with time, *each* oligomer appears to aggregate to the same extent after 24 hours of exposure to pre-fixed cells.

5.1.2 Internalization of Pre-Aggregated Oligomers of α −Syn post SH-SY5Y Cell Fixation

We wanted to determine if enforced aggregation of oligomers prior to exposure to fixed cells would affect the degree of aggregation of oligomers in cells, in comparison to the work shown in Chapter 5.1.1. Thus, cells were first fixed and blocked with BSA as previously shown.

However, prior to exposure to fixed SH-SY5Y cells, monomers and tetramers were maintained in a temperature controlled shaking device overnight.

The concentrations of monomers and tetramers prepared for the temperature controlled shaking device were twelve-fold greater than their respective concentrations used for cellular uptake. After remaining in the temperature controlled shaker overnight, oligomers were diluted to their appropriate concentrations for cell uptake, then exposed to pre-fixed cells. Pre-aggregated monomers and tetramers were exposed to pre-fixed cells for 1, 2, 4, and 24 hours. Pre-aggregated oligomers were able to passively diffuse through fixed cell membranes into the cytoplasm of SH-SY5Y cells. The experimental procedure can be found in Chapter 2.8.3.3. Laser scanning confocal microscopy imaging of one oligomer can be found in Chapter 2.10.3.1 Image Correlation Spectroscopy can be found Chapter 2.11.1.

5.1.2.1 Internalization of Pre-Aggregated Monomers after Variable Exposure, Post SH-SY5Y Cell Fixation

Pre-Aggregated monomers were exposed to fixed SH-SY5Y cells to study the passive diffusion of pre-aggregated monomers into cells.

Figure 5.8 shows confocal fluorescence microscopy images of pre-fixed cells after being exposed to pre-aggregated monomers. Images A, B, C, and D each correspond to one image of one SH-SY5Y cell with internalized pre-aggregated monomers. Images vary based on exposure time of pre-aggregated monomers to cells in a sample; 1, 2, 4, and 24 hours, respectively.

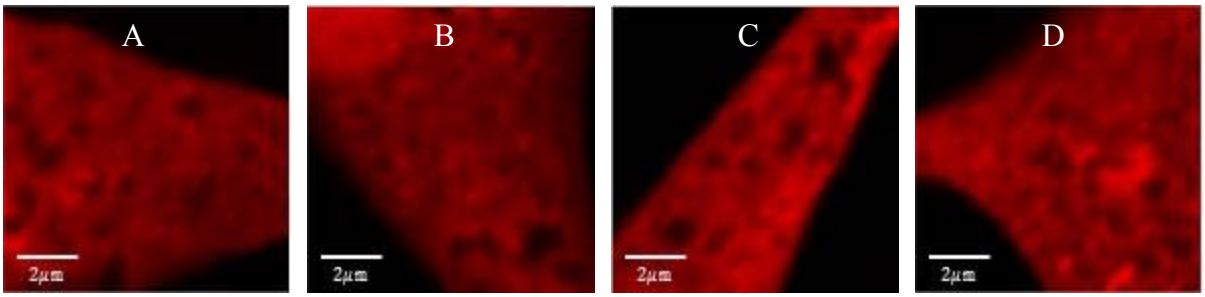

Figure 5.8 Images of Internalized Pre-Aggregated Monomers after Variable Exposure, Post SH-SY5Y Cell Fixation

Confocal fluorescence microscopy images of pre-fixed cells after being exposed to pre-aggregated monomers. Images A, B, C, and D each correspond to one image of one SH-SY5Y cell with internalized pre-aggregated monomers. Images vary based on exposure time of pre-aggregated monomers to cells in a sample; 1, 2, 4, and 24 hours, respectively.

The pre-aggregated monomers distribute to a very large extent, as shown similarly in Figure 5.1.

Table 5.7 shows the averages of the auto correlation amplitude, fitted laser beam width, and average intensity of pre-aggregated monomers. Approximately 20-30 images were obtained for each variable exposure time interval.

Table 5.7 Averages of ICS Parameters for Images of Pre-Aggregated Monomers after Variable Exposure, Post SH-SY5Y Cell Fixation

Pre-Aggregated Post Fix Exposure Variable Time (hours)	$\langle g(0,0) \rangle$	$\langle \omega\ (\mu m) \rangle$	$\langle I_{avg.} \rangle$
1	0.06 ± 0.01[1]	0.49 ± 0.02	164 ± 6
2	0.09 ± 0.01	0.53 ± 0.02	287 ± 12
4	0.14 ± 0.02	0.58 ± 0.02	336 ± 15
24	0.10 ± 0.01	0.53 ± 0.02	660 ± 27

1 Standard error.

There is a slight trend observed with average intensity as there is a gradual increase with average intensity of pre-aggregated monomers with time. The auto correlation amplitude obtained for pre-aggregated monomers ranges between 0.06-0.14 with the progression of time. The values for the auto correlation amplitudes are similar to the observed auto correlation amplitudes previously shown for non-pre-aggregated monomers in Table 5.1. Additionally, the

fit obtained for the width of the laser beam is between 0.49-0.58 microns. These values are similar to the observed fit for the laser beam width for non pre-aggregated monomers.

Table 5.8 shows the average values of the calculations corresponding to pre-aggregated monomers after variable exposure, post SH-SY5Y cell fixation. The average number of clusters containing pre-aggregated monomers, the average number of clusters containing pre-aggregated monomers per square micron, and the average relative degree of aggregation of pre-aggregated monomers per cluster were calculated for 20-30 images per sample. The calculations correspond to data obtained in Table 5.7.

Table 5.8 Averages of Derived ICS Parameters for Images of Pre-Aggregated Monomers after Variable Exposure, Post SH-SY5Y Cell Fixation

Pre-Aggregated Post Fix Exposure Variable Time (hours)	$\langle N_{Ms} \rangle$	$\langle CD \rangle$	$\langle DA \rangle$
1	22.6 ± 2.4[1]	39.0 ± 6.4	9.8 ± 1.0
2	20.2 ± 2.9	32.8 ± 7.3	23.1 ± 3.1
4	10.9 ± 1.5	15.1 ± 3.6	43.9 ± 4.2
24	15.7 ± 2.1	24.9 ± 4.9	65.0 ± 9.5

1 Standard error.

The number of clusters containing pre-aggregated monomers in the observation region of the laser beam is between 15-23 clusters. Similarly, the number of clusters containing pre-aggregated monomers observed per square micron is between 15-40 clusters per square micron. The relative degree of aggregation of pre-aggregated monomers increases gradually with exposure time. The source of this increase is due to the increase in intensity of pre-aggregated monomers with exposure time, as the auto correlation amplitude does not change with time of exposure.

These results indicate that the average number of clusters observed per square micron is somewhat constant, but the extent to which these pre-aggregated monomers aggregate within clusters increases with time. The same trends were observed for non-pre-aggregated monomers.

5.1.2.2 Internalization of Pre-Aggregated Tetramers after Variable Exposure, Post SH-SY5Y Cell Fixation

Pre-Aggregated tetramers of α −syn were exposed to fixed SH-SY5Y cells to study the passive diffusion of pre-aggregated tetramers into cells.

Figure 5.9 shows confocal fluorescence microscopy images of pre-fixed cells after being exposed to pre-aggregated tetramers. Images A, B, C, and D each correspond to one image of one SH-SY5Y cell with internalized pre-aggregated tetramers. Images vary based on exposure time of pre-aggregated tetramers to cells in a sample; 1, 2, 4, and 24 hours, respectively.

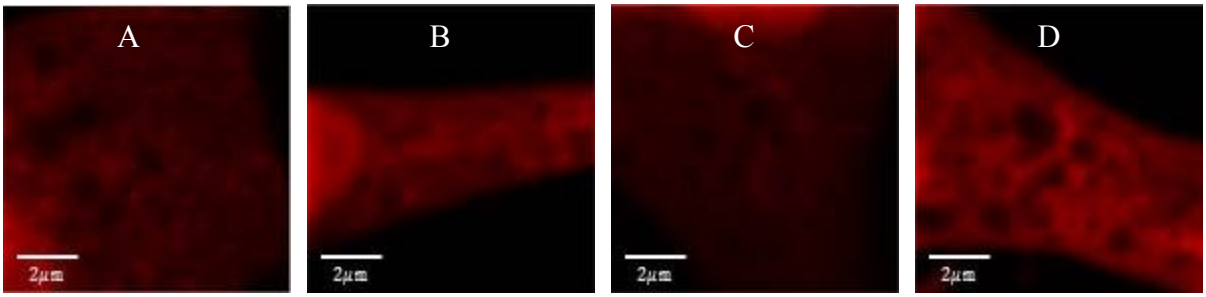

Figure 5.9 Images of Internalized Pre-Aggregated Tetramers after Variable Exposure, Post SH-SY5Y Cell Fixation

Confocal fluorescence microscopy images of pre-fixed cells after being exposed to pre-aggregated tetramers. Images A, B, C, and D each correspond to one image of one SH-SY5Y cell with internalized pre-aggregated tetramers. Images vary based on exposure time of pre-aggregated tetramers to cells in a sample; 1, 2, 4, and 24 hours, respectively.

The pre-aggregated tetramers distribute amongst the cytoplasm of the cell to a very large extent. However, the "brightness" of images A and C is less in comparison to the brightness of images B and D.

Table 5.9 shows the averages of the auto correlation amplitude, fitted laser beam width, and average intensity of pre-aggregated tetramers after being exposed to pre-fixed cells. Approximately 20-30 images were obtained for each variable exposure time interval.

Table 5.9 Averages of ICS Parameters for Images of Pre-Aggregated Tetramers after Variable Exposure, Post SH-SY5Y Cell Fixation

Pre-Aggregated Post Fix Exposure Variable Time (hours)	$\langle \mathbf{g(0,0)} \rangle$	$\langle \boldsymbol{\omega}\ (\boldsymbol{\mu m}) \rangle$	$\langle I_{avg.} \rangle$
1	0.06 ± 0.01[1]	0.50 ± 0.02	27.4 ± 1.0
2	0.10 ± 0.02	0.58 ± 0.03	226 ± 12
4	0.07 ± 0.01	0.51 ± 0.02	45.2 ± 2.0
24	0.10 ± 0.02	0.59 ± 0.01	190 ± 12

1 Standard error.

The intensities of pre-aggregated tetramers after 1 and 4 hours of exposure is low in comparison to the intensities of tetramers at 1 and 4 hours in Table 5.5. The average auto correlation amplitudes obtained for each exposure time are relatively constant, ranging between 0.06-0.10. In addition, the values obtained for the fitted laser beam width for each time of exposure ranges between 0.50-0.59 microns. The measured fit arises from convolution.

Table 5.10 shows the average values of the calculations corresponding to pre-aggregated tetramers after variable exposure, post SH-SY5Y cell fixation. The average number of clusters containing pre-aggregated tetramers, the average number of clusters containing pre-aggregated tetramers per square micron, and the average relative degree of aggregation of pre-aggregated tetramers per cluster was calculated for 20-30 images per sample. The calculations correspond to data obtained in Table 5.9.

Table 5.10 Averages of Derived ICS Parameters for Images of Pre-Aggregated Tetramers after Variable Exposure, Post SH-SY5Y Cell Fixation

Pre-Aggregated Post Fix Exposure Variable Time (hours)	$\langle N_{Ts} \rangle$	$\langle CD \rangle$	$\langle DA \rangle$
1	28.9 ± 3.0[1]	50.8 ± 8.8	1.68 ± 0.36
2	23.0 ± 4.7	32.2 ± 8.4	20.2 ± 3.3
4	23.0 ± 2.6	35.4 ± 6.4	2.70 ± 0.35
24	14.7 ± 1.5	14.8 ± 2.0	18.8 ± 3.5

1 Standard error.

The number of clusters containing pre-aggregated tetramers ranges between 23-30 for the initial four hours of exposure to pre-fixed cells. After 24 hours have progressed, approximately 14.7 clusters contain pre-aggregated tetramers. The number of clusters containing pre-aggregated tetramers per square micron fluctuates with time, but decreases after 24 hours has elapsed. However, as shown in Table 5.9 with low intensity at 1 and 4 hours, it is expected the aggregation of pre-aggregated tetramers per cluster would also be small in magnitude.

5.1.3 Comparisons for Binding of Pre-Aggregated Oligomers of α −Syn post SH-SY5Y Cell Fixation

The purpose of this section is to compare pre-aggregated monomers and tetramers in SH-SY5Y cells with the use of bar graphs.

Figure 5.10 is a bar graph of the average intensity of pre-aggregated oligomers plotted as a function of exposure time.

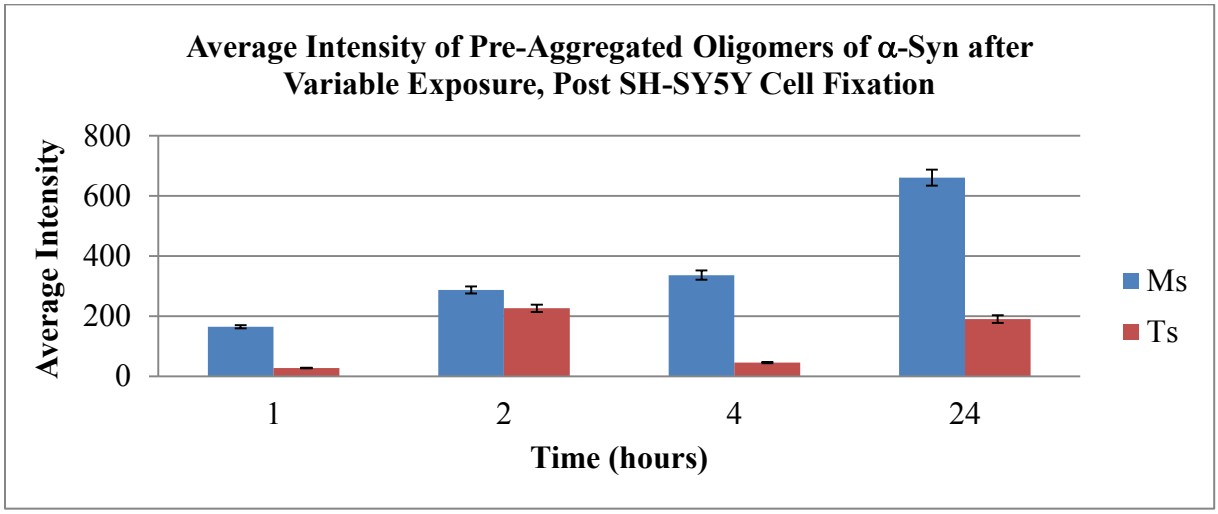

Figure 5.10 Bar Graph of Average Intensity of Pre-Aggregated Oligomers of α-syn after Variable Exposure, Post SH-SY5Y Cell Fixation

The average intensity of pre-aggregated oligomers of α-syn after variable exposure, post SH-SY5Y cell fixation is plotted as a function of variable exposure time.

In Figure 5.10, the intensity of pre-aggregated monomers increases with exposure time to pre-fixed cells whereas the intensity of pre-aggregated tetramers fluctuates with exposure time.

Generally speaking, the average intensity of pre-aggregated monomers is greater in comparison to the intensity of pre-aggregated tetramers.

Figure 5.11 is a bar graph for the average number of clusters containing pre-aggregated oligomers after variable exposure, post SH-SY5Y cell fixation.

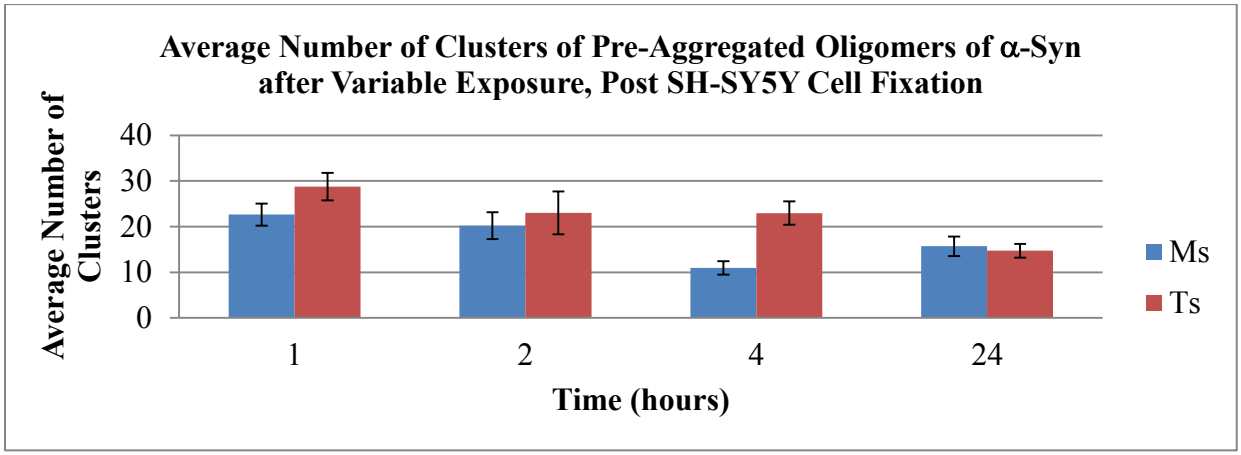

Figure 5.11 Bar Graph for Average Number of Clusters of Pre-Aggregated Oligomers of α-Syn After Variable Exposure, Post SH-SY5Y Cell Fixation

The average number of clusters of pre-aggregated oligomers of α-syn after variable exposure, post SH-SY5Y cell fixation is plotted as a function of variable exposure time.

The number of clusters of pre-aggregated monomers and tetramers are of the same magnitude. Generally speaking, the number of clusters containing pre-aggregated monomers is constant within 24 hours. However, for pre-aggregated tetramers, the number of clusters containing pre-aggregated tetramers decreases after 24 hours has elapsed. An interesting feature to this bar graph is the relative similarity of the number of clusters of monomers and tetramers after 24 hours has elapsed.

Figure 5.12 is a bar graph of the average number of clusters containing pre-aggregated oligomers per square micron after variable exposure, post SH-SY5Y cell fixation.

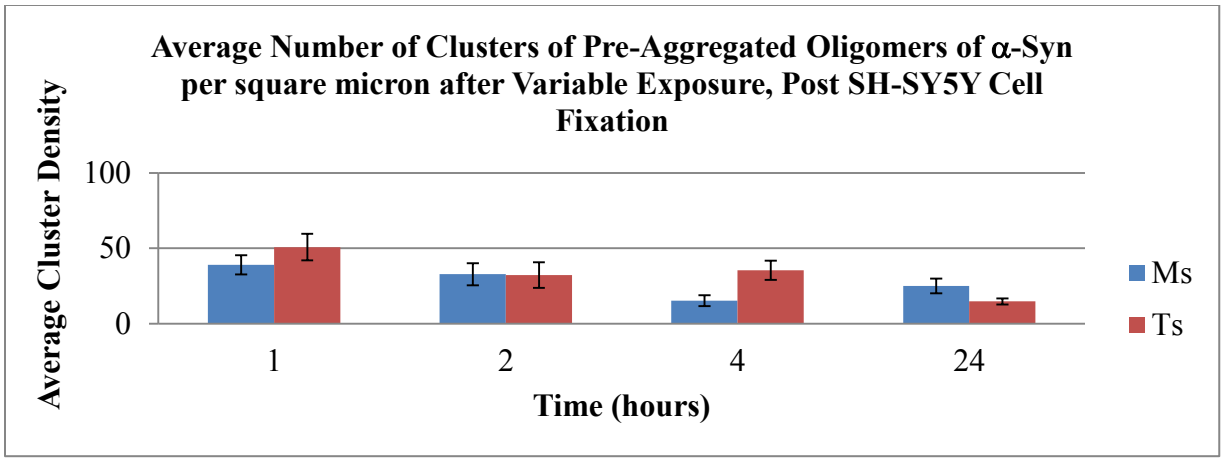

Figure 5.12 Bar Graph of Average Number of Clusters of Pre-Aggregated Oligomers of α-Syn per square micron after Variable Exposure, Post SH-SY5Y Cell Fixation

The average number of clusters of pre-aggregated oligomers of α-syn per square micron after Variable Exposure, Post SH-SY5Y Cell Fixation is plotted as a function of variable exposure time.

Based on the bar graph presented in Figure 5.12, there is no absolute trend with the number of monomeric clusters observed per square micron. However, after 24 hours has elapsed, the number of clusters observed per square micron that contain pre-aggregated tetramers is constant within the first four hours of exposure and then decreases after 24 hours has elapsed. In addition, the magnitude for each oligomer is similar.

Figure 5.13 is a bar graph for the average relative degree of aggregation of pre-aggregated oligomers of α −Syn after variable exposure, post SH-SY5Y cell fixation.

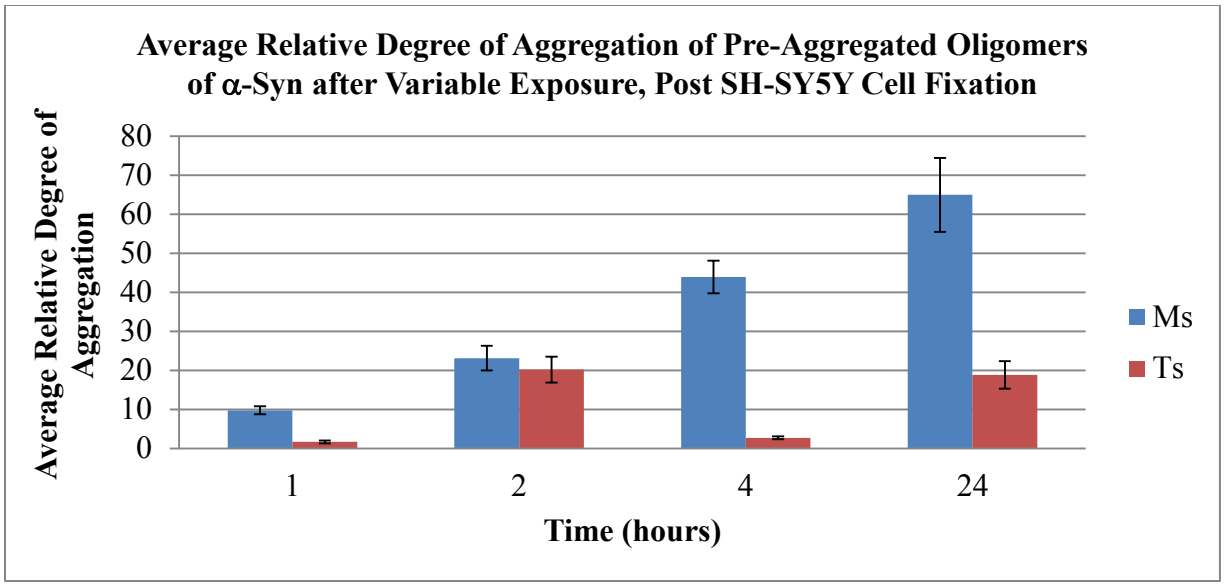

Figure 5.13 Bar Graph for Average Degree of Aggregation of Pre-Aggregated Oligomers of α-Syn after Variable Exposure, Post SH-SY5Y Cell Fixation

The average degree of aggregation of pre-aggregated oligomers of α-Syn after Variable Exposure, Post SH-SY5Y Cell Fixation is plotted as a function of variable exposure time.

As expected with the proportionality to intensity, the average relative degree of aggregation of monomers per cluster increases with time. In addition, the tetramers fluctuate with time; a greater degree of aggregation of tetramers is observed after 2 and 24 hours of exposure. An interesting trend is the similarity of the data after 2 hours has progressed, contrary to the plot shown in Figure 5.7 when a similarity was observed after 24 hours had progressed. In addition, this plot is similar to the plot of intensities as a function of exposure time shown Figure 5.10 because the relative degree of aggregation is weighted heavily on the intensity as the experimental fitted laser beam width is constant.

5.1.4 Fixed Exposure, Variable Uptake of Oligomers of α −Syn in SH-SY5Y Cells

Oligomers were exposed to living cells for 2 hours. Samples were then washed, replaced with fresh media, and placed back in the incubator for 1, 2, 4, and 24 hours prior to cell fixation. Recall, this experiment was also done for phospholipid coated gold nanoparticle uptake in Chapters 4.1.2 and 4.5.2

Thus, SH-SY5Y cells were exposed to monomeric, dimeric, and tetrameric forms α −syn by a fixed exposure, variable uptake experiment as discussed in Chapter 2.3.2. Laser scanning confocal microscopy can be found in 2.10.3.1. Image Correlation Spectroscopy can be found in Chapter 2.11.1

5.1.4.1 Fixed Exposure, Variable Uptake of Monomers in SH-SY5Y Cells

This section is based on the study of the internalization of monomers in SH-SY5Y cells by a fixed exposure, variable uptake experiment.

In Figure 5.14, Images A, B, C, and D each correspond to one confocal fluorescence microscopy image of one SH-SY5Y cell with internalized monomers. Each image corresponds to a cell from a different sample, varying based on time of sample re-incubation after washing; 1, 2, 4, and 24 hours.

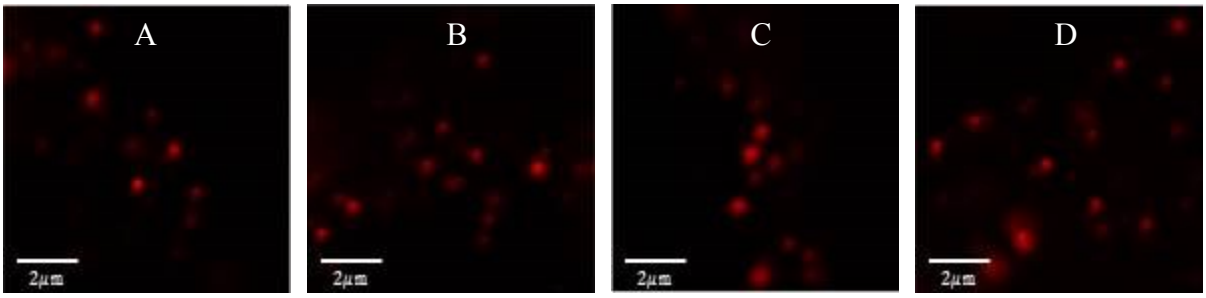

Figure 5.14 Images of Monomers after Fixed Exposure, Variable Uptake in SH-SY5Y Cells

Images A, B, C, and D each correspond to one confocal fluorescence microscopy image of one SH-SY5Y cell with internalized monomers. Each image corresponds to a cell from a different sample, varying based on time of sample re-incubation after washing; 1, 2, 4, and 24 hours.

In contrast to passive diffusion, the monomers cluster in fewer red regions in the cell as opposed to homogeneously distributing within the entire cytoplasm of the cell; the red circular regions represent compartments that contain monomers after uptake via endocytosis.

Table 5.11 shows the average auto correlation amplitude, average fitted laser beam width, and average intensity for 20-30 images of each sample of monomers after fixed exposure, variable uptake in SH-SY5Y cells.

Table 5.11 Averages of ICS Parameters Corresponding to Images of Monomers after Fixed Exposure, Variable Uptake in SH-SY5Y Cells

Variable Uptake Time (hours)	$\langle \mathbf{g}(\mathbf{0},\mathbf{0}) \rangle$	$\langle \boldsymbol{\omega}\ (\boldsymbol{\mu}\mathbf{m}) \rangle$	$\langle I_{avg.} \rangle$
1	1.70 ± 0.18[1]	0.40 ± 0.01	141. ± 9
2	1.76 ± 0.23	0.38 ± 0.01	146 ± 10
4	1.54 ± 0.19	0.39 ± 0.02	144 ± 13
24	1.19 ± 0.28	0.39 ± 0.02	69.2 ± 7.8

1 Standard error.

The average intensity pertaining to experiments of varying uptake time reveal that the intensity of monomers is constant within the first four hours, and then reduces to approximately half after 24 hours of uptake has progressed. The average auto correlation function obtained for each variable uptake time is relatively consistent within the first four hours of uptake, ranging in magnitude between 1.54-1.76. The average auto correlation amplitude obtained at 24 hours is approximately 1.19, which is less in magnitude compared to 1-4 hours of uptake. Additionally, the average values obtained for the fitted laser beam width ranges between 0.38-0.40, which indicates this measurement arises from convolution.

Table 5.12 shows the average values of the calculations corresponding to monomers after fixed exposure, variable uptake in SH-SY5Y cells. The average number of clusters monomers, the average number of clusters of monomers per square micron, and the average relative degree of aggregation of monomers per cluster was calculated for 20-30 images per sample. The calculations presented are in reference to the data obtained in Table 5.11. The average values for each parameter are shown with standard error.

Table 5.12 Averages of Derived ICS Parameters for Images of Monomers after Fixed Exposure, Variable Uptake in SH-SY5Y Cells

Variable Uptake Time (hours)	$\langle N_{Ms} \rangle$	$\langle CD \rangle$	$\langle DA \rangle$
1	0.83 ± 0.09[1]	1.72 ± 0.21	225 ± 23
2	0.82 ± 0.10	1.94 ± 0.25	234 ± 24
4	0.89 ± 0.08	2.05 ± 0.22	190 ± 17
24	1.73 ± 0.48	3.57 ± 0.71	85 ± 24

1 Standard error.

The calculations presented in Table 5.12 reflect that the number of monomers observed in the observation region of the laser beam is approximately 0.82-0.89 within the initial four hours of uptake. After 24 hours of uptake has progressed, there are a greater number of clusters containing monomers in the observation region of the laser beam. The observed average number of clusters containing monomers per square micron is also relatively consistent, ranging between 1.72-2.05 clusters per square micron. After 24 hours has progressed, there are a greater number of clusters containing monomers per square micron, specifically 3.57 clusters per square micron. Lastly, the relative degree of aggregation is constant for the first four hours of uptake, then decreases to approximately 85 monomers per cluster.

Monomers aggregate to a large extent in clusters within four hours of uptake. After 24 hours have progressed for uptake, monomers are observed in more clusters per square micron, but aggregate to a lesser extent in these clusters. To argue a time interval in which aggregates of these oligomers are observed, between 1-4 hours, even as early as 1 hour of uptake, is enough time for efficient aggregation of this oligomer in *one* cell.

5.1.4.2 Fixed Exposure, Variable Uptake of Dimers in SH-SY5Y Cells

This section is based on the study of the internalization of dimers in SH-SY5Y cells by a fixed exposure, variable uptake experiment.

In Figure 5.15, images A, B, C, and D each correspond to one confocal fluorescence microscopy image of one SH-SY5Y cell with internalized dimers. Each image corresponds to a cell from a different sample, varying based on time of sample re-incubation after washing; 1, 2, 4, and 24 hours.

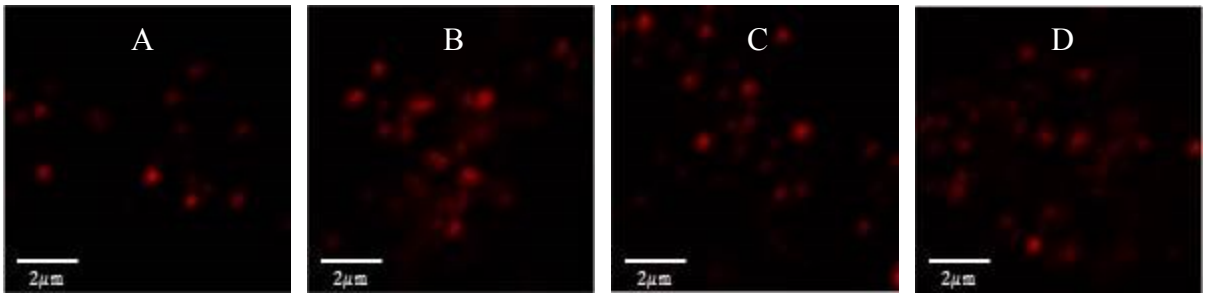

Figure 5.15 Images of Dimers after Fixed Exposure, Variable Uptake in SH-SY5Y Cells

Images A, B, C, and D each correspond to one confocal fluorescence microscopy image of one SH-SY5Y cell with internalized dimers. Each image corresponds to a cell from a different sample, varying based on time of sample re-incubation after washing; 1, 2, 4, and 24 hours.

Similar to the uptake of monomers, there is very little difference between Images A, B, C, and D; the dimers appear to cluster to the same extent amongst images.

Table 5.13 shows the average of the auto correlation amplitude, average fitted laser beam width, and average intensity for 20-30 images of each sample of dimers after fixed exposure, variable uptake in SH-SY5Y cells.

Table 5.13 Averages of Derived ICS Parameters for Images of Dimer after Fixed Exposure, Variable Uptake in SH-SY5Y Cells

Variable Uptake Time (hours)	$\langle g(0,0) \rangle$	$\langle \omega\ (\mu m) \rangle$	$\langle I_{avg.} \rangle$
1	2.10 ± 0.23[1]	0.39 ± 0.01	76.8 ± 6.4
2	2.18 ± 0.25	0.38 ± 0.01	81.3 ± 6.4
4	2.98 ± 0.38	0.38 ± 0.01	74.0 ± 12.1
24	1.78 ± 0.54	0.39 ± 0.02	49.1 ± 5.1

1 Standard error.

The average intensity is constant within the first four hours of uptake and decreases after 24 hours have progressed, similar to monomers in Table 5.11. The average auto correlation function obtained for each variable uptake time is relatively consistent within the first four hours of uptake, ranging between 2.10-2.98. The average auto correlation function obtained at 24 hours is less in magnitude, approximately 1.78. Additionally, the average values obtained for the fitted laser beam width ranges between 0.38-0.39. The values obtained from the fit of the laser beam reflect the measurement arises from convolution.

Table 5.14 shows the average values of the calculations corresponding dimers after fixed exposure, variable uptake in SH-SY5Y cells. The average number of clusters containing dimers, the average number of clusters containing dimers per square micron, and the average relative degree of aggregation of dimers per cluster was calculated for 20-30 images per sample. The calculations presented are in reference to the data obtained in Table 5.14. The average values for each parameter are shown with standard error.

Table 5.14 Averages of Calculations Corresponding to Data for Images of Dimers after Fixed Exposure, Variable Uptake in SH-SY5Y Cells

Variable Uptake Time (hours)	$\langle N_{Ds} \rangle$	$\langle CD \rangle$	$\langle DA \rangle$
1	0.63 ± 0.06[1]	1.39 ± 0.14	145 ± 13
2	0.71 ± 0.10	1.65 ± 0.24	168 ± 23
4	0.46 ± 0.07	1.06 ± 0.21	208 ± 42
24	1.05 ± 0.17	2.68 ± 0.59	100 ± 35

1 Standard error.

The calculations presented in Table 5.14 reflect the number of dimers observed in the observation area of the laser beam is approximately 0.46-0.71 within the first four hours of uptake. After 24 hours of uptake has progressed, there are a greater number of clusters containing dimers in the observation region of the laser beam. As one would expect, the observed average number of clusters containing dimers per square micron is also relatively consistent, ranging between 1.06-1.65 clusters per square micron. After 24 hours has progressed, there are a greater number of clusters containing dimers per square micron, specifically 2.68 clusters per square micron. Lastly, the relative degree of aggregation is again constant for the first four hours of uptake, then decreases to approximately 100 dimers per fluorescent cluster.

In conclusion, dimers aggregate to a large extent in clusters within four hours of uptake. After 24 hours have elapsed for uptake, dimers are observed in more clusters per square micron, but aggregate to a lesser extent in these clusters. To argue a time interval in which aggregates of these oligomers are observed, between 1-4 hours, even as early as 1 hour of uptake, is enough time for efficient aggregation of this oligomer in *one* cell.

5.1.4.3 Fixed Exposure, Variable Uptake of Tetramers in SH-SY5Y Cells

This section is based on the study of the internalization of tetramers in SH-SY5Y cells via a fixed exposure, variable uptake experiment.

In Figure 5.16, images A, B, C, and D each correspond to one confocal fluorescence microscopy image of one SH-SY5Y cell with internalized tetramers. Each image corresponds to a cell from a different sample, varying based on time of re-incubation after washing; 1, 2, 4, and 24 hours.

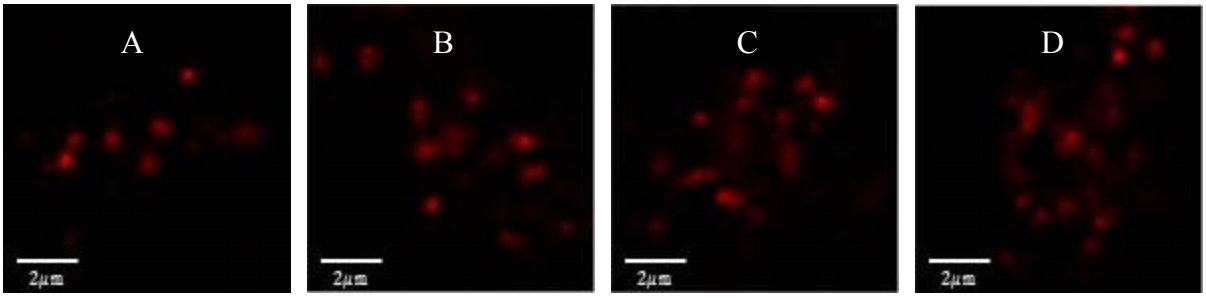

Figure 5.16 Images of Tetramers after Fixed Exposure, Variable Uptake in SH-SY5Y Cells

Images A, B, C, and D each correspond to one confocal fluorescence microscopy image of one SH-SY5Y cell with internalized tetramers. Each image corresponds to a cell from a different sample, varying based on time of re-incubation after washing; 1, 2, 4, and 24 hours.

There is little difference between images A, B, C, and D shown in the figure.

Table 5.15 shows the average of the auto correlation amplitude, average fitted laser beam width, and average intensity for 20-30 images of each sample of SH-SY5Y cells with internalized tetramers.

Table 5.15 Averages of ICS Parameters for Images of Tetramers after Fixed Exposure, Variable Uptake in SH-SY5Y Cells

Variable Uptake Time (hours)	$\langle g(0,0) \rangle$	$\langle \omega\ (\mu m) \rangle$	$\langle I_{avg.} \rangle$
1	3.53 ± 0.69[1]	0.44 ± 0.02	77.1 ± 7.2
2	3.65 ± 0.64	0.47 ± 0.04	83.9 ± 6.7
4	3.61 ± 0.77	0.41 ± 0.02	98.3 ± 11.6
24	2.54 ± 0.35	0.38 ± 0.01	95.0 ± 12.1

1 Standard error.

The average intensity pertaining to experiments of varying uptake time reveal that the intensity is constant within 24 hours of uptake. The average auto correlation amplitude obtained for each variable uptake time is relatively consistent within the first four hours of uptake, ranging in magnitude between 3.53-3.61. The average auto correlation function obtained at 24 hours is less in magnitude, approximately 2.54. Additionally, the average values obtained for the fitted laser beam width ranges between 0.38-0.47. As discussed in Chapter 4, the fitted ω value is a convolution of the size of the beam and the system of interest imaged in the observation area of the laser beam. These values reflect that the measured width arises from convolution.

Table 5.16 shows the average values of the calculations corresponding tetramers after fixed exposure, variable uptake in SH-SY5Y cells. The average number of clusters containing tetramers, the average number of clusters containing tetramers per square micron, and the average relative degree of aggregation of tetramers per cluster was calculated for 20-30 images per sample. The calculations presented in Table 5.16 are in reference to the data obtained in Table 5.15.

Table 5.16 Averages of Derived ICS Parameters for Images of Tetramers after Fixed Exposure, Variable Uptake in SH-SY5Y Cells

Variable Uptake Time (hours)	$\langle N_{Ts} \rangle$	$\langle CD \rangle$	$\langle DA \rangle$
1	0.72 ± 0.14[1]	1.23 ± 0.27	239 ± 39
2	0.59 ± 0.12	0.94 ± 0.20	309 ± 65
4	0.68 ± 0.13	1.41 ± 0.24	337 ± 68
24	0.55 ± 0.07	1.25 ± 0.17	230 ± 39

1 Standard error.

Based on the calculations presented in Table 5.16, there is no specific trend, apart from each measured parameter being constant with time.

5.1.4.4 Comparisons for Fixed Exposure, Variable Uptake of Oligomers of α-Syn in SH-SY5Y Cells

The purpose of this section is to compare the number of clusters, number of clusters per square micron, intensity, and degree of aggregation of monomers, dimers, and tetramers in SH-SY5Y cells.

Figure 5.17 is a bar graph of the average intensity of oligomers of α-Syn after fixed exposure, variable uptake in SH-SY5Y cells.

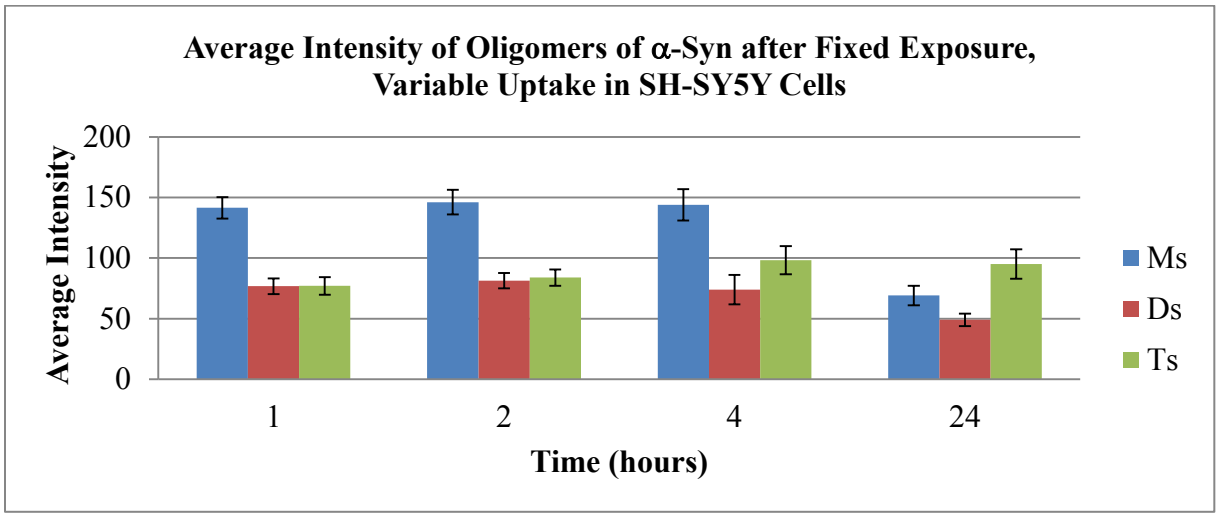

Figure 5.17 Bar Graph of Average Intensity of Oligomers of α-Syn after fixed Exposure, Variable Uptake in SH-SY5Y Cells

The average Intensity of each oligomer of α-Syn after Fixed Exposure, Variable Uptake is plotted as a function of Variable Uptake time in SH-SY5Y cells.

The average intensity of each oligomer observed is within magnitude. However, monomeric intensity after 24 hours has elapsed is much less in comparison to that of the intensity observed within 4 hours. The dimers also exhibit a decrease in intensity, but a larger decrease in intensity between 4 and 24 hours is observed for monomers.

Figure 5.18 is a bar graph of the average number of clusters of oligomers of α-Syn after fixed exposure, variable uptake in SH-SY5Y cells.

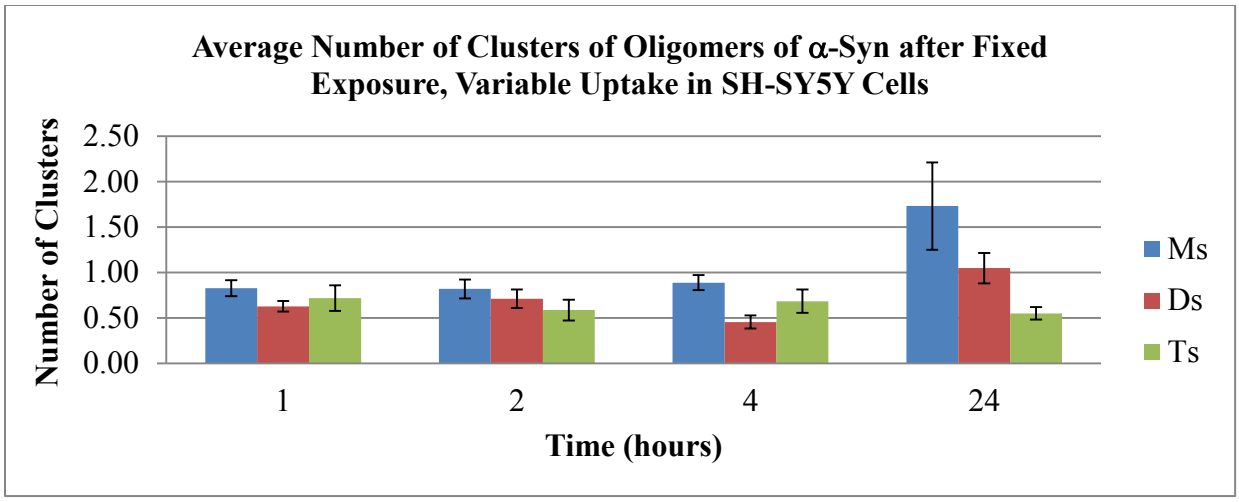

Figure 5.18 Bar Graph of Average Number of Clusters of Oligomers of α-Syn after fixed Exposure, Variable Uptake in SH-SY5Y Cells

The average number of clusters of each oligomer of α −Syn after fixed exposure, variable uptake is plotted as a function of variable uptake time in SH-SY5Y cells.

Generally speaking, the number of clusters observed for each oligomer is of similar magnitude. Differences observed include the following; the number of clusters containing monomers and number of clusters containing dimers increases with the progression of uptake time, but to a larger extent with monomers. The number of tetramers observed remains unchanged with the progression of time.

Figure 5.19 is a bar graph of the average number of clusters containing oligomers of α −Syn after fixed exposure, variable uptake in SH-SY5Y cells.

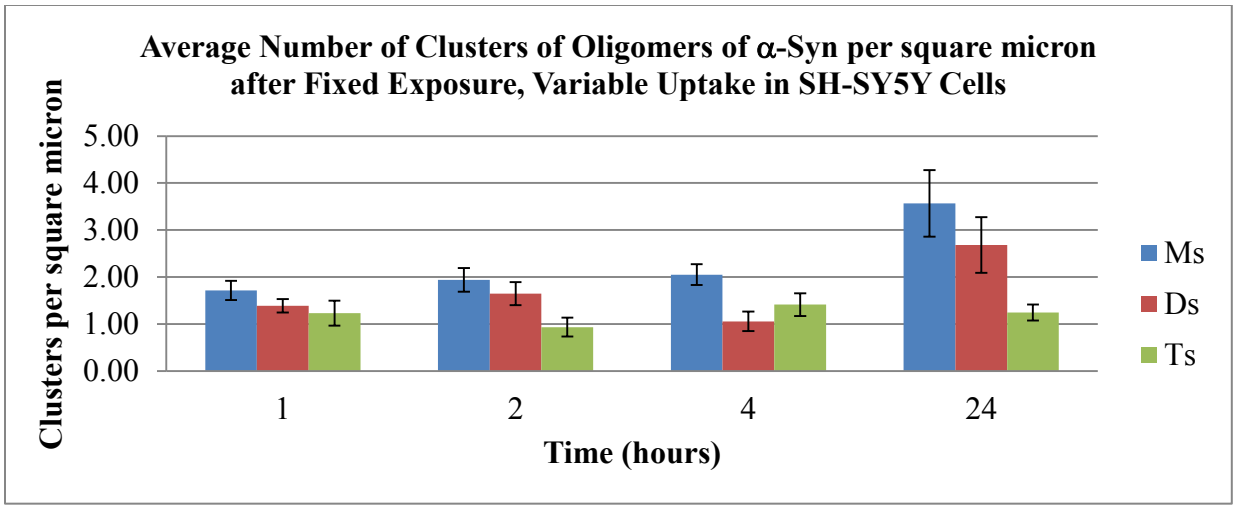

Figure 5.19 Bar Graph of Average Number of Clusters of Oligomers of α-Syn per square micron after fixed exposure, variable uptake in SH-SY5Y Cells

The average number of clusters of each oligomer of α −Syn per square micron after fixed exposure, variable uptake is plotted as a function of Variable Uptake time in SH-SY5Y cells.

As expected, the magnitude corresponding to each cluster containing an oligomer compares; however the monomer is of slightly larger magnitude. By observation, the number of clusters per square micron containing monomers and dimers increases after 24 hours has progressed, and the number of clusters of tetramers is constant within 24 hours of uptake.

Figure 5.20 is a bar graph of the average relative degree of aggregation of oligomers of α −Syn observed per cluster after fixed exposure, variable uptake in SH-SY5Y cells.

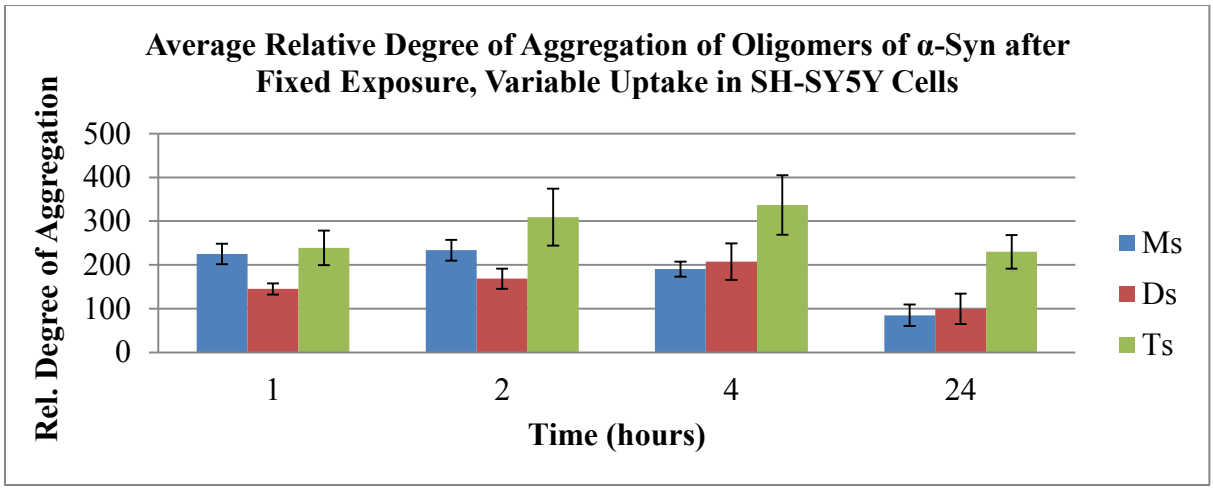

Figure 5.20 Bar Graph of Average Degree of Aggregation of Oligomer of α-Syn after Fixed Exposure, Variable Uptake in SH-SY5Y Cells

The average degree of aggregation of each oligomer of α −Syn after fixed exposure, variable uptake is plotted as a function of Variable Uptake time in SH-SY5Y cells.

The average relative degree of aggregation for monomers and dimers decreases after 24 hours has elapsed; tetramers remain consistent.

5.1.5 Data & Calculations for Exposure and Fixed Uptake of Oligomers of α-Syn to SH-SY5Y Cells

The data and calculations presented in this section pertain to images of monomers, dimers, and tetramer by a variable exposure, fixed uptake experiment however the uptake is referred to as time *zero;* each of these images were obtained separately from the experiments previously presented for variable exposure, fixed uptake in Chapter 5.1.4 for which they are not plotted with respect to other uptake times.

Figure 5.21 shows images of three individual cells singly exposed to monomers, dimers, and tetramers for two hours and then fixed.

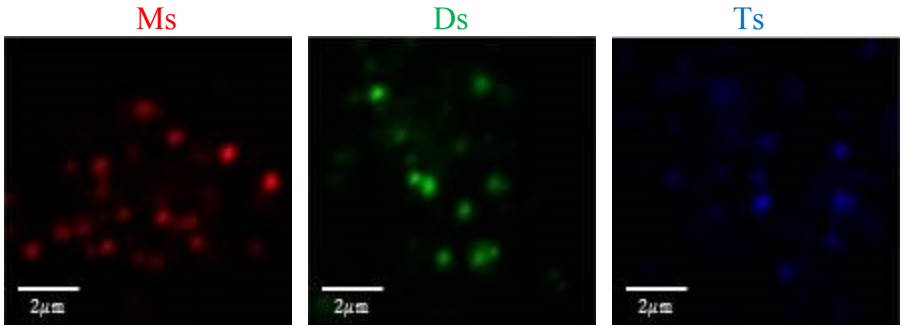

Figure 5.21 Images of Two hours of Exposure, Fixed Uptake of Oligomers of α-Syn to SH-SY5Y Cells

The images in Figure 5.21 show each oligomer appears to be similarly distributed over the entire image, with no major differences.

Table 5.17 shows the averages of the auto correlation amplitude, fitted laser beam width, and average intensity corresponding to 20-30 images of monomers, dimers, and tetramers.

Table 5.17 ICS Parameters for Images of Two hours of Exposure, Fixed Uptake of Oligomers of α-Syn to SH-SY5Y Cells

Species	$\langle g(0,0) \rangle$	$\langle \omega\ (\mu m) \rangle$	$\langle I_{avg.} \rangle$
Monomers	2.41 ± 0.32[1]	0.38 ± 0.01	186 ± 17
Dimers	2.28 ± 0.30	0.41 ± 0.01	167 ± 14
Tetramers	3.87 ± 0.55	0.47 ± 0.02	181 ± 28

1 Standard error.

The average intensity for each species is similar in magnitude, specifically ranging between 167-186. The auto correlation amplitude for each oligomer ranges between 2.28-3.87. The value obtained for the fitted beam width is slightly increasing with size of oligomer, but is more or less constant and approximately 0.40 microns.

Table 5.18 shows the average number of clusters, average number of clusters per square micron, and the average relative degree of aggregation of oligomers, corresponding to data obtained in Table 5.17.

Table 5.18 Average Calculations Corresponding to Data for Images of Two hours of Exposure, Fixed Uptake of Oligomers of α −Syn to SH-SY5Y Cells

Species	$\langle N_{Species} \rangle$	$\langle CD \rangle$	$\langle DA \rangle$
Monomers	0.50 ± 0.04[1]	1.15 ± 0.10	393 ± 31
Dimers	0.60 ± 0.06	1.22 ± 0.13	325 ± 29
Tetramers	0.45 ± 0.07	0.76 ± 0.12	521 ± 58

1 Standard error.

The number of clusters containing each species ranges between 0.45-0.60. Lastly, the number of clusters observed of monomers and tetramers are similar in magnitude, approximately 1cluster per square micron. Lastly, the degree of aggregation of monomers and dimers are similar, approximately 300 oligomers observed per fluorescent cluster. The relative degree of aggregation of tetramers in a cluster is approximately 521 tetramers per cluster.

Although complete direct comparison cannot be made with the previous variable exposure, fixed uptake experiments in Chapter 5.1.4 as the intensity of light emitted is dependent on the amount of light at the sample and detector gain on the day of the experiment; however, the average number of clusters containing each of these oligomers per square micron in Table 5.18 are of the same magnitude as the values obtained for the cluster density plotted in Figure 5.19. At this time zero, there are slightly fewer clusters; this is somewhat expected and a good measure such that immediately after exposure to cells, there would be fewer clusters containing oligomers in cells then there would be after 1 hour has progressed for uptake.

5.2 Co-localization of Two Oligomers of α −Syn in SH-SY5Y Cells

Chapter 5.2 is based on the study of the co-localization of two oligomers in SH-SY5Y cells. SH-SY5Y cells were simultaneously exposed to two oligomers for two hours and fixed prior to imaging to determine the extent to which two oligomers exist in the same cluster, such that they follow the same pathway once internalized in cells.

The experimental protocol corresponding to simultaneously labelling cells with two oligomers can be found in Chapter 2.8.2. The protocol required for laser scanning confocal

imaging of two species can be found in 2.10.3.2. Last, image cross correlation spectroscopy analysis methods can also be referred to in Chapter 2.11.2.

5.2.1 Co-localization of Monomers (Ms-561) & Dimers (Ds-633) in SH-SY5Y Cells

Figure 5.22 shows original (not contrast enhanced) confocal fluorescence microscopy images of one cell exposed to monomers and dimers for two hours prior to immediate fixation. The monomers and dimers are shown in green and red, respectively. The merge image is the overlay of the green and red images.

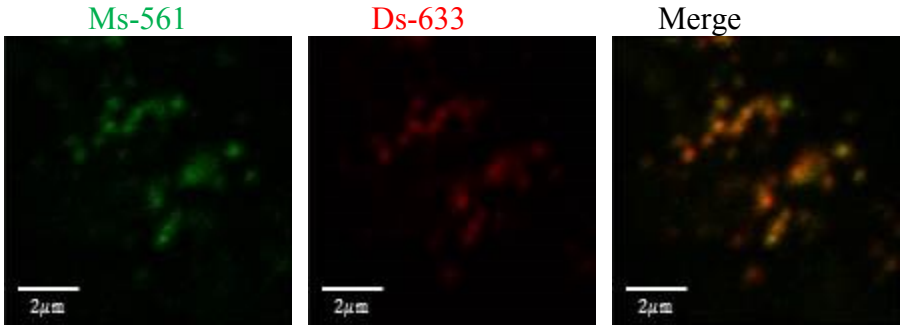

Figure 5.22 Images of Monomers & Dimers in SH-SY5Y Cells

Confocal fluorescence microscopy images of monomers and tetramers, shown in green and red, respectively, in one cell. The Merge image is an overlay of the green and red images.

Due to the copious amount of yellow color in the Merge image, Figure 5.22 shows the monomers and dimers are in the same compartments.

Table 5.19 shows the average number of clusters denoted by $\langle N_{Species} \rangle$ and the average fractions of co-localization of monomers and dimers. The average fraction of clusters containing monomers that also contain dimers is denoted by $\langle F(Ms|Ds) \rangle$. Likewise, the average fraction of clusters containing dimers that also contain monomers is denoted by $\langle F(Ds|Ms) \rangle$.

Table 5.19 Average Number of Clusters and Fractions of Co-Localization of Ms & Ds in SH-SY5Y Cells

Species	$\langle N_{Species} \rangle$	$\langle F(Ms\|Ds) \rangle$	$\langle F(Ds\|Ms) \rangle$
Ms-561	0.59 ± 0.21[1]		
Ds-633	0.33 ± 0.09		
Ms-561 & Ds-633	0.38 ± 0.11	0.79 ± 0.07	1.09 ± 0.04

[1]Standard error.

There are approximately 0.59 clusters containing monomers and approximately 0.33 clusters containing dimers. Lastly, there are approximately 0.38 clusters that contain both monomers and dimers. The similarity in clusters consisting of two oligomers with clusters of one oligomer is in good agreement with the images presented in Figure 5.22.

The calculations presented in Table 5.19 reflect that approximately 79% of clusters containing monomers also contain dimers and approximately 109% of clusters containing dimers also contain monomers. Recall the lower limit of data rejection was data for fractions of co-localization were greater than 1.20; therefore, a majority of the samples measured consisted of data with fractions greater than 1.00.

5.2.2 Co-localization of Monomers (Ms-561) & Tetramers (Ts-561) in SH-SY5Y Cells

Figure 5.23 shows the original (not contrast enhanced) confocal fluorescence microscopy images of one cell after being exposed to monomers and tetramers for two hours prior to fixation. The monomers and dimers are shown in green and red, respectively. The merge image is the overlay of the green and red images.

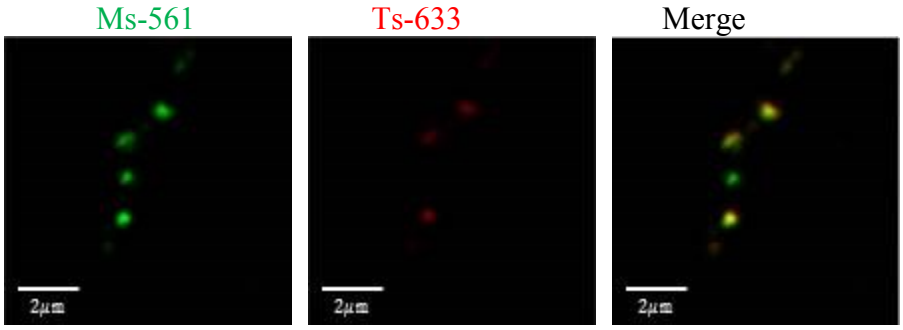

Figure 5.23 Images of Monomers & Tetramers in SH-SY5Y Cells

Original confocal fluorescence microscopy images of monomers and tetramers, shown in green and red, respectively, in one cell. The Merge image is an overlay of the green and red images.

Visually speaking, there is a very high degree of co-localization as shown with the copious amount of yellow color in the Merge image.

Table 5.20 reflects the average number of clusters denoted by $\langle N_{Species} \rangle$ and the average fractions of co-localization of monomers and tetramers. The average fraction of clusters containing monomers that also contain tetramers is denoted by $\langle F(Ms|Ts) \rangle$. Likewise, the average fraction of clusters containing tetramers that also contain monomers is denoted by $\langle F(Ts|Ms) \rangle$.

Table 5.20 Average Number of Clusters and Fractions of Co-Localization of Monomers & Tetramers in SH-SY5Y Cells

Species	$\langle \boldsymbol{N_{Species}} \rangle$	$\langle \boldsymbol{F(Ms\|Ts)} \rangle$	$\langle \boldsymbol{F(Ts\|Ms)} \rangle$
Ms-561	0.21 ± 0.02[1]		
Ts-633	0.21 ± 0.03		
Ms-561 & Ts-633	0.20 ± 0.02	0.93 ± 0.03	0.98 ± 0.04

There are approximately 0.21 clusters containing monomers and approximately 0.21 clusters containing tetramers. Lastly, there are approximately 0.20 clusters that contain both monomers and tetramers. The similarity in clusters consisting of two oligomers with clusters of one oligomer is in good agreement with the images presented in Figure 5.23.

The calculations presented in Table 5.20 show that approximately 93% of clusters containing monomers also contain dimers and 98% of clusters containing tetramers also contain monomers.

5.2.3 Co-localization of Dimers (Ds-561) & Tetramers (Ts-633) in SH-SY5Y Cells

Figure 5.24 shows confocal fluorescence microscopy images of one cell after being exposed to dimers and tetramers for two hours prior to immediate fixation. The monomers and dimers are shown in green and red, respectively.

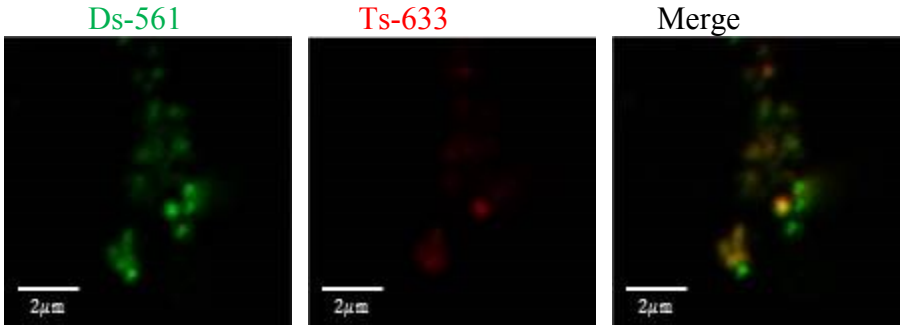

Figure 5.24 Images of Ds-561 & Ts-561 in SH-SY5Y Cells

The copious amount of yellow color in the Merge image indicates dimers and tetramers are located in the same clusters.

Table 5.21 reflects the average number of clusters denoted by $\langle N_{Species} \rangle$ and the average fractions of co-localization of dimers and tetramers. The average fraction of clusters containing dimers that also contain tetramers is denoted by $\langle F(Ds|Ts) \rangle$. Likewise, the average fraction of clusters containing tetramers that contain dimers is denoted by $\langle F(Ts|Ds) \rangle$.

Table 5.21 Average Number of Clusters and Fractions of Co-Localization of Dimers & Tetramers in SH-SY5Y Cells

Species	$\langle N_{Species} \rangle$	$\langle F(Ds\|Ts) \rangle$	$\langle F(Ts\|Ds) \rangle$
Ds-561	0.29 ± 0.05[1]		
Ts-633	0.22 ± 0.03		
Ds-561 & Ts-633	0.23 ± 0.04	1.00 ± 0.01	1.05 ± 0.01

1 Standard error.

There are approximately 0.29 clusters containing dimers and there are approximately 0.22 clusters containing tetramers. Lastly, there are approximately 0.23 clusters that contain both dimers and tetramers. The similarity in clusters consisting of two oligomers with clusters of one oligomer is in good agreement with the images presented in Figure 5.24.

The calculations presented in Table 5.21 reflect that approximately 100% of clusters containing dimers also contain tetramers and approximately 105% of clusters containing tetramers also contain dimers with an error of ± 0.01 that of the measured value.

5.3 Distribution of Endocytic Marked Compartments in SH-SY5Y Cells

Chapter 5.3 focusses on the distribution and co-localization of markers for endocytic compartments in SH-SY5Y cells.

Methods corresponding to labelling of markers in cells can be found in Chapter 2.4. Laser scanning confocal microscopy imaging of one marker can be found in Chapter 2.10.3.1. Image Correlation Spectroscopy can be found in Chapter 2.11.1.

Figure 5.25 shows the original fluorescence microscopy images of three different cells. Approximately 20-30 images were obtained for each single label experiment. Rab5, Rab7, and LAMP-1 markers were studied.

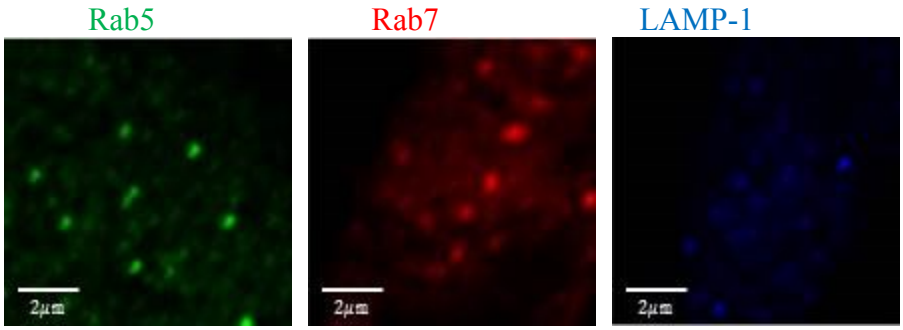

Figure 5.25 Images of Rab5, Rab7, and LAMP-1 Endocytic Marked Compartments in SH-SY5Y Cells

The images shown in Figure 5.25 show that the bright regions of clusters of Rab7 are larger than the bright regions labelled with Rab5 and LAMP-1 markers.

Table 5.22 shows the average auto correlation amplitude, average fitted laser beam width, and average intensity corresponding to 20-30 images of markers for endocytic compartments in SH-SY5Y cells.

Table 5.22 ICS Parameters for Images of Endocytic Marked Compartments in SH-SY5Y Cells

Species	$\langle \mathbf{g(0,0)} \rangle$	$\langle \boldsymbol{\omega}\ (\boldsymbol{\mu m}) \rangle$	$\langle I_{avg.} \rangle$
Rab5	0.51 ± 0.05[1]	0.35 ± 0.02	370 ± 24
Rab7	0.22 ± 0.02	0.51 ± 0.01	692 ± 39
LAMP-1	0.58 ± 0.11	0.31 ± 0.01	251 ± 12

1 Standard error.

The average intensities for each species ranges between 251-692. The average auto correlation amplitudes obtained for Rab5 and LAMP-1 are similar, approximately 0.51 and 0.58 respectively. The auto correlation amplitude obtained for Rab7 is 0.22, approximately two-fold less in comparison. The fit obtained for the laser beam width is in agreement for Rab5 and LAMP-1 markers. This is expected due to the fluorescent probe of the secondary antibodies used for Rab5 and LAMP-1 were the same wavelength, 561 nm. The average fit for the laser beam width corresponding to images of Rab5 marked endocytic compartments is 0.35 microns and the average fit for the laser beam width for LAMP-1 marked compartments is 0.31 microns. Rab7 is somewhat larger in comparison, approximately 0.51 microns.

Table 5.23 shows the average values corresponding to the number of clusters, the number of clusters per square micron, and the relative degree of aggregation of markers per cluster.

Table 5.23 Averaged Calculations Corresponding to Data of Images of Endocytic Marked Compartments in SH-SY5Y Cells

Species	$\langle N_{Species} \rangle$	$\langle CD \rangle$	$\langle DA \rangle$
Rab5	2.70 ± 0.37[1]	7.87 ± 1.15	175 ± 15
Rab7	1.29 ± 0.07	7.29 ± 0.84	143 ± 10
LAMP-1	2.26 ± 0.21	7.46 ± 0.73	133 ± 17

On average there are approximately 2.70 clusters containing Rab5 markers and there are approximately 1.29 clusters containing Rab7 markers. Lastly, there are approximately 2.26 clusters containing LAMP-1 markers. An interesting feature to these calculations is the relative similarity among the number of clusters per square micron that contain each of these markers. Specifically, 7.87 clusters contain Rab5 markers, 7.29 clusters contain Rab7, and 7.46 clusters contain LAMP-1. The relative degree of aggregation is also similar for each marker; there are 175 Rab5 markers per cluster, 143 Rab7 markers per cluster, and 133 LAMP-1 markers per cluster.

5.4 Co-localization of Two Endocytic Markers in SH-SY5Y Cells

Chapter 5.4 is based on the study of the co-localization of two markers specific for two endocytic compartments in SH-SY5Y cells.

In this section, the following experimental combinations were studied; Rab5-561 & Rab7-633, Rab5-561 & LAMP-1-633, and Rab7-633 & LAMP-1-561. The experimental procedure for immunofluorescent labelling of two markers in cells can be found in Chapter 2.6.1. Laser scanning confocal microscopy imaging of two markers can be found 2.10.3.2. Image Cross Correlation Spectroscopy analysis can be found in Chapter 2.11.2.

5.4.1 Rab5-561 & Rab7-633 Endocytic Marked Compartments in SH-SY5Y Cells

Figure 5.26 shows the original confocal fluorescence microscopy images of one cell marked with Rab5-561 and Rab7-633. The Merge image is an overlay of the Rab5-561 and Rab7-633 images.

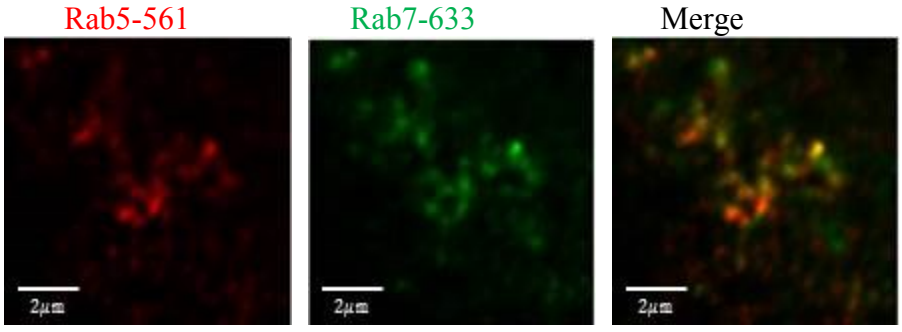

Figure 5.26 Images of Rab5-561 & Rab7-633 Endocytic Marked Compartments in SH-SY5Y Cells

Due to the presence of yellow regions in the Merge image in Figure 5.26, Rab5-561 and Rab7-633 markers appear to be located in the same clusters.

Table 5.24 reflects the average number of clusters denoted by $\langle N_{Species} \rangle$ and the average fractions of co-localization of Rab5 and Rab7. The average fraction of clusters containing Rab5 that also contain Rab7 markers is denoted by $\langle F(Rab5|Rab7) \rangle$. Likewise, the average fraction of clusters containing Rab7 markers that also contain Rab5 markers is denoted by $\langle F(Rab7|Rab5) \rangle$.

Table 5.24 Average Number of Clusters and Fractions of Co-Localization of Rab5-561 & Rab7-633 Markers in SH-SY5Y Cells

Species	$\langle N_{Species} \rangle$	$\langle F(Rab5\|Rab7) \rangle$	$\langle F(Rab7\|Rab5) \rangle$
Rab5-561	1.73 ± 0.43[1]		
Rab7-633	3.55 ± 0.66		
Rab5-561 & Rab7-633	1.73 ± 0.35	1.04 ± 0.04	0.57 ± 0.12

1 Standard error.

The calculations for the average number of clusters in Table 5.24 reflect that there are approximately 1.73 clusters containing Rab5-561 markers and there are also approximately 3.55 clusters containing Rab7-633 markers. Lastly, there are approximately 1.73 clusters containing both Rab5-561 and Rab7-633 markers.

The calculations for the average fractions of co-localization represented in Table 5.24 reflect approximately 104% of clusters containing Rab5-561 markers also contain Rab7-633 markers and approximately 57% of the clusters containing Rab7 -633 markers also contain Rab5-561 markers.

5.4.2 Rab5-561 & LAMP-1-633 Endocytic Marked Compartments in SH-SY5Y Cells

Figure 5.27 shows the original confocal fluorescence microscopy images of one cell marked with Rab5-561 and LAMP-1-633. The Merge image is an overlay of the Rab5-561 and LAMP-1-633 images.

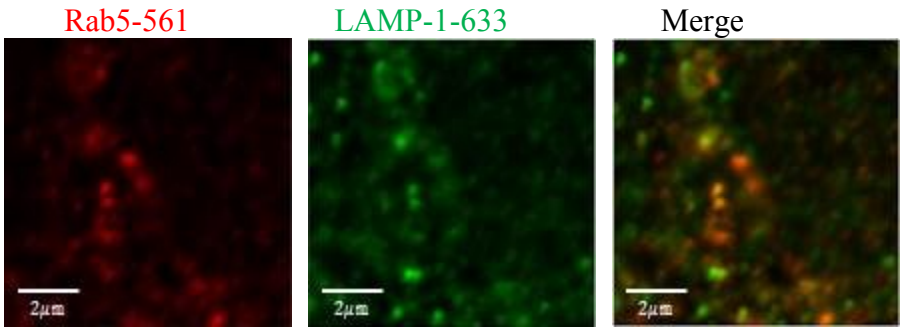

Figure 5.27 Images of Rab5-561 & LAMP-1-633 Endocytic Marked Compartments in SH-SY5Y Cells

Similar to the association of Rab5 with Rab7, the Merge image in Figure 5.27 shows Rab5 and LAMP-1 markers occupy the same clusters.

Table 5.25 reflects the average number of clusters denoted by $\langle N_{Species} \rangle$ and the average fractions of co-localization of Rab5-561 and LAMP-1-633. The average fraction of clusters containing Rab5-561 that also contain LAMP-1-633 markers is denoted by $\langle F(Rab5|LAMP-1) \rangle$. Likewise, the average fraction of clusters containing LAMP-1-633 markers that also contain Rab5-561 markers is denoted by $\langle F(LAMP-1|Rab5) \rangle$.

Table 5.25 Average Number of Clusters and Fractions of Co-Localization of Rab5-561 & LAMP-1-633 Markers in SH-SY5Y Cells

Species	$\langle N_{Species} \rangle$	$\langle F(Rab5\|LAMP-1) \rangle$	$\langle F(LAMP-1\|Rab5) \rangle$
Rab5-561	4.46 ± 0.54[1]		
Lamp-1-633	4.73 ± 0.47		
Rab5-561 & Lamp-1-633	3.44 ± 0.37	0.82 ± 0.04	0.74 ± 0.03

1 Standard error.

The calculations for the average number of clusters in Table 5.25 reflect that there are approximately 4.46 clusters containing Rab5-561 markers and there are also approximately 4.73 clusters containing LAMP-1-633 markers. Lastly, there are approximately 3.44 clusters containing both Rab5-561 and LAMP-1-633 markers.

The calculations for the average fractions of co-localization represented in Table 5.25 reflect approximately 82% of clusters containing Rab5-561 markers also contain LAMP-1-633

markers and approximately 74% of the clusters containing LAMP-1-633 markers also contain Rab5-561 markers.

5.4.3 Rab7-633 & LAMP-1-561 Endocytic Marked Compartments in SH-SY5Y Cells

Figure 5.28 shows original (not contrast enhanced) confocal fluorescence microscopy images of one cell marked with Rab7-633 and LAMP-1-561. The Merge image is the overlay of the Rab7-633 and LAMP-1-561 images.

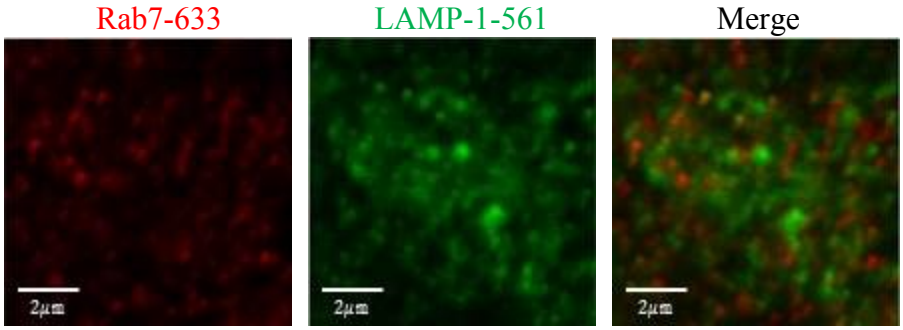

Figure 5.28 Images of Rab7-633 & LAMP-1-561 Endocytic Marked Compartments in SH-SY5Y Cells

From a visual perspective, the Merge image in Figure 5.27 reflects very little degree of co-localization of Rab7-633 and LAMP-1-561 marked compartments, judging by the merge image.

Table 5.26 reflects the average number of clusters denoted by $\langle N_{Species} \rangle$ and the average fractions of co-localization of Rab7-633 and LAMP-1-561. The average fraction of clusters containing Rab7-633 that also contain LAMP-1-561 markers is denoted by $\langle F(Rab7|LAMP-1) \rangle$. Likewise, the average fraction of clusters containing LAMP-1-561 markers that also contain Rab7-633 markers is denoted by $\langle F(Rab7|LAMP-1) \rangle$.

Table 5.26 Average Number of Clusters and Fractions of Co-Localization of Rab7-633 & LAMP-1-561 Marked Endocytic Compartments in SH-SY5Y Cells

Species	$\langle N_{Species} \rangle$	$\langle F(Rab7 \mid LAMP-1) \rangle$	$\langle F(LAMP-1 \mid Rab7) \rangle$
Rab7-633	3.65 ± 0.38 [1]		
LAMP-1-561	1.43 ± 0.18		
Rab7-633 & LAMP-1-561	0.63 ± 0.09	0.19 ± 0.03	0.46 ± 0.05

1 Standard error.

The calculations for the average number of clusters in Table 5.26 reflect that there are approximately 3.65 clusters containing Rab7-633 markers and there are also approximately 1.43 clusters containing LAMP-1-561 markers with standard error ± 0.18 the average value. Lastly, there are approximately 0.63 clusters containing both Rab7-633 and LAMP-1-561 markers with standard error ± 0.09.

The calculations for the average fractions of co-localization represented in Table 5.26 reflect approximately 19% of clusters containing Rab7-633 markers also contain LAMP-1-633 markers and approximately 46% of the clusters containing LAMP-1 markers also contain Rab7 markers.

5.5 Co-localization of a Labelled Endocytic Compartment Containing Oligomers of α −Syn in SH-SY5Y Cells

Chapter 5.5 focusses on the study of the extent to which endocytic compartments contain oligomers of α −syn. In addition, the extent to which clusters of oligomers of α −syn contain markers for endocytic compartments was also studied. Each oligomer was studied in relation to Rab5, Rab7, and LAMP-1 markers of endocytic compartments.

The double labelling procedure of oligomers and primary and secondary antibodies required for labelling of one marker can be found in Chapter 2.6.2. Procedure required for obtaining images via laser scanning confocal microscopy can be found in Chapter 2.10.3.2. Lastly, Image cross correlation spectroscopy analysis can be found in Chapter 2.11.2.

5.5.1 Co-localization Endocytic Compartments containing Monomers in SH-SY5Y Cells

The extent to which monomers (Ms) associate with Rab5, Rab7, and LAMP-1 marked compartments was studied.

Figure 5.29 shows the original confocal fluorescence microscopy images of one cell of Ms-488 and Rab5-561 marked compartments in one cell. The Merge image is an overlay of the Ms-488 and Rab5-561 images.

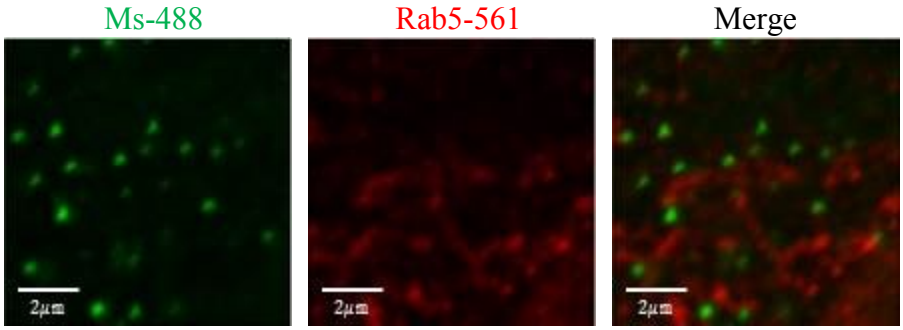

Figure 5.29 Images of Ms-488 and Rab5-561 Endocytic Marked Compartments in SH-SY5Y Cells

The lack of yellow regions in the Merge image in Figure 5.29 reflects very little degree of co-localization of Ms-488 and Rab5-561 marked compartments.

Table 5.27 reflects the average number of clusters denoted by $\langle N_{Species} \rangle$ and the average fractions of co-localization of Ms-488 and Rab5-561. The average fraction of clusters containing Ms-488 that also contain Rab5-561 markers is denoted by $\langle F(Ms|Rab5) \rangle$. Likewise, the average fraction of clusters containing Ms-488 that also contain Rab5 markers is denoted by $\langle F(Rab5|Ms) \rangle$.

Table 5.27 Average Number of Clusters and Fractions of Co-Localization of Ms-488 & Rab5-561 Marked Endocytic Compartments in SH-SY5Y Cells

Species	$\langle N_{Species} \rangle$	$\langle F(Ms\|Rab5) \rangle$	$\langle F(Rab5\|Ms) \rangle$
Ms-488	0.66 ± 0.15[1]		
Rab5-561	4.82 ± 0.76		
Ms-488 & Rab5-561	0.32 ± 0.11	0.58 ± 0.09	0.08 ± 0.02

1 Standard error.

The calculations for the average number of clusters in Table 5.27 reflect that there are approximately 0.66 clusters containing Ms-488 and there are also approximately 4.82 clusters containing Rab5 markers. Lastly, there are approximately 0.32 clusters containing both Ms-488 and Rab5 markers.

The calculations for the average fractions of co-localization represented in Table 5.27 reflect approximately 58% of clusters containing Ms-488 also contain Rab5 markers and approximately 8% of the clusters containing Rab5 markers also contain Ms-488.

Figure 5.30 shows the original confocal fluorescence microscopy images of one cell of Ms-488 and Rab7 marked compartments in one cell. The Merge image is the overlay of the Ms-488 and Rab7 images.

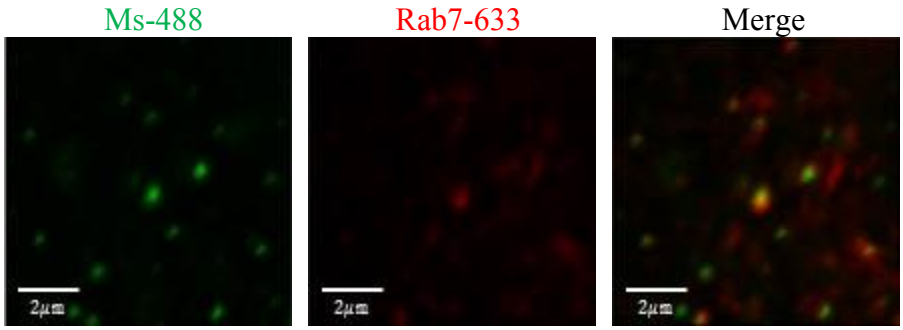

Figure 5.30 Images of Ms-488 and Rab7-633 Endocytic Marked Compartments in SH-SY5Y Cells

There are some faint yellow regions in the Merge image in Figure 5.30 to reflect some degree of co-localization of Ms-488 and Rab7 marked compartments.

Table 5.28 reflects the average number of clusters denoted by $\langle N_{Species} \rangle$ and the average fractions of co-localization of Ms-488 and Rab7-633. The average fraction of clusters containing Ms-488 that also contain Rab7-633 markers is denoted by $\langle F(Ms|Rab7) \rangle$. Likewise, the average fraction of clusters containing Rab7-633 markers that also contain Ms-488 is denoted by $\langle F(Rab7|Ms) \rangle$.

Table 5.28 Average Number of Clusters and Fractions of Co-Localization of Ms-488 & Rab7-633 Marked Endocytic Compartments in SH-SY5Y Cells

Species	$\langle N_{Species} \rangle$	$\langle F(Ms\|Rab7) \rangle$	$\langle F(Rab7\|Ms) \rangle$
Ms-488	0.56 ± 0.12[1]		
Rab7-633	3.19 ± 0.58		
Ms-488 & Rab7-633	0.35 ± 0.07	0.64 ± 0.11	0.16 ± 0.05

1 Standard error.

The calculations for the average number of clusters in Table 5.28 reflect that there are approximately 0.56 clusters containing Ms-488 and there are also approximately 3.19 clusters containing Rab7 markers and there are approximately 0.35 clusters containing both Ms-488 and Rab7 markers.

The calculations for the average fractions of co-localization represented in Table 5.28 reflect approximately 64% of clusters containing Ms-488 also contain Rab7-633 markers and approximately 16% of the clusters containing Rab7-633 markers also contain Ms-488.

Figure 5.30 is a visual representation of original confocal fluorescence microscopy images of one cell of Ms-488 and LAMP-1-561 marked compartments in one cell. The Merge image is an overlay of the monomers and LAMP-1-561 images.

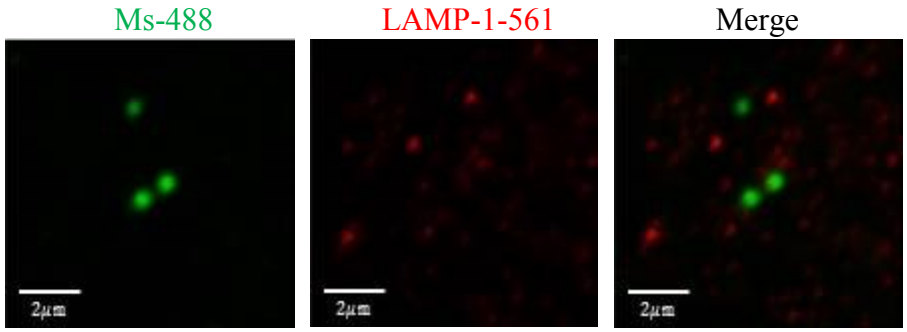

Figure 5.31 Images of Ms-488 and LAMP-1-561 Endocytic Marked Compartments in SH-SY5Y Cells

The Merge image in Figure 5.31 shows no yellow regions, thus there is likely no degree of co-localization of Ms-488 and LAMP-1-561 marked compartments.

Table 5.29 reflects the average number of clusters denoted by $\langle N_{Species} \rangle$ and the average fractions of co-localization of Ms-488 and LAMP-1-561. The average fraction of clusters containing Ms-488 that also contain LAMP-1-561 markers is denoted by $\langle F(Ms|LAMP-1) \rangle$. Likewise, the average fraction of clusters containing LAMP-1-561 markers that also contain Ms-488 is denoted by $\langle F(LAMP-1|Ms) \rangle$.

Table 5.29 Average Number of Clusters and Fractions of Co-Localization of Ms-488 & LAMP-1-561 Marked Endocytic Compartments in SH-SY5Y Cells

Species	$\langle N_{Species} \rangle$	$\langle F(Ms\|LAMP-1) \rangle$	$\langle F(LAMP-1\|Ms) \rangle$
Ms-488	0.51 ± 0.15[1]		
LAMP-1-561	1.87 ± 0.41		
Ms-488 & LAMP-1-561	0.13 ± 0.03	0.35 ± 0.07	0.10 ± 0.02

1 Standard error.

The calculations for the average number of clusters in Table 5.29 reflect that there are approximately 0.51 clusters containing Ms-488 and there are also approximately 1.87 clusters containing LAMP-1-561 markers. There are approximately 0.13 clusters containing both Ms-488 and LAMP-1-561 markers with standard error ± 0.03.

The calculations for the average fractions of co-localization represented in Table 5.29 reflect approximately 35% of clusters containing Ms-488 also contain LAMP-1-561 markers and there are approximately 10% of the clusters containing LAMP-1-561 markers also contain Ms-488.

5.5.2 Co-localization Endocytic Compartments containing Dimers in SH-SY5Y Cells

The extent to which dimers (Ds) associate with Rab5, Rab7, and LAMP-1 marked compartments was studied.

Figure 5.32 shows original confocal fluorescence microscopy images of one cell of Ds-633 and Rab5-561 marked compartments in one cell. The Merge image is an overlay of the dimers and Rab5 images.

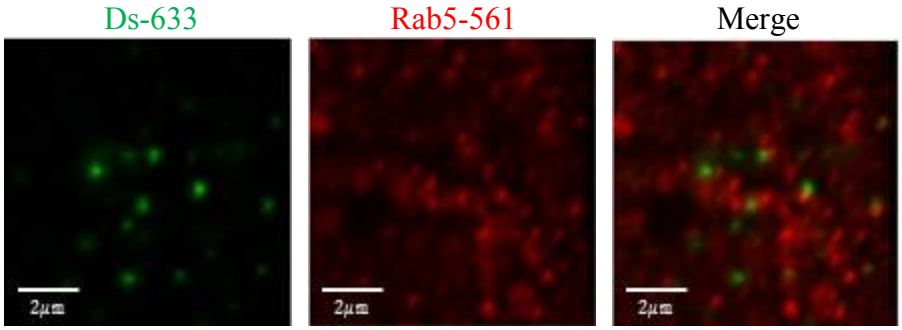

Figure 5.32 Images of Ds-633 & Rab5 Endocytic Marked Compartments in SH-SY5Y Cells

From a visual perspective, the Merge image in Figure 5.32 reflects no degree of co-localization of Ds-633 and Rab5-561 marked compartments, judging by the merge image.

Table 5.30 reflects the average number of clusters denoted by $\langle N_{Species} \rangle$ and the average fractions of co-localization of Ds-633 and Rab5-561. The average fraction of clusters containing Ds-633 that also contain Rab5-561 markers is denoted by $\langle F(Ds|Rab5) \rangle$. Likewise, the average fraction of clusters containing Rab5-561 markers that also contain Ds-633 is denoted by $\langle F(Rab5|Ds) \rangle$.

Table 5.30 Average Number of Clusters and Fractions of Co-Localization of Ds-633 & Rab5-561 Marked Endocytic Compartments in SH-SY5Y Cells

Species	$\langle N_{Species} \rangle$	$\langle F(Ds\|Rab5) \rangle$	$\langle F(Rab5\|Ds) \rangle$
Ds-633	1.23 ± 0.33[1]		
Rab5-561	5.58 ± 0.50		
Ds-633 & Rab5-561	0.35 ± 0.07	0.41 ± 0.07	0.06 ± 0.01

1 Standard error.

The calculations for the average number of clusters in Table 5.30 reflect that there are approximately 1.23 clusters containing Ds-633 and there are also approximately 5.58 clusters containing Rab5-561. Lastly, there are approximately 0.35 clusters containing both Ds-633 and Rab5-561 markers.

The calculations for the average fractions of co-localization represented in Table 5.30 reflect approximately 41% of clusters containing Ds-633 also contain Rab5-561 markers and approximately 6% of the clusters containing Rab5-561 markers also contain Ds-633.

Figure 5.33 shows original confocal fluorescence microscopy images of one cell of Ds-633 and Rab7-488 marked compartments in one cell. The Merge image is an overlay of the Ds-633 and Rab7-488 images.

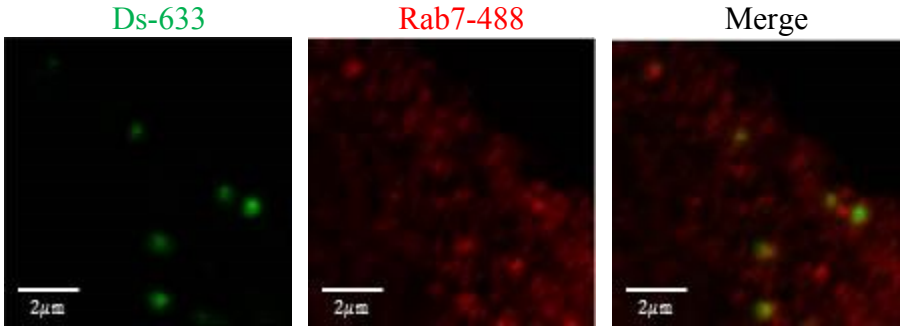

Figure 5.33 Images of Ds-633 & Rab7-488 Endocytic Marked Compartments in SH-SY5Y Cells

From a visual perspective, the Merge image in Figure 5.33 reflects some degree of co-localization of Ds-633 and Rab7-488 marked compartments, judging by the merge image.

Table 5.31 reflects the average number of clusters denoted by $\langle N_{Species} \rangle$ and the average fractions of co-localization of Ds-633 and Rab7-488. The average fraction of clusters containing Ds-633 that also contain Rab7-488 markers is denoted by $\langle F(Ds|Rab7) \rangle$. Likewise, the average fraction of clusters containing Rab7-488 markers that also contain Ds-633 is denoted by $\langle F(Rab7|Ds) \rangle$.

Table 5.31 Average Number of Clusters and Fractions of Co-Localization of Ds-633 & Rab7-488 Marked Endocytic Compartments in SH-SY5Y Cells

Species	$\langle N_{Species} \rangle$	$\langle F(Ds\|Rab7) \rangle$	$\langle F(Rab7\|Ds) \rangle$
Ds-633	3.94 ± 1.09[1]		
Rab7-488	3.09 ± 0.44		
Ds-633 & Rab7-488	1.48 ± 0.28	0.49 ± 0.06	0.47 ± 0.08

1 Standard error.

The calculations for the average number of clusters in Table 5.31 reflect that there are approximately 4.31 clusters containing Ds-633 and there are approximately 3.06 clusters containing Rab7-488 markers with standard error ± 0.39 the average value. Lastly, there are approximately 1.84 clusters containing both Ds-633 and Rab7-488 markers.

The calculations for the average fractions of co-localization represented in Table 5.31 reflect approximately 62% of clusters containing Ds-633 also contain Rab7-488 markers with and approximately 62% of the clusters containing Rab7-488 markers also contain Ds-633.

Figure 5.34 shows the original confocal fluorescence microscopy images of one cell of Ds-633 and LAMP-1-561 marked compartments in one cell. The Merge image is an overlay of the Ds-633 and LAMP-1-561 images.

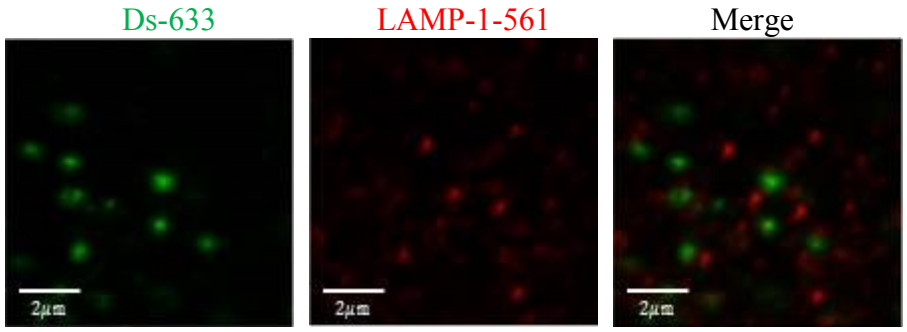

Figure 5.34 Images of Ds-633& LAMP-1-561 Endocytic Marked Compartments in SH-SY5Y Cells

From a visual perspective, the Merge image in Figure 5.34 reflects no degree of co-localization of Ds-633 and LAMP-1-561 marked compartments, judging by the merge image.

Table 5.32 reflects the average number of clusters denoted by $\langle N_{Species} \rangle$ and the average fractions of co-localization of DS-633 and LAMP-1-561. The average fraction of clusters containing Ds-633 that also contain LAMP-1-561 markers is denoted by $\langle F(Ds|LAMP-1) \rangle$. Likewise, the average fraction of clusters containing LAMP-1-561 markers that also contain Ds-633 is denoted by $\langle F(LAMP-1|Ds) \rangle$.

Table 5.32 Average Number of Clusters and Fractions of Co-Localization of DS-633 & LAMP-1-561 Marked Endocytic Compartments in SH-SY5Y Cells

Species	$\langle N_{Species} \rangle$	$\langle F(Ds\|LAMP-1) \rangle$	$\langle F(LAMP-1\|Ds) \rangle$
Ds-633	0.32 ± 0.06[1]		
LAMP-1-561	1.48 ± 0.18		
Ds-633 & LAMP-1-561	0.12 ± 0.03	0.42 ± 0.08	0.07 ± 0.01

1 Standard error.

The calculations for the average number of clusters in Table 5.32 reflect that there are approximately 0.32 clusters containing Ds-633 and there are also approximately 1.48 clusters containing LAMP-1-561 markers. Lastly, there are approximately 0.12 clusters containing both Ds-633 and LAMP-1-561 markers.

The calculations for the average fractions of co-localization represented in Table 5.32 reflect approximately 42% of clusters containing Ds-633 also contain LAMP-1-561 markers and approximately 7% of the clusters containing LAMP-1-561 markers also contain Ds-633.

5.5.3 Co-localization Endocytic Compartments containing Tetramers in SH-SY5Y Cells

The extent to which tetramers (Ts) associate with Rab5, Rab7, and LAMP-1 marked compartments was studied.

Figure 5.35 is a visual representation of original confocal fluorescence microscopy images of one cell of Ts-633 and Rab5-561 marked compartments in one cell. The Merge image is an overlay of the Ts-633 and Rab5-561 images.

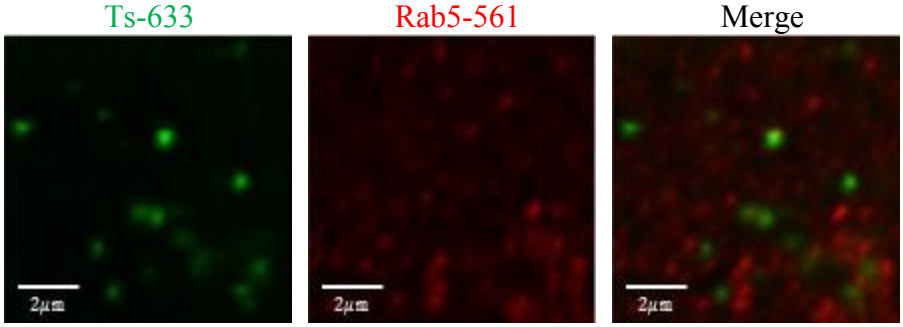

Figure 5.35 Images of Ts-633 & Rab5-561 Endocytic Marked Compartments in SH-SY5Y Cells

From a visual perspective, the Merge image in Figure 5.35 reflects no degree of co-localization of Ts-633 and Rab5-561 marked compartments, judging by the merge image.

Table 5.33 reflects the average number of clusters denoted by $\langle N_{Species} \rangle$ and the average fractions of co-localization of Ts-633 and Rab5-561. The average fraction of clusters containing Ts-633 that also contain Rab5-561 markers is denoted by $\langle F(Ts|Rab5) \rangle$. Likewise, the average fraction of clusters containing Rab5-561 markers that also contain Ts-633 is denoted by $\langle F(Rab5|Ts) \rangle$.

Table 5.33 Average Number of Clusters and Fractions of Co-Localization of Ts-633 & Rab5-561 Marked Endocytic Compartments in SH-SY5Y Cells

Species	$\langle N_{Species} \rangle$	$\langle F(Ts\|Rab5) \rangle$	$\langle F(Rab5\|Ts) \rangle$
Ts-633	0.73 ± 0.09[1]		
Rab5-561	4.67 ± 0.58		
Ts-633 & Rab5-561	0.31 ± 0.05	0.45 ± 0.07	0.07 ± 0.01

1 Standard error.

The calculations for the average number of clusters in Table 5.33 reflect that there are approximately 0.73 clusters containing tetramers and there are also approximately 4.67 clusters containing Rab5-561 markers. Lastly, there are approximately 0.31 clusters containing both Ts-633 and Rab5-561 markers.

The calculations for the average fractions of co-localization represented in Table 5.33 reflect approximately 45% of clusters containing Ts-633 also contain Rab5-561 markers and approximately 7% of the clusters containing Rab5-561 markers also contain Ts-633.

Figure 5.36 is a visual representation of original confocal fluorescence microscopy images of one cell of Ts-633 and Rab7-488 marked compartments in one cell. The Merge image is an overlay of the dimers and Rab7 images.

Ts-633 Rab7-488 Merge

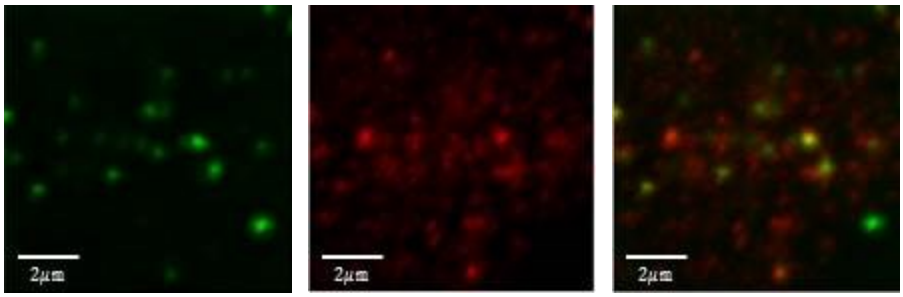

Figure 5.36 Images of Ts-633 & Rab7-488 Endocytic Marked Compartments in SH-SY5Y Cells

From a visual perspective, the Merge image in Figure 5.36 reflects some degree of co-localization of Ts-633 and Rab7-488 marked compartments, judging by the merge image.

Table 5.34 reflects the average number of clusters denoted by $\langle N_{Species} \rangle$ and the average fractions of co-localization of Ts-633 and Rab7-488. The average fraction of clusters containing Ts-633 that also contain Rab7-488 markers is denoted by $\langle F(Ts|Rab7) \rangle$. Likewise, the average fraction of clusters containing Ts-633 that also contain Rab7 markers is denoted by $\langle F(Rab7|Ts) \rangle$.

Table 5.34 Average Number of Clusters and Fractions of Co-Localization of Ts-633 & Rab7-488 Marked Endocytic Compartments in SH-SY5Y Cells

Species	$\langle N_{Species} \rangle$	$\langle F(Ts\|Rab7) \rangle$	$\langle F(Rab7\|Ts) \rangle$
Ts-633	2.33 ± 0.72[1]		
Rab7-488	2.81 ± 0.22		
Ts-633 & Rab7-488	1.14 ± 0.14	0.74 ± 0.07	0.43 ± 0.05

1 Standard error.

The calculations for the average number of clusters in Table 5.34 reflect that there are approximately2.33 clusters containing Ts-633 and there are also approximately 2.81 clusters containing Rab7-488 markers. Lastly, there are approximately 1.14 clusters containing both Ts-633 and Rab7-488 markers.

The calculations for the average fractions of co-localization represented in Table 5.34 reflect approximately 74% of clusters containing Ts-633 also contain Rab7-488 markers and approximately 43% of the clusters containing Rab7-488 markers also contain Ts-633.

Figure 5.37 is a visual representation of original confocal fluorescence microscopy images of one cell of Ts-633 and LAMP-1-561 marked compartments in one cell. The Merge image is an overlay of the Ts-633 and LAMP-1-561 images.

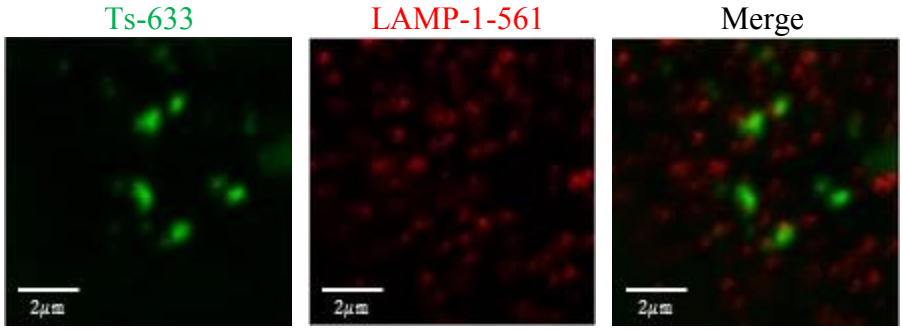

Figure 5.37 Images of Ts-633 & LAMP-1-561 Endocytic Marked Compartments in SH-SY5Y Cells

The Merge image in Figure 5.37 reflects no degree of co-localization of Ts-633 and LAMP-1-561 marked compartments.

Table 5.35 reflects the average number of clusters denoted by $\langle N_{Species} \rangle$ and the average fractions of co-localization of Ts-633 and LAMP-1-561. The average fraction of clusters containing Ts-633 that also contain LAMP-1-561 markers is denoted by $\langle F(Ts|LAMP-1) \rangle$. Likewise, the average fraction of clusters containing LAMP-1-561 markers that also contain Ts-633 is denoted by $\langle F(LAMP-1|Ts) \rangle$.

Table 5.35 Average Number of Clusters and Fractions of Co-Localization of Ts-633 & LAMP-1-561 Marked Endocytic Compartments in SH-SY5Y Cells

Species	$\langle N_{Species} \rangle$	$\langle F(Ts\|LAMP-1) \rangle$	$\langle F(LAMP-1\|Ts) \rangle$
Ts-633	0.73 ± 0.13[1]		
LAMP-1-561	1.66 ± 0.14		
Ts-633 & LAMP-1-561	0.24 ± 0.03	0.45 ± 0.07	0.17 ± 0.03

1 Standard error.

The calculations for the average number of clusters in Table 5.35 reflect that there are approximately 0.73 clusters containing Ts-633 and there are approximately 1.66 clusters containing LAMP-1-561 markers. Lastly, there are approximately 0.24 clusters containing both Ts-633 and LAMP-1-561 markers.

The calculations for the average fractions of co-localization represented in Table 5.35 reflect approximately 45% of clusters containing Ts-633 also contain LAMP-1-561 markers with and approximately 17% of the clusters containing LAMP-1-561 markers also contain Ts-633.

5.6 Chapter Conclusions

The work presented in this chapter was performed as a means to further inquire about the various oligomeric forms of α −Syn to determine if any similarities or differences exist with oligomers. Based on these findings, this information will be useful for creating better detection methods and lead to the development of more therapeutic applications due to the varying nature of each oligomer studied.

There were seven findings made from this work; 1) these oligomers are able to passively internalized in cells, 2) the passive entry of enforced pre-aggregated oligomers does not affect the amount of internalized oligomers, 3) there are differences observed in regard to the amount of time cells are able to withhold oligomers internally after fixed exposure, variable uptake, 4) there is almost 100% interaction observed between two oligomers, 5) oligomers are located in the same compartment and the distributions of each endocytic marker in cells are similar, 6) the pairwise interaction of markers is somewhat unexpected and different from the fusion/maturation model, and 7) the extent to which oligomers associate with markers in one compartment are similar between oligomers.

The use of PFA was used to fix cells and observe if potential binding of oligomers to the membrane would occur; however, to our surprise, the oligomers were able to internalize into cells despite this fixation. PFA was used for fixation because it cross links cytosolic proteins and molecules in the cell.[94] Thus, the cytosolic proteins required to assist with active transport and uptake of materials via endocytosis are effected and unable to perform their specific functions for endocytosis to occur. From simple observation of monomers, dimers, and tetramers within the

cytoplasm after cells were fixed prior to exposure of oligomers, it was concluded that these oligomers were able to passively enter cells, meaning they enter cells without active transport.

Upon passive entry, there was a relative *increase* in intensity with time of exposure in monomers and dimers. Therefore, these oligomers are indeed able to passively diffuse into cells but actually accumulate in the same relative number of clusters with time, on average about 20 clusters per square micron. In contrast, tetramers actually reflect a *decrease* in intensity after exposure to fixed cells and there is some fluctuation with the intensity within 24 hours. Thus, these findings imply that these oligomers can enter cells without the influence of intracellular proteins to enable active transport; in addition, the monomers and dimers passively enter cells to a larger extent than do tetramers.

It was also determined that there was no clear differences in terms of time dependent trends observed for monomers nor tetramers by enforcing aggregation from simple agitation and heating of oligomers prior to exposing said oligomers to pre-fixed cells, as opposed to exposing these oligomers to cells without this agitation and heating.

In addition to passive entry into cells, the internalization of oligomers by an assumed active transport pathway was studied; one can observe the major differences between images such that passive diffusion of these oligomers distribute to quite an extent unlike oligomers taken up actively, which appear in bright circular regions, or endosomes. In this work, the key oligomer of interest exhibiting differences in uptake was the monomer; after 24 hours progressed for uptake, although the number of clusters remains somewhat constant, if not slightly more, the intensity of the species decreases after 24 hours reflecting a decrease in the degree of aggregation of monomers in clusters. The dimers behave in a similar fashion, but not to the same extent as monomers. The uptake of tetramers revealed no trend; the relative number of clusters and degree of aggregation remains constant with time. Therefore, this data suggests that monomers are perhaps either cleared from cells or may begin to be degraded in some fashion when cells contain monomers for times longer than 24 hours.

After studying the internalization of each oligomer, it was desired to study the extent to which two oligomers simultaneously exist in the same cluster. Despite differences observed in uptake, each experiment conducted showed that each cluster for which one oligomer was present

also contained one other oligomer. Specifically, approximately 100% co-existence between monomers and dimers, monomers and tetramers, and dimers and tetramers was observed. These reported fractions are greatest in magnitude compared to the previous fractions reported in Chapters 3 and 4. Based on the significant amount of yellow regions in the Merge images, these fractions reflect specific co-localization.

As with previous chapters, the distribution of endocytic markers was also studied; contrary to previous findings in this work, the distribution of Rab5, Rab7, and LAMP-1 markers are distributed equally in images, however Rab7 markers are somewhat larger in comparison to the similar size of Rab5 and LAMP-1 marked compartments.

In addition to the individual distribution of these markers for endocytic compartments, the pairwise interaction of markers was also studied. As a result, these fractions of co-localization reflect findings that two markers are able to simultaneously exist on one cluster but are not unique for one endocytic compartment. In addition, these co-localizations are somewhat unexpected; specifically, there is a relatively high co-existence of Rab5 and LAMP-1 markers in comparison to Rab7 and LAMP-1 markers. The associations of two markers in SH-SY5Y cells are very similar in comparison to the associations observed for A549 cells in Chapter 3.

Lastly, the association of each oligomer with one endocytic marker was studied. Similarities were observed between each oligomer. Between 40-60% of each cluster containing one type of oligomer also contained Rab5 markers, approximately 60-70% of each cluster containing one type of marker also contained Rab7 markers, and approximately 30-40% of each cluster containing one oligomer also contained LAMP-1 markers. Lastly, the association of Rab5 and LAMP1 markers with one type of oligomer ranged between 10-17% however the association of Rab7 markers with one oligomer was a greater, ranging between 16-62%.

This chapter provided a wealth of information; each oligomer studied was effectively internalized by cells, by endocytosis and passive transport. In addition, although each oligomer associates with endocytic compartments in the same fashion, the relative amount of *time* of uptake and internalization varies, in large part with the monomer.

Chapter 6

The Intracellular Dynamics of Oligomers of α −synuclein in Live SH-SY5Y Cells

6 The Intracellular Dynamics of Oligomers of α −synuclein in Live SH-SY5Y Cells

In Chapter 5, we determined that oligomers of α −synuclein were able to undergo both passive and active transport for internalization into SH-SY5Y cells. In addition, differences in uptake were observed, such that monomers and dimers can passively diffuse to greater extents than tetramers into cells. However, monomers are less frequently observed in cells after 24 hours of uptake via endocytosis. Despite differences with internalization over time, each oligomer associated similarly with an endocytic marker and we observed the pairwise association of two oligomers to be almost 100% in cells.

The motivation for the work presented in this chapter was to observe oligomers in SH-SY5Y cells in real time to inquire about α −synuclein dynamics. Data corresponding to monomers, dimers, and tetramers will be discussed.

The dynamics of oligomers of α −synuclin were studied via laser scanning confocal microscopy and temporal image correlation spectroscopy analysis of images of live SH-SY5Y cells. In contrast to previous work in this thesis, 80-100 images were obtained, but of the *same cell* to study the diffusion of oligomers in one cell.

Materials and methods corresponding to labelling of oligomers of α −synuclein in cells can be found in 2.9.1. Laser scanning confocal microscopy imaging of one oligomer can be found in Chapter 2.10.4.1. Temporal Image Correlation Spectroscopy can be found in Chapter 2.11.4.

6.1 Monomers

Chapter 6.1 focusses on the dynamics of monomers of α −synuclein in SH-SY5Y cells.

Figure 6.1 shows nine images, each image corresponding to the same cell, taken over a series of 244.51 seconds (the microscope has the ability to acquire images in milliseconds). Cells in the sample were exposed to monomers for two hours and imaged immediately after washing. Image A is the first image of one cell exposed to monomers in the series, collected at $\tau = 0$ seconds. Images B, C, D, E, F, G, H, and I each correspond to an image of the cell at times $\tau =$

4.99, $\tau = 19.96, \tau = 34.93$ $\tau = 44.91, \tau = 94.81$, $\tau = 144.71$, $\tau = 194.61$, and $\tau = 244.51$ seconds, respectively. Each image presented in Figure 6.1 has not been contrast enhanced.

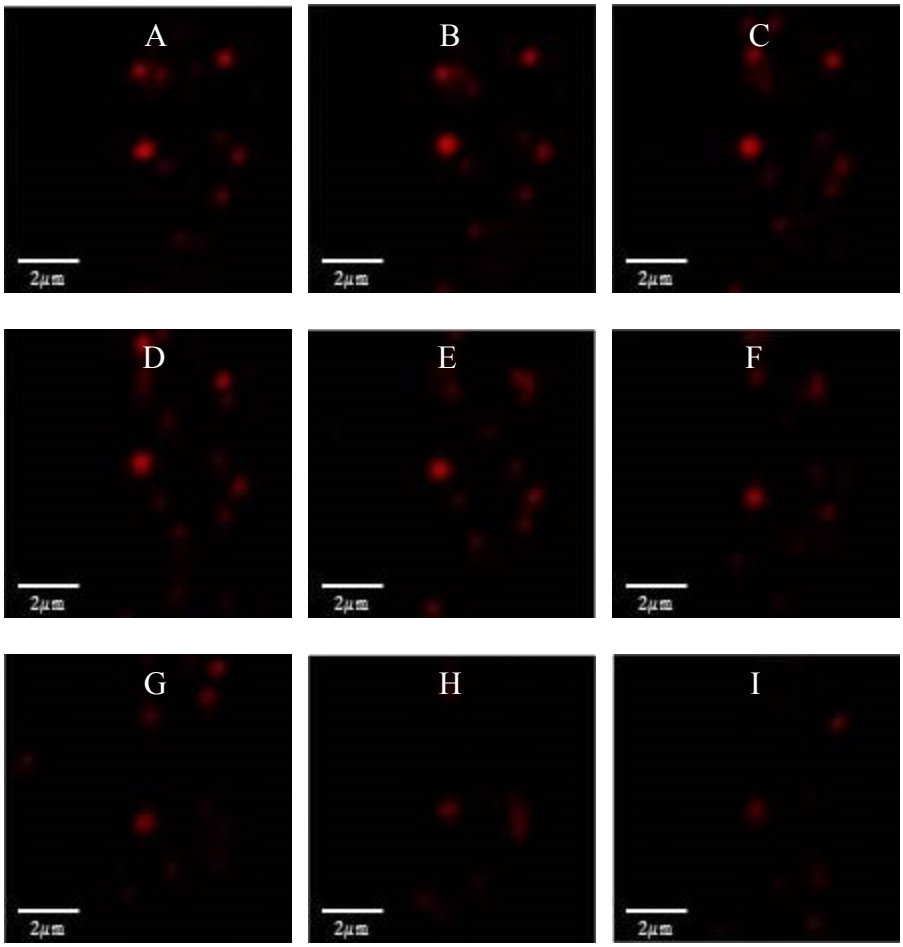

Figure 6.1 Monomers in Real Time

Images A, B, C, D, E, F, G, H, and I each correspond to an image of the cell with monomers at times $\tau = 0, \tau = 4.99, \tau = 19.96, \tau = 34.93$ $\tau = 44.91, \tau = 94.81, \tau = 144.71, \tau = 194.61$, and $\tau = 244.51$ seconds.

Similar to the images presented in Chapter 4 for monomers internalized in cells by a fixed exposure, variable uptake experiment, each red region represents a cluster or aggregation of monomers. The images shown in Figure 6.1 show Images A, B, and C are similar. However with the progression of time, specifically for images G, H, and I, the red regions are not quite as bright as a result of photobleaching. Photobleaching is a phenomena defined as the photochemical modification of a dye that results in an irreversible loss of the species' ability to fluoresce[95].

Photobleaching is very common with fluorescent imaging in which the fluorescence of a species fades as it is under observation.

To extract quantitative information in regard to photobleaching from the images, Figure 6.2 is a scatter plot of the intensity corresponding to each image in the series of 50 images collected as a function of the image in the series.

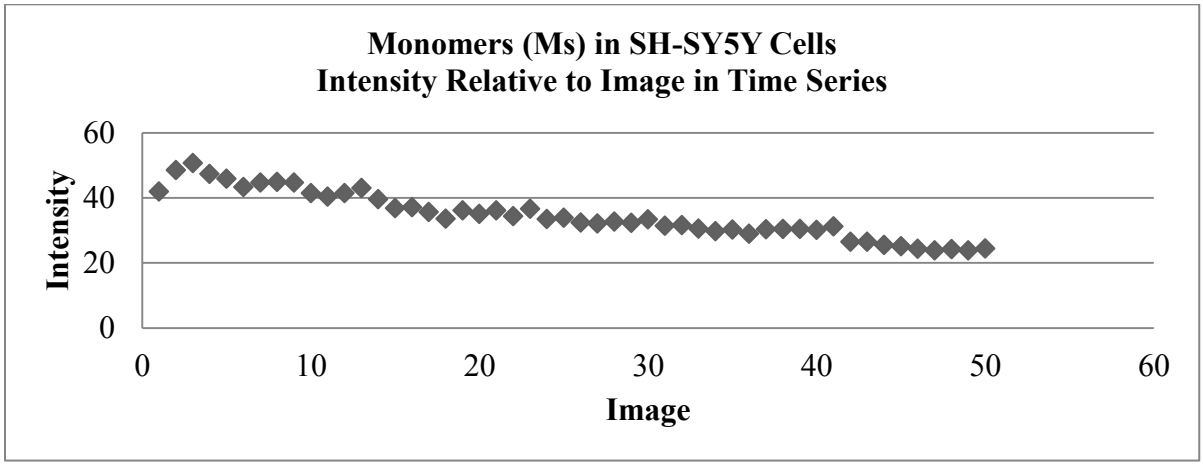

Figure 6.2 Scatter Plot of Intensity of Monomers in SH-SY5Y cells as a Function of Image in Time Series

In relation to Figure 6.1, the intensity is somewhat consistent for the first 20 images obtained in the series. However, the intensity begins to decrease two fold within the last ten images in the series, which is consistent with the relative faint brightness of images G, H, and I. Since the *same region* is now being constantly illuminated by the laser beam, photo bleaching is occurring. Constant intensity is expected for a system that has not been photobleached.

Figure 6.3 is a scatter plot of the auto correlation amplitude plotted with respect to the image in the time series.

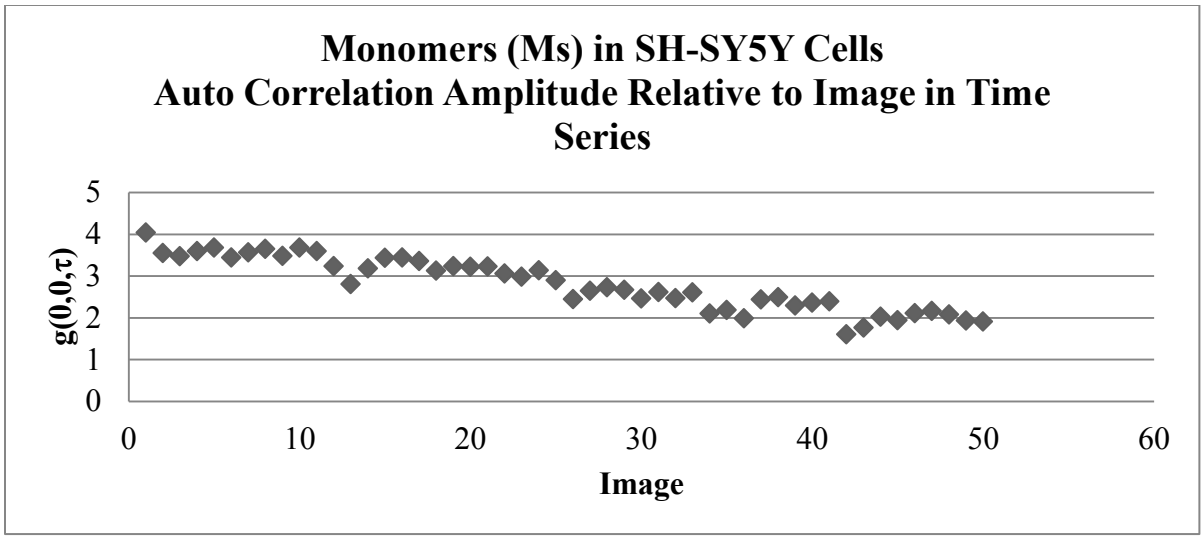

Figure 6.3 Scatter Plot of Auto Correlation Amplitude of Monomers in SH-SY5Y cells as a Function of Image in Time Series

As with intensity, the auto correlation amplitude decreases with time. As the number of clusters in the observation area is inversely proportional to the auto correlation amplitude, a greater number of clusters could be observed as the monomers diffuse in the region defined by the laser beam as time progresses. However, the decrease in auto correlation amplitude is more likely explained by the photobleaching as the background noise becomes more prominent.

To better visualize the diffusion of monomers with time, Figure 6.4 shows the same images as presented in Figure 6.1 that have been *overlaid* with the image at $\tau = 0$ seconds. ImageJ software was used to merge the image obtained at $\tau = 0$ seconds in red with an image collected at a later time in green. Thus, Image A in Figure 6.4 is yellow as it is the merge of the same image.

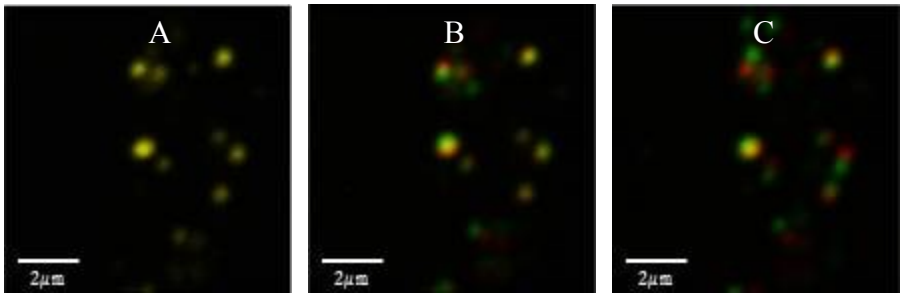

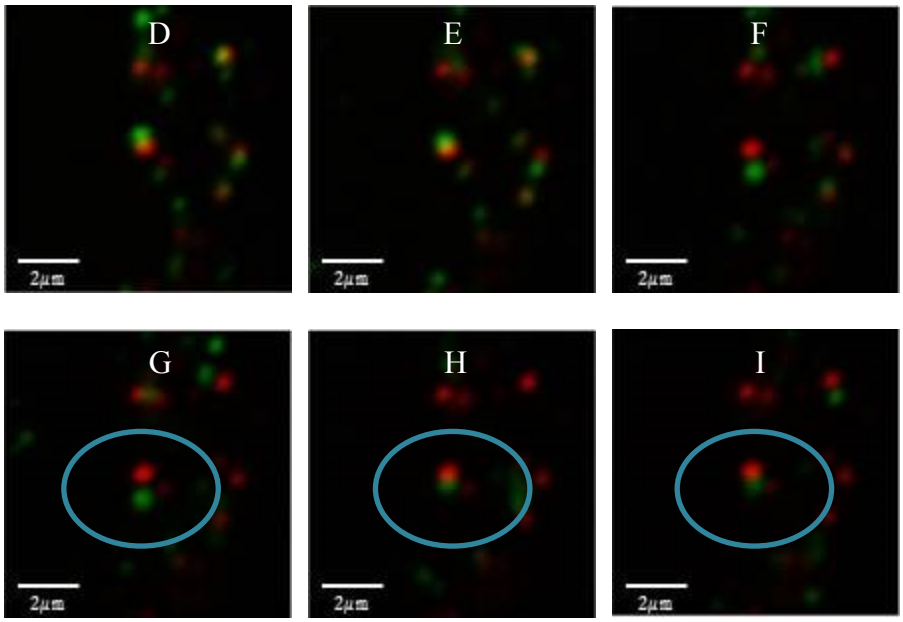

Figure 6.4 Images of Monomers in Real Time Merged with Image at $\tau = 0$

Images A, B, C, D, E, F, G, H, and I each correspond to a merge of monomers at $\tau = 0$ in red with monomers at times $\tau = 0$, $\tau = 4.99, \tau = 19.96, \tau = 34.93$ $\tau = 44.91, \tau = 94.81$, $\tau = 144.71$, $\tau = 194.61$, and $\tau = 244.51$ seconds, respectively in green.

Overlaying two images in a time series is useful for visualizing the intracellular movement of these monomers in a cell. Thus, Image A reflects only yellow regions because it is the overlay of the *same image.* Image B shows several yellow regions, however there are faint green and red regions present in the image; the presence of red and green indicate the monomers are moving from their initial position at $\tau = 0$, however the remaining yellow regions indicate that the monomers in that specific position in the cell have not moved. Thus, the relative number of yellow regions observed in the image disappears with image F, after 94.81 seconds has progressed. An interesting feature with images H and I is that the monomers appear to be diffusing back into the center to their original position, as shown by the blue circles in Images G (for comparison), H, and I.

Table 6.1 corresponds to the temporal image correlation spectroscopy (TICS) data corresponding to the amplitude of the auto correlation function, $g(0,0,0)$, delay time between images, $\Delta\tau$, and the fit obtained for the laser beam width, ω.

Table 6.1 Raw Data Corresponding to first Image of Monomers in Real Time Series

$\boldsymbol{g(0,0,0)}$	4.04
$\boldsymbol{\Delta\tau}$	4.99 sec
$\boldsymbol{\omega}$	0.43 μm

The data presented in Table 6.1 indicate that the amplitude for the temporal auto correlation amplitude is 4.04. In addition, the value for $\Delta\tau$ indicates that each image in the series was obtained with an approximate 4.99 second lag between images. The fit for the laser beam was approximately 0.43. As shown in previous chapters, this measured beam radius arises from convolution.

Recall, for temporal image correlation spectroscopy analysis, the decay of the amplitude of the auto correlation function as a function of time, τ, is fit to a three parameter hyperbolic decay expression;

$$g(0,0,\tau) = \frac{A}{1+\frac{\tau}{\tau_d}} + C \tag{31}$$

Figure 6.5 is a scatter plot for the temporal auto correlation function for monomers (Data) compared to the three parameter hyperbolic decay fit (Fit).

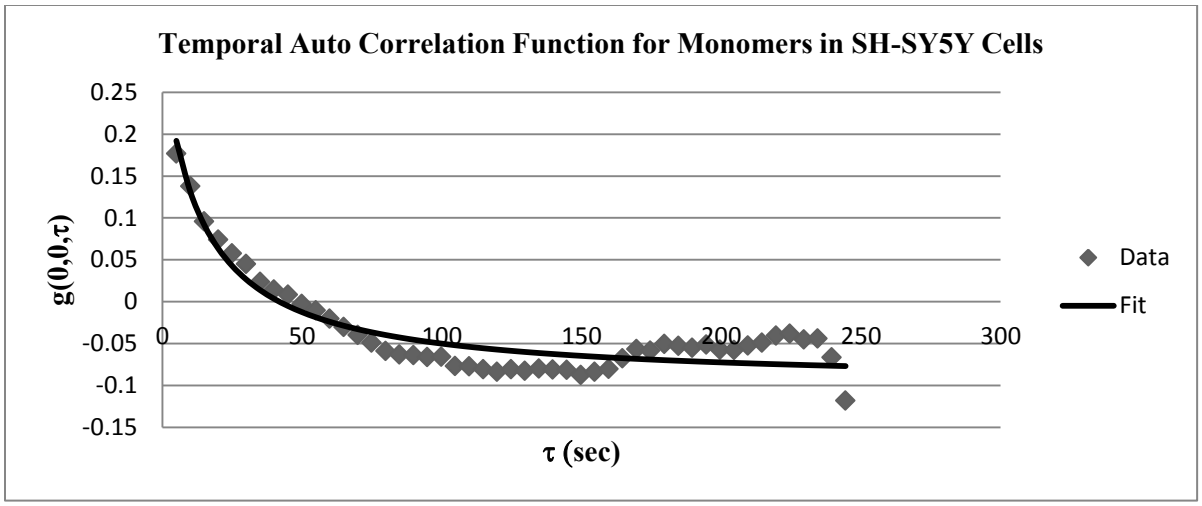

Figure 6.5 Temporal Auto Correlation Function for Monomers in Real Time in SH-SY5Y Cells

The three parameter hyperbolic fit is in agreement with the data. The curve corresponding to the data decays at a constant rate until about 150 seconds has progressed. At a τ value of 150 seconds, the value for the temporal auto correlation begins to increase; recall, the monomers appear to be diffusing back to their original position in the center of the image as shown with Image G in Figure 6.4. This phenomena could explain the increase in the temporal auto correlation. Likewise, the decrease in the temporal auto correlation at a tau value of 250 seconds decreases due to the bleaching of the image and also due to the fact that the monomers are no longer correlated as they have moved from their initial position.

Table 6.2 shows the fit parameters corresponding to the fitted function in Figure 6.5. The values are shown with standard deviation. Goodness of fit can be represented by a small value (less than 1) for chi square, χ^2.

Table 6.2 Fit parameters obtained for One Monomer Experiment of 50 Images in Real Time in SH-SY5Y Cells

A	0.40 ± 0.04[1]
τ_d	$13.8 \pm 3.5\ sec$
C	$(-0.100) \pm 0.007$

[1] Standard deviation. $\chi^2 = 0.02$.

The global fit produces a chi square value of 0.02. This value indicates the fit of the data consisting of 50 images is reasonable, and the measured parameters are specific to the monomers.

The diffusion coefficient can be calculated using the fitted diffusion time, τ_d and fit for the experimental laser beam width, ω;

$$D = \frac{4\tau_d}{\omega^2} \tag{32}$$

Thus, the diffusion coefficient can be calculated;

$$D = 3.35\, x\, 10^{-11}\, cm^2/sec \tag{33}$$

Since this was the first time live cell analysis was performed in this thesis, it was unclear for how many images should be collected from one cell to accurately sample and obtain precise estimates of parameters of species in live time. To address this question, eight different cells were imaged, 100 images pertaining to each cell. Imaging of one cell defined one experiment.

For each experiment, the data was analyzed in batches, such that a batch was defined by data consisting of 20, 40, 50, 60, 80, or 100 images. Temporal image correlation spectroscopy was completed for all data sets within each batch. Each data set in a batch was then fit with the three parameter hyperbolic decay function and parameters were obtained.

All batches consisting of the same number of images for all experiments were then compared by averaging the measured parameters and performing global fits. Table 6.3 is a representation of the average temporal auto correlation amplitude, average fitted auto correlation amplitude, average temporal auto correlation constant to account for incomplete decay of the correlation function, average diffusion time, and average diffusion coefficient calculated for the data sets from each experiment in a specific batch consisting of n_{images}. The average values are shown with standard error.

Table 6.3 Average Auto Correlation Amplitude, Fitted Auto Correlation Amplitude, Diffusion Time, and Average Diffusion Coefficient for Monomers in Batches

$\langle n_{images} \rangle$	$\langle g(0,0,0) \rangle$	$\langle A \rangle$	$\langle C \rangle$	$\langle \tau_d\ (sec \rangle$	$\langle D(\text{cm\^2/sec}) \rangle$
20	2.76 ± 0.83[1]	0.41 ± 0.05	(-0.11) ± 0.04	9.71 ± 1.44	4.81E-11 ± 1.30E-11
40	2.36 ± 0.71	0.52 ± 0.08	(-0.14) ± 0.01	18.3 ± 6.2	3.46E-11 ± 8.32E-12
50	**3.31 ± 0.94**	**0.51 ± 0.11**	**(-0.13) ± 0.03**	**16.7 ± 2.4**	**3.15E-11 ± 9.28E-12**
60	2.63 ± 0.70	0.78 ± 0.27	(-0.12) ± 0.03	12.4 ± 4.3	7.32E-11 ± 4.52E-11
80	1.99 ± 0.38	0.82 ± 0.29	(-0.11) ± 0.03	9.17 ± 1.67	3.34E-11 ± 1.18E-12
100	2.16 ± 0.14	1.19 ± 0.30	(-0.13) ± 0.10	10.8 ± 12.0	7.74E-11 ± 9.09E-11

[1] Standard error.

The average auto correlation amplitudes for data within each defined batch ranges between 1.99-3.31. The average auto correlation amplitude obtained from the fit, $\langle A \rangle$, is approximately 10% less, specifically with values ranging between 0.41-1.19. The parameter to account for incomplete decay of the correlation function ranges between -0.14-(-0.11). The incomplete decay of the auto correlation function has been accounted for in the fit. The average diffusion time for monomers in each defined batch ranges between approximately 9.71-18.3 seconds. Lastly, the diffusion coefficient on average is on the scale of 10^{-11} square centimeters per second.

Figure 6.6 is a bar graph of the average auto correlation amplitude for monomers in reference to Table 6.3. The average auto correlation amplitude is plotted as a function of the batch.

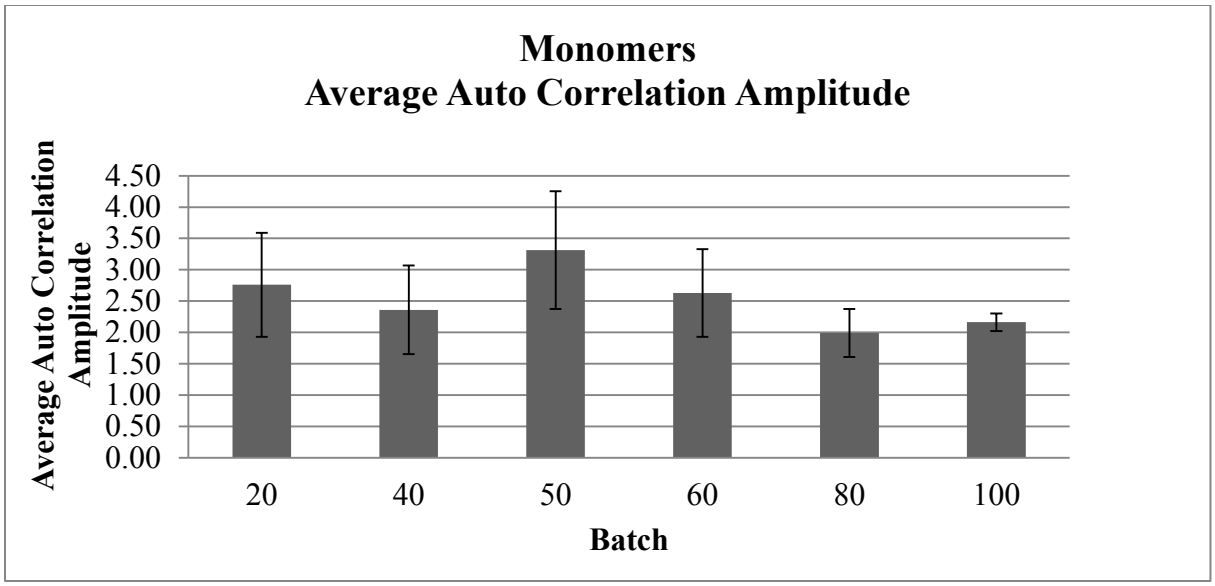

Figure 6.6 Bar Graph of Average Auto Correlation Amplitude as a Function of the Batch for Monomers

The auto correlation amplitude does not change or depend on the number of images in a data set.

Figure 6.7 is a bar graph of the *average fitted* auto correlation amplitude as a function of the batch.

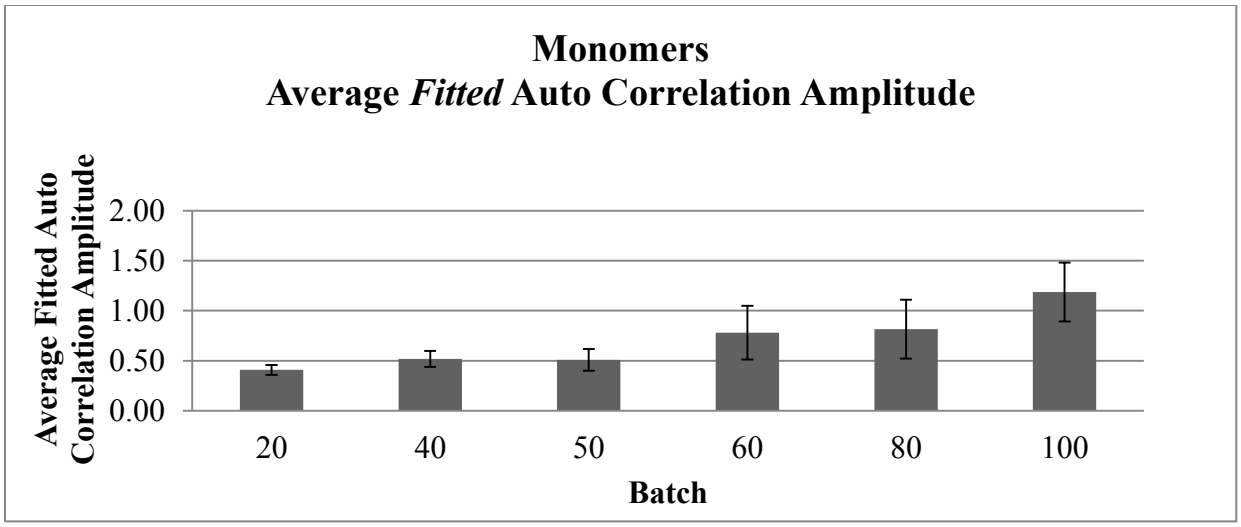

Figure 6.7 Bar Graph of the Average Fitted Auto Correlation Amplitude as a Function of Batch for Monomers

The fitted auto correlation amplitude is relatively consistent for analyses of batches defined by 20-50 images. The fitted auto correlation amplitude increases for batches defined by 60-100 images. Thus, there is a slight dependency on the number of images to calculate the fitted auto correlation amplitude, such that larger magnitudes for the fitted auto correlation amplitude will be observed for batches defined by 60 images or more.

Figure 6.8 is a bar graph of the average fitted auto correlation amplitude as a function of the batch.

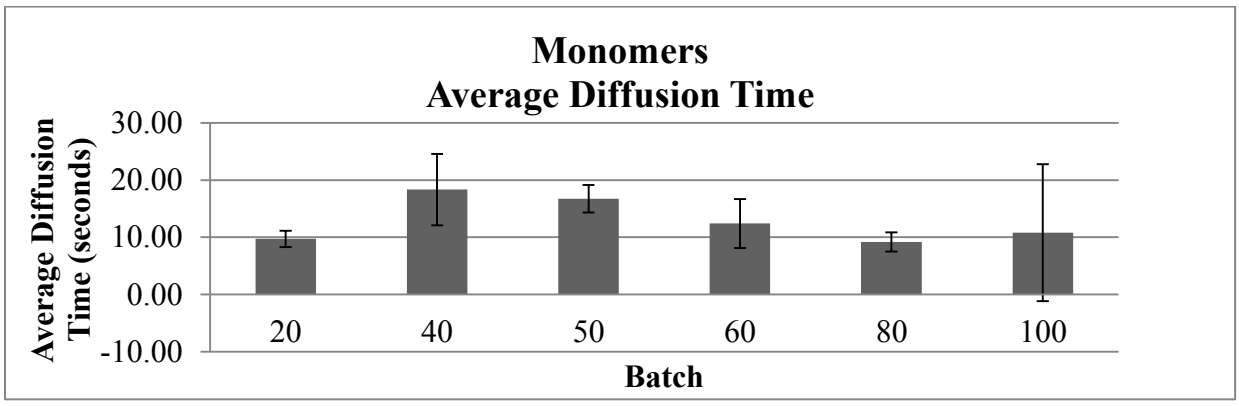

Figure 6.8 Bar Graph of Average Diffusion Time as a Function of Batch for Monomers

The diffusion time corresponding to monomers fluctuates however the standard error with respect to the batch defined by data containing 100 images is quite large in comparison to a batch defined by fewer images in a data set.

Figure 6.9 is a bar graph of the average diffusion coefficient as a function of the batch.

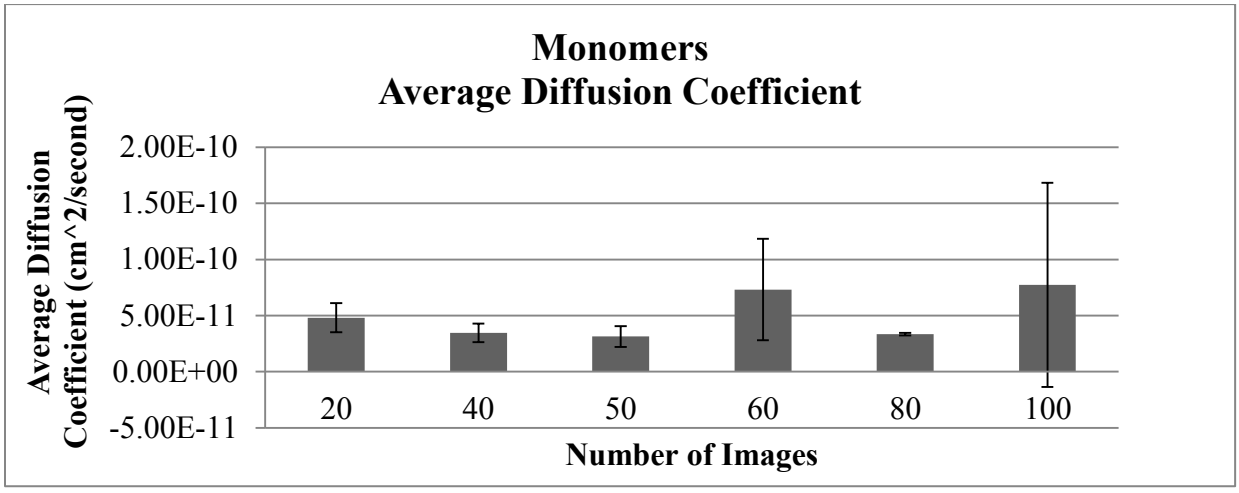

Figure 6.9 Bar Graph of the Average Diffusion Coefficient as a Function of Batch for Monomers

The average diffusion coefficient is relatively consistent depending on the analysis of batches defined by data containing 20-50 images. However, batches consisting of data with 60-100 images start to reflect a significant amount of error for the measured average diffusion coefficient.

This data confirms that the appropriate number of images to analyze the monomer in real time is 50 images. This is based on the standard error corresponding to the average fit of the auto correlation amplitude, average diffusion time, and average diffusion coefficient is low. In addition, the average values of parameters of data consisting of 50 images compares to that of batches defined by either 20 or 40 images.

An important point to understand is the temporal auto correlation function never fully decays to zero. For temporal image correlation spectroscopy, the auto correlation should decay to approximately 10% of the temporal auto correlation amplitude, $g(0,0,0)$. For this monomeric diffusion data, the correlation function in Figure 6.5 decays to approximately 5% after 244

seconds has progressed for 50 images obtained approximately every 5 seconds. However, the temporal correlation function decays to approximately 9% after only 150 seconds have elapsed for 30 images of the monomers. Thus, it can be argued 30 images is a useful number of images to analyze monomers. However, 50 images has been chosen for analysis because the standard error for parameters measured from 50 images is about the same as the averages of parameters measured for batches consisting of 20 and 40 images. Also, a greater number of images in an experiment is important for ICS analysis.

A global fit was then obtained for the data consisting of 50 images to determine the goodness of the fit and determine if each data set within this batch for all experiments followed the same distribution. Table 6.4 shows the fit parameters obtained for the global fit.

Table 6.4 Global Fit of Data Sets within Batches Defined by 50 Images of Monomers

A	0.51 ± 0.03
τ_d	15.5 ± 2.4 sec
C	(-0.13) ± 0.01

[1]Standard error. $\chi^2 = 0.48$.

The global fit indicates that the temporal auto correlation amplitude is approximately 0.51. The diffusion time for monomers is approximately 15.5 seconds and the constant to allow for incomplete decay of the auto correlation amplitude was (-0.13). The chi square value is approximately 0.48. As this value is small, and more specifically less than 1.0, the fit is reasonably good. In addition, the parameters strongly compare with the average of the fit parameters of the experiments consisting of 50 images (bolded in Table 6.3).

6.2 Dimers

Chapter 6.2 focusses on the dynamics of dimers of α −synuclein in SH-SY5Y cells.

Figure 6.10 shows nine images, each image corresponding to the same cell, taken over a series of 245.49 seconds. Cells in the sample were exposed to dimers for two hours and imaged immediately after washing. Image A is the first image of one cell exposed to dimers in the series, collected at $\tau = 0\ seconds$. Images B, C, D, E, F, G, H, and I each correspond to an image of the cell at $\tau = 5.01, \tau = 20.04, \tau = 35.07\ \tau = 45.09, \tau = 95.19, \tau = 145.29, \tau = 195.39$, and

$\tau = 245.49$ seconds, respectively. Each image presented in Figure 6.10 has been contrast enhanced for better visualization of dimers.

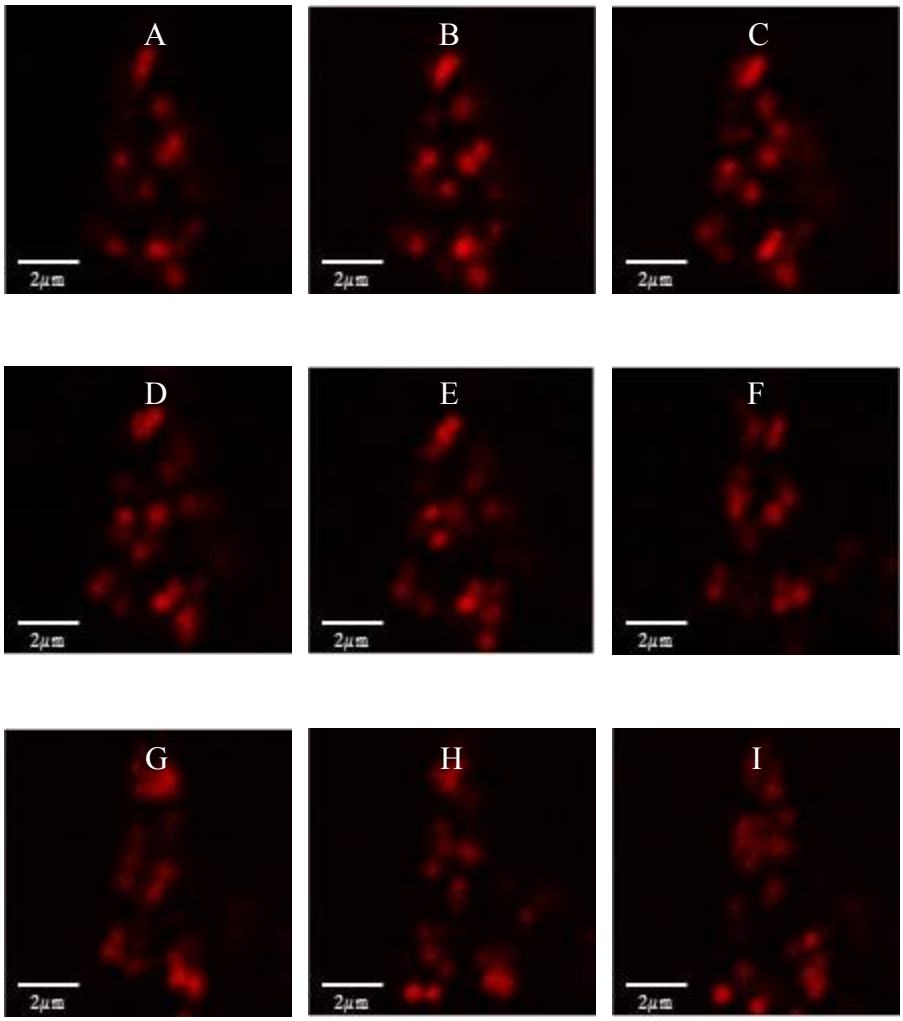

Figure 6.10 Dimers in Real Time

Images A, B, C, D, E, F, G, H, and I each correspond to an image of the cell with dimers at times $\tau = 0$, $\tau = 5.01, \tau = 20.04, \tau = 35.07$ $\tau = 45.09, \tau = 95.19$, $\tau = 145.29$, $\tau = 195.39$, and $\tau = 245.49$ seconds, respectively in green merged with Image A at $\tau = 0$ in red.

These images are similar to the images presented in Chapter 4 for dimers internalized in cells via a fixed exposure, variable uptake experiment; each red region in the image is expected to be a cluster or aggregation of dimers. The images shown in Figure 6.10 reflect minor changes between Images A and B; however the brightness of the images is relatively consistent with time.

To extract quantitative information from the images, Figure 6.11 is a scatter plot of the intensity corresponding to each image in the series of 50 images collected as a function of the image number.

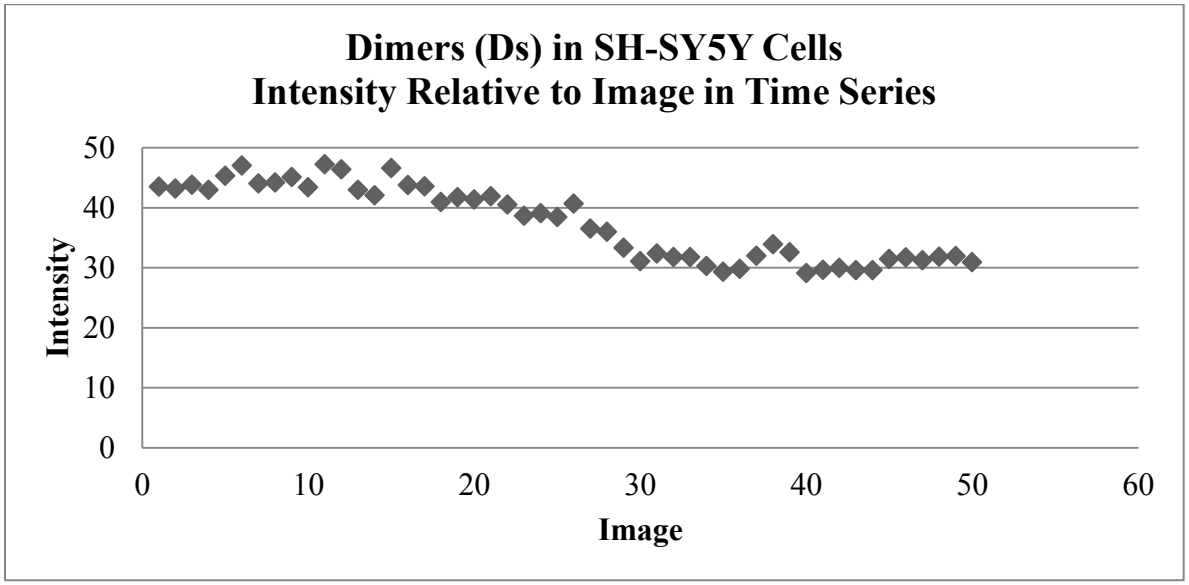

Figure 6.11 Scatter Plot of Intensity of Dimers in SH-SY5Y cells as a Function of Image in Time Series

The intensity of dimers as shown in Figure 6.11 shows the intensity of each image is approximately 40 but decreases to approximately 30 for the remaining twenty images in the series. Therefore, there is some degree of photobleaching occurring but not to the same extent as with monomers.

Figure 6.12 is a scatter plot of the auto correlation amplitude plotted with respect to the image number in the time series.

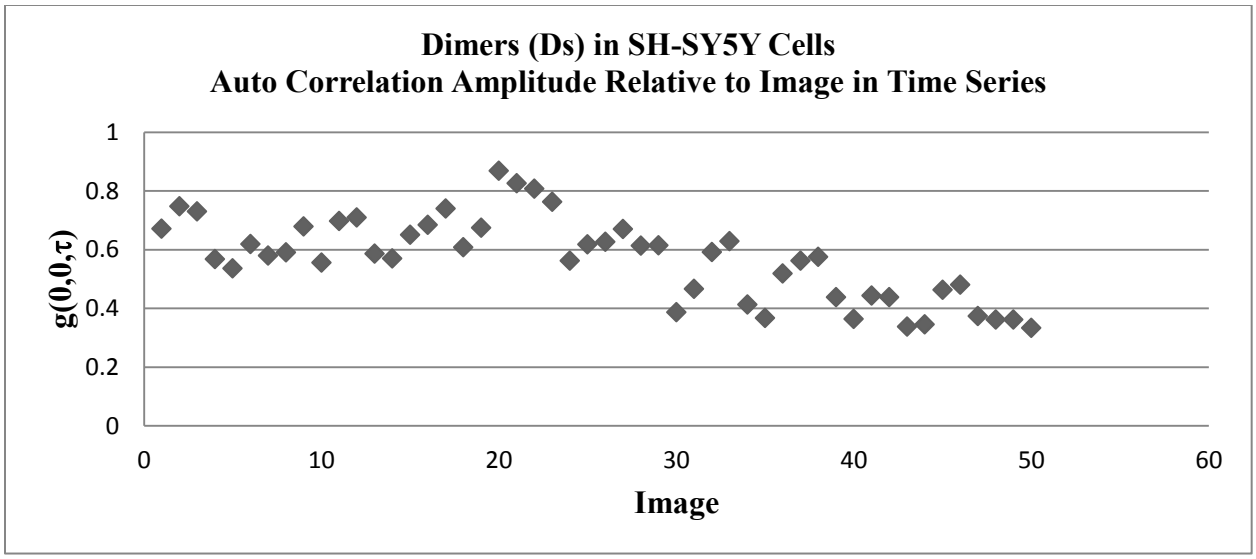

Figure 6.12 Scatter Plot of Auto Correlation Amplitude of Dimers Relative to Image in Time Series

Similar to the intensity, the auto correlation amplitude decreases to approximately half its initial value with the progression of time. As the number of clusters in the observation area is inversely proportional to the auto correlation amplitude, a greater number of clusters would be observed as the dimers diffuse in the region defined by the laser beam as time progresses. However, as a result of photobleaching, the decrease in the auto correlation amplitude is more likely due to the background noise that comes into effect.

Table 6.5 corresponds to the temporal image correlation spectroscopy (TICS) data corresponding to the amplitude of the auto correlation function, $g(0,0,0)$, delay time between images, $\Delta\tau$, and the fit obtained for the laser beam width, ω.

Table 6.5 Data Corresponding to Images of Dimers in Real Time

$\boldsymbol{g(0,0,0)}$	0.67
$\boldsymbol{\Delta\tau}$	5.01 sec
$\boldsymbol{\omega}$	0.42 μm

The auto correlation amplitude for dimers is approximately 0.67, which is quite a bit less than the auto correlation amplitude observed for monomers. The delay time between images is

approximately 5.01 seconds. Lastly, the fit obtained for the laser beam width is approximately 0.42 which is similar to the fit for monomers and reflects the sizes of clusters containing either monomers or dimers are the same. In addition, the measurement of the fitted laser beam width arises from convolution.

Figure 6.13 is a scatter plot of the temporal auto correlation amplitude plotted with respect to time, τ.

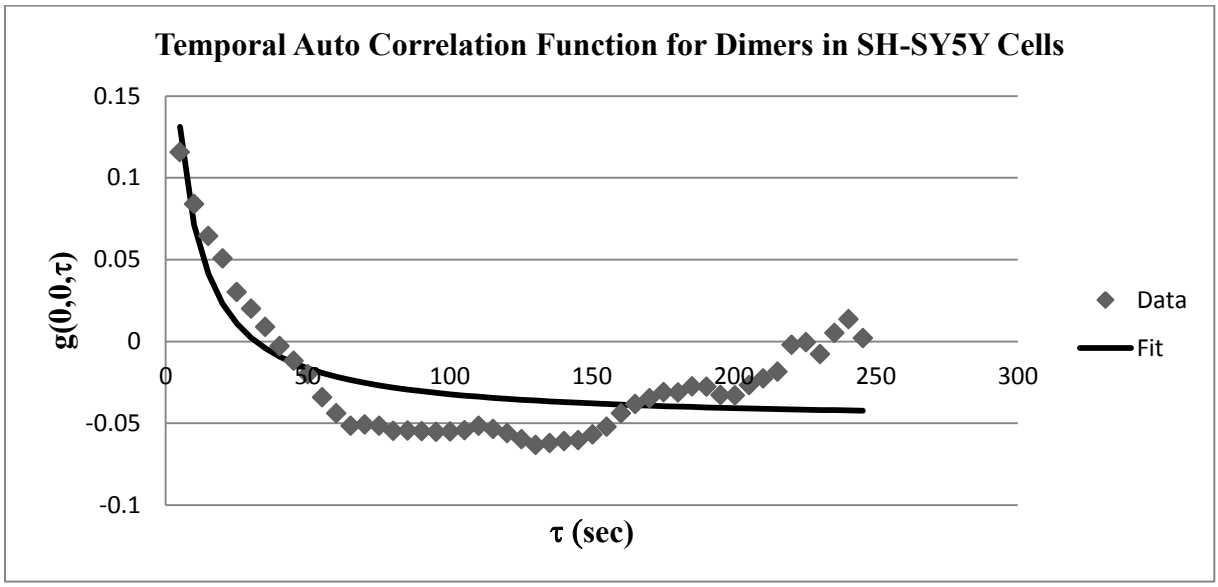

Figure 6.13 Temporal Auto Correlation Function for Dimers in SH-SY5Y Cells

In contrast to the monomers, the fit for the decay of the temporal auto correlation is not quite as good for this particular experiment. This may be a result of molecules diffusing back into the region of observation which is why the correlation function is increasing after 150 seconds.

Table 6.6 shows the fit parameters corresponding to the fitted function in Figure 6.13. The values are shown with standard deviation.

Table 6.6 Fit parameters obtained for One Dimer Experiment of 50 Images in Real Time in SH-SY5Y Cells

A	0.36 ± 0.15[1]
τ_d	$5.09 \pm 3.67\ sec$
C	$(-0.049) \pm 0.006$

[1] Standard deviation. $\chi^2 = 0.03$.

The fit calculated for the auto correlation amplitude is 0.36. The diffusion time of dimers is 5.09, which is a third of the time of monomers. In addition, the calculated constant to allow for incomplete decay of the temporal correlation function is -0.049. The chi square value is only 0.03 which reflects the goodness of the fitted curve to the data.

To obtain a visual representation for the diffusive behavior of dimers with time, Figure 6.14 shows the same images as presented in Figure 6.10 that have been *overlaid* with the image at $\tau = 0$ seconds . ImageJ software was used to merge the image obtained at $\tau = 0$ seconds in red with an image collected at a later time, τ, in green. Thus, image A in Figure 6.14 is yellow as it is the merge of the same image.

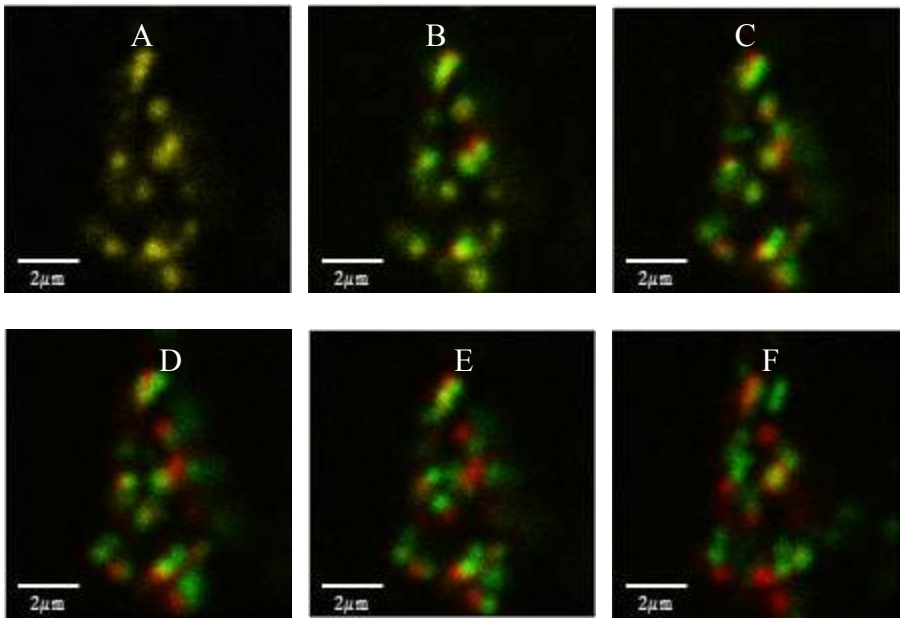

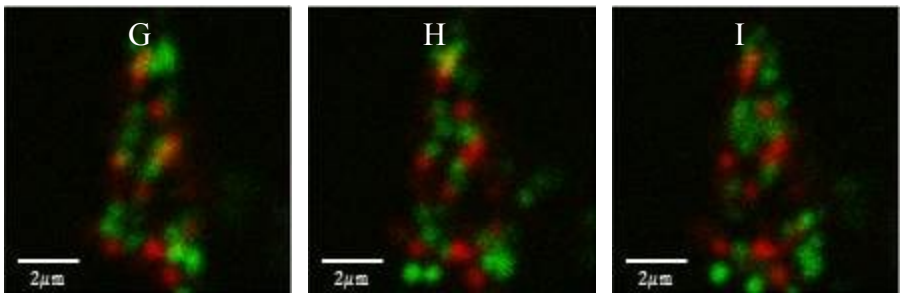

Figure 6.14 Images of Dimers in Real Time Merged with Image at $\tau = 0$

Images A, B, C, D, E, F, G, H, and I each correspond to an overlay of dimers imaged at $\tau = 0$ in red with $\tau = 0$, $\tau = 5.01$, $\tau = 20.04$, $\tau = 35.07$ $\tau = 45.09$, $\tau = 95.19$, $\tau = 145.29$, $\tau = 195.39$, and $\tau = 245.49$ seconds, respectively in green.

Table 6.7 is a representation of the average temporal auto correlation amplitude, average fitted auto correlation amplitude, average incomplete decay constant, average diffusion time, and average diffusion coefficient for data sets consisting of n_{images} defining a batch. The average values are shown with standard error.

Table 6.7 Average Auto Correlation Amplitude, Average Fitted Auto Correlation Average Amplitude, Average Diffusion Time, and Diffusion Coefficient for Dimers in Batches

$\langle n_{images} \rangle$	$\langle g(0,0,0) \rangle$	$\langle A \rangle$	$\langle C \rangle$	$\langle \tau_d\,(sec) \rangle$	$\langle D(\mathrm{cm2/sec}) \rangle$
20	0.64 ± 0.21[1]	0.18 ± 0.03	(-0.13) ± 0.02	16.4 ± 7.2	7.77E-11 ± 2.40E-11
40	0.86 ± 0.29	0.32 ± 0.12	(-0.10) ± 0.01	14.8 ± 9.4	5.32E-11 ± 1.91E-11
50	**0.82 ± 0.11**	**0.30 ± 0.05**	**(-0.07) ± 0.01**	**10.9 ± 5.0**	**6.25E-11 ± 1.93E-11**
60	0.82 ± 0.30	0.38 ± 0.08	(-0.08) ± 0.01	7.69 ± 1.36	6.22E-11 ± 9.07E-12
80	0.97 ± 0.36	0.45 ± 0.09	(-0.07) ± 0.02	7.93 ± 2.21	7.05E-11 ± 1.58E-11

[1] Standard error.

The average auto correlation amplitudes for each image batch ranges between approximately 0.64-0.97. The average auto correlation amplitude obtained from the fit, $\langle A \rangle$, is approximately 10% less, values ranging between 0.18-0.45, specifically. The average fit of the auto correlation amplitude is expected to be less. The parameter to account for incomplete decay of the correlation function ranges between -0.13-(-0.07). The incomplete decay of the auto correlation function has been accounted for in the fit. The average diffusion time for monomers

for each defined batch ranges between approximately 7.69-16.4 seconds. Lastly, the diffusion coefficient on average is on the scale of 10^{-11} square centimeters per second.

Figure 6.15 is a bar graph of the average auto correlation amplitude for dimers in reference to Figure 6.7. The average auto correlation amplitude is plotted as a function of the number of images in a batch.

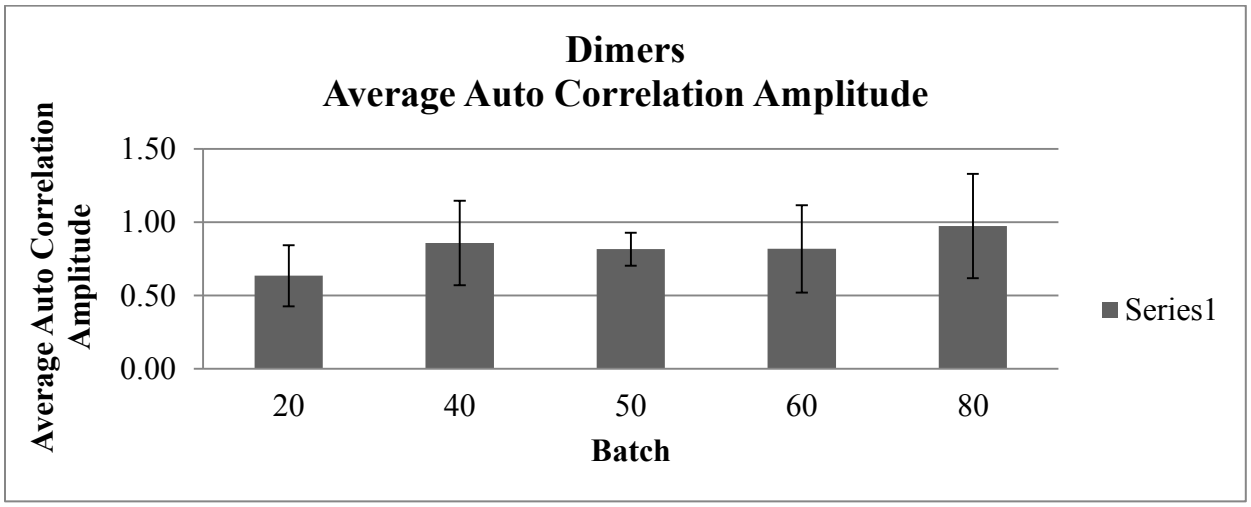

Figure 6.15 Bar Graph for Average Auto Correlation Amplitude as a Function of Batch for Dimers

Similar to monomers, the average auto correlation amplitude is relatively consistent, thus does not depend on the number of images in a data set. However, the standard error corresponding to data consisting of 50 images is quite a bit less in comparison to the average auto correlation amplitude measured for other batches.

Figure 6.16 is a bar graph for the fitted auto correlation amplitude as a function of image batch.

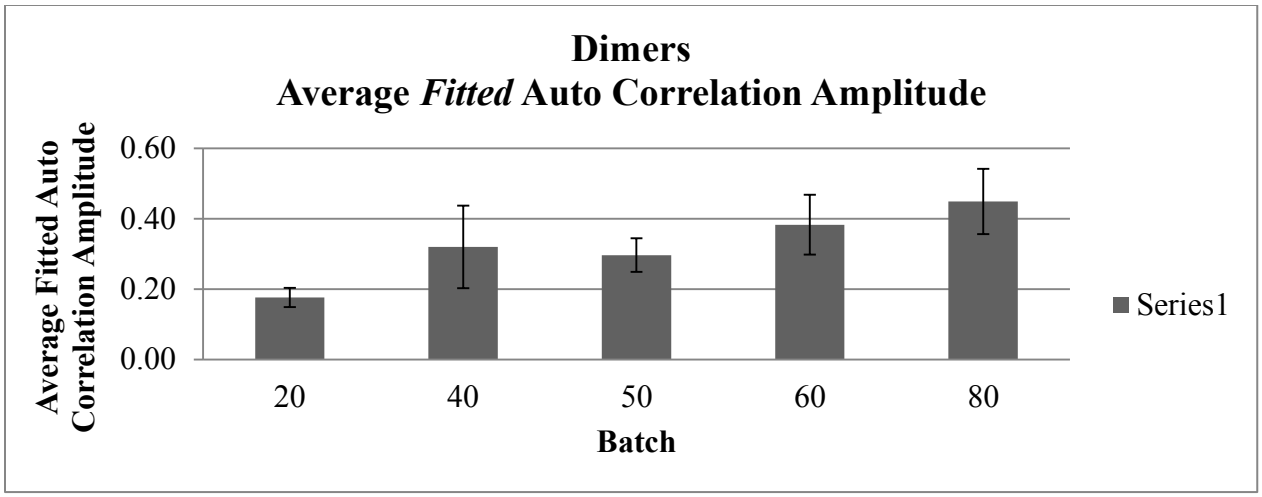

Figure 6.16 Bar Graph of Average Fitted Auto Correlation Amplitude as a Function of Batch for Dimers

The average fitted auto correlation amplitude for each image batch defined by data consisting of 20- 50 images is within the same magnitude then increases almost two fold for batches of data containing 60 and 80 images. Similar behavior was also exhibited with the case of the monomers.

Figure 6.17 is a bar graph of the average diffusion time as a function of the batch.

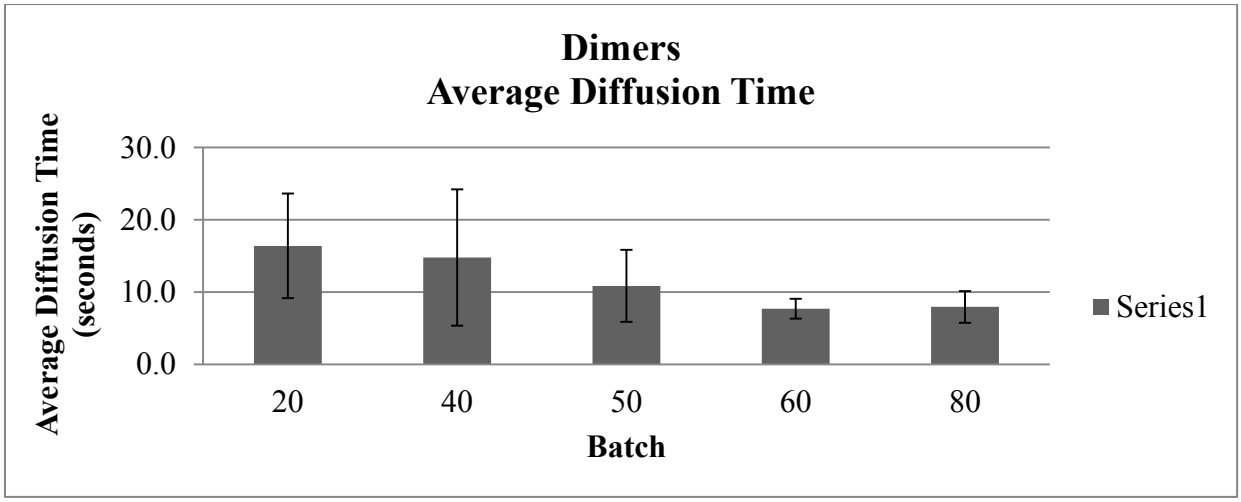

Figure 6.17 Average Diffusion Time of Dimers as a Function of Number of Images in Batch

The average diffusion time for batches containing data of a certain number of images decreases depending on the number of images within the batch. However, the standard error with respect to the diffusion time for batches defined by data consisting of 20 and 40 images is high and thus not a precise measurement of the diffusion time.

Figure 6.18 is a bar graph for the average diffusion coefficient for dimers as a function of batch.

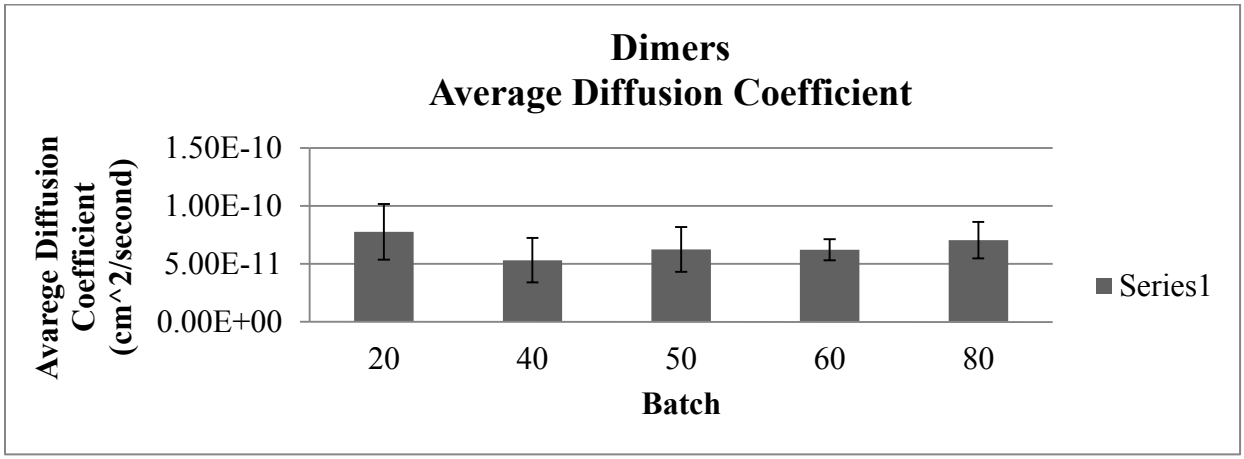

Figure 6.18 Average Diffusion Coefficient of Dimers as a Function of Number of Images in Batch

The average diffusion coefficient is somewhat consistent with image batch.

Similar to the case with the monomers, analysis of dimers was based on data sets within a batch consisting of 50 images. Therefore, a global fit of data consisting of 50 images was calculated for the dimers in Table 6.8;

Table 6.8 Global Fit for Data Sets for Batches Defined by 50 Images of Dimers

A	0.28 ± (-0.04)[1]
τ_d	8.56 ± (-2.24) sec
C	(-0.059) ± (-0.003)

[1] Standard error. $\chi^2 = 0.05$.

The global fit indicates that the temporal auto correlation amplitude is approximately 0.28. The diffusion time for dimers is approximately 8.56 seconds and the constant to allow for incomplete decay of the auto correlation amplitude was (-0.059). The chi square value is approximately 0.05 to reflect a good fit for all sets of data corresponding to 50 images of dimers. However, the diffusion time obtained in the global fit strongly compares with the average of the fit parameters of the experiments consisting of 50 images (bolded in Table 6.7).

6.3 Tetramers

Chapter 6.3 focusses on the dynamics of tetramers of α −synuclein in SH-SY5Y cells.

Figure 6.19 shows nine images, each image corresponding to the same cell, taken over a series of 100 seconds. Cells in the sample were exposed to tetramers for two hours and imaged immediately after washing. Image A is the first image of one cell exposed to tetramers in the series, collected at $\tau = 0\ seconds$. Images B, C, D, E, F, G, H, and I each correspond to an image of the cell at times $\tau = 1.97, \tau = 7.98, \tau = 14.0\ \tau = 18,\ = 38,\ \tau = 58,\ \tau = 78,$ and $\tau = 98$ seconds, respectively.

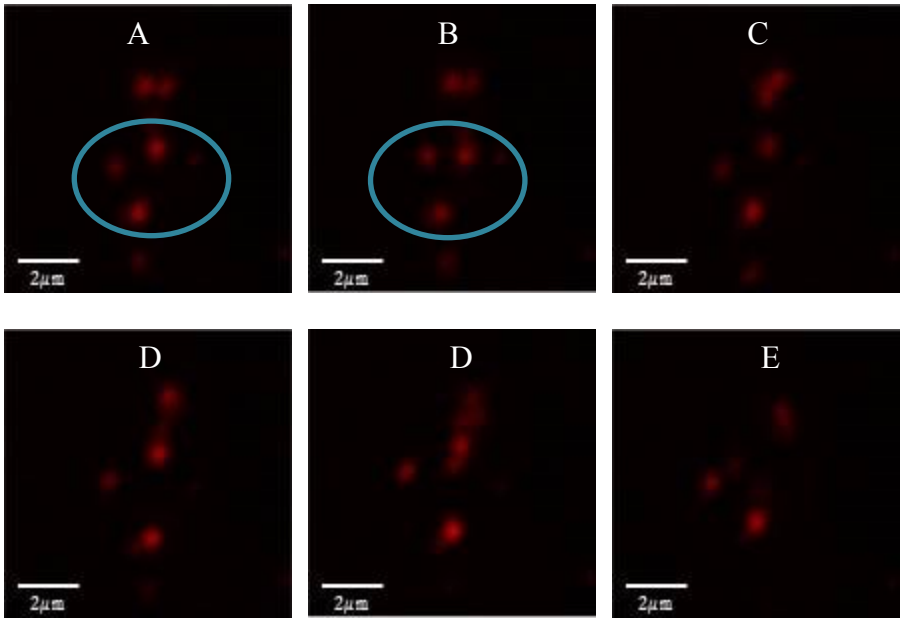

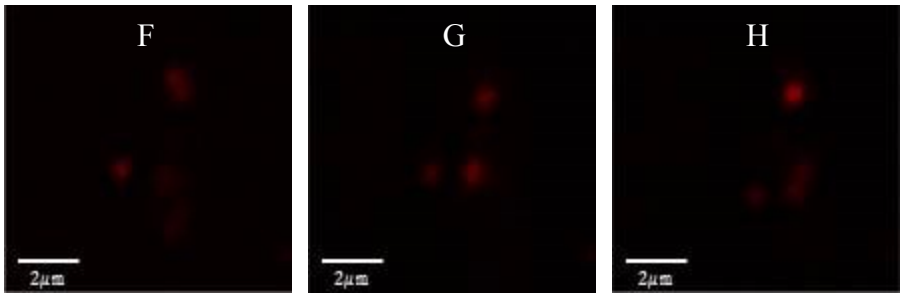

Figure 6.19 Tetramers in Real Time

Each image corresponds to the same cell with internalized monomers, each varying based on delta time, t, from time zero. Images A, B, C, D, E, F, G, H, and I each correspond to an image of the cell at times $\tau = 0, \tau = 1.97, \tau = 7.98, \tau = 14.0\ \tau = 18, \tau = 38, \tau = 58, \tau = 78$, and $\tau = 98$ seconds, respectively.

These images are similar to the images in Chapter 4 for tetramers internalized in cells via a fixed exposure, variable uptake experiment, each red region represents a cluster or aggregation of tetramers. The images shown in Figure 6.19 show that there are differences observed in the image as early as 1.97 seconds in Image B, due to the variation in red regions, circled in blue in Images A and B.

To extract quantitative information from the images, Figure 6.20 is a scatter plot of the intensity corresponding to each image in the series of 50 images collected as a function of the image in the series.

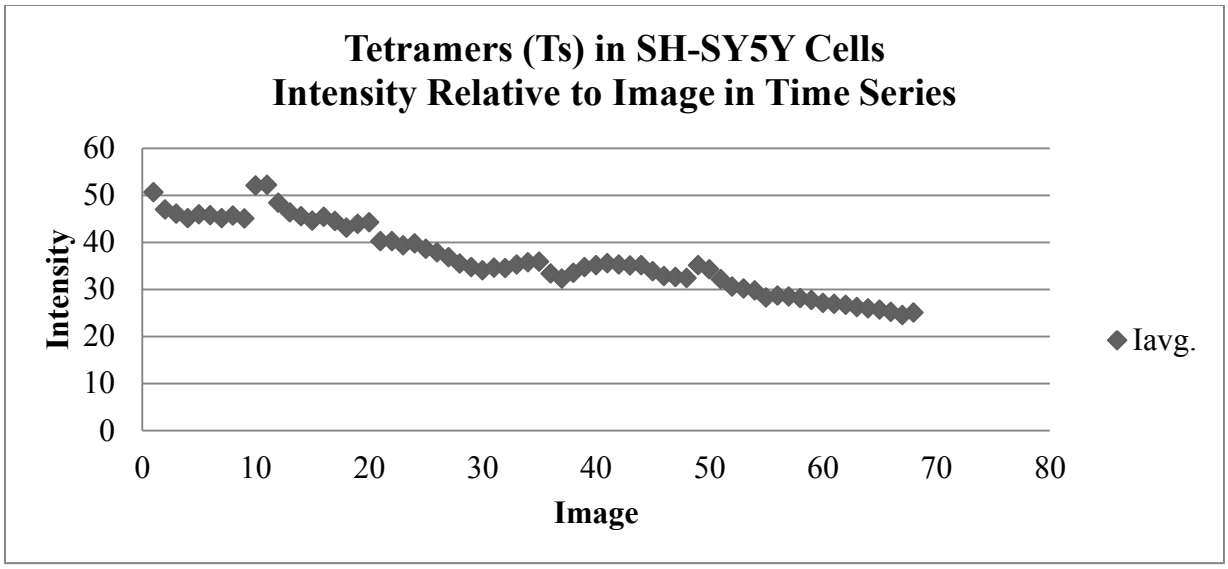

Figure 6.20 Scatter Plot of Intensity of Tetramers in SH-SY5Y cells as a Function of Image in Time Series

The average intensity of the tetramers is relatively consistent for the first 20 images obtained in the time series followed by some photobleaching for the remaining 30 images. However, the intensity is somewhat consistent, on average approximately 30 for 20-50 images.

Figure 6.21 is a scatter plot of the auto correlation amplitude plotted with respect to the image number in the time series.

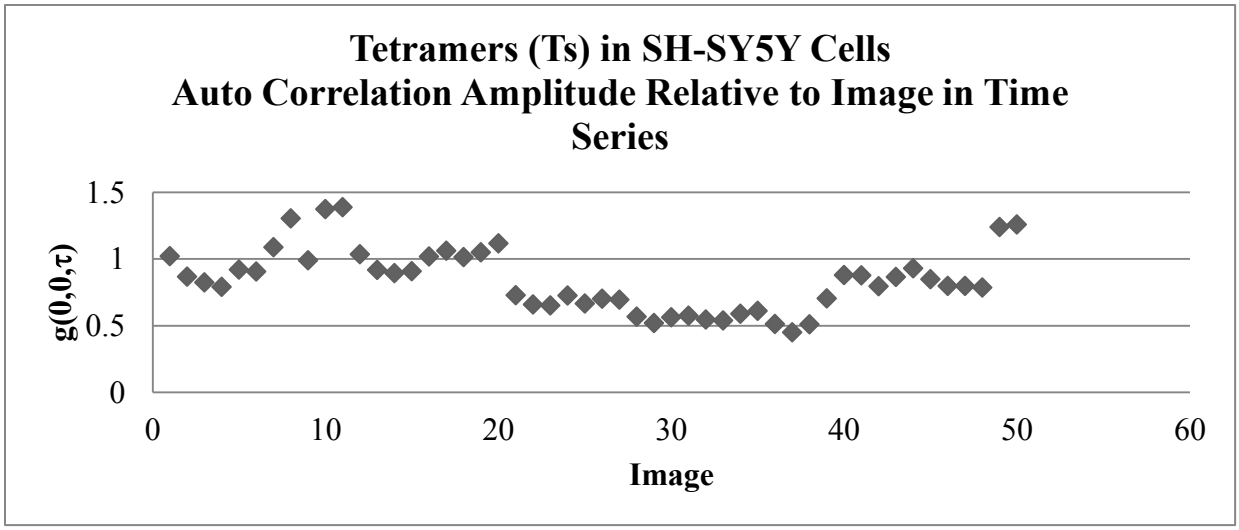

Figure 6.21 Scatter Plot of Average Auto Correlation Amplitude for Tetramers

Contrary to previous findings, the auto correlation amplitude fluctuates over the course of fifty images obtained for the time series.

Table 6.9 corresponds to the temporal image correlation spectroscopy (TICS) data corresponding to the amplitude of the auto correlation function, $g(0,0,0)$, delay time between images, $\Delta\tau$, and the fit obtained for the laser beam width, ω.

Table 6.9 Raw Data Corresponding to Images of Tetramers in Real Time

$\boldsymbol{g(0,0,0)}$	1.02
$\boldsymbol{\Delta\tau}$	1.97 sec
$\boldsymbol{\omega}$	0.46 μm

The auto correlation amplitude for dimers is approximately 1.02. The delay time between images is approximately 1.97 seconds. Lastly, the fit obtained for the laser beam width is approximately 0.46 which is similar to the fit for monomers and dimers and reflects these clusters are larger than the laser beam itself.

Figure 6.22 is the temporal auto correlation function in comparison to the three parameter hyperbolic decay fit for tetramers in SH-SY5Y cells.

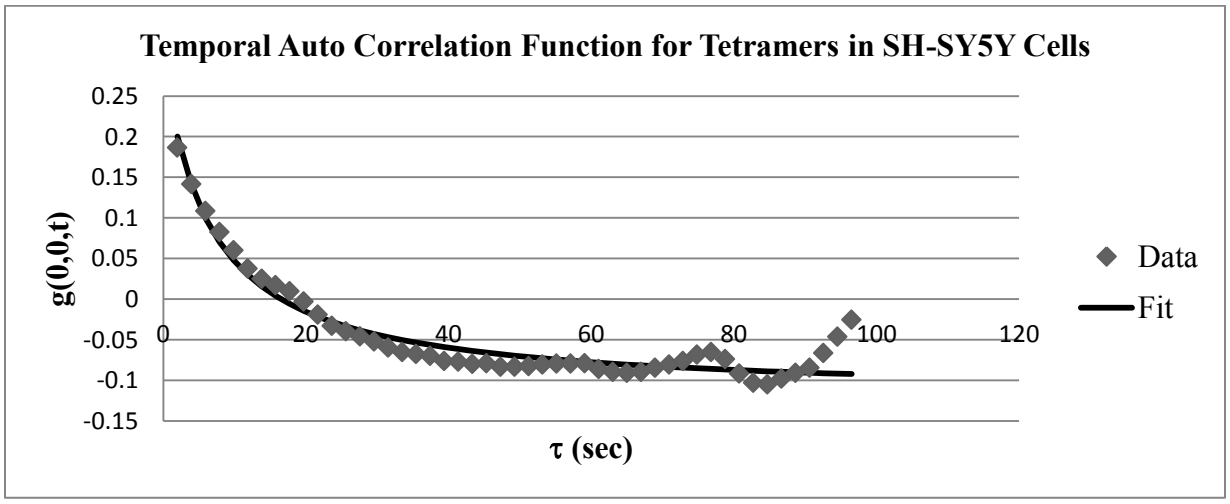

Figure 6.22 Temporal Auto Correlation Function for Tetramers in Real Time in SH-SY5Y Cells

The hyperbolic decay fits well with the data shown in Figure 6.22.

Table 6.10 shows the parameters corresponding to the fit in Figure 6.22.

Table 6.10 Fit parameters obtained for One Tetramer Experiment of 50 Images in Live Time in SH-SY5Y Cells

A	0.41 ± 0.03[1]
τ_d	6.69 ± 1.23 sec
C	(-0.119) ± 0.006

[1] Standard deviation. $\chi^2 = 0.01$

The fitted auto correlation amplitude is approximately 0.41. The diffusion time of tetramers is 6.69. In addition, the calculated constant to allow for incomplete decay of the temporal correlation function is -0.119. The chi square value is only 0.01 which reflects the goodness of the fitted curve to the data.

To obtain a visual representation for the diffusive behavior of dimers with time, Figure 6.23 shows the same images as presented in Figure 6.19 that have been *overlaid* with the image at $\tau = 0$ seconds . ImageJ software was used to merge the image obtained at $\tau = 0$ seconds with an image collected at a later time in green. Thus, Image A in Figure 6.23 is yellow as it is the merge of the same image.

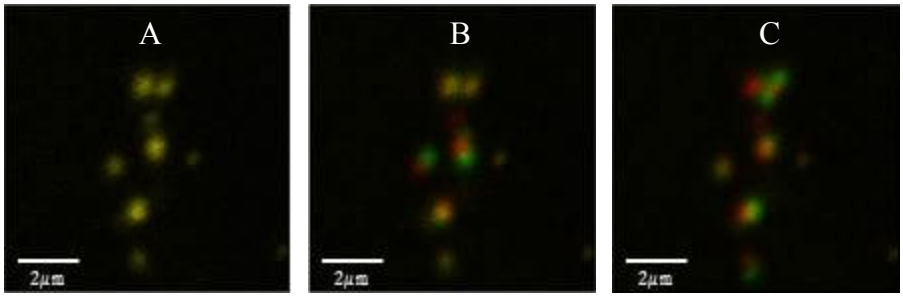

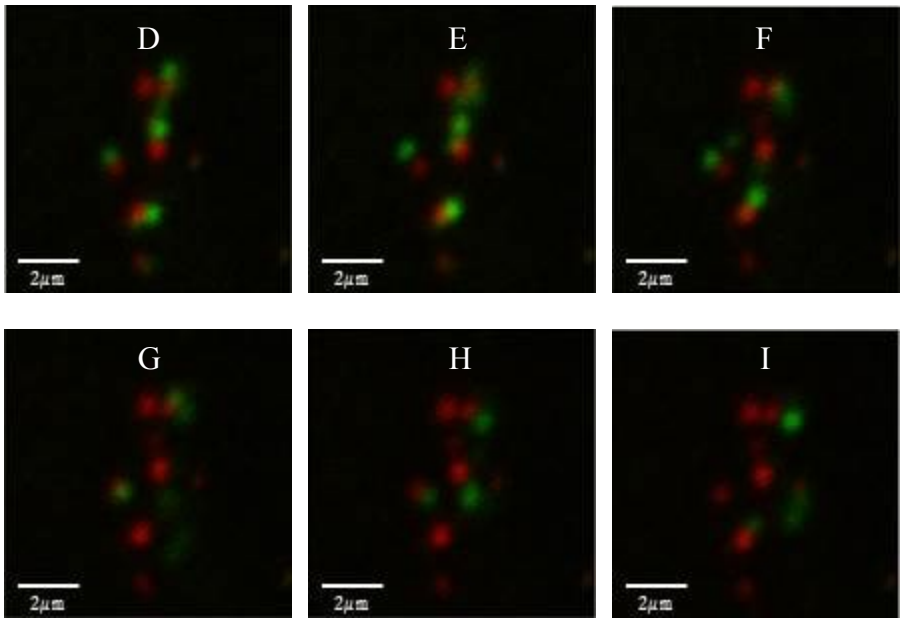

Figure 6.23 Images of Tetramers in Real Time Merged with Image at $\tau = 0$

Images A, B, C, D, E, F, G, H, and I each correspond to a merge of the tetramers at $\tau = 0$ in red with tetramers at times $\tau = 0, \tau = 1.97, \tau = 7.98, \tau = 14.0\ \tau = 18, \tau = 38, \tau = 58, \tau = 78,$ and $\tau = 98$ seconds, respectively.

Red and green regions are visualized as early as early as in image B, after approximately 1.97seconds have elapsed. Thus, contrary to the monomer and dimer, these tetramers diffuse even more quickly.

Table 6.11 is a representation of the average temporal auto correlation amplitude, fitted auto correlation amplitude, incomplete decay constant, diffusion time, and diffusion coefficient for data sets in a batch consisting of n_{images}. The average values are shown with standard error.

Table 6.11 Average Auto Correlation Amplitude, Average Fitted Auto Correlation Amplitude, Average Diffusion Time, and Average Diffusion Coefficient for Tetramers

$\langle n_{images} \rangle$	$\langle g(0,0,0) \rangle$	$\langle A \rangle$	$\langle C \rangle$	$\langle \tau_d(sec) \rangle$	$\langle D(\mathrm{cm\^2/sec}) \rangle$
20	1.53 ± 0.21[1]	0.23 ± 0.04	(-0.10) ± 0.01	4.78 ± 0.73	1.03E-10 ± 1.34E-11
40	2.01 ± 0.27	0.49 ± 0.08	(-0.14) ± 0.02	6.49 ± 1.56	9.33E-11 ± 3.83E-11
50	**1.77 ± 0.39**	**0.51 ± 0.08**	**(-0.13) ± 0.02**	**5.66 ± 0.65**	**8.04E-11 ± 1.07E-11**
60	1.97 ± 0.28	0.57 ± 0.06	(-0.15) ± 0.04	9.16 ± 4.31	6.63E-11 ± 1.99E-11
80	1.84 ± 0.20	0.69 ± 0.06	(-0.18) ± 0.08	11.6 ± 9.2	4.66E-11 ± 3.62E-11

[1]Standard error.

The average auto correlation amplitudes for each image batch ranges between approximately 1.53-2.01. The average auto correlation amplitude obtained from the fit, $\langle A \rangle$, is approximately 50% less, values ranging between 0.23-0.69, specifically. The average fit of the auto correlation amplitude is expected to be less. The parameter to account for incomplete decay of the correlation function ranges between -0.18-(-0.10). The incomplete decay of the auto correlation function has been accounted for in the fit. The average diffusion time for tetramers in each batch ranges between approximately 4.78-11.6 seconds. Lastly, the diffusion coefficient on average is on the scale of 10^{-11} square centimeters per second.

Figure 6.24 is a distribution of the average auto correlation amplitude for tetramers in reference to Figure 6.9. The average auto correlation amplitude is plotted as a function of the number of images defining a batch

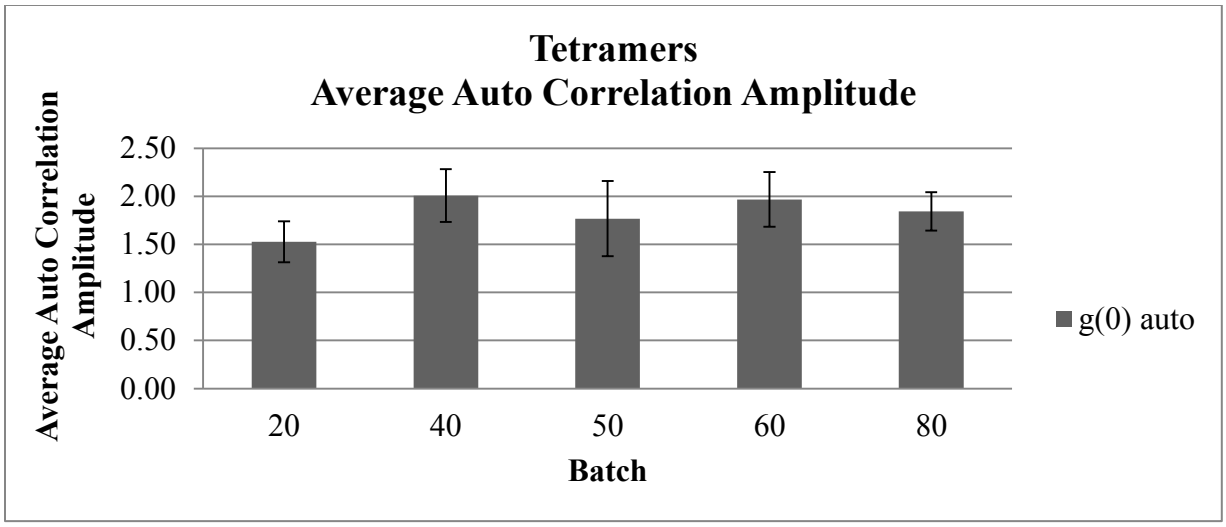

Figure 6.24 Bar Graph of the Average Auto Correlation Amplitude as a Function of Batch for Tetramers

The average auto correlation amplitude is relatively consistent between batches; there are no outliers or specific trends.

Figure 6.24 is bar graph for the average fitted auto correlation amplitude as a function of batch.

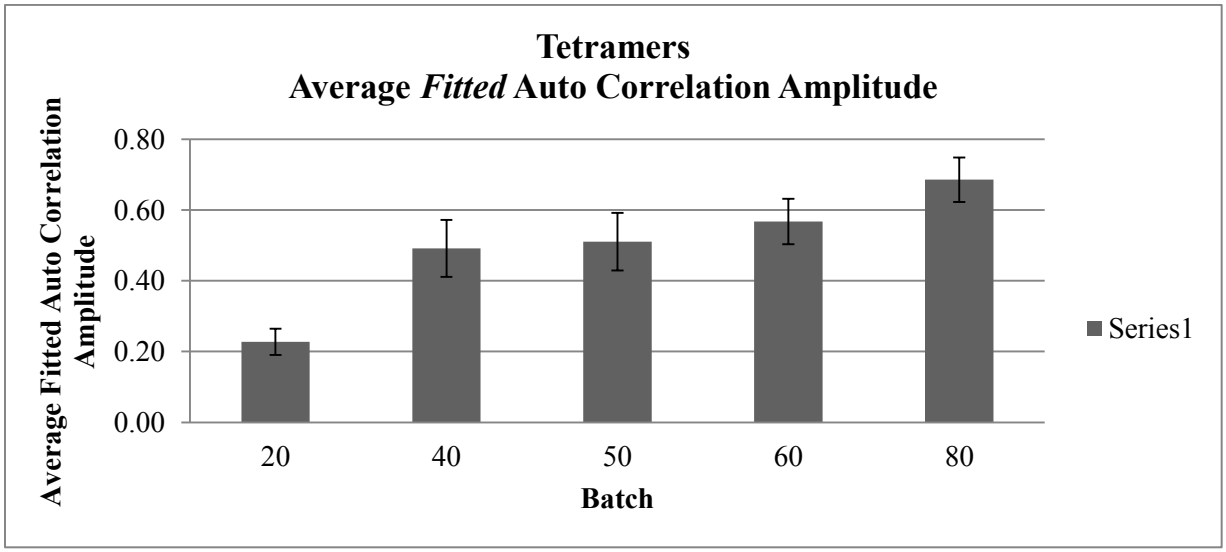

Figure 6.25 Bar Graph of Average Fitted Auto Correlation Amplitude as a Function of Batch for Tetramers

The fitted auto correlation amplitude for data sets in a batch of 20 images is much less in comparison to batches consisting of data with 40 images or more.

Figure 6.26 is a bar graph of the average diffusion time of tetramers as a function of images within a batch.

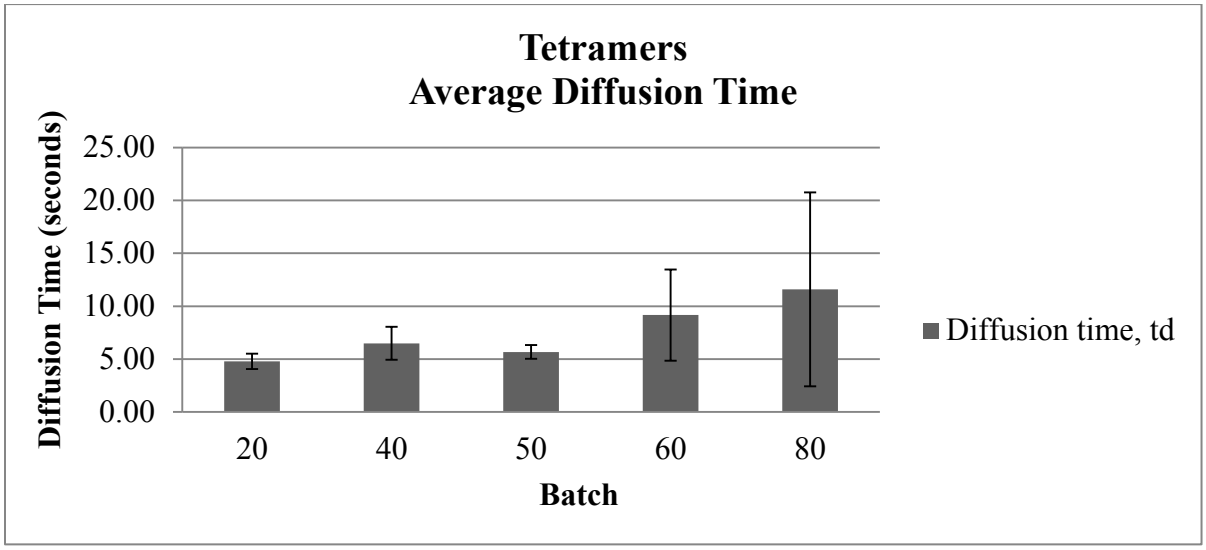

Figure 6.26 Bar Graph of Average Diffusion Time as a Function of Batches for Tetramers

The average diffusion time is consistent for batches containing data consisting of 20-50 images. However, the diffusion time for tetramers in batches of data containing 60 and 80 images is somewhat larger, but also reflecting a relatively high standard error.

Figure 6.27 is a plot of the average diffusion coefficient of tetramers as a function of images in a batch.

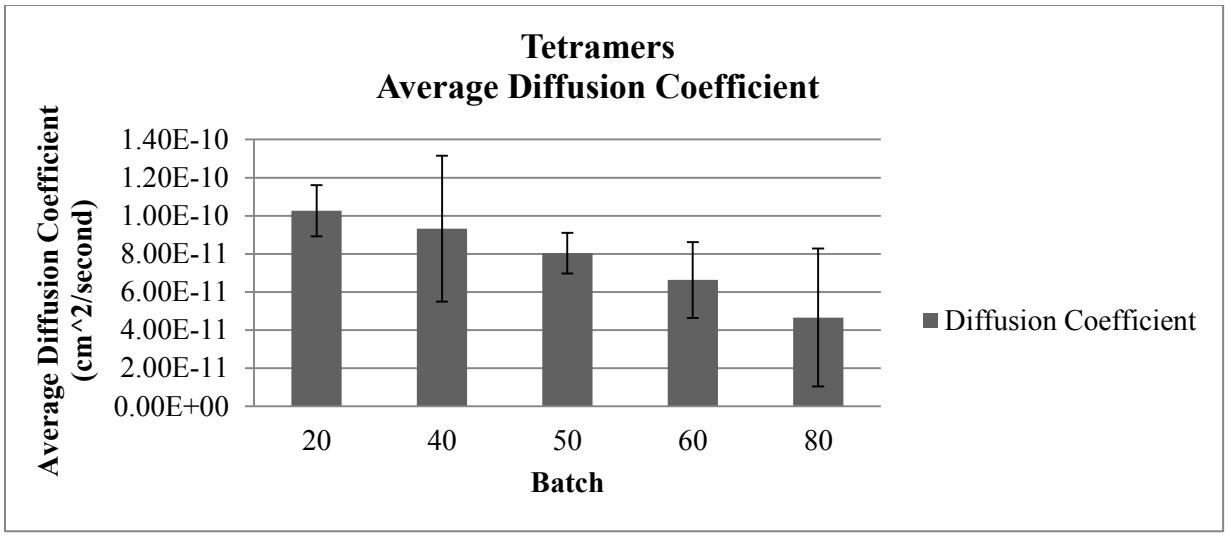

Figure 6.27 Bar Graph of Average Diffusion Coefficient as a Function of Batch for Tetramers

There is a steady decrease in magnitude for the average diffusion coefficient of tetramers dependent on the number of images in the batch. However, the diffusion coefficient represented for batches of 50 images reflects a low standard error, thus is a reasonable measurement for the diffusion coefficient of tetramers.

As with monomers and dimers, analysis of tetramers was based on data consisting of 50 images. Therefore, a global fit of data was obtained for the data sets in the 50 image batch.

Table 6.12 represents the parameters obtained for the global fit of data sets consisting of 50 images.

Table 6.12 Global Fit for Data Sets within a Defined Batch of 50 Images of Tetramers

A	0.50 ± -0.02[1]
τ_d	5.58 ± -0.65 sec
C	-0.129 ± -0.004

[1] Standard error. $\chi^2 = 0.17$

The global fit indicates that the temporal auto correlation amplitude is approximately 0.50. The diffusion time for tetramers is approximately 5.58 seconds and the constant to allow for incomplete decay of the auto correlation amplitude was (-0.129). The chi square value to assess goodness of fit is approximately 0.17, which reflects a good fit. In addition, the diffusion time obtained in the global fit strongly compares with the average of the fit parameters of the experiments consisting of 50 images (bolded in Table 6.11).

6.4 Summary

The purpose of section Figure 6.4 is to summarize the results obtained for each oligomer as represented in Table 6.3, and Table 6.7, and Table 6.11.

Figure 6.28 is a bar graph of both the fitted auto correlation amplitude and the auto correlation amplitude from the raw data for each oligomer.

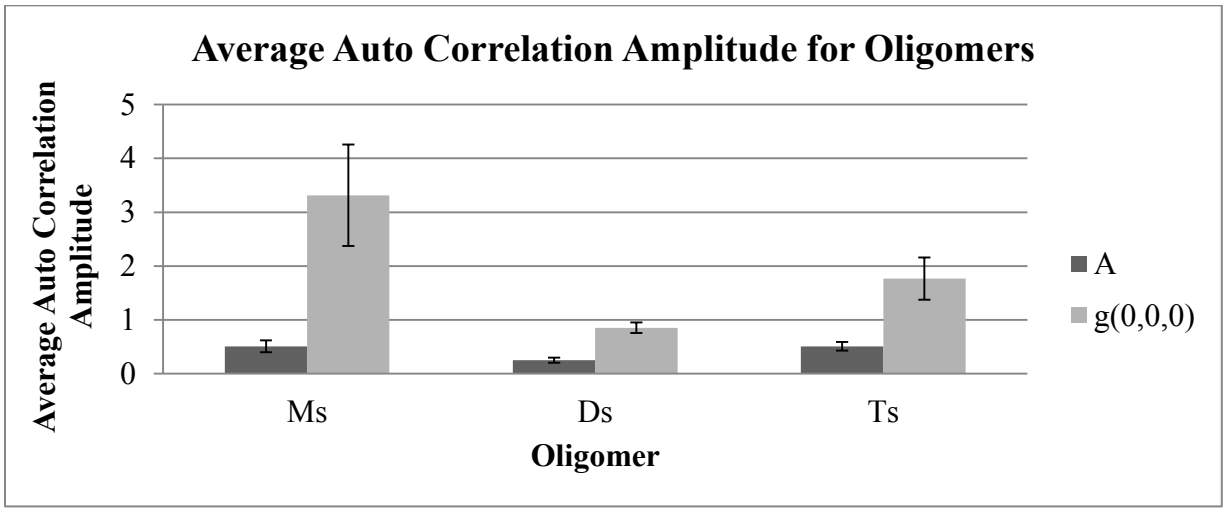

Figure 6.28 Bar Graph of Fitted and Raw Auto Correlation Amplitude of Oligomers
Based on batch defined by data consisting of 50 images.

The most notable feature of Figure 6.28 is the greater difference in magnitude between the auto correlation amplitude for the raw data and the fitted auto correlation amplitude. This is somewhat unexpected as this implies the total number of oligomers in the observation area is greater than the number of oligomers that the beam is able to illuminate. Thus, this requires further analysis. Second, the fitted auto correlation amplitudes for the monomers and tetramers are both approximately 0.50 whereas the dimer has an auto correlation amplitude of 0.25. In

addition, there is a striking difference between the fitted auto correlation amplitude and the raw auto correlation amplitude for monomers then there are in comparison for tetramers and dimers.

Figure 6.29 is a bar graph of the average diffusion time for each oligomer.

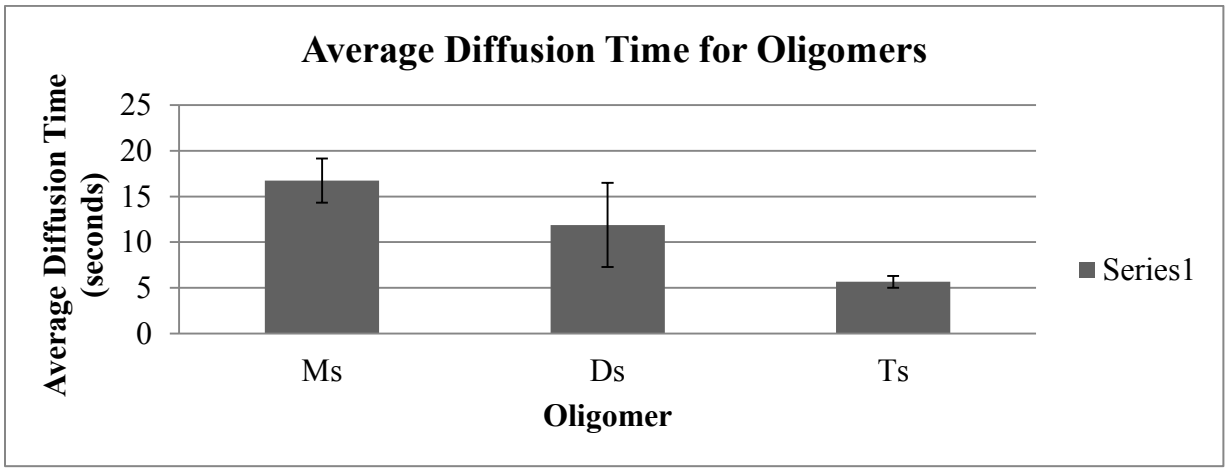

Figure 6.29 Bar Graph of Average Diffusion Time for Oligomers
Based on batch defined by data consisting of 50 images.

This plot reflects that the monomers have the greater diffusion time in comparison to dimers and tetramers.

Figure 6.30 is a plot of the average diffusion coefficient for each oligomer.

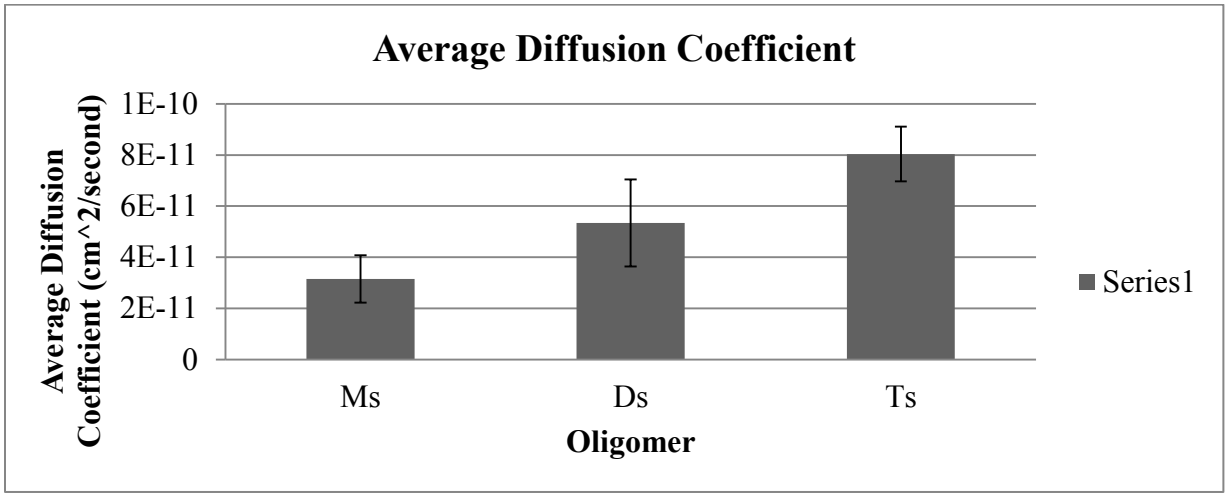

Figure 6.30 Average Diffusion Coefficient for Oligomers
Based on batch defined by data consisting of 50 images.

As there is no change observed for the fit for the laser beam, ω, the diffusion coefficient for each oligomer is weighed heavily upon the inverse relationship to the diffusion time. Thus, the diffusion coefficient increases with the size of the oligomer.

6.5 Chapter Conclusions

The purpose of this chapter was to demonstrate the process and expectations for studying the dynamics of a system via temporal image correlation spectroscopy analysis of live cells. The dynamics of oligomeric forms of α −syn were studied. The following conclusions can be made; 1.) A total of 50 images for one experiment is sufficient for estimation of parameters, 2) photobleaching is expected to occur but to a minor extent, and 3) the diffusion time decreases with oligomeric size and thus the diffusion coefficient increases with oligomeric size. Lastly, there is a large difference between the fitted auto correlation amplitude and auto correlation amplitude from the raw data; this was unexpected and requires some further interpretation.

The increased diffusion coefficient with oligomeric size is somewhat unusual; however, it must be interpreted as the diffusion coefficient of *endosomes* which contain the oligomers. However, the question as to why endosomes containing oligomers have a larger diffusion coefficient than endosomes containing monomers is a bit unclear. Recall, the aggregation of oligomers leads to the eventual formation of larger oligomers and fibrils. For example, in Chapter 6.1, the study of monomers with a 633 fluorescent probe in real time is useful but from this experiment alone, it is impossible to isolate which species may also be dimers and tetramers, since it is likely the monomers are aggregating and larger oligomers or even fibrils are forming.[35] To address this, real time imaging of two oligomers in cells was completed for this thesis however the analysis and understanding of this data has yet to be completed. Results from this study may provide some further insight as to why this phenomenon is occurring; given that oligomers aggregate to form fibrils, the aggregation of one type of oligomer in the presence of another may be effected.

Temporal Image Correlation Spectroscopy analysis has been widely used to study dynamics of biological systems of interest. It has been shown that membrane lipids and proteins diffuse on average between 10^{-12} to 10^{-10} square centimeters per second inside cells or within the

cell membrane. This slower rate of diffusion can be explained by the viscous nature of the cell membrane.[96]

In addition, small molecules, cytosolic proteins, transmembrane proteins, and large protein aggregates all vary with diffusion time, specifically ranging in time from microseconds to seconds. As an example, studies have used TICS to calculate the diffusion coefficient of α-actinin and α5-integrin to assess the roles of these proteins in cell migration.[97] Studies have also used TICS to calculate the lateral diffusion of GPI-anchored proteins across cell membranes.[98]

On average, the movement of these oligomers in cells is much slower, on the order of seconds, in comparison to the diffusion of species in solution, which is generally on the order of milliseconds.[99] This study has demonstrated a useful technique for analyzing species in real time. Specifically, parameters calculated from an experiment consisting of 50 images will be most precise and specific to your system of interest. More importantly, the rate at which oligomers diffuse in cells varies; this study has shown that the larger the oligomer of α −synuclein, the more quickly it will diffuse in cells.

Chapter 7

Conclusion

7 Conclusion

7.1 Thesis Summary

The work performed for this thesis provided insight into the relative distribution and association of markers in C2C12, A549 and SH-SY5Y cells. It was determined that the distribution of each of these markers and association of two and three markers is cell type specific, contrary to the proposed hypothesis in Chapter 1.5 in the introduction that the distribution is *not* cell type specific. While C2C12 cells reflect the expected association of two markers in reference to the commonly understood maturation/fusion model, A549 and SH-SY5Y cells share similarities in association but somewhat different to that of the understood pathway. These markers have been shown to localize to *specific* compartments, but to the best of our knowledge, this is the first study performed to determine the extent to which these markers exist on multiple compartments and that the markers are *not unique* to one endosomal compartment.

In addition, it has been demonstrated that two different nanomaterial systems, phospholipid coated gold nanoparticles and oligomeric forms of $\alpha-$synuclein associate with Rab5, Rab7, Rab11 (only studied for phospholipid coated gold nanoparticles), and LAMP-1 markers in various combinations to undergo clathrin mediated endocytosis. These results are also contrary to the proposed hypotheses in the introduction of this thesis that although phospholipid coated gold nanoparticles and $\alpha-$synuclein associate with endocytic markers, the association is not one hundred percent. An important point to consider is the phospholipid coated gold nanoparticles in endocytic compartments were studied *first* prior to the association of $\alpha-$synuclein with markers. This was done for two purposes; to study the uptake of this particular type of gold nanoparticle system in mammalian cells and to also serve as a model and ensure the pair wise and three color co-localization study was reliable for studying other nanomaterial systems of interest, like $\alpha-$synuclein.

In addition to the endocytic uptake pathway taken by phospholipid coated gold nanoparticles and oligomeric forms of $\alpha-$synuclein, these systems were studied individually to determine the extent of uptake in a time dependent manner. The extent of uptake of phospholipid coated gold nanoparticles in C2C12 and A549 cells varies from the standpoint that C2C12 cells appear to have a maximum amount of time in which they can *withhold* phospholipid coated gold

nanoparticles in a nanoparticle free media extracellular environment, whereas phospholipid coated gold nanoparticles were still observed in cells within a full 24 hours with continuous exposure. In the case of the α−synuclein studies, the relative uptake of α−synuclein varied with the three different oligomers chosen for this study; specifically, no obvious trends were reflected for dimers and tetramers, such that the relative degree of aggregation was relatively constant but decreased with time for tetramers to a minor extent. However, the relative degree of aggregation of monomeric forms of α−synuclein decreased after 24 hours of being retained in cells.

Experiments were also performed to assess other non-receptor mediated dependent cellular uptake pathways; it was determined that oligomers of α−synuclein *can* enter cells passively, more so for monomers and dimers than observed with tetramers with time. Additionally, enforced pre-aggregation of oligomers prior to their exposure to cells reflected no differences in the trend of uptake in cells.

In real time studies, the relative diffusion time of each of these species varies in cells, which was unexpected. The diffusion coefficient was greatest for the tetramer in comparison to the monomers and dimers of α−synuclein.

Collectively, all of these results reflect there exist a cell specific distribution of endocytic markers. In reference to GNPs, there is a cell specific uptake of phospholipid coated gold nanoparticles and association with endocytic compartments. Lastly, there are variations in uptake and dynamics for different oligomers of α−synuclein in neuroblastoma cells.

All of the results in this thesis were obtained using image correlation spectroscopy analysis of laser scanning confocal fluorescence microscopy images. The experimental and imaging procedures can be performed with relative ease, but care and caution must be taken into consideration for analysis and that a large number of images need to be obtained to reflect reliable estimates of parameters. Additionally, control samples are critical for comparison in experiments to ensure accurate sampling of systems of interest.

7.2 Significance and Contribution to the field of Nanotechnology and Cell Biology

In this work, membrane trafficking and possible roles of endocytic proteins was studied along with the endocytic uptake of two nanomaterial systems of interest for potential therpuetic and diagnostic applications. This is the first ICS analysis of endocytic marker and gold nanoparticle association and distribution. Additionally, this is the first time a successful *quantitative* three color co-localization was performed in-vitro in mammalian cells, C2C12 and A549 cells using Image Correlation Spectroscopy analysis.

7.3 Future Work

There are a few studies that must be performed to complete the understanding of the distribution and association of endocytic markers in cell lines, the association of nanomaterial systems with these markers in cell lines, and the efficiency of uptake and internalization of nanomaterial systems in a time dependent manner. This work has also provided motivation to explore potential platforms for therapeutic applications for Parkinson's disease.

From a technical standpoint, further cross correlations of random sets of images is required to address the question of coincidental fluorescence. Although shown for one instance that the cross correlation of random images only implies an approximate 16% over-estimate of fractions, additional calculations for all of these systems should also be calculated to inquire about potential coincidental fluorescence, especially for publication purposes.

Also, the question of anticorrelation requires attention. Some co-localizations may not quite appear as "yellow" as expected for green and red overlay; in particular for phospholipid coated gold nanoparticle and marker association in Chapter 4; however ICCS calculations show there is a high degree of co-localization. Although this may be true, the calculations may be a slight over estimate and there may be some anticorrelation. Thus, for publication purposes in the future, anticorrelation analysis should be addressed.

Real-time analysis study of markers of endocytosis is needed. This work has shown that these markers are not unique and exist on multiple compartments. However, work for the future requires real time analysis of these markers to determine the actual times for which these markers begin to associate with one another, in addition to the times for which they co-localize.

Specifically, the number of clusters in the observation area and the extent to which markers co-localize can *also* be determined as a function of time.

There have been many studies performed, specifically at the Rockafeller University in New York in the Simon laboratory to determine the dynamics specific for clathrin recruitment to the cell membrane to localize with specific receptors,[100,101] the dynamics specific for adapter proteins to recruit to the plasma membrane and subsequently get removed from vesicles,[102] and the amount of time required for dynamin to assist with pinching of the invaginated pit. [103] Thus, work has been done to understand the timing of endocytosis in its initial stages. However, few studies have been done to determine the temporal dependence on the extent of co-localization and clustering of Rab5, Rab7, Rab11, and LAMP-1 markers in cells. Figure 7.1 is an illustration to demonstrate the work to be determined for understanding association of markers in a time dependent manner;

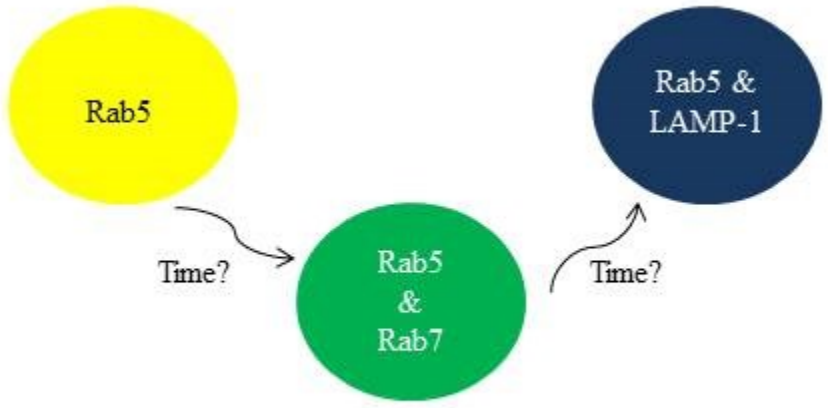

Figure 7.1 Timing for Marker Association with Compartments Still to be Determined

As cells are always in a steady state, it may be a challenge, or perhaps even impossible, to measure the clathrin mediated endocytic proteins individually, thus it may be useful to study these systems in relation to phospholipid coated gold nanoparticles.

Phospholipid coated gold nanoparticles have been fully characterized via scanning electron microscopy, UV Vis Spectroscopy, and transmission electron microscopy in previous studies.[2] In this thesis, the association with endocytic compartments and the internalization of phospholipid coated gold nanoparticles in fixed cells was determined to assess the internalization and clathrin mediated endocytic behavior in two cell types. However, quantitative information in relation to the dynamics of this material has yet to be unveiled. Thus, real time analysis of the phospholipid coated gold nanoparticles is still required. In doing so, parameters such as the diffusion coefficient and time of diffusion will ultimately be determined. The motive to study this particular nanomaterial system was to assess the potential as a platform for drug delivery applications. Thus, an important question to address is how *quickly* these gold nanoparticles progress from early endosomes to lysosomes. In addition, live cell imaging will also answer the question of the ultimate *fate* of these gold nanoparticles; are they degraded or eventually cleared by exocytosis.

In order to determine if phospholipid coated gold nanoparticles could be used for drug delivery purposes, experiments need to be performed to determine the toxicity of phospholipid coated gold nanoparticles. Due to the phospholipid bilayer coating, these nanoparticles are already more biocompatible than gold nanoparticles that lack any coating.[104,105] However, there are many toxicity studies one can perform to measure oxidative stress, mitochondrial damage, and presence of lactate dehydrogenase. In addition, pharmacokinetic studies of gold are also required to assess if these particular phospholipid coated gold nanoparticles can be disposed from the body.

Last, if the phospholipid coated gold nanoparticles show to be non-toxic in-vitro and tested in-vivo, the work provided in this thesis has provided motivation to develop a phospholipid coated gold nanoparticle bi-functionalized with tyrosine kinase (can also use Epidermal Growth factor receptors that are expressed on breast cancer cells). In doing so, these nanoparticles can be directed to specific cell types such as SH-SY5Y cells or other neuroblastoma cells which express tyrosine kinase receptors.[106] Thus, phospholipid coated gold nanoparticles can serve as a platform and specifically target various cell types. For example, cisplatin and doxorubicin (DOX) are commonly used drugs to treat cancer; gold nanoparticles have been loaded with DOX and cisplatin as a means to increase efficiency of uptake and drug delivery.[107,108]

As discussed in Chapter 6, the real time *analysis* of two oligomers in cells is underway and to be completed for further understanding of α −synuclein oligomer dynamics.

References

[1] Wang, M.; Petersen, N. O. Lipid-coated gold nanoparticles promote lamellar body formation in A549 cells. *Biochim. Biophys. Acta - Mol. Cell Biol. Lipids* **2013,** *1831* (6), 1089–1097.

[2] Wang, M.; Petersen, N. O. Characterization of phospholipid-encapsulated gold nanoparticles: a versatile platform to study drug delivery and cellular uptake mechanisms. *Can. J. Chem.* **2015,** *93*, 265–271.

[3] Jones, R. Biology, Drexler, and nanotechnology. *Mater. Today* **2005,** *8* (8 SUPPL.), 56.

[4] Martín-Palma, R.J.; Lakhtakia, Akhlesh. N*anotechnology: A Crash Course*; SPIE Pres: Bellinghan, 2010.

[5] Nuzzo, R. G.; Zegarski, B. R.; Dubois, L. H. Fundamental studies of the chemisorption of organosulfur compounds on gold(111). Implications for molecular self-assembly on gold surfaces. *J. Am. Chem. Soc.* **1987,** *109* (3), 733–740.

[6] Collard, D. M.; Fox, M. A. Use of Electroactive Thiols To Study the Formation and Exchange of Alkanethiol Monolayers on Gold. *Langmuir* **1991,** *7* (13), 1192–1197.

[7] Dreaden, E. C.; Austin, L. A; Mackey, M. A; El-Sayed, M.A. Size matters: gold nanoparticles in targeted cancer drug delivery. *Ther. Deliv.* **2012,** *3* (4), 457–478.

[8] Mei, B.C.; Susumu, K.; Medintz, I. L.; Delehanty, J. B.; Mountziaris, T. J.; Mattoussi, H. Modular poly(ethylene glycol) ligands for biocompatible semiconductor and gold nanocrystals with extended pH and ionic stability. *J. Mater. Chem.* **2008,** *18*, 4949-4958.

[9] El-Gogary, R. I.; Rubio, N.; Wang, J. T. W.; Al-Jamal, W. T.; Bourgognon, M.; Kafa, H.; Naeem, M.; Klippstein, R.; Abbate, V.; Leroux, F.; Bals, S.; Van Tendeloo, G.; Kamel, A. O.; Awad, G. A. S.; Mortada, N. D.; Al-Jamal, K. T. Polyethylene Glycol Conjugated Polymeric Nanocapsules for Targeted Delivery of Quercetin to Folate-Expressing Cancer Cells in Vitro and in Vivo. *ACS. Nano.* **2014,** *8,* (2), 1384–1401.

[10] Jokerst, J. V; Lobovkina, T.; Zare, R. N.; Gambhir, S. S. Nanoparticle PEGylation for imaging and therapy. *Nanomedicine (Lond).* **2011,** *6* (4), 715–728.

[11] Mukherjee, P.; Bhattacharya, R.; Bone, N.; Lee, Y. K.; Patra, C. R.; Wang, S.; Lu, L.; Secreto, C.; Banerjee, P. C.; Yaszemski, M. J.; Kay, N. E.; Mukhopadhyay, D. Potential therapeutic application of gold nanoparticles in B-chronic lymphocytic leukemia (BCLL): enhancing apoptosis. *J. Nanobiotechnology.* **2007,** *5* (4),1-13.

[12] Gautier, J.; Allard-Vannier, E.; Munnier, E.; Soucé, M.; Chourpa, I. Recent advances in theranostic nanocarriers of doxrubicin based on iron oxide and gold nanoparticles. *J. Control. Release.* **2013,** *169* (1-2), 48–61.

[13] Brown, S. D.; Nativo, P.; Smith, J. A.; Stirling, D.; Edwards, P. R.; Venugopal, B.; Flint, D. J.; Plumb, J. A.; Graham, D.; Wheate, N. J. Gold Nanoparticles for the Improved

Anticancer Drug Delivery of the Active Component of Oxaliplatin. *J. Am. Chem. Soc.* **2010,** *132* (13), 4678–4684.

[14] Kratz, F.; Müller, I. A.; Ryppa, C.; Warnecke, A. Prodrug Strategies in Anticancer Chemotherapy. *Chem. Med. Chem* **2008,** *3* (1), 20–53.

[15] Huang, X.; Jain, P. K.; El-Sayed, I. H.; El-Sayed, M. A. Determination of the Minimum Temperature Required for Selective Photothermal Destruction of Cancer Cells with the Use of Immunotargeted Gold Nanoparticles. *Photochem. Photobiol.* **2006,** *82* (2), 412–417.

[16] Arruebo, M.; Valladares, M.; González-Fernández, Á. Antibody-Conjugated Nanoparticles for Biomedical Applications. *J. Nanomater.* **2009,** *2009,* 1-25.

[17] Gao, J.; Huang, X.; Liu, H.; Zan, F.; Ren, J. Colloidal Stability of Gold Nanoparticles Modified with Thiol Compounds: Bioconjugation and Application in Cancer Cell Imaging. *Langmuir* **2012,** *28* (9), 4464–4471.

[18] Mirkin, C. a; Letsinger, R. L.; Mucic, R. C.; Storhoff, J. J. A DNA-based method for rationally assembling nanoparticles in macroscopic materials. *Nature*. **1996,** *382 (15),* 607–609.

[19] Li, F.; Zhang, H.; Dever, B.; Li, X.-F.; Le, X. C. Thermal Stability of DNA Functionalized Gold Nanoparticles. *Bioconjug. Chem.* **2013,** *24* (11), 1790–1797.

[20] Dhar, S.; Daniel, W. L.; Giljohann, D. A.; Mirkin, C. A.; Lippard, S. J. Polyvalent Oligonucleotide Gold Nanoparticle Conjugates as Delivery Vehicles for Platinum(IV) Warheads. *J. Am. Chem. Soc.* **2009,** *131* (41), 14652–14653.

[21] Jain, P. K.; Qian, W.; El-Sayed, M. A. Ultrafast Cooling of Photoexcited Electrons in Gold Nanoparticle-Thiolated DNA Conjugates Involves the Dissociation of the Gold-Thiol Bond. *J. Am. Chem. Soc.* **2006,** *128* (7), 2426–2433.

[22] Alkilany, A. M.; Murphy, C. J. Toxicity and cellular uptake of gold nanoparticles: what we have learned so far? *J. Nanoparticle. Res.* **2010,** *12* (7), 2313–2333.

[23] Luna, E.; Luk, K. C. Bent out of shape: α-Synuclein misfolding and the convergence of pathogenic pathways in Parkinson's disease. *FEBS Lett.* **2015,** *589* (24), 3749–3759.

[24] Lees, A. J.; Hardy, J.; Revesz, T. Parkinson's disease. *Lancet.* **2009,** *373* (9680), 2055–2066.

[25] Spillantini, M. G.; Schmidt, M. L.; Lee, V. M.; Trojanowski, J. Q.; Jakes, R.; Goedert, M. α-Synuclein in Lewy Bodies. *Nature.* **1997,** *388* (6645), 839–840.

[26] Cooper, A.A.; Gitler, A.D.; Cashikar, A.; Haynes, C.M.; Hill, K.J.; Bhullar, B; Kangning, L.; Xu, Kexiang.; Strathearn, K,; Liu, F..; Cao, S.; Caldwell, K.A.; Caldwell, G.A.; Marsischky, G.; Kolodner, R.D.; LaBaer, J.; Rochet, J.; Bonini, N.M.; Lindquist, S. α-Synuclein Blocks ER-Golgi Traffic and Rab1 Rescues Neuron Loss in Parkinson's Models. *Science.* **2006,** *313* (5785), 3324-328.

[27] Brundin, P.; Melki, R.; Kopito, R. Prion-like transmission of protein aggregates in neurodegenerate diseases. *Nat. Rev. Mol. Cell Biol.* **2010,** *11,* 301–307.

[28] Breydo, L.; Wu, J. W.; Uversky, V. N. α-Synuclein misfoldering and Parkinson's disease. *Biochim. Biophys. Acta.* **2012,** *1822* (2), 261–285.

[29] Jakes, R.; Spillantini, M. G.; Goedert, M. Identification of two distinct syynucleins from human brain. *FEBS Lett.* **1994,** *345* (1), 27–32.

[30] Macchi, F.; Deleersnijder, A.; Van den Haute, C.; Munck, S.; Pottel, H.; Michiels, A.; Debyser, Z.; Gerard, M.; Baekelandt, V. High-content analysis of α-synuclein aggregation and cell death in a cellular model of Parkinson's disease. *J. Neurosci. Methods* **2016,** *261*, 117–127.

[31] Lashuel, H.A.; Overk, C.R.; Oueslati, A.; Masliah, E. The many faces of α-synuclein: from structure and toxicity to therapeutic target. *Nat. Rev. Neurosci.* **2013,** *14* (1), 38-48.

[32] Bisaglia, M.; Greggio, E.; Maric, D.; Miller, D. W.; Cookson, M. R.; Bubacco, L. α-Synuclein overexpression increases dopamine toxicity in BE(2)-M17 cells. *BMC Neurosci.* **2010,** *11*, 41-46.

[33] Winner, B.; Jappelli, R. Maji, S.; Desplats, P.A.; Boyer, A.; Aigner, S.; Hetzer, C.; Loher, T.; Vilar, M.; Campioni, S.; Tzitzilonis, C.; Soragni, A.; Jessberger, S.; Mira, H.; Consiglio, A.; Pham, E.; Masliah, E.; Gage, F.; Riek, R. In-vivo demonstration that α-synuclein oligomers are toxic. *Proc. Natl. Acad. Sci.* **2011,** *108* (10), 4194–4199.

[34] Lee, H. J.; Suk, J. E.; Bae, E. J.; Lee, J. H.; Paik, S. R.; Lee, S. J. Assembly-dependent endocytosis and clearance of extracellular α-synuclein. *Int. J. Biochem. Cell Biol.* **2008,** *40* (9), 1835–1849.

[35] Marques, O.; Outeiro, T. F. Alpha-synuclein: from secretion to dysfunction and death. *Cell Death Dis.* **2012,** *3* (7), e350.

[36] Conway, K. a; Lee, S. J.; Rochet, J. C.; Ding, T. T.; Williamson, R. E.; Lansbury, P. T. Acceleration of oligomerization, not fibrillization, is a shared property of both α-synuclein mutations linked to early-onset Parkinson's disease: Implications for pathogensis and therapy. *Proc. Natl. Acad. Sci. U. S. A.* **2000,** *97* (2), 571–576.

[37] Karpinar, D. P.; Balija, M. B. G.; Kügler, S.; Opazo, F.; Rezaei-Ghaleh, N.; Wender, N.; Kim, H.-Y.; Taschenberger, G.; Falkenburger, B. H.; Heise, H.; Kumar, A.; Riedel, D.; Fichtner, L.; Voigt, A.; Braus, G. H.; Giller, K.; Becker, S.; Herzig, A.; Baldus, M.; Jäckle, H.; Eimer, S.; Schulz, J. B.; Griesinger, C.; Zweckstetter, M. Pre-fibrillar α-synuclein variants with impaired β-structure increase neurotoxicity in Parkinson's disease models. *EMBO J.* **2009,** *28* (20), 3256–3268.

[38] Chithrani, B. D.; Ghazani, A. A.; Chan, W. C. W. Determining the Size and Shape Dependence of Gold Nanoparticle Uptake into Mammalian Cells. *Nano Lett.* **2006,** *6* (4), 662–668.

[39] Oh, N.; Park, J. H. Endocytosis and exocytosis of nanoparticles in mammalian cells. *Int. J.*

Nanomedicine. **2014,** *9* (SUPPL.1), 51–63.

[40] Maderna, P.; Godson, C. Phagocytosis of apoptotic cells and the resolution of inflammation. *Biochim. Biophys. Acta - Mol. Basis Dis.* **2003,** *1639* (3), 141–151.

[41] Guo, S.; Zhang, X.; Zheng, M.; Zhang, X.; Min, C.; Wang, Z.; Cheon, S. H.; Oak, M. H.; Nah, S. Y.; Kim, K. M. Selectivity of commonly used inhibitors of clathrin-mediated and caveolae-dependent endocytosis of G protein-coupled receptors. *Biochim. Biophys. Acta - Biomembr.* **2015,** *1848* (10), 2101–2110.

[42] Hillaireau, H.; Couvreur, P. Nanocarriers' entry into the cell: relevance to drug delivery. *Cell. Mol. Life Sci.* **2009,** *66* (17), 2873–2896.

[43] Gordon, S. Elie Methnikoff: Father of natural immunity. *Eur. J. Immunol.* **2008,** *38,* 3257-3264.

[44] Straus, W. Cytochemical Observations on the Relationship Between Lysosomes and Phagosomes in Kidney and Liver By Combined Staining for Acid Phosphatase and Intravenously Injected Horseradish Peroxidase. *J. Cell Biol.* **1964,** *20* (3), 497–507.

[45] Huotari, J.; Helenius, A. Endosome maturation. *EMBO J.* **2011,** *30* (17), 3481–3500.

[46] Luzio, J.P.; Pryor, P.R.; Bright, N.A.; Lysosomes: fusion and function. *Biochim. Biophys. Acta - Mol. Cell Res.* **2009,** *1793* (4), 615–624.

[47] Le Roy, C.; Wrana, J. L. Clathrin- and non-clathrin-mediated endocytic regulation of cell signaling. *Nat. Rev. Mol. Cell Biol.* **2005,** *6* (2), 112–126.

[48] Takei, K.; Haucke, V. Clathrin-mediated endocytosis: membrane factors pull the trigger. *Trends Cell Biol.* **2001,** *11* (9), 385–391.

[49] International University Receptor Mediated Endocytosis. http://khunsunly.blogspot.ca/2010/09/receptor-mediated-endocytosis.html (accessed July 7, 2016).

[50] Stenmark, H.; Olkkonen, V. M. The Rab GTPase family. *Genome Biol.* **2001,** *2* (5), reviews3007.1-3007.7.

[51] Grosshans, B. L.; Ortiz, D.; Novick, P. Rabs and their effectors: Achieving specificity in membrane traffic. *Proc. Natl. Acad. Sci. U. S. A.* **2006,** *103* (32), 11821–11827.

[52] Hutagalung, A. H.; Novick, P. J. Role of Rab GTPases in Membrane Traffic and Cell Physiology. *Physiol. Rev.* **2011,** *91* (1), 119–149.

[53] Gorvel, J.-P.; Chavrier, P.; Zerial, M.; Gruenberg, J. rab5 Controls Early Endosome Fusion In Vitro. *Cell.* **1991,** *64* (5), 915–925.

[54] Bucci, C.; Parton, R. G.; Mather, I. H.; Stunnenberg, H.; Simons, K.; Hoflack, B.; Zerial, M. The Small GTPase rab5 Functions as a Regulatory Factor in the Early Endocytic Pathway. *Cell* **1992,** *70* (5), 715–728.

[55] Alejandro Barbieri, M.; Hoffenberg, S.; Roberts, R.; Mukhopadhyay, A.; Pomrehn, A.; Dickey, B. F.; Stahl, P. D. Rab5, an Early Acting Endosomal GTPase, Supports in Vitro Endosome Fusion without GTP Hydrolysis. *J. Biol. Chem.* **1998,** *273* (40), 25850–25855.

[56] Nielsen, E.; Severin, F.; Backer, J. M.; Hyman, A.A.; Zerial, M. Rab5 regulates motility of early endosomes on microtubules. *Nat. Cell Biol.* **1999,** *1* (6), 376–382.

[57] Epp, N.; Rethmeier, R.; Krämer, L.; Ungermann, C. Membrane dynamics and fusion at late endosomes and vacuoles - Rab regulation, multisubunit tethering complexes and SNAREs. *Eur. J. Cell Biol.* **2011,** *90* (9), 779–785.

[58] Wang, T.; Ming, Z.; Xiaochun, W.; Hong, W. Rab7: Role of its protein interaction cascades in endo-lysosomal traffic. *Cell. Signal.* **2011,** *23* (3), 516–521.

[59] Rink, J.; Ghigo, E.; Kalaidzidis, Y.; Zerial, M. Rab Conversion as a Mechanism of Progression from Early to Late Endosomes. *Cell* **2005,** *122* (5), 735–749.

[60] Poteryaev, D.; Datta, S.; Ackema, K.; Zerial, M.; Spang, A. Identification of the Switch in Early-to-Late Endosome Transission. *Cell* **2010,** *141* (3), 497–508.

[61] Bucci, C.; Thomsen, P.; Nicoziani, P.; McCarthy, J.; van Deurs, B. Rab7: A Key to Lysosome Biogenesis. *Mol. Biol. Cell* **2000,** *11* (2), 467–480.

[62] Jäger, S.; Bucci, C.; Tanida, I.; Ueno, T.; Kominami, E.; Saftig, P.; Eskelinen, E. Role for Rab7 in maturation of late autophagic vacuoles. *J. Cell Sci.* **2004,** *117* (20), 4837–4848.

[63] Eskelinen, E. L. Roles of LAMP-1 and LAMP-2 in lysosome biogenesis and autophagy. *Mol. Aspects Med.* **2006,** *27*, 495–502.

[64] Kornfeld, S.; Mellman, I. The Biogenesis of Lysosomes. *Annu. Rev. Cell Biol.* **1989,** *5,* 483–525.

[65] Grant, B. D.; Donaldson, J. G. Pathways and mechanisms of endocytic recycling. *Nat. Rev. Mol. Cell Biol.* **2011,** *10* (9), 597–608.

[66] Ullrich, O.; Reinsch, S.; Urbé, S.; Zerial, M.; Parton, R.; Rab11 Regulates Recycling through the Pericentriolar Recycling Endosome. **1996,** *135* (4), 913–924.

[67] Sönnichsen, B.; De Renzis, S.; Nielsen, E.; Rietdorf, J.; Zerial, M. Distinct Membrane Domains on Endosomes in the Recycling Pathway Visualized by Multicolor Imaging of Rab4, Rab5, and Rab11. *J. Cell Biol.* **2000,** *149* (4), 901–913.

[68] Lafourcade, C.; Sobo, K.; Kieffer-Jaquinod, S.; Garin, J.; van der Goot, F. G. Regulation of the V-ATPase along the Endocytic Pathway Occurs through Reversible Subunit Association and Membrane Localization. *PLoS One* **2008,** *3* (7), e2758.

[69] Wang,C.; Transmission Electron Microscopy I. Introduction. http://web.eng.fiu.edu/wangc/EMA6518-1.pdf. (accessed July 8, 2016).

[70] Tai, L. A.; Kang, Y. T.; Chen, Y. C.; Wang, Y. C.; Wang, Y. J.; Wu, Y. T.; Liu, K. L.; Wang, C. Y.; Ko, Y. F.; Chen, C. Y.; Huang, N. C.; Chen, J. K.; Hsieh, Y. F.; Yew, T. R.;

Yang, C. S. Quantitative Characterization of Nanoparticles in Blood by Transmission Electron Microscopy with a Window-Type Microchip Nanopipet. *Anal. Chem.* **2012,** *84* (15), 6312–6316.

[71] Tsai, D. H.; Cho, T. J.; Delrio, F. W.; Gorham, J. M.; Zheng, J.; Tan, J.; Zachariah, M. R.; Hackley, V. A. Controlled Formation and Characterization of Dithiothreitol-Conjugated Gold Nanoparticle Clusters. *Langmuir* **2014,** *30,* (12), 3397–3405.

[72] Yoonessi, M.; Seikel, E.; Pender, M. J. Characterization and Modeling of Stable Colloids of Organically Surface Tailored Gold Nanoparticle Liquids. *Langmuir* **2009,** *25* (6), 3369–3373.

[73] Nie, B.; Shortreed, M. R.; Smith, L. M. Quantitative Detection of Individual Cleaved DNA Molecules on Surfaces Using Gold Nanoparticles and Scanning Electron Microscop Imaging. *Anal. Chem.* **2006,** *78* (5), 1528–1534.

[74] Srinivasan, C.; Mullen, T. J.; Hohman, J. N.; Anderson, M. E.; Dameron, A. A.; Andrews, A. M.; Dickey, E. C.; Horn, M. W.; Weiss, P. S. Scanning Electron Microscopy of Nanoscale Chemical Patterns. *ACS Nano* **2007,** *1* (3), 191–201.

[75] Tiensuu, A.L.; Bexell, M.; Schweitz, J.Å; Smith, L.; Johnsson, S. Assembling three-dimensional microstructures using gold-silicon etectic bonding. *Sensors Actuators A. Phys.* **1994,** *45* (3), 227–236.

[76] Thorn, K. A quick guide to light microscopy in cell biology. *Mol. Biol. Cell* **2016,** *27* (2), 219–222.

[77] Kolin, D. L.; Wiseman, P. W. Advances in Image Correlation Spectroscopy: Measuring Number Densities, Aggregation States, and Dynamics of Fluorescently labeled Macromolecules in Cells. *Cell Biochem. Biophys.* **2007,** *49* (3), 141–164.

[78] Malvern Instruments Ltd. Characterisation of Colloidal Gold Using Dynamic Light Scattering. **2007,** 1–4.

[79] Nano Research Facility, Washington University in St. Louis.

[80] Edward, J. T. Molecular Volumes and the Stokes-Einstein Equation. *J. Chem. Educ.* **1970,** *47* (4), 261.

[81] Mukherjee, S.; Ghosh, N.; Maxfield, R. Endocytosis. *Physiol. Rev.* **1997,** *77* (3), 759–803.

[82] Li, X.; Wang, M.; Hoffmann, M.; Woodside, M.; Petersen, N. O.*Under Review.*

[83] Petersen, N. O.; Brown, C.; Kaminski, A; Rocheleau, J.; Srivastava, M.; Wiseman, P. W. *Faraday Discuss.* **1998,** *111*, 289–305; discussion 331–343.

[84] Keating, E.; Nohe, A.; Petersen, N. O. Studies of distribution, location and dynamic properties of EGFR on the cell surface measured by image correlation spectroscopy. *Eur. Biophys. J.* **2008,** *37*, 469–481.

[85] ATCC. C2C12 (ATCC® CRL-1772). http://www.atcc.org/~/ps/CRL-1772.ashx (accessed

July 7,2016).

[86] ATCC. A549 (ATCC® CCL-185). http://www.atcc.org/~/ps/CCL-185.ashx (accessed July 7, 2016).

[87] Everett, T.; Kell, C.; *Human Movement An Introductory Text*; 6th ed. Elsevier Ltd: Edinburgh, 2010.

[88] Burattini, S.; Ferri, P.; Battistelli, M.; Curci, R.; Luchetti, F.; Falcieri, E.;C2C12 murine myoblasts as a model of skeletal muscle development: morpho-functional characterization. *Eur. J. Histochem.* **2004,** *48* (3), 223-234.

[89] Bragdon, B.; Thinakaran, S.; Moseychuk, O.; King, D.; Young, K.; Litchfield, D.W.; Petersen, N.O.; Casein kinase 2 β-subunit is a regulator of bone morphogenetic protein 2 signaling. *Biophys. J.* **2010,** *99*, 897-904.

[90] Foster, K.A.; Oster, C.G.; Mayer, M.M.; Avery, M.L.; Audus, K.L.; Characterization of the a549 cell line as a type ii pulmonary epithelial cell model for drug metabolism. *Exp. Cell. Res.* **1998,** *243*, 359-366.

[91] Yu, S.H.; Possmayer, F.; Lipid compositional analysis of pulmonary surfactant monolayers and monolayer-associated reservoirs. *J. Lipid. Res.* **2003,** *44* (3), 621-629.

[92] Angeletti, C.; Nichols, J.W. Dithionite quenching rate measurement of the inside-outside membrane bilayer distribution of 7-nitrobenz-2-oxa-1,3-diazol-4-yl-labeled phospholipids. *Biochemistry.* **1998,** *37*, 15114-15119.

[93] El-Agnaf, O.M.A.; Salem, S.A.; Paleologou, K.E.; Curran, M.D.; Gibson, M.J.; Court, J.A.; Scholossmacher, M.G.; Allsop, D.; Detection of oligomeric forms of α−synuclein protein in human plasma as a potential biomarker for Parkinson's disease. *FASEBJ.* **2006,** *20* (3), 419-425.

[94] Thavarajah, R.; Kazhiyur Mudimbaimannar, V.; Elizabeth, J.; Krishnamohan Rao, U.; Ramganathan, K.; Chemical and physical basics of routine formaldehyde fixation. *J. Oral. Maxillofac. Pathol.* **2012,** *16* (3), 400-405.

[95] Bressloff, P. C. *Stochastic Processes in Cell Biology*; Springer: Salt Lake City, 2014.

[96] Honerkamp-Smith, A. R.; Woodhouse, F. G.; Kantsler, V.; Goldstein, R. E. Membrane Viscosity Determined from Shear-Driven FLow in Giant Vesicles. *Phys. Rev. Lett.* **2013,** *111* (3), 1–5.

[97] Wiseman, P. W.; Brown, C. M.; Webb, D. J.; Hebert, B.; Johnson, N. L.; Squier, J.A; Ellisman, M. H.; Horwitz, A.F. Spatial mapping of integrin interactions and dynamics during cell migration by Image Correlation Microscopy. *J. Cell Sci.* **2004,** *117* (Pt 23), 5521–5534.

[98] Nohe, A.; Keating, E.; Fivaz, M.; Van Der Goot, F. G.; Petersen, N. O. Dynamics of GPI-anchored proteins on the surface of living cells. *Nanomedicine Nanotechnology, Biol. Med.* **2006,** *2* (1), 1–7.

[99] Fujii, F.; Horiuchi, M.; Ueno, M.; Sakata, H.; Nagao, I.; Tamura, M.; Kinjo, M. Detection of prion protein immune complex for bovine spongiform encephalopathy diagnosis using fluorescence correlation spectroscopy and fluorescence cross-correlation spectroscopy. *Anal. Biochem.* **2007,** *370* (2), 131–141.

[100] Rappoport, J. Z.; Simon, S. M. Endocytic Trafficking of activated EGFR is AP-2 dependent and occurs through preformed clathrin spots. *J. Cell Sci.* **2009,** *122* (9), 1301–1305.

[101] Jouvenet, N.; Zhadina, M.; Bieniasz, P. D.; Simon, S. M. Dynamics of ESCRT protein recruitment during retroviral assembly. *Nat. Cell Biol.* **2011,** *13* (4), 394–401.

[102] Rappoport, J. Z.; Kemal, S.; Benmerah, A.; Simon, S. M. Dynamics of clathrin and adaptor proteins during endocytosis. *Am. J. Physiol. Cell Physiol.* **2006,** *291* (5), C1072–C1081.

[103] Rappoport, J. Z.; Heyman, K. P.; Kemal, S.; Simon, S. M. Dynamics of Dynamin during Clathrin Mediated Endocytosis in PC12 Cells. *PLoS One.* **2008,** *3* (6), 1-9.

[104] Weingart, J.; Vabbilisetty, P.; Sun, X. L. Membrane mimetic surface functionalization of nanoparticles: Methods and applications. *Adv. Colloid Interface Sci.* **2013,** *197-198*, 68–84.

[105] Possmayer, F.; Hall, S. B.; Haller, T.; Petersen, N. O.; Zuo, Y. Y.; Bernardino de la Serna, J.; Postle, A. D.; Veldhuizen, R. a W.; Orgeig, S. Recent advances in alveolar biology: Some new looks at the alveolar interface. *Respir. Physiol. Neurobiol.* **2010,** *173* (SUPPL.), S55–S64.

[106] Edsjö, A.; Lavenius, E.; Nilsson, H.; Hoehner, J. C.; Simonsson, P.; Culp, L. a; Martinsson, T.; Larsson, C.; Påhlman, S. Expression of trkB in Human Neuroblastoma in Relation to MYCN Expression and Retinoic Acid Treatment. *Lab. Invest.* **2003,** *83* (6), 813–823.

[107] Tsai, D.-H.; Cho, T. J.; Elzey, S. R.; Gigault, J. C.; Hackley, V. A. Quantitative analysis of dendron-conjugated cisplatin-complexed gold nanoparticles using scanning particle mobility mass spectrometry. *Nanoscale.* **2013,** *5* (12), 5390–5395.

[108] Lee, K. Y. J.; Lee, G. Y.; Lane, L. A.; Li, B.; Wang, J.; Lu, Q.; Wang, Y.; Nie, S. Functionalized, Long-Circulating, and Ultrasmall Gold Nanocarriers for Overcoming the Barriers of Low Nanoparticle Delivery Efficiency and Poor Tumor Penetration. *Bioconjug. Chem.* **2016**.

Appendix A

Appendix for Chapter 3

Appendix A

The purpose of this appendix is meant to serve as a guide to understand ICS parameters for C2C12 and A549 Cells as discussed in Chapter 3.

A.1 Statistical Analysis: Histograms of ICS Parameters in C2C12 Cells

This section is meant to serve as a guide to understand the distribution of markers of endocytic marked compartments in C2C12 cells as in reference to Chapter 3.1.

A.1.1 Number of Clusters Containing Markers of Endocytic Compartments in C2C12 cells

Recall in Chapter 3.1, approximately 30-40 images of C2C12 cells were obtained for each marker. Figure A.1 is a histogram for the number of clusters containing markers that are observed in one imaging experiment for each marker.

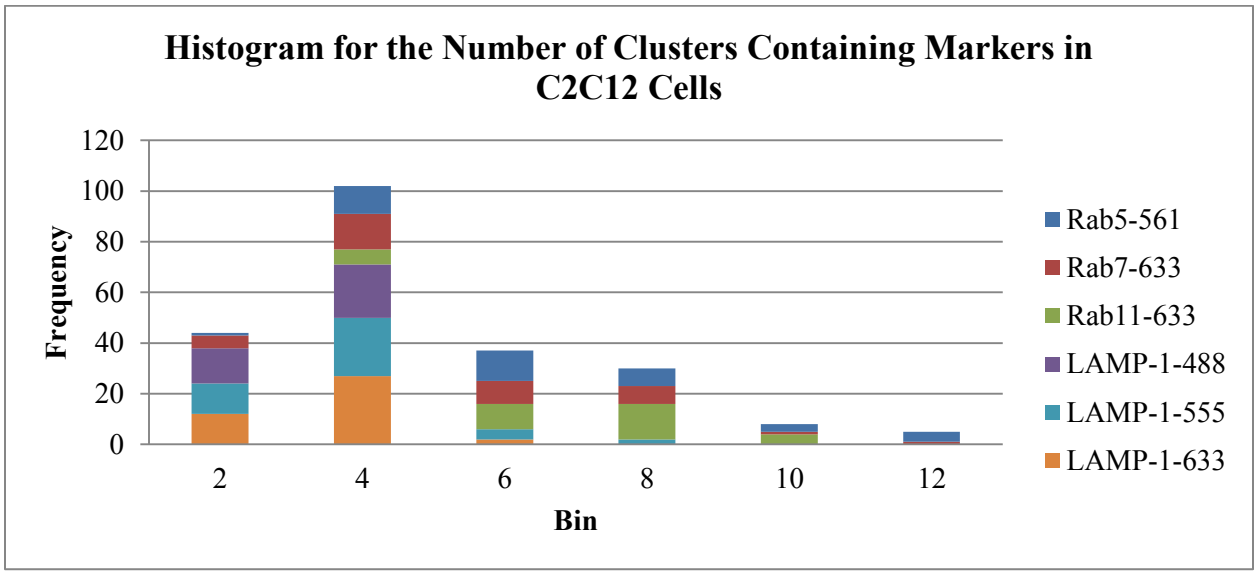

Figure A.1 Histogram for the $N_{species}$ of each Cluster Containing Markers of Endocytic Compartments in C2C12 Cells

Histogram is a reflection of values between n and n-2. For example; the frequency at bin 2 is a reflection of values of CD of Rab5 that lie between 0.00-2.00.

In Figure A.1 on average, the most frequently observed number of clusters consisting of a marker in C2C12 cells is 2.01-4.00 clusters. In addition, the distribution of clusters containing

LAMP-1-488, LAMP-1-555, and LAMP-1-633 are in agreement; therefore, this observation is proof that the labelling of LAMP-1 marked endocytic compartments is consistent between experiments and the efficiency of labelling has no dependence on fluorophore.

A.1.2 Number of Clusters Containing Markers of Endocytic Compartments per square micron in C2C12 Cells

Figure A.2 represents a histogram for the number of clusters containing markers of endocytic compartments per square micron that were observed for each marker as discussed in Chapter 3.1.

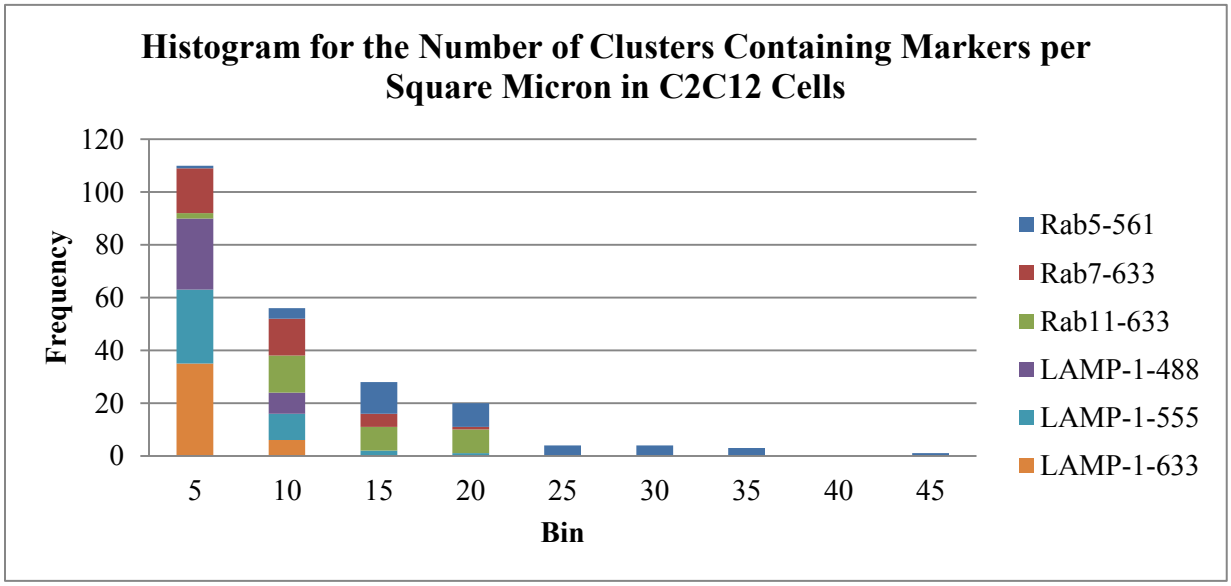

Figure A.2 Histogram for the CD of each Endocytic Marked Compartment in C2C12 Cells

In Figure A.2, the most frequent number of clusters per square micron containing a marker is between 0.00-5.00 clusters per square micron. The number of LAMP-1 clusters per square micron experimented using different fluorescent secondary antibodies are also in agreement. Thus, the labelling of LAMP-1 marked endocytic compartments is consistent between experiments and the efficiency of labelling has no dependence on fluorophore.

A.1.3 Intensity of Markers in C2C12 Cells

Figure A.3 is a histogram for the intensity of markers observed for each marker as discussed in Chapter 3.1.

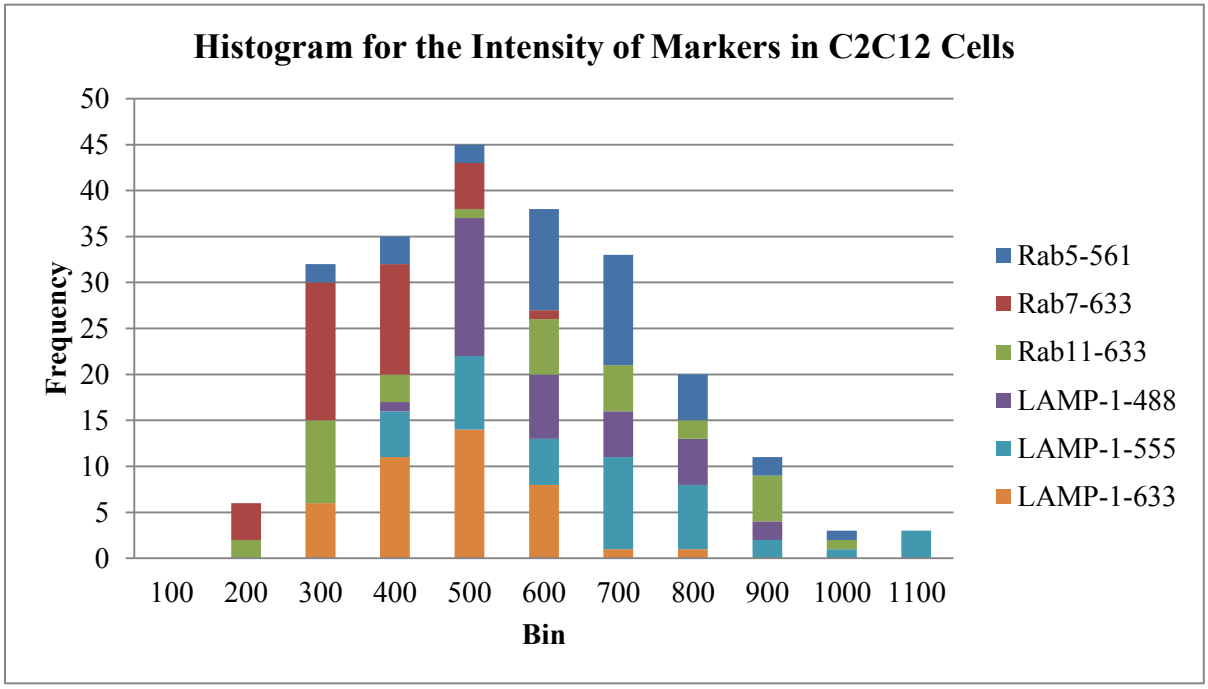

Figure A.3 Histogram for the Intensity of Species in C2C12 Cells

In Figure A.3, the distribution of intensities Rab5, Rab7, Rab11, and LAMP-1 markers follows a normal distribution. In addition, the most frequently observed magnitude of intensities of markers ranges between 400.01-500.00. As shown with the number of clusters and number of clusters per square micron, the distributions of intensities for each LAMP-1 marker labelled with a different secondary antibody of LAMP-1 are similar.

A.1.4 Relative Degree of Aggregation of Endocytic Markers in C2C12 Cells

Figure A.4 shows a histogram for the relative degree of aggregation for each marker discussed in Chapter 3.1.

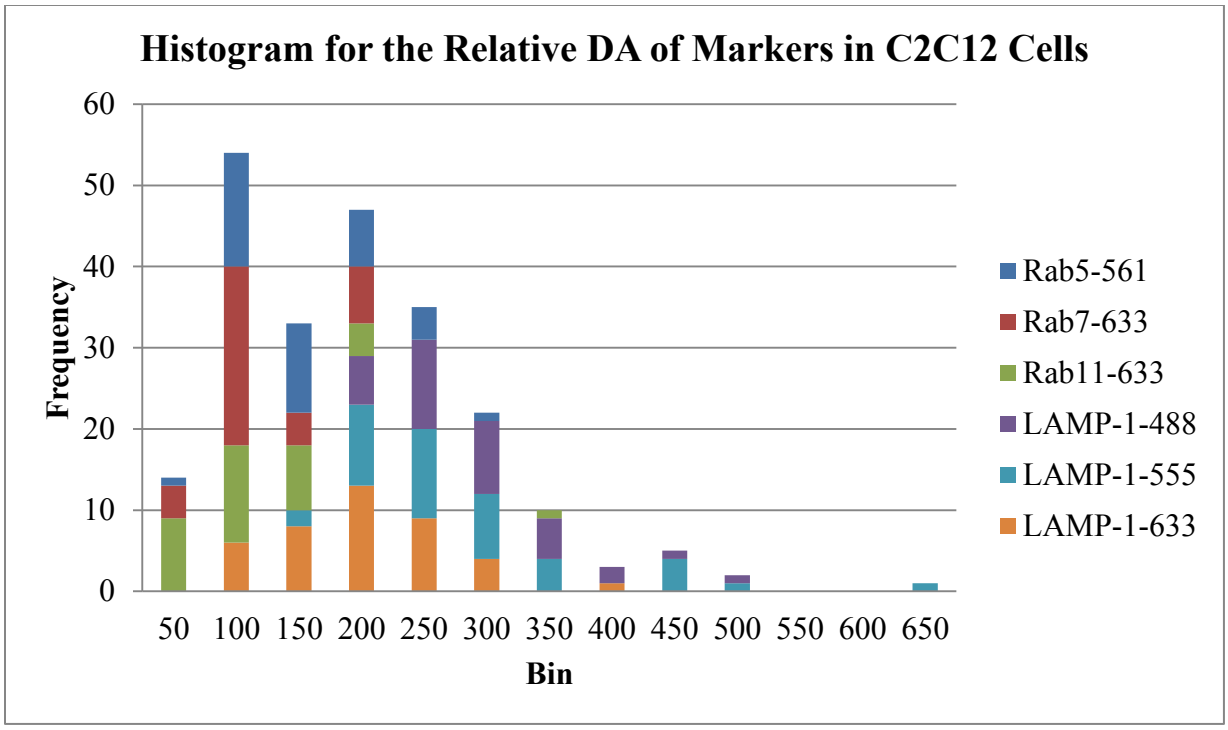

Figure A.4 Histogram for the Relative DA of each Endocytic Marked Compartment in C2C12 Cells

In Figure A.4, the relative degree of aggregation of Rab5, Rab7, Rab11, and LAMP-1 markers per cluster from one experiment follows a normal distribution. In addition, the most frequently observed magnitude for the relative degree of aggregation for each marker ranges between 50.01-100.00.

A.2 Statistical Analysis of Parameters in A549 Cells

This section is meant to serve as a guide to understand the overall distribution of markers for endocytic compartments in A549 cells as shown in Chapter 3.4.

A.2.1 Number of Clusters Containing Markers of Endocytic Compartments in A549 cells

Figure A.5 is a histogram for the number of clusters containing markers for each marker experiment as shown in Chapter 3.4.

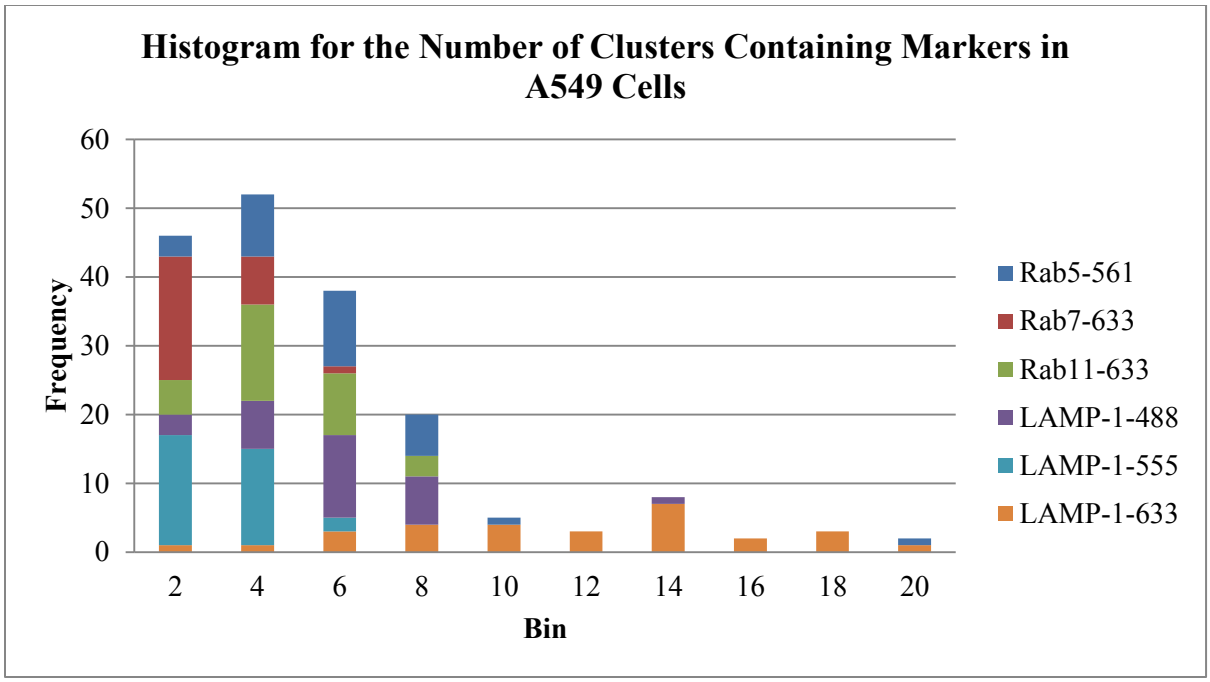

Figure A.5 Histogram for the Number of Fluorescent Endocytic Marked Compartment in A549 Cells

In Figure A.5, the number of clusters containing Rab5, Rab7, Rab11, and LAMP-1 markers of endocytic compartments calculated from one experiment corresponding to each marker does not follow a normal distribution. The most frequently observed number of clusters for each marker ranges between 2.01-4.00 clusters. However, approximately 0.00-2.00 clusters of each marker are also frequently observed.

A.2.2 Number of Clusters Containing Markers per Square micron in A549 Cells

Figure A.6. represents a histogram for the number of clusters containing markers per square micron for each marker studied in Chapter 3.4.

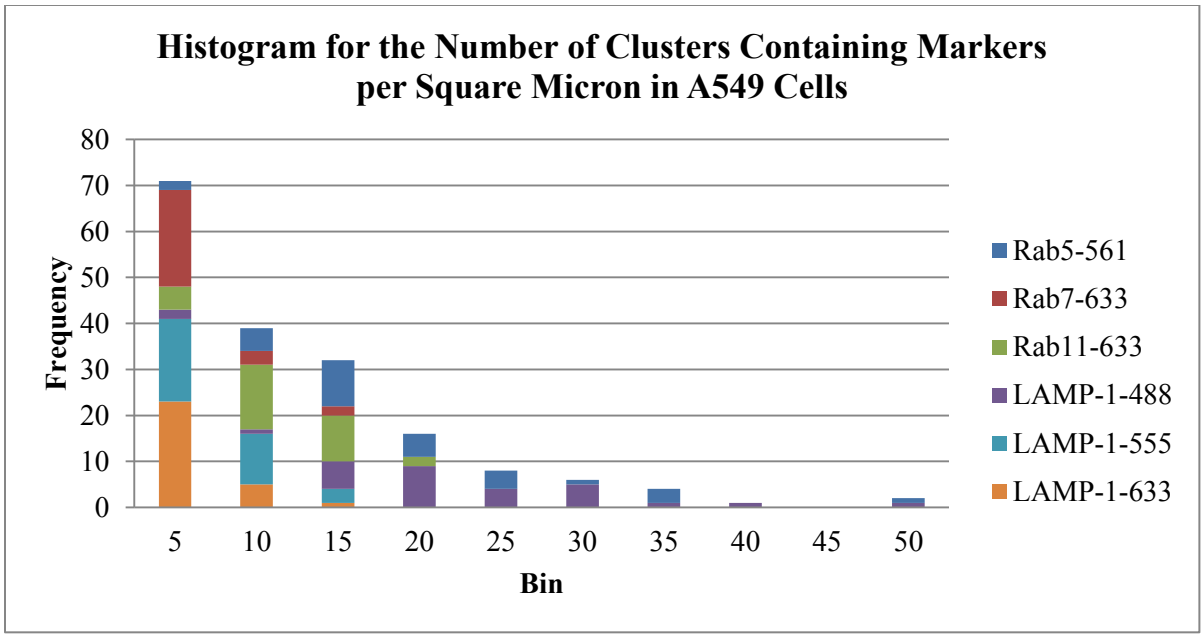

Figure A.6 Histogram for the CD Endocytic Marked Compartment in A549 Cells

Based on the histogram plotted in Figure A.6, the distribution of clusters per square micron does not follow a normal distribution. The most frequently observed number of clusters per square micron ranges between 0.00-5.00 clusters per square micron.

A.2.3 Intensity of Markers in A549 Cells

Figure A.7 is a histogram of intensities for each endocytic marker discussed in Chapter 3.4.

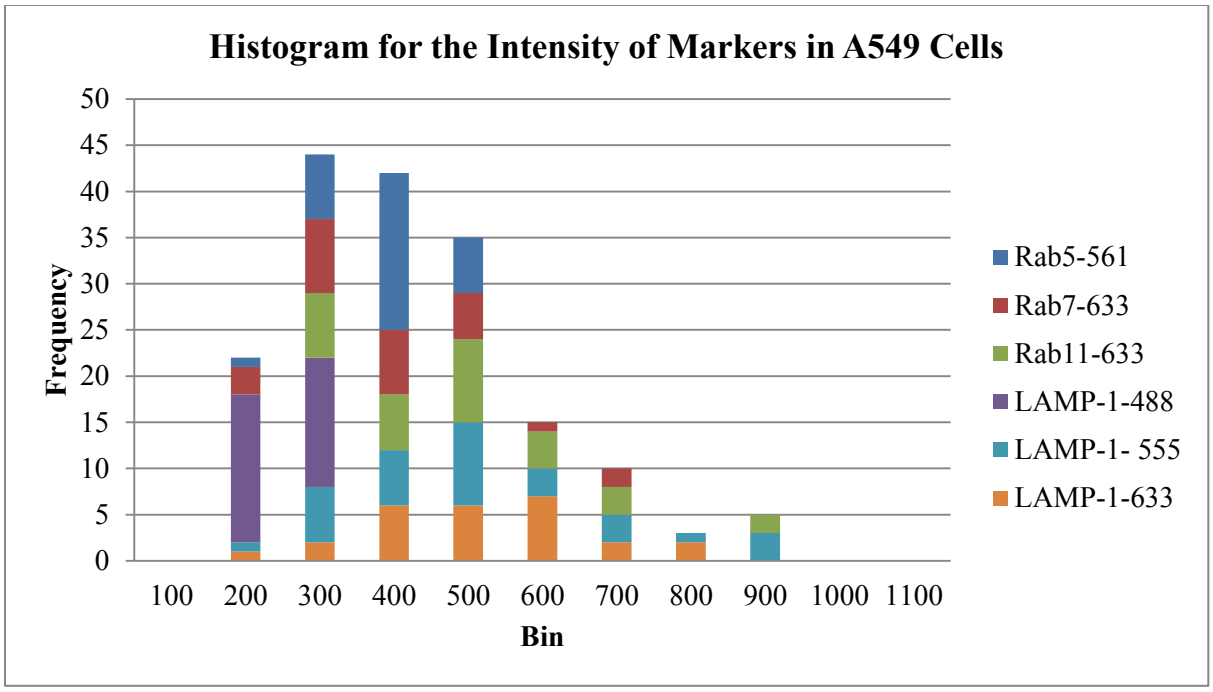

Figure A.7 Histogram for the Intensity of Species in A549 Cells

In Figure A.7, the distribution of intensities follows a normal distribution. The most frequently observed magnitude of intensities observed for markers ranges between 200.01-300.00. However, there are also a large number of intensities observed that range between 300.00-500.00.

A.2.4 Relative Degree of Aggregation of Markers in A549 Cells

Figure A.8 represents a histogram for the relative degree of aggregation for each marker discussed in Chapter 3.4.

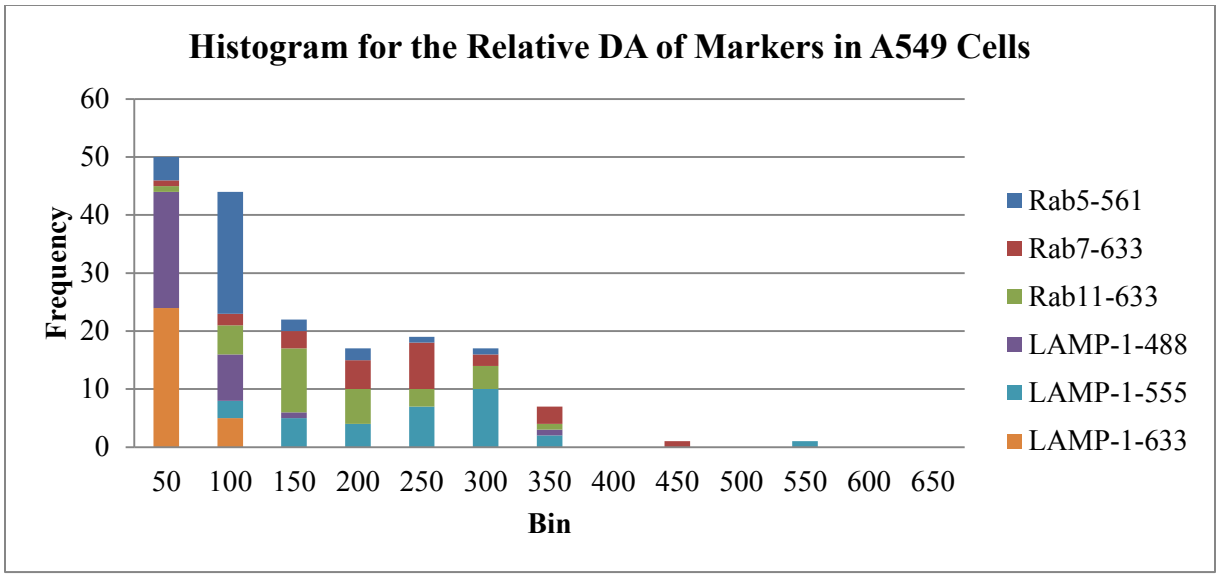

Figure A.8 Histogram for the Degree of Aggregation of Markers in A549 Cells

The most frequently observed magnitude for the relative degree of aggregation ranges between 0.00-50.00. However, intensities between 50.01-100.00 are also frequently observed for markers.

Appendix B

Appendix for Chapter 4

Appendix B

The purpose of this appendix is to provide additional material for the claims and observations discussed in Chapter 4.1. DLS spectra is shown for phospholipid coated gold nanoparticles to be approximately 20 nm. In addition, Student's T-tests were performed to assess the similarity in magnitude for a measured or calculated parameter between two sets of data.

Three types of t-tests were calculated; 1) t-tests for two different time intervals within *one* phospholipid coated gold nanoparticle internalization experiment of the same cell type 2) t-tests for the same time interval for different phospholipid coated gold nanoparticle internalization experiments for the same cell type, and 3) t-tests for data of the same experiment, same time interval, for two different cell types.

P-values calculated that were greater than 0.05 imply that the measured values for each parameter in both sets of data are similar. P-values greater than 0.20 were used as a lower limit to indicate that the measured values for a parameter compared between two sets of data are similar.

B.1 Dynamic Light Scattering

Figure B.1 is a dynamic light scattering spectrum for the size of phospholipid coated gold nanoparticles.

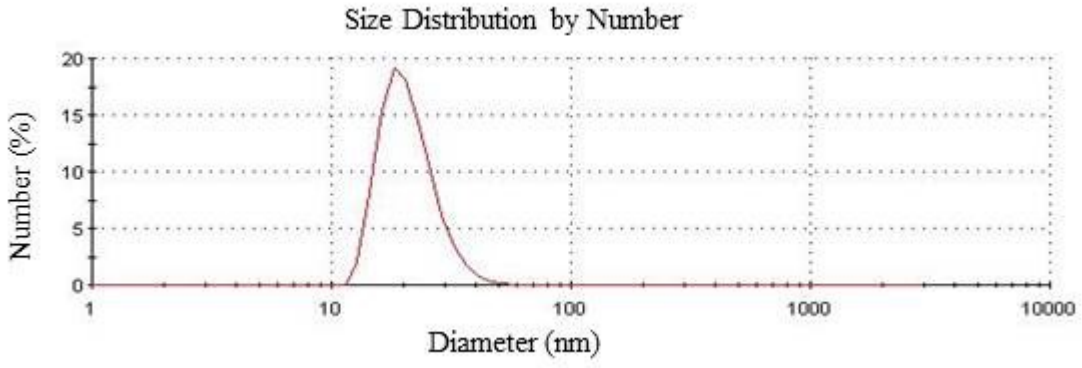

Figure B.1 DLS Spectra for Phospholipid Coated Gold Nanoparticles

Phospholipid coated gold nanoparticles are approximately 21.13 nanometers in diameter.

Gold nanoparticles are approximately 20 nm.

B.2 Student's T-Tests for Variable Exposure, Fixed Uptake Experiment in C2C12 Cells

Table B-1 is a representation of the p-values calculated from Student's T-test analysis for two different time intervals within a variable exposure, fixed uptake experiment in C2C12 cells.

Table B-1 Student's T-Test p-values for Two different Time Intervals Within a Variable Exposure, Fixed Uptake Experiment in C2C12 cells

ttest	N_{GNPs}	$I_{avg.}$	CD	DA
1 hour with 2 hour	0.09	0.07	0.01	0.01
1 hour with 4 hour	**0.23**	0.00	0.13	0.05
1 hour with 24 hour	0.01	0.00	0.00	0.00
2 hour with 4 hour	0.03	0.01	0.03	0.01
2 hour with 24 hour	**0.30**	0.01	**0.34**	**0.24**
4 hour with 24 hour	0.00	0.00	0.01	0.00

Values presented in the table refer to the $p - value$ calculated from a t-test of two independent samples of data of equal variance.

The bold faced values are a reflection of the measurements of calculations corresponding for two similar data sets. For a variable exposure, fixed uptake experiment in C2C12 cells, the number of clusters containing gold nanoparticles in the observation area appears to be similar at 1 and 4 hours, as indicated with a bold face p-value of 0.23. In addition, the average number of clusters in the observation area appears to also be similar at 2 and 24 hours, as indicated with a bold face p-value of 0.30.

In addition, the average number of clusters containing phospholipid coated gold nanoparticles for a variable exposure; fixed uptake experiment is in agreement with p-values of 0.34 and 0.24 respectively.

These t-tests suggest that the data obtained for phospholipid coated gold nanoparticles continuously exposed to cells for either 2 or 24 hours are similar.

B.3 Student's T-Tests for Fixed Exposure, Variable Uptake Experiment in C2C12 Cells

Table B-2 is a representation of the p-values calculated from Student's T-test analysis for two time intervals for data obtained for the fixed exposure, variable uptake experiment in C2C12 cells.

Table B-2 Student's T-Test p-values for Time Intervals within a Fixed Exposure, Variable Uptake Experiment of Phospholipid Coated Gold Nanoparticles in C2C12 cells

ttest	N_{GNPs}	$I_{avg.}$	CD	DA
1 hour with 2 hour	**0.42**	0.01	**0.32**	0.05
1 hour with 4 hour	0.01	0.02	0.14	0.00
1 hour with 24 hour	0.00	0.00	0.00	0.00
2 hour with 4 hour	0.02	0.13	0.04	0.03
2 hour with 24 hour	0.00	0.00	0.00	0.00
4 hour with 24 hour	0.00	0.00	0.00	0.00

Values presented in the table refer to the $p - value$ calculated from a t-test of two independent samples of data of equal variance.

The only similarities observed between data occur at 1 and 2 hours; p-values corresponding to the number of clusters containing phospholipid coated gold nanoparticles and number of clusters per square micron is 0.42 and 0.32, respectively. This is expected because at earlier times, C2C12 cells are more likely to withhold phospholipid coated gold nanoparticles when nanoparticles are no longer present in the extracellular environment (cell culture media).

B.4 Student's T-Tests for Variable Exposure, Fixed Uptake Experiment in A549 Cells

Table B-3 is a representation of the p-values calculated from Student's T-test analysis for two sets of data from a variable exposure, fixed uptake experiment in A549 cells.

Table B-3 Student's T-Test p-values for time points within a Variable Exposure, Fixed Uptake Experiment in A549 cells

ttest	N_{GNPs}	$I_{avg.}$	CD	DA
1 hour with 2 hour	0.08	0.00	0.11	0.03
1 hour with 4 hour	0.00	0.00	0.01	0.00
1 hour with 24 hour	0.00	0.00	0.00	0.00
2 hour with 4 hour	0.01	**0.33**	0.02	0.08
2 hour with 24 hour	0.00	0.00	0.00	0.00
4 hour with 24 hour	0.00	0.00	0.00	0.00

Values presented in the table refer to the $p-value$ calculated from a t-test of two independent samples of data of equal variance.

These t-tests reflect the variation in values between each time point for a continuous exposure fixed chase experiment. Thus, each time point is unique. The p-value of 0.33 for 2-4 hour intensities reflects that the data obtained for the intensities are in agreement. In addition, the magnitudes of the cluster density measurements calculated at time points 1 and 2 hour in a continuous exposure, fixed chase experiment in A549 cells are also in agreement.

These t-tests don't reflect any similarities, apart from the intensities of species observed at 2 and 4 hours.

B.5 Student's T-Tests for Fixed Exposure, Variable Uptake Experiment in A549 Cells.

Table B-4 is a representation of the p-values calculated from Student's T-test analysis for sets of data obtained for a variable exposure, fixed uptake experiment.

Table B-4 Student's T-Test p-values for time points within a Fixed Exposure, Variable Uptake Experiment in A549 cells

ttest	N_{GNPs}	$I_{avg.}$	CD	DA
1 hour with 2 hour	0.01	0.07	0.07	0.02
1 hour with 4 hour	0.00	0.06	0.00	0.02
1 hour with 24 hour	0.00	0.00	0.00	0.00
2 hour with 4 hour	0.01	0.00	0.00	**0.32**
2 hour with 24 hour	0.00	0.00	0.00	0.00
4 hour with 24 hour	0.00	0.00	0.00	0.00

Values presented in the table refer to the $p-value$ calculated from a t-test of two independent samples of data of equal variance.

In reference to Table B-4, the relative degree of aggregation values calculated for 2 and 4 hours are in agreement. This observation is expected due to the strong correlation among data sets for the measured intensities at 2 and 4 hours, as previously shown in Table B-3.

Similar to Chapter B.4, the only similarity between two data sets is in reference to the calculated degree of aggregation after 2 and 24 hours of variable uptake in cells.

B.6 Statistical Analysis Comparison of Phospholipid Coated Gold Nanoparticles in C2C12 and A549 Cells

The final section of this chapter focusses on the Student's T-tests results obtained to compare phospholipid coated gold nanoparticle internalization in C2C12 and A549 cells.

Table B-5 is a representation of the p-values calculated from Student's T-test analysis for the sets of data obtained for the variable exposure, fixed uptake experiment between C2C12 and A549 cells undergoing variable exposure, fixed uptake of phospholipid coated gold nanoparticles.

Table B-5 Student's T-Test p-values for C2C12 and A549 Cells in Continuous Exposure, Fixed Uptake Experiment

ttest	N_{GNPs}	$I_{avg.}$	CD	DA
1 hour	0.01	0.00	0.01	0.00
2 hour	0.01	0.02	0.00	0.01
4 hour	0.09	0.03	0.00	0.05
24 hour	0.00	0.00	0.00	0.00

Values presented in the table refer to the $p - value$ calculated from a t-test of two independent samples of data of equal variance.

As a result, there is no similarity among the values obtained for the data between C2C12 and A549 cells, granted there are no p-values greater than 0.05 in Table B-5. This is expected as complete opposite trends were observed and discussed in Chapter 4.

Table B-6 is a representation of the p-values calculated from Student's T-test analysis for the sets of data obtained for the Fixed Exposure, Variable Uptake experiment between C2C12

and A549 cells undergoing Fixed Exposure, Variable Uptake of phospholipid coated gold nanoparticles.

Table B-6 Student's T-Test p-values for C2C12 and A549 Cells in a Fixed Exposure, Variable Uptake Experiment.

ttest	N_{GNPs}	$I_{avg.}$	CD	DA
1 hour	0.00	0.00	0.00	0.00
2 hour	0.00	0.00	0.00	0.00
4 hour	0.00	**0.49**	0.00	0.00
24 hour	0.00	0.00	0.00	0.00

Values presented in the table refer to the $p - value$ calculated from a t-test of two independent samples of data of equal variance.

The bold face p-values in Table B-6 refer to sets of data that are similar, as previously done in this chapter. The only similarity observed for A549 and C2C12 cells in a fixed exposure, variable uptake experiment is occurred in which both cell types were exposed to phospholipid coated gold nanoparticles for 2 hours and proceeded to uptake nanoparticles for an additional 4 hours. This similarity is indicated by the bold face p-value of 0.49 for the intensity at 4 hours. Although an interesting find, comparison of intensity between two separate experiments is important. One can conclude these p-values are expected for this particular experiment, as both cell lines have exhibited completely different phenomena for phospholipid coated gold nanoparticle internalization.

Appendix C

Appendix for Chapter 5

Appendix C

The purpose of this appendix is to compare and contrast data sets from Chapter 5.

C.1 Student's T-tests for Binding of Pre-Aggregated Oligomers of α-syn post SH-SY5Y Cell Fixation

The purpose of this section is to compare and contrast data sets for pre-aggregated oligomers of α-syn exposed to pre-fixed cells. This was accomplished through the use of t-tests. Bold face pvalues represent similarities in data.

Table C-1 shows student's t-tests for data obtained for pre-aggregated monomers post SH-SY5Y cell fixation. Calculated p-values were performed for two time points within an experiment.

Table C-1 Student's T-Tests for Binding of Pre-Aggregated Monomers post SH-SY5Y Cell Fixation

ttest	N_{Ms}	$I_{avg.}$	CD	DA
1 hour with 2 hour	**0.26**	0.00	**0.26**	0.00
1 hour with 4 hour	0.00	0.00	0.00	0.00
1 hour with 24 hour	0.02	0.00	0.04	0.00
2 hour with 4 hour	0.00	0.01	0.01	0.00
2 hour with 24 hour	0.11	0.00	**0.18**	0.00
4 hour with 24 hour	0.03	0.00	0.05	0.02

Values presented in the table refer to the $p - value$ calculated from a t-test of two independent samples of data of equal variance.

Table C-1 reflects that average number of clusters of monomers observed after 1 hour and 2 hours of exposure are in agreement, such that a p-value of 0.26 was obtained. There are no similarities in relation to intensity for any two time intervals of monomeric exposure. The number of clusters observed per square micron for 1 and 2 hours of exposure and 4 and 24 hours of exposure are in agreement; p-values calculated for each test were 0.26 and 0.18. Lastly, there are no similarities observed for the degree of aggregation.

Table C-2 shows students t-tests for data obtained for pre-aggregated tetramers, post SH-SY5Y cell fixation. Calculated p-values were performed for two time points within an experiment.

Table C-2 Student's T-Tests p-values for Binding of Pre-Aggregated Tetramers post SH-SY5Y Cell Fixation

ttest	N_{Ds}	$I_{avg.}$	CD	DA
1 hour with 2 hour	0.15	0.00	0.06	0.00
1 hour with 4 hour	0.07	0.00	0.08	0.02
1 hour with 24 hour	0.00	0.00	0.00	0.00
2 hour with 4 hour	**0.50**	0.00	**0.39**	0.00
2 hour with 24 hour	0.05	0.02	0.03	**0.39**
4 hour with 24 hour	0.00	0.00	0.00	0.00

Values presented in the table refer to the $p - value$ calculated from a t-test of two independent samples of data of equal variance.

The calculations corresponding to the average number of clusters of tetramers observed after 2 and 4 hours of exposure to pre-fixed cells are in agreement, reflecting a p-value of approximately 0.50. In addition, the average number of clusters observed per square micron after 2 and 4 hours have elapsed are also in agreement, reflecting a p-value of 0.39. The degree of aggregation after 2 and 24 hours is in agreement reflecting a p-value of 0.39.

Table C-3 is a representation of students t-tests for data obtained for pre-aggregated monomers and tetramers, post SH-SY5Y cell fixation. Calculated p-values were performed for the same time interval of exposure between both oligomers.

Table C-3 Student's T-Tests p-values for Binding of Pre-Aggregated Monomers and Tetramers at same time interval post SH-SY5Y Cell Fixation

ttest	$N_{Species}$	$I_{avg.}$	CD	DA
1 hour	0.06	0.00	0.14	0.00
2 hour	**0.31**	0.00	**0.48**	**0.26**
4 hour	0.00	0.00	0.00	0.00
24 hour	**0.35**	0.00	0.03	0.00

Values presented in the table refer to the $p - value$ calculated from a t-test of two independent samples of data of equal variance.

The number of clusters of oligomers after 2 and 24 hours of exposure are in agreement, reflecting p-values of 0.31 and 0.35, respectively. In addition, the number of clusters observed per square micron after 2 hours of exposure is in agreement, reflecting a p-value of approximately 0.48. Lastly, the degree of aggregation of oligomers observed after 2 hours is approximately 0.26.

These t-tests suggest that the data corresponding to the presence of monomers and tetramers after 2 hours of exposure to pre-fixed cells are similar.

C.2 Student's T-Tests for Variable Exposure, Fixed Uptake of Oligomers of α-syn post SH-SY5Y Cell Fixation

Student's T-tests were performed to assess similarities in the data for oligomers of α-syn variously exposed to pre-fixed cells.

Table C- 4 is a representation of p-values obtained for t-tests comparing two sets of data from two different exposure times of monomers to pre-fixed cells. Bold face values indicate similarity in data sets.

Table C- 4 Student's T-Test p-values for Variable Exposure of Monomers post SH-SY5Y Cell Fixation

ttest	N_{MS}	$I_{avg.}$	CD	DA
1 hour with 2 hour	0.14	**0.41**	**0.36**	0.17
1 hour with 4 hour	**0.28**	0.01	0.07	**0.27**
1 hour with 24 hour	0.09	0.00	**0.45**	0.01
2 hour with 4 hour	**0.26**	0.00	0.08	0.04
2 hour with 24 hour	**0.31**	0.00	**0.38**	0.00
4 hour with 24 hour	0.16	0.00	0.07	0.05

Values presented in the table refer to the $p - value$ calculated from a t-test of two independent samples of data of equal variance.

The average number of clusters containing monomers is similar for data at 1 and 4 hours, 2 and 4 hours, and 2 and 24 hours. The average intensity of monomers is only similar for data obtained at 1 hour and 2 hours. The cluster density of monomers is in agreement at 1 and 2 hours, 1 and 24 hours, and 2 and 24 hours. Lastly, the degree of aggregation shows similarities

among data obtained at 1 hour and 4 hours. Similarities were expected for comparing any two data sets as there was no trend or differences observed in the experiment.

Table C-5 is a representation of p-values obtained for t-tests comparing two sets of data corresponding to two different exposure times of dimers to pre-fixed cells. Bold face values indicate similarity in data sets.

Table C-5 Student's T-Test p-values for Variable Exposure of Dimers post SH-SY5Y Cell Fixation

ttest	N_{Ds}	$I_{avg.}$	CD	DA
1 hour with 2 hour	**0.36**	0.01	**0.41**	0.16
1 hour with 4 hour	**0.21**	0.16	**0.34**	0.06
1 hour with 24 hour	0.12	0.00	0.07	0.00
2 hour with 4 hour	0.14	0.00	**0.42**	0.18
2 hour with 24 hour	0.07	0.00	0.11	0.00
4 hour with 24 hour	**0.36**	0.00	0.17	0.00

Values presented in the table refer to the $p - value$ calculated from a t-test of two independent samples of data of equal variance.

The average number of clusters containing dimers is similar among data obtained at 1 and 2 hours, 1 and 4 hours, and 4 and 24 hours. There are no observed similarities for the average intensity of species for two data sets. Lastly, the density of clusters of dimers is similar between 1 and 2 hours, 1 and 4 hours, and 2 and 4 hours. There are no observed similarities in the degree of aggregation of dimers for two sets of data.

Table C-6 is a representation of p-values obtained for t-tests comparing two sets of data corresponding to two different exposure times of tetramers to pre-fixed cells. Bold face values indicate similarity in data sets.

Table C-6 Student's T-Tests p-values for Variable Exposure of Tetramers post SH-SY5Y Cell Fixation

ttest	N_{Ts}	$I_{avg.}$	CD	DA
1 hour with 2 hour	0.09	0.00	0.08	**0.42**
1 hour with 4 hour	**0.43**	**0.44**	**0.36**	0.20
1 hour with 24 hour	0.14	0.03	0.08	**0.37**
2 hour with 4 hour	0.05	0.00	0.03	0.16
2 hour with 24 hour	0.02	0.00	0.02	**0.33**
4 hour with 24 hour	0.10	0.02	0.06	**0.36**

The $p - value$ calculated from a t-test of two independent samples of data of equal variance.

The only similarities observed for two time points of data for the number of clusters of tetramers is at 1 and 4 hours. Similarities in the average intensity for tetramer at two time intervals is observed at 1 and 4 hours. The average cluster density of tetramers is in agreement at 1 and 4 hours. Lastly, the average degree of aggregation of tetramers is in agreement at 1 and 2 hours, 1 and 24 hours, 2 and 24 hours, and 4 and 24 hours.

Table C-7 is a representation of p-values obtained for t-tests comparing exposure of monomers and dimers to pre-fixed cells. Bold face values indicate similarity in data sets.

Table C-7 Student's T-Tests p-values for Variable Exposure of Monomers & Dimers at same time post SH-SY5Y Cell Fixation

ttest	$N_{Species}$	$I_{avg.}$	CD	DA
1 hour	**0.35**	0.00	0.19	0.00
2 hour	0.08	0.00	**0.35**	0.00
4 hour	**0.33**	0.00	0.12	0.00
24 hour	**0.43**	0.00	**0.24**	**0.21**

Values presented in the table refer to the $p - value$ calculated from a t-test of two independent samples of data of equal variance.

After 1 hour of exposure, the number of clusters containing monomers and clusters containing dimers are in agreement at 1, 4, and 24 hours. Lastly, average number of clusters observed per square micron is in agreement at 2 and 24 hours. Lastly, the average degree of aggregation of monomers and dimers is similar for 24 hours of exposure.

Table C-8 is a representation of p-values obtained for t-tests comparing exposure of monomers and tetramers to pre-fixed cells. Bold face values indicate similarity in data sets.

Table C-8 Student's T-Tests p-values for Variable Exposure of Monomers & Tetramers at same time post SH-SY5Y Cell Fixation

ttest	$N_{Species}$	$I_{avg.}$	CD	DA
1 hour	0.04	0.12	0.13	0.01
2 hour	**0.46**	0.00	**0.42**	0.00
4 hour	0.01	0.20	0.01	0.07
24 hour	0.01	0.00	0.00	**0.41**

Values presented in the table refer to the $p - value$ calculated from a t-test of two independent samples of data of equal variance.

The average number of clusters of monomers and clusters of tetramers are similar for data sets obtained after 2 hours of post cell fixation exposure. Additionally, the average cluster density of monomers and cluster density of tetramers are similar for data sets obtained after 2 hours of post cell fixation exposure.

Table C-9 is a representation of p-values obtained for t-tests comparing exposure of dimers and tetramers to pre-fixed cells. Bold face values indicate similarity in data sets.

Table C-9 Student's T-Tests p-values for Variable Exposure of Dimers & Tetramers at same time post SH-SY5Y Cell Fixation

ttest	$N_{Species}$	$I_{avg.}$	CD	DA
1 hour	0.01	0.00	0.01	0.00
2 hour	0.14	0.00	**0.46**	0.00
4 hour	0.03	0.00	0.01	0.00
24 hour	0.02	0.38	0.03	**0.23**

Values presented in the table refer to the $p - value$ calculated from a t-test of two independent samples of data of equal variance.

The cluster density at 2 hours and degree of aggregation after 24 hours are in agreement for dimers and tetramers.

C.3 Student's T-Tests for Fixed Exposure, Variable Uptake of Oligomers of α −syn in SH-SY5Y Cells

Student's T-tests were performed to assess similarities in magnitude for data and calculations. T-tests are deemed useful to provide further support or to argue interpretation of results.

Table C- 10 contains student's t-tests to assess the similarity for the number of clusters containing monomers, average intensity, cluster density, and degree of aggregation of monomers in the observation area for two different times of cell uptake. Bold face numbers indicate the magnitude of the data and calculations are similar.

Table C- 10 Student's T-Tests p-values for Two Times of Variable Exposure of Monomers after Fixed Exposure, Variable Uptake of Monomers SH-SY5Y Cells

ttest	N_{Ms}	$I_{avg.}$	CD	DA
1 hour with 2 hour	**0.48**	**0.36**	**0.24**	**0.40**
1 hour with 4 hour	**0.31**	**0.44**	0.13	0.12
1 hour with 24 hour	0.01	0.00	0.00	0.00
2 hour with 4 hour	**0.30**	**0.44**	**0.37**	**0.07**
2 hour with 24 hour	0.01	1.27E-06	5.89E-03	5.72E-05
4 hour with 24 hour	0.01	6.09E-05	7.23E-03	2.87E-04

Values presented in the table refer to the $p - value$ calculated from a t-test of two independent samples of data of equal variance.

As expected, there is similarity in magnitude for the observed number of clusters of intensity, cluster density, and degree of aggregation of monomers for each time of variable uptake compared for times between 1 and 4 hours. Thus, due to the variability at 24 hours in comparison to uptake between 1-4 hours, p-values calculated in reference to 24 hours are less than 0.05 to indicate that the data is not similar.

Table C-11 shows student's t-tests to assess the similarity for the number of clusters containing dimers, average intensity, cluster density, and degree of aggregation of dimers in the observation area for two different times of cell uptake. Bold face numbers indicate the magnitude of the data and calculations are similar.

Table C-11 Student's T-Tests p-values for Two Times of Variable Exposure of Dimers after Fixed Exposure, Variable Uptake of Dimers in SH-SY5Y Cells

ttest	N_{Ds}	$I_{avg.}$	CD	DA
1 hour with 2 hour	**0.24**	**0.31**	0.18	0.19
1 hour with 4 hour	0.03	**0.41**	0.09	0.04
1 hour with 24 hour	0.00	0.00	0.00	0.07
2 hour with 4 hour	0.04	**0.28**	0.05	0.18
2 hour with 24 hour	0.03	0.00	0.03	0.04
4 hour with 24 hour	0.00	0.03	0.01	0.02

Values presented in the table refer to the $p - value$ calculated from a t-test of two independent samples of data of equal variance.

Between 1 and 2 hours of variable uptake, the number of clusters and intensity of dimers are similar in magnitude. Additionally, the intensities of dimers are similar in magnitude between 1 and 4 hours of uptake. In addition, there are also similarities in the data between 2 and 4 hours in terms of intensity.

Table C-12 shows student's t-tests to assess the similarity for the number of clusters containing tetramers, average intensity, cluster density, and degree of aggregation of tetramers in the observation area for two different times of cell uptake. Bold face numbers indicate the magnitude of the data and calculations are similar.

Table C-12 Student's T-Tests p-values for Two Times of Variable Exposure of Tetramers after Fixed Exposure, Variable Uptake of Tetramers SH-SY5Y Cells

ttest	N_{Ts}	$I_{avg.}$	CD	DA
1 hour with 2 hour	**0.24**	**0.24**	0.19	0.17
1 hour with 4 hour	**0.43**	0.05	**0.30**	0.10
1 hour with 24 hour	0.17	0.09	**0.48**	**0.43**
2 hour with 4 hour	**0.28**	0.14	0.06	**0.38**
2 hour with 24 hour	**0.40**	**0.20**	0.12	0.15
4 hour with 24 hour	0.19	**0.39**	**0.29**	0.10

Values presented in the table refer to the $p - value$ calculated from a t-test of two independent samples of data of equal variance.

The data obtained exhibits similarities for almost every parameter and calculation at different times of variable uptake of tetramers. Thus, this data suggest that the relative uptake of tetramers does not vary with time.

Table C-13 is a representation of student's t-tests performed for monomers and dimers observed at same times of variable uptake.

Table C-13 Student's T-Tests p-values for Monomers & Dimers at same time intervals after Fixed Exposure, Variable Uptake in SH-SY5Y Cells

ttest	$N_{Species}$	$I_{avg.}$	CD	DA
1 hour	0.03	0.00	0.10	0.00
2 hour	**0.22**	0.00	**0.20**	0.02
4 hour	0.00	0.00	0.00	**0.33**
24 hour	0.09	0.02	0.16	**0.36**

Values presented in the table refer to the $p - value$ calculated from a t-test of two independent samples of data of equal variance.

After 2 hours of uptake, both oligomers have similar values obtained in the data corresponding to the number of clusters and number of clusters per square micron. In addition, the degree of aggregation pertaining to monomers and dimers at 4 and 24 hours is also similar. This is expected as the relative number of monomers and dimers present in cells after longer times is less, more so for monomers.

Table C-14 is a representation of student's t-tests performed for monomers and tetramers observed at same times of variable uptake.

Table C-14 Student's T-Tests p-values for Monomers & Tetramers at same time intervals after Fixed Exposure, Variable Uptake in SH-SY5Y Cells

ttest	$N_{Species}$	$I_{avg.}$	CD	DA
1 hour	**0.25**	0.00	0.07	**0.38**
2 hour	0.07	0.00	0.00	0.12
4 hour	0.09	0.01	0.03	0.01
24 hour	0.00	0.05	0.00	0.00

Values presented in the table refer to the $p - value$ calculated from a t-test of two independent samples of data of equal variance.

Similarities in the data are observed for monomers and tetramers after 1 hour; the number of clusters of these oligomers and the degree of aggregation of these oligomers observed are similar after 1 hour of uptake. This is expected as the number of monomers present in cells would not be in agreement with the magnitude corresponding to the number of tetramers in cells at longer times.

Table C-15 is a representation of student's t-tests performed for dimers and tetramers observed at same times of variable uptake.

Table C-15 Student's T-Tests p-values for Dimers & Tetramers at same time intervals after Fixed Exposure, Variable Uptake in SH-SY5Y Cells

ttest	$N_{Species}$	$I_{avg.}$	CD	DA
1 hour	**0.27**	**0.49**	**0.30**	0.01
2 hour	0.21	**0.39**	0.02	0.01
4 hour	0.08	0.08	0.14	0.07
24 hour	0.00	0.00	0.01	0.01

Values presented in the table refer to the $p-value$ calculated from a t-test of two independent samples of data of equal variance.

As with monomers and tetramers, there is similarities observed at 1 hour; however, the intensity is also similar in magnitude after 1 and 2 hours of uptake have progressed.

C.4 Student's T-tests for Fixed Exposure and Uptake of Oligomers of $\alpha-$syn to SH-SY5Y Cells

Student's T-tests were calculated between two sets of oligomers for a statistical representation for similarities among data and calculations corresponding to each oligomer. Table C- 16 is a representation of the p-values obtained for t-tests.

Table C- 16 Student's T-Tests p-values for Fixed Exposure and Uptake of Oligomers of a-syn to SH-SY5Y Cells

t-test	$N_{Species}$	$I_{avg.}$	CD	DA
Monomers & Dimers	0.08	**0.20**	**0.35**	0.06
Monomers & Tetramers	**0.29**	**0.45**	0.01	0.05
Dimers & Tetramers	0.04	**0.33**	0.01	0.00

Values presented in the table refer to the $p-value$ calculated from a t-test of two independent samples of data of equal variance.

The average numbers of species are in similar magnitude for monomers and tetramers. The average intensity compared between two oligomers for each of the three oligomers all similar. Lastly, the average number of clusters per square micron is similar for monomers and dimers.